THE EFFECT OF MOLECULAR PROPERTIES ON MECHANICAL BEHAVIOUR IN POLY(METHYLMETHACRYLATE)

TRUONG VAN-TAN
(B.Eng.Sci., M.Eng.Sci.)

awarded 4/Dec/1981

Department of Physical
& Inorganic Chemistry,
University of Adelaide.

Ph.D. Thesis
July, 1981.

For my Parents

Brothers and Sisters

TABLE OF CONTENTS

SUMMARY

It was found that the molecular properties of polymers such as molecular weight (MW), molecular weight distribution (MWD) and stereoregularity strongly influence the fracture toughness of poly(methylmethacrylate) (PMMA) in air as well as in methanol. Dependence of fracture behaviours on these molecular properties could be understood in terms of the entanglement density.

Narrow MWD PMMA of various MW were prepared by anionic polymerization and controlled tacticity PMMA by pseudo-anionic polymerization. A method of measuring the glass transition temperature of methanol-equilibrated PMMA was developed and the depression of the glass transition temperature in the presence of solvent was discussed.

The fracture energy and the crack opening displacement (COD) in air were examined as a function of MW. The fracture energy and the COD increased rapidly with MW in the region of MW $\gtrsim M_c$, the critical MW (approximate 30,000 for PMMA), and remained constant in the high MW range. On the basis of entanglement concept, a theory has been proposed to predict the effect of MW on the fracture energy and a good agreement between theoretical values and experimental data verified the role of entanglement network in craze stabilization. The theory using the critical MW, M_c, as the main parameter to calculate the density of entanglement network has shown a marked improvement over previous reported theory and predicted that if the number-average MW, M_n, is used in relation to the fracture energy, the effect of MWD on the fracture energy can be neglected.

While the fracture in air is predominantly a cracking process, the fracture in methanol is naturally divided into two main categories: stress-cracking and stress-crazing. The stress relaxation behaviour of methanol-equilibrated PMMA exhibited an interesting relationship with the fracture behaviour in methanol. Samples

of MW > M_{sc} (the critical MW of PMMA in the presence of methanol) showing rubbery behaviour from the stress relaxation curves gave long craze growth, whereas samples of MW $\leq M_{sc}$ that did not show rubbery behaviour would fracture via cracking. This relationship between stress relaxation behaviour and fracture behaviour implied the role of entanglements in the breakdown process of PMMA in the presence of methanol.

Theoretical analysis of cracking data of low MW samples in methanol led to the conclusion that the fracture mechanism was governed by a viscous flow process. In this process, the molecular chains slipped by each other leading to the breakage of the secondary bonds. The analysis has also shown that plasticization at the crack tip by methanol resulted in the reduction of crazing stress and the COD, and that the crack velocity was controlled by the diffusion rate of methanol. Thus, the enhancement of diffusion coefficient by stress or temperature facilitated the development of a longer craze at the crack tip.

In the craze predominant regime, there were two kinds of crazes, strong mature craze in high MW samples and weak premature craze in medium MW samples. Fracture behaviour of medium MW PMMA was sensitive to temperature. At low temperature (e.g. T = 0°C), medium MW showed crazing behaviour whereas at high temperature (e.g. T = 40°C), the sample behaved similarly to low MW, i.e. cracking behaviour. This dependence on temperature of fracture behaviour was also understood in terms of entanglement density. The time dependent stress crazing and COD were analysed by the Williams-Marshall theory. The higher MW samples showed less relaxation of the stress crazing and a higher ability of stretching of craze fibrils. The enhanced stretching ability of craze fibrils of high MW samples in the presence of methanol resulted in a large

COD (~75 μm cf. 2 μm in air) and the enhancement in the ability of absorbing energy. Due to a large COD, the magnitude of the fracture toughness in methanol could exceed that in air in a range of craze velocities larger than a given velocity. However, the relaxation of crazing stress became more rapid and the stretching ability of craze fibrils reduced as MW decreased or MWD became broader. The stability of craze fibrils which led to a strong mature craze or a weak premature craze could be understood by the magnitude of primordial craze thickness (the height of original bulk material). The thickness of a strong craze (1 μm) was larger than that of weak craze (50 nm).

The co-crystallization in blends of isotactic PMMA (i-PMMA) and syndiotactic PMMA (s-PMMA) was induced by thermal treatment or by immersion in methanol. The stereocomplexes induced by these two crystallization processes exhibited different melting points. This suggested different crystal structures between thermal induced crystallites and solvent induced crystallites. The fracture toughness of s-PMMA was enhanced by blending with i-PMMA. The enhancement of the fracture toughness was attributed to the formation of crystalline stereocomplexes at the crack tip. The crystallites act as pseudo-crosslinks inhibiting chain disentanglement and thus reinforcing the entanglement network to promote craze formation.

The fracture toughness vs. entanglement correlation was shown to be a more fundamental concept than the fracture toughness vs. glass transition temperature or the fracture toughness vs. solubility parameter correlation of current thinking in predicting the effects of MW, MWD and stereoregularity on the fracture behaviour of PMMA.

DECLARATION

To the author's knowledge and belief, the material in this thesis, except where due reference is made or where common knowledge is assumed, is original. No part of this work has been submitted for any degree or award in any university.

The work was performed in the University of Adelaide from May 1977 to July 1980.

TRUONG VAN-TAN

ACKNOWLEDGMENTS

I am deeply indebted to my supervisors Dr. D.R.G. Williams and Dr. P.E.M. Allen for their warm guidance, interest and encouragement throughout the work.

I am grateful for the assistance rendered by the Glass Blowers, the workshop and laboratory staff in the Department of Physical and Inorganic Chemistry and Materials Engineering Group of the University of Adelaide. The assistance of Mr. I. Brown and Miss V. Greenwood with photography and Miss J. Nash with typing is acknowledged with gratitude.

Thanks are also due to my colleagues Mr. M.C. Fisher and Mr. C. Mair for their advice and assistance in method of polymerization and to Ms. Tuong-Vi for much assistance in the experimental works of Chapter 4.

Gratitude is expressed to the University of Adelaide for support in the form of a University Research Grant.

I would also like to express appreciation to my friend T.V. Hung whose idea encouraged me to come to Australia and created a turning point in my social and research life, and with whom I share many memories of the good old days.

Reserved until las is praise for the understanding and perseverance of my wife Setsuko to whom I failed to keep my promise on many sunny weekends. The writing of this thesis was marked by the birth of my son, Laptrung Takuya.

LIST OF IMPORTANT SYMBOLS

a_T	shift factor
A	pore area
B	thickness of specimen
B_c	crack width
C	concentration
$\mathcal{C}$	compliance
c	material constant
C_p	heat capacity
D	diffusion coefficient
d_o	primodial craze thickness
E	modulus
E^o_{eN}	modulus of rubbery zone
ΔE	flex energy
ΔE_v	energy of vaporization of solvent
f	fractional free volume
f_g	fractional free volume at glass transition temperature
G	energy release rate
G_A	energy absorbed by craze matter
G_c	critical energy release rate
G_p	energy required to propagate the crack tip
$\mathcal{G}$	shear modulus
G'	storage shear modulus
G"	loss shear modulus
h	Planck's constant
I	X-ray intensity
J	jump distance of penetrant
K	stress intensity factor (SIF)

k	time factor of the crack opening displacement
K_c	SIF at fracture
K_g, K_{og}, K_{sg}	constants in molecular weight and glass transition temperature relationship.
K_i	initial SIF
ℓ	thickness
ℓ_v	void spacing
M	molecular weight (MW)
m	time factor of the crazing stress
M_c	critical MW
M_{oc}	M_c of dry polymer (0% absorbed solvent)
M_{sc}	M_c of solvent-equilibrated polymer
M_e	MW between entanglement loci
M_n	number-average MW
M_w	weight average MW
M_p	geometric mean MW
M_{KT}	Kusy and Turner's characteristic MW
m_d	mass of diluent
m_p	mass of polymer
m_u	mass of monomer unit
N	number of moles
N_A	Avogadro's number
$\bar{N}_e$	density of entanglements
n	time factor of the modulus
$\bar{n}$	number-average of stereoblock
$\bar{n}_m$	number-average of isotactic block
$\bar{n}_r$	number-average of syndiotactic block
P	load
p	pressure at the crack tip

q	time factor of the load or the SIF
R	gas constant
$\bar{r}_o$	average end-to-end distance of polymer molecule
r_y	radius of plastic zone at the crack tip
S	weight fraction
S_c	configurational entropy
T	temperature
t	time
T_{cr}	crystallization temperature
T_g	glass transition temperature
T_{og}	T_g of dry polymer (0% absorbed solvent)
T_{sg}	T_g of solvent-equilibrated polymer
T_{dg}	T_g of diluent
T_{pg}	T_g of polymer
T_r	reference temperature
T_o	Vogel temperature
U	stored energy
u_c	critical crack opening displacement (COD)
U_o	activation energy of flow process
U_r	potential energy of relaxation process
U_b	barrier energy
V	volume
v	crack/craze velocity
V_e	evolution volume
V_d	molar volume of diluent
$v_{\bar{D}}$	front velocity of case II absorption
V_s	molar volume of solvent
V_u	molar volume of monomer unit
v_i	initial craze velocity
v_o	limiting crack velocity

W	weight
W_p	weight ratio
W_t	plate width
w_c	degree of crystallinity
x_o	crack length
x_s	number of mainchain segment
Y	displacement distance
Z	lattice coordinate number
α	reduction factor
α_ε	reduction factor of stress (or strain)
α_u	reduction factor of the COD
α_f	free volume temperature coefficient
α_p	free volume temperature coefficient of polymer
α_d	free volume temperature coefficient of diluent
β	fraction of fracture energy
γ_c	fracture energy
γ_{c_1}	surface energy
γ_{c_2}	plastic deformation energy
γ_F, γ_F'	constants in Zhurkov's equation
Δ	craze length
δ_s	solubility parameter of solvent
δ_p	solubility parameter of polymer
ε	strain
$\dot{\varepsilon}$	strain rate
ε_c	critical strain
ε_y	yield strain
θ	total released free volume
θ_1	free volume released by chain ends
θ_2	free volume released by disentanglement
τ	time scale of crack propagation
τ_r	relaxation time

ν	specific real volume of liquid
ν_o	specific occupied volume of liquid
ρ	density
ρ_p	density of polymer
ρ_s	density of solvent-equilibrated polymer
σ	applied bulk stress
σ_D	standard deviation in normal distribution
σ_r	steric hindrance factor
σ_c	crazing stress
σ_y	yield stress
ϕ	volume fraction
λ	spacing distance of intermolecular bond
λ_e	extension ratio
η	viscosity
η_o	zero-shear viscosity
ξ	correction factor for craze length
χ	Flory-Huggin's parameter
μ	Poisson's constant

CHAPTER 1

INTRODUCTION

Fracture, a well known phenomena in solid materials, is customarily associated with cracking. The investigation of cracking may have a history as long as the history of materials engineering, but crazing which is another form of fracture was discovered only three decades ago. Craze is a distinct deformation inherent to organic polymers and originates from long chain nature of macromolecules. Fracture processes in polymers can be illustrated by tearing a piece of tissue paper. Under the high hydrostatic tension at the crack tip, voids are formed and polymer chains are oriented with the direction of stress forming the craze fibrils. The formation of voids and craze fibrils are the characteristics of crazing. If the external stress exceeds a limit which depends on the molecular properties of the polymer, the breakdown of craze fibrils will lead to void coalescence and cause failure by subsequent cracking.

The fracture behaviour of polymers has been studied in depth in recent years. The investigation of the cracking and crazing mechanism can be divided into two main streams: fracture in air and fracture in an active environment. The fracture process in air is a crack-predominant process whereas fracture process in an active environment includes two phenomena: stress-cracking and stress-crazing. The environmental stress-cracking can be observed in the fracture behaviour of polyethylene in detergent solution or poly(methylmethacrylate) (PMMA) in benzene. The environmental stress-crazing, on the other hand, occurs mainly in amorphous polymers. For example, the crazing of PMMA in methanol shows a long craze growth without cracking (i.e. without breakdown of craze fibrils) and the material can be subjected to a high stress as the

craze matter is able to absorb energy.

Although there have been a considerable number of studies concerned with elucidating the mechanism of fracture process in air and in environment, little attention has been paid to a unified mechanism for cracking and crazing in particular to the search of a main factor which governs the cracking or the crazing in fracture process. Most of the previous works have concentrated on the evaluation of fracture energy in amorphous polymers (1-4), the study of craze morphology and structure (5-7), the environmental effects on cracking /crazing (8-10) and theoretical description of micromechanism of craze fibrils at the crack tip (11-14).

It is the basic hypothesis that the bulk properties of solid materials are to be understood in terms of the properties of the molecules, their arrangement in space and the interactions between them. Establishment of relationship between the mechanical properties (e.g. fracture behaviour) and basic molecular parameters (molecular weight, molecular weight distribution and stereoregularity), however , has been impeded by scarcity of well-defined samples for testing hypothesis. Recently narrow molecular weight distribution (MWD) stereorandom (atactic) polystyrene has become commercially available, therefore the effects of molecular weight (MW) and MWD can be properly tested . We chose to work instead with another common and long-established thermoplastic, PMMA. The commercial product has changed little over the years and is broad MWD stereorandom polymer. In our laboratories, we have developed methods of preparing reasonably narrow MWD stereorandom PMMA as well as isotactic and a variety of stereoblock polymers. The former enable us to investigate the effects of MW and MWD, the latter of chain configuration and in particular the effects of blending isotactic PMMA with the normal commercial material. The present work aims at improving the understanding of the mechanism of fracture process

in air and in methanol of PMMA on the basis of chain entanglement concept by investigating the relationship between the molecular properties and the fracture behaviour.

The fracture mechanics approach has proved to be a successful method for the quantitative study of propagation phenomena (15-17). Using the fracture toughness parameter expressed by the energy release rate at fracture, G_c, or the corresponding stress intensity factor (SIF), K_c, this approach enables the development of a quantitative criteria for crack/craze stability and propagation behaviour. Because of the viscoelastic effects in organic polymers, measurement of the K_c as a function of crack/craze velocity, v, provides the most acceptable description of the fracture process. Analysis of the data for fracture in this work which is based on the K_c vs. v relationship will include the calculation of basic parameters of the fracture mechanics approach such as the crack opening displacement, the craze length, the fracture energy, the absorbed energy by craze matter and the time dependent of fracture process at the tip.

This thesis is divided into eight chapters. An overview of the fracture process in amorphous polymers and the application of fracture mechanics concept is outlined in Chapter 2. Synthesis and characterization of PMMA is described in Chapter 3. In Chapter 4, to understand physical properties of the plasticized crack tip, the glass transition temperature of methanol-equilibrated PMMA being an approximation of the glass transition temperature of the plasticized tip is determined. Depression of the glass transition temperature in the presence of methanol will be discussed in the framework of free volume concept and statistical thermodynamics theories. In Chapter 5, the fracture mechanics approach and Zhurkov's modified Rhee-Eyring theory are applied to the analysis of the effect of MW and MWD on the fracture toughness. The effect

of stereoregularity on fracture toughness is investigated by blending isotactic PMMA with syndiotactic-like PMMA, and the associated physical properties of these blends such as the glass transition temperature and the melting point of crystalline stereocomplexes are discussed in Chapter 6. A general discussion and further comments on the influence of the molecular properties on the fracture toughness are referred in Chapter 7 to support the fracture toughness and the entanglement correlation in predicting the cracking and crazing behaviour in polymers. Research topics for further development are suggested in Chapter 8.

CHAPTER 2

DEVELOPMENT OF THE UNDERSTANDING OF THE FRACTURE PROCESS IN AMORPHOUS POLYMERS AND THE APPLICATION OF FRACTURE MECHANICS

2.1 Overview of the Fracture Process in Amorphous Polymers

There have been a number of reviews on the cracking and crazing behaviours of polymers. The earliest review was written by Andrews (18), but the most wide ranging of these subjects concerning the mechanism of fracture process in air and in active environment, the mechanism of toughness enhancement and fatigue fracture was contributed by Rabinowitz and Beardmore (19), and by Kambour (20). Recently, Kramer (21) has reviewed the effect of environment on the fracture behaviour of polymers with the emphasis on the micromechanics of the craze and craze fibril stability. Because of the breadth of the subjects, only previous studies on the fracture behaviour of amorphous polymers forming the background of this work will be outlined.

2.1.1 Fracture Process in Air

Most of the studies in this area have been dealt with the crack mechanism, the phenomenology of air cracking and the evaluation of the fracture energy as a function of MW, crosslink density and temperature. Dependence of fracture energy on MW has been investigated for a wide range of broad MWD amorphous polymers. Robertson (3) established a relationship between fracture energy and MW for narrow MWD polystyrene but the MW of samples was in low MW range (MW < 70,000). Fracture energy of polycarbonate was reported by Pittman and Ward (4). Berry (1) measured the fracture energy for high MW PMMA (MW > 10^5), Kusy and co-workers (2,22) found a

sigmoid-like relationship between the fracture energy and MW for a wide range of MW (MW = 10^4 to 10^6) of broad MWD PMMA. The fracture energy in these amorphous polymers has the same tendency in MW dependence. In the MW range smaller than the critical MW, M_c (low MW range), the fracture energy is of the order of surface energy. The fracture energy increased rapidly in the range of MW just larger than M_c (medium MW range) and become constant at very high MW. The fracture energy of high MW polymers which is mainly contributed by the work of plastic deformation at the crack tip is about three decades larger than the surface energy.

The plastic deformation can be prohibited by crosslinks and this leads naturally to a reduction of the fracture energy. Berry (23) found that a copolymer of 10% ethylene glycol dimethacrylate (crosslinking agent) with methyl methacrylate possessed only 25% to 30% fracture energy of PMMA. Broutman and McGarry (24) obtained similar results for crosslinked PMMA showing that the fracture energy decreases with increasing crosslink density. On the other hand, the addition of rubber particles to amorphous polymers resulted in an enhancement of impact toughness (20). The fracture energy of rubber-modified PMMA can be at least two decades greater than unmodified PMMA. Similarly, rubber-modified polystyrene (high impact polystyrene, HIPS) possesses not only excellent high impact properties in comparison to polystyrene, but also good ductility. The enhancement of mechanical properties by the addition of rubber particles largely arises from numerous stress-induced microcrazing in amorphous matrix occurring between two rubber particles (25).

Although only few studies have reported the crack mechanism and kinetics of crack propagation the most comprehensive study of the kinetics of fracture in air of solid materials ranging from metals to polymers were contributed by Zhurkov (26). He

adopted a molecular model and proposed that the failure process is characterised by an activation energy of Rhee-Eyring stress-biased kinetics, where the height of the energy barrier is reduced by some function of the applied stress. Zhurkov calculated the activation energy from fracture data and found this energy is close to the carbon-carbon bond energy for the polymers. He suggested that main chain bond rupture is responsible for the failure in polymers. Marshall et al. (27) assumed the temperature dependence of the fracture toughness expressed by stress intensity factor, K, (see next section) can be described by the Arrhenius equation. These authors noted that the activation energy is equal to that of the β transition of viscoelastic process in polymers. There appears to be similarity between Zhurkov's Rhee-Eyring stress-biased expression and Arrhenius equation, but which is the main process governing the failure mechanism, main chain rupture process or β transition, is still not clear. Admittedly, while Zhurkov's approach was theoretically developed on a molecular model and successfully applied to a wide range of solids, Marshall's et al. unjustified assumption of Arrhenius-type temperature dependence of the fracture toughness may cast doubt on the role of the β transition in failure mechanism.

2.1.2 Fracture Process in an Active Environment

The study of environmental stress cracking/crazing (ESC) has been largely dealt with the effect of environment on fracture process and the associated mechanism and morphology. The role of organic solvents in craze and crack initiation of poly(2,6-dimethyl-1,4-phenyleneoxide) has been comprehensively studied by Benier and Kambour (8). According to these authors, the two major hypotheses for the action of organic agents in craze and crack initiation have been surface energy reduction and plasticization. They suggested

the correlation between the cracking or crazing behaviour and the glass transition temperature of plasticized crack tip, T_{sg}. The critical strain, ε_c, which expressed the initiation of cracking or crazing was found to have a linear relationship with T_{sg}. The cracking behaviour of amorphous polymers showed that the critical strain increased with T_{sg} and approached zero when T_{sg} is close to or below room temperature. Following Benier and Kambour's pioneer work, a number of studies have been reported for polystyrene by Boyer and Keskkula (28), Kambour et al. (10), for polar polymer such as PMMA, polyvinylchloride and polysulfone by Vincent and Raha (9). The correlation of ε_c vs. T_{sg} (or alternatively ε_c vs. the solvent solubility parameter, δ_s) used by these workers in predicting the cracking and crazing of polymers is open to speculation and this problem will be scrutinized in the light of the present work (Chapter 7). Kramer has recently attempted to classify the environmental fracture systems depending on whether the environment (gas or organic solvent) promotes degradation in polymers, chain cross-linking or neither (21).

Kambour and co-workers' correlation between the fracture behaviour and a physical quantity (T_{sg} or δ_s), or Kramer's classification of environmental fracture systems does not encompass the essence of ESC, because neither of these approaches has been concerned with the influence of molecular properties of polymer in elucidating the fracture behaviour of polymer. Rather, in this conventional thinking the nature of environment and the action of environment to polymers have been considered as the controlling factors in the cracking or crazing. Although investigation of the effect of molecular properties on the fracture toughness could provide a fundamental approach to understanding of the fracture mechanism, few studies have been reported. The importance of molecular properties on the fracture behaviour is clearly revealed

by the results of Rudd (29). He investigated the effect of MW and MWD on time-to-fracture of polystyrene under a constant load in butanol. Decay of stress with time during craze growth showed a curve similar to stress relaxation curve with a longer stress plateau for higher MW polymer. The stress plateau may imply the role of entanglement network in stabilizing craze fibrils at the crack tip. In his review, Kramer (21) repeatedly referred to the importance of the chain entanglement in the fracture mechanism of polymers, but this proposal has not yet been confirmed because of limited experimental data.

2.2 Application of Linear Elastic Fracture Mechanics to the Analysis of Crack and Craze Growth in Polymers

The earliest theory of fracture mechanics was proposed by Griffith (30) who suggested that the energy required to commence crack propagation must be larger than the surface energy of the material. Following Griffith, Orowan (31) recognised that the energy required for crack growth is generally much larger than the surface energy and came to the conclusion that the region at the crack tip was not entirely elastic. Griffith's and Orowan's theoretical treatments were further developed by Irwin (32) who derived equations for the intensity of the stress field around a crack expressed by a stress intensity factor (SIF). Irwin's approach was based on the assumption of linear elasticity and infinitesimal strain and thus is referred as linear elastic fracture mechanics (LEFM).

The following sections will outline the basic concept of LEFM and in particular the application of this concept to the analysis of fracture data in polymers.

2.2.1 Linear Elastic Fracture Mechanics

2.2.1.1 Energy Release Rate, G

Considering a cracked body of thickness, B, exposed to load P (Fig.2.1) the body displaces a distance, Y, from it's unloaded position. The stored energy, U_1, in the body becomes (region OAD in Fig.2.2)

$$U_1 = \tfrac{1}{2}PY \tag{2.1}$$

An increase of load δP causes an increase in displacement of δY and crack will propagate from x_o to $(x_o + \delta x_o)$. The new stored energy, U_2, is given by (region OCB)

$$U_2 = \tfrac{1}{2}(P + \delta P)(Y + \delta Y) \tag{2.2}$$

which requires an external work, U_3, to be done on the body (region ABCD), that is

$$U_3 = \left(P + \frac{\delta P}{2}\right) \delta Y \tag{2.3}$$

Thus the energy δU is released when the crack grows a distance of δx_o is given by

$$\begin{aligned} \delta U &= U_2 - U_1 - U_3 \\ &= \tfrac{1}{2}(Y\delta P - P\delta Y) \end{aligned} \tag{2.4}$$

That corresponds to the region ODC in Fig.2.2. The energy release rate, G, defined as the energy released per unit area of crack growth is expressed by

$$G = -\frac{\delta U}{B\delta x_o} = -\frac{1}{B}\left(Y\frac{\delta P}{\delta x_o} - P\frac{\delta Y}{\delta x_o}\right) \tag{2.5}$$

To initiate fracture in a body, a minimum energy (a critical energy release rate), G_c, is required, that is

$$G \geq G_c \tag{2.6}$$

For the Griffith's criterion, G_c can be expressed by

$$G_c = 2\gamma_{cl} \tag{2.7}$$

Fig.2.1 The cracked body.

Fig.2.2 Relationship between the displacement distance, Y, and the required load, P.

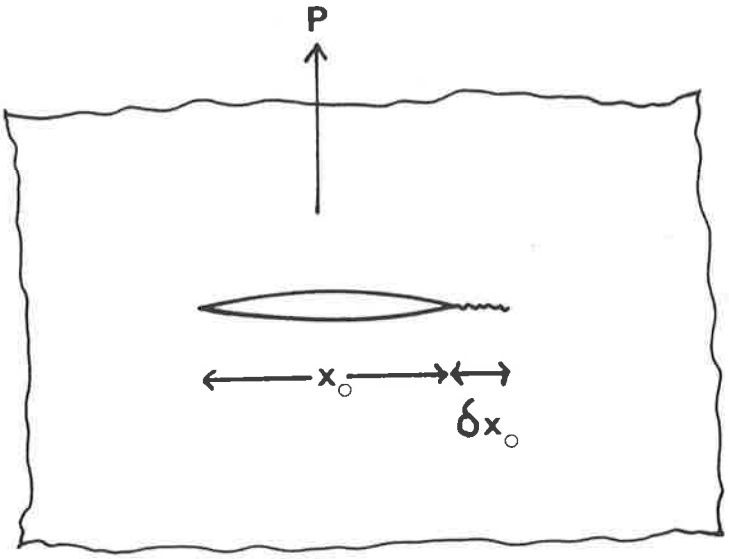
P
x_o
δx_o

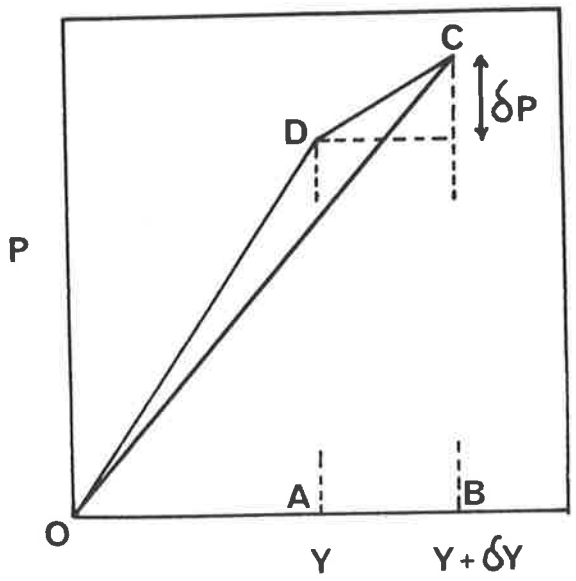
C
δP
D
P
A
B
O
Y
Y + δY

where γ_{cl} = surface energy of material

The fracture initia criterion can be written as

$$G_c = \frac{1}{2B}\left(-Y\frac{\delta P}{\delta x_o} + P\frac{\delta P}{\delta x_o}\right) \tag{2.8}$$

Let C be the compliance of the cracked body

$$C = Y/P \tag{2.9}$$

so that, in the case of fixed grips $Y = 0$, G_c becomes

$$G_c = \frac{P^2}{2B}\frac{dC}{dx_o} \tag{2.10}$$

and in the case of constant load $\delta P = 0$

$$G_c = \frac{Y^2}{2B}\frac{1}{C^2}\frac{dC}{dx_o} \tag{2.11}$$

The compliance,, C, is a function of specimen geometrical factors, if dC/dx_o is known, G_c will be determined from the above equations.

2.2.1.2 The Crack Tip Stress Field and Stress Intensity Factor

There are three modes of crack propagation under external load, Mode I: opening, Mode II: edge sliding or shearing and Mode III: tearing. Because the fracture process investigated in this work is Mode I propagation, the results are relevant to this mode only.

Using Westergaard's complex stress function, Irwin (32) demonstrated that the elastic stress field around the crack of $2x_o$ length in an infinite sheet for Mode I could be described by

$$\sigma_x = \sigma\sqrt{\frac{x_o}{2r}}\cos\frac{\theta}{2}\left(1 - \sin\theta\sin\frac{3\theta}{2}\right) \tag{2.12a}$$

$$\sigma_y = \sigma\sqrt{\frac{x_o}{2r}}\cos\frac{\theta}{2}\left(1 + \sin\frac{\theta}{2}\sin\frac{3\theta}{2}\right) \tag{2.12b}$$

$$\tau_{xy} = \sigma\sqrt{\frac{x_o}{2r}}\sin\frac{\theta}{2}\cos\frac{\theta}{2}\cos\frac{3\theta}{2} \tag{2.12c}$$

where σ is the applied bulk stress, r and θ is co-ordinate in polar dimension of an infestimal volume as shown in Fig.2.3.

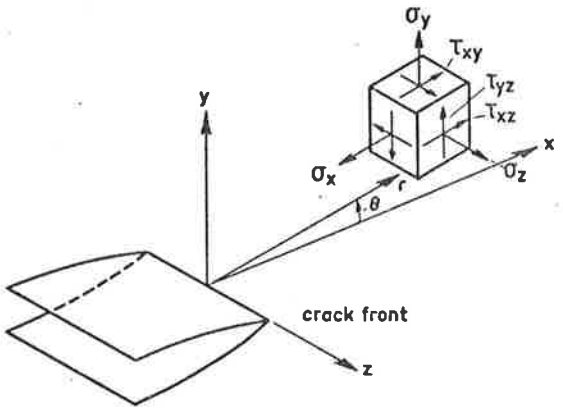

FIG.2.3: The crack tip stress field.

The stress intensity factor (SIF), K, for mode I in an infinite sheet is defined by

$$K = \sigma\sqrt{\pi x_o} \tag{2.13}$$

For finite bodies, equation (2.20) is given by

$$K = Y_c \sigma\sqrt{x_o} \tag{2.14}$$

where Y_c is geometrical correction factor and is a function of the dimension of the body.

In plane strain, the corresponding displacement in x and y direction are obtained as

$$u = \frac{2K\ (1+\mu)}{E}\sqrt{\frac{r}{2\pi}}\cos\frac{\theta}{2}\left(1 - 2\mu + \sin^2\frac{\theta}{2}\right) \tag{2.15}$$

$$v = \frac{2K\ (1+\mu)}{E}\sqrt{\frac{r}{2\pi}}\sin\frac{\theta}{2}\left(2 - 2\mu - \cos^2\frac{\theta}{2}\right) \tag{2.16}$$

The relationship between K and G can be found in the calculation of the energy change when crack propagates an increment of δx_o (34). It can be expressed as

$$G\,\delta x_o = \int_0^{\delta x_o} \sigma\, v\, dr \qquad (2.17)$$

so that in plane strain G becomes

$$G = \frac{K^2}{E}(1 - \mu^2) \qquad (2.18)$$

and in plane stress

$$G = \frac{K^2}{E} \qquad (2.19)$$

For PMMA μ = 0.33, difference between Eqs. 2.18 and 2.19 is about 10%.

Combining Eqs. 2.11 and 2.19 gives

$$K_c^2 = E\,G_c = \frac{EP^2}{2B}\frac{dC}{dx_o} \qquad (2.20)$$

where K_c is the SIF at fracture and corresponds to G_c.

2.2.1.3 Effect of the Plastic Zone. Modification of LEFM

The elastic stresses acting near the crack tip are extremely high and will reach the yield stress, σ_y, to form plastic zone ahead of sharp crack tip. Linear elasticity is no longer applied to the plastic zone. By using the concept of effective crack length, however, Irwin (34) calculated radius, r_y, of the plastic zone to be

$$r_y = \frac{K_c^2}{2\pi\sigma_y^2} \qquad r_y << x_o \qquad (2.21)$$

so that the effective crack length is now $2(x_o + r_y)$. The new elastic stress distribution is given by

$$\sigma_c = \sigma_y = \frac{K_c}{\sqrt{2\pi r_y}} \qquad (2.22)$$

where $K_c = \sigma\sqrt{\pi(x_o + r_y)}$.

This modification using the effective crack length, $2(x_o + r_y)$, enables the application of the LEFM into the inelastic region providing that the plastic zone is small in comparison with crack length, i.e. $r_y << x_o$ (Fig.2.4).

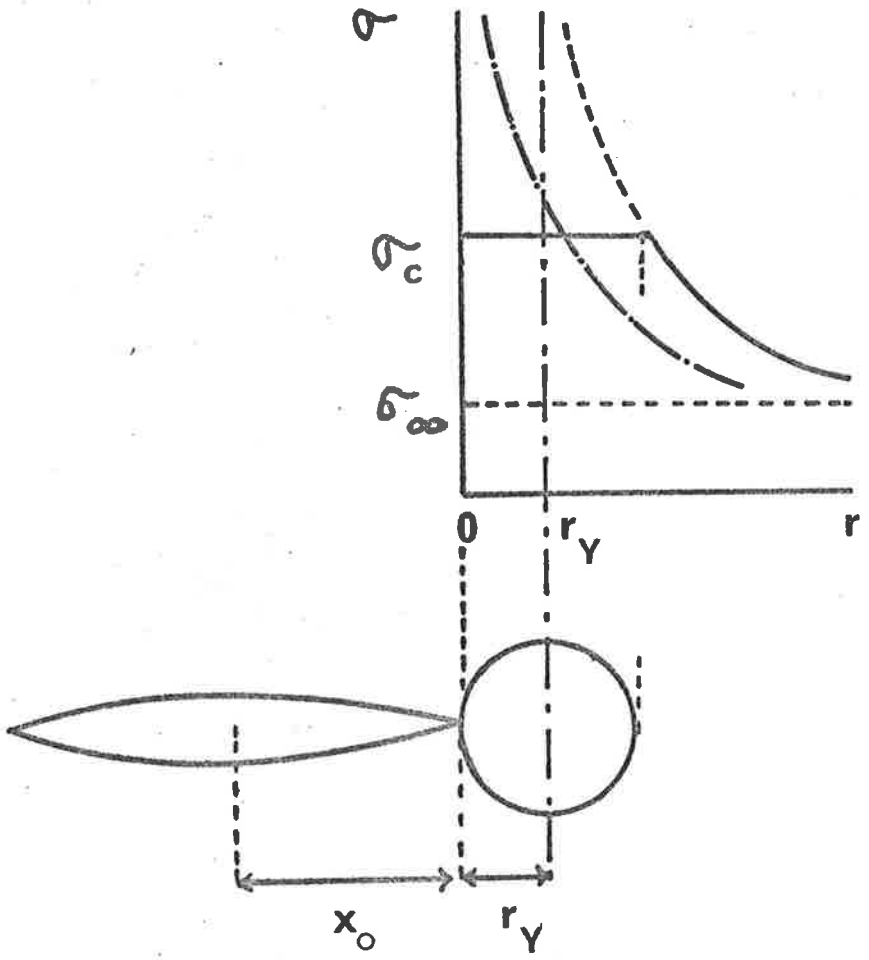

Fig.2.4 Increase in effective crack length due to the plastic zone at the tip.

Dugdale (35) used similar mathematical analysis to yield

$$\Delta = 2r_y = x_o \left[\sec \left(\frac{\pi}{2} \frac{\sigma}{\sigma_c} \right) - 1 \right] \tag{2.23}$$

where Δ is the craze length. The critical work done at the crack tip is given by

$$G_c = u_c \sigma_c \tag{2.24}$$

From Eqs. 2.20, 2.23 and 2.24, we obtain

$$\Delta = \frac{\pi}{8} \frac{K_c^2}{\sigma_c^2} \tag{2.25}$$

and

$$\frac{8}{\pi} x_o^2 \sigma_c \ln \sec \left(\frac{\pi}{2} \frac{\sigma}{\sigma_c} \right) = u_c \sigma_c E \tag{2.26}$$

The approximation of Eq.2.26 is given by

$$K_c^2 = u_c \sigma_c E = \frac{u_c \sigma_c^2}{\varepsilon_y} \tag{2.27}$$

where $E = \sigma_c / \varepsilon_y$ and ε_y is the yield strain.

Eq.2.27 is a good approximation for either $\Delta < x_o$ or $\Delta > x_o$, but Eq.2.27 is only true when $\Delta \ll x_o$ (17). Combining Eqs. 2.25 and 2.27 gives

$$\Delta = \frac{\pi}{8} \frac{K_c}{\varepsilon_y} \tag{2.28}$$

2.2.2 Application to Polymers

2.2.2.1 Description of Cracking and Crazing by the LEFM Concept

LEFM have been widely used in the theoretical analysis of fracture behaviour in metals for some time, but application of this concept to cracking and crazing in polymers was initiated by Marshall et al. (15-16) only ten years ago.

The log K_c vs. log v (or K_c vs. v) diagram is widely used to describe the fracture behaviour of brittle materials and the

most well-documented data of air cracking in polymers is that for PMMA (17,97). Williams (97) suggested that the general form of cracking behaviour for PMMA in terms of the SIF, K_c, and the crack velocity, v, can be represented by the graph in Fig.2.5. The description of the cracking behaviour in air can be divided into three regions: regions AB, BC and CD. In region AB ($0.73\ MNm^{-3/2} \lesssim K_c \lesssim 1.7\ MNm^{-3/2}$) crack propagation is stable, since an increase in K_c is required to accelerate the crack. Stable crack propagation occurring in region AB is the most common fracture process. When the crack velocity exceeds $10^{-2} m\ sec^{-1}$, K_c starts to drop (region BC) and Williams (97) attributed this behaviour to the onset of thermal effects arising from the plastic work performed at the crack tip. In region CD, the curve is assumed to rise again when the crack velocity approaches sonic speed. Conclusive data for this last region, however, has not yet been obtained.

The general breakdown process of polymers in the presence of an aggressive environment can be divided into two main categories: predominantly stress-crazing and predominantly stress-cracking. For the case of stress cracking, Williams (33) has suggested a model where complete plasticization at the tip leads to a drop in the load carrying capacity of the material, i.e. a decrease in the total crazing stress distribution at the tip. This situation can be viewed on the log K_c vs. log v schematic diagram of crack propagation in a cracking solvent (Fig.2.6). The diagram consists of three regions: Region I, Region II and Region III. Region I illustrates a drop in K_c from the corresponding K_c in air at a given crack velocity, v, due to plasticization at the tip. Region III shows a non-solvent crack growth (dry crack growth)

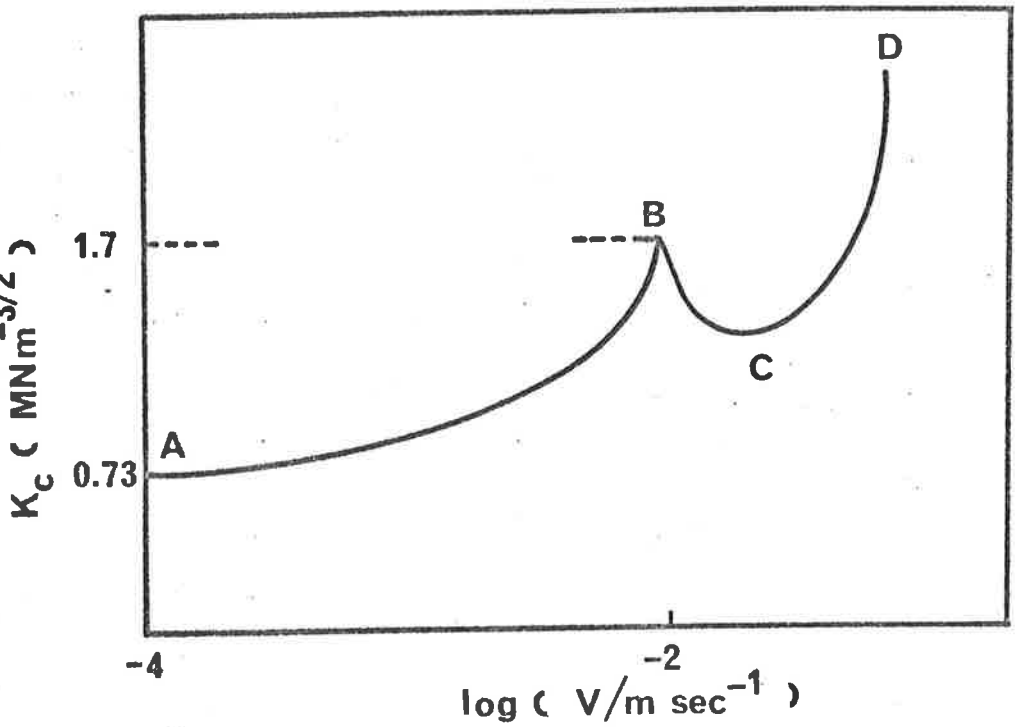

Fig.2.5 Schematic K_c vs. log v diagram of cracking behaviour in air for PMMA at room temperature.

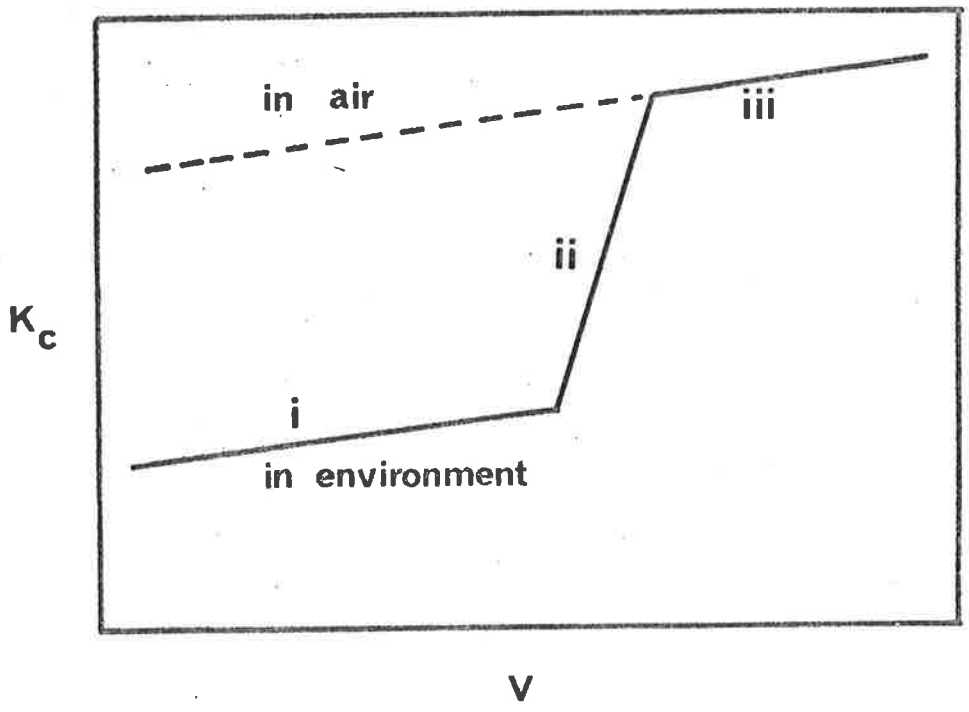

Fig.2.6 Schematic K_c vs. v diagram of environmental stress-cracking.

where the diffusion rate of the fluid is exceeded by the crack speed, so that the craze zone fails to be plasticized leaving the dry tip propagating in the same manner as cracking in air. Region II is the transition region where the crack velocity, v, is equal to the diffusion rate of the penetrant and K_c becomes sensitive to v (17,33).

The three distinct regions have been widely observed in the ESC of inorganic glasses (17,98) but only portion (Regions I and II) of this general behaviour has been reported for polymers (e.g. ESC of polyethylene in ethanol) (17). Fig.2.6 can currently only be regarded as a schematic diagram of the probable log K_c vs. log v relation for polymers.

The log K_c vs. log v relationship for solvent crazing in PMMA can be found in Marshall and Williams' work (17) and Mai's work (99), but the general behaviour of crazing in solvent expressed in the log K_c vs. log v diagram has not been reported.

2.2.2.2 Williams and Marshall's Theoretical Treatment of Crack and Craze Growth

On the basis of LMFM concept Williams and Marshall have proposed a comprehensive theory to describe the time-dependent crack and craze growth in both an inert and an active environment. The theory, which has been successfully applied to the analysis of experimental data for various amorphous polymers, was developed on a basic assumption that a time scale, τ, describing the process at the crack tip, can be defined as

$$\frac{1}{\tau} = \frac{v}{\Delta} + \frac{1}{t} \qquad (2.29)$$

where t = the total elapsed "macro" time from the onset of loading and, v = the crack velocity. For the crack growth, because sufficient time has elapsed for the crack growth to exceed a distance

of craze length, Δ, i.e. $l/t \simeq 0$, Eq.2.29 becomes

$$\frac{l}{\tau} = \frac{v}{\Delta} \tag{2.30}$$

For the craze growth, crack remains stationary or v = 0, therefore

$$\tau = t \tag{2.31}$$

Furthermore, due to viscoelastic behaviours of polymers Williams and Marshall assumed the time dependence of the crazing stress, σ_c, and the modulus E, to be of the form

$$\sigma_c = \sigma_o \tau^{-m} \tag{2.32}$$

$$E = E_o \tau^{-n} \tag{2.33}$$

Where σ_o and E_o = the unit time values, m and n = the time factors.

Fracture behaviours of polymers have been treated by the Williams-Marshall (WM) theory in four mechanisms

(a) Relaxation controlled crack growth

(b) Flow controlled crack growth

(c) Relaxation controlled craze growth

(d) Flow controlled craze growth.

Derivation of equations describing the above mechanisms in terms of the SIF and the crack (craze) velocity will be outlined in the following section.

(a) Relaxation Controlled Crack Growth

This mechanism can be found in crack growth in air or in organic solvent (Region I in Fig.2.6). Combining Eqs.2.25, 2.27, 2.30, 2.32 and 2.33 gives

$$\tau^{1-m+n} = \frac{\pi}{8} \frac{u_c E_o}{\sigma_o} \frac{l}{v} \tag{2.34}$$

and

$$v = \frac{\pi}{8} \frac{K_c^{2(1-m+n)/(m+n)}}{(u_c E_o)^{(1-2m)/(m+n)} \sigma_c^{(1+2n)(m+n)}} \tag{2.35}$$

In air, m and n were determined to be around 0.1 and the K_c vs. v relationship becomes

$$K_c \propto v^{0.1}$$

The power term of 0.1 is in good agreement with the experimental data of cracking (0.08 to 0.1)

(b) Flow Controlled Crack Growth

The flow controlled crack growth is presumed to correspond with Region II (Fig.2.6) where the crack velocity, v, is equal to the flow velocity. Williams and Marshall suggested that in the flow controlled cracking the fluid flows into the dry craze zone at the front tip, and therefore, d'Arcy's law for flow in a porous system can be used, that is

$$v = \frac{A}{12\eta}\left(\frac{dP}{dx}\right) \tag{2.36}$$

where A = the pore area, dP/dx = pressure gradient along the craze and η = the fluid viscosity.

Although Williams and Marshall have shown that crack propagation of high density polyethylene in a detergent environment obeys d'Arcy's law, theoretical confirmation of Region II mechanism still awaits a well-established K_c vs. v relationship for environmental crack growth behaviour as shown by a schematic diagram in Fig.2.6, especially the connection between Region II and Region III.

(c) Relaxation Controlled Craze Growth

Using the Dugdale's model of uniform crazing stress distribution (35), the average crazing stress from time 0 to time t can be approximated by

$$\bar{\sigma}_c = \frac{1}{t}\int_0^t \sigma_c \, dt \tag{2.37}$$

Combining Eqs.2.31, 2.32 and 2.37 gives

$$\bar{\sigma}_c = \frac{\sigma_o \, t^{-m}}{1-m} \tag{2.38}$$

The craze length developing with time is expressed by

$$\Delta = \frac{\pi}{8}\frac{K_c^2}{\bar{\sigma}_c^2} = \frac{\pi}{8}\frac{K_c^2}{\sigma_o^2}(1-m)^2 t^{2m} \qquad (2.39)$$

Differentiating Eq.2.39 so that the craze velocity is given by

$$v(\text{craze}) = 2m(1-m)^2 \frac{\pi}{8}\frac{K_c^2}{\sigma_o^2} t^{2m-1} \qquad (2.40)$$

(d) Flow Controlled Craze Growth

The craze growth at shorter times (initiation step) is governed by this mechanism. The pore area, A, can be expressed by

$$A = c\, u_c \qquad (2.41)$$

where c = the material constant depending on void content. Using Eq.2.27, Eq.2.41 can be written as

$$A = c\frac{K_c}{E\sigma_c} \qquad (2.42)$$

Substituting d'Arcy's formulation (Eq.2.36) gives

$$v(\text{craze}) = \frac{c}{12\eta}\frac{K_c^2}{\sigma_o E_o}(1-m)\, t^{m+n}\left(\frac{dP}{dx}\right) \qquad (2.43)$$

If the pressure drops linearly from the craze base to the craze tip dP/dx can be expressed by

$$\frac{dP}{dx} = \frac{P}{\Delta}$$

$$v(\text{craze}) = \frac{P}{\Delta}\frac{c}{12\eta}\frac{K_c^2}{\sigma_o E_o}(1-m)\, t^{m+n} \qquad (2.44)$$

If $M = n \simeq 0$, Eq.2.44 can be rewritten as

$$v(\text{craze}) = \frac{P}{\Delta}\frac{c}{12\eta}\frac{K_c^2}{\sigma_o E_o} \qquad (2.45)$$

CHAPTER 3

POLYMERIZATION AND POLYMER CHARACTERIZATION

3.1 Introduction

Discovery of anionic vinyl polymerization can be dated back as far as in the 1940's. In his discussion of anionic polymerization of cyclic acids and acidanhydrides, Flory clearly foreshadowed the possibility of a controlled synthesis (36), but it was not until Szwarc's discovery of "living" anionic systems several years later (37) that the anionic polymerization was realised as an ideal method to produce polymers with a certain specific desired MW or molecular structure. Using the "living" polymer, it was possible to synthesize not only two-phase block polymers or graft polymers, but also polymers of predetermined MW, MWD and configuration. With the technique of anionic polymerization, suitable reaction conditions can yield very narrow MWD or stereoregular polymers (38). Considerable work on preparing narrow MWD PMMA, polystyrene and poly (α-methystyrene) by an electron transfer reaction of alkali metal complexes in an ether under high vacuum has been reported (39-42).

The "living" polymer concept, however, does not necessarily represent anionic polymerization. Polymerization of methyl methacrylate initiated by alkyl magnesium compounds in tetrahydrofuran (THF)/toluene mixture is based on a "living" polymer concept but is in fact pseudo-anionic polymerization (43). According to recent development in our laboratory (44), the conditions of the pseudo-anionic polymerization which control the MW and MWD have not been defined yet, but the stereoregularity of a polymer chain is known to be dependent on three variables: temperature; ratio of concentration of solvent mixture (tetrahydrofuran/toluene) used as the reaction media and ratio of concentrations of solvent mixture and monomer.

The main object, however, was not a detailed analysis of reaction mechanism, but to scale up the reaction to produce a quantity of 10 to 20g of polymer for bulk properties testing. Polymerizations of narrow MWD with different MW polymers were carried out with sodium biphenyl as initiator. Polymers of controlled stereoregularity (74%, 100% isotacticity and 73% syndiotacticity) were synthesized with t-butyl or phenyl magnesium compounds as initiator. Details of polymerization technique will be described in next section.

3.2 Polymerization Technique

3.2.1. High Vacuum System

Initiator complexes for the polymerization are quite sensitive to traces of air or water and therefore it is necessary to use high vacuum apparatus to remove all impurities. The all-glass system consists of a rotary oil pump and the mercury diffusion pump to reduce the pressure to 10^{-4} mm Hg. Liquid nitrogen traps are located between the oil pump, the diffusion pump and the glass manifolds. The traps are used to condense any solvent gases during vacuum drying, also to prevent the mercury in the diffusion pump from entering the manifolds. The separable manifolds are designed to suit the requirements of each reaction.

All glass assemblies for polymerization are attached to the manifolds by Viton ring greaseless taps or ground glass taps lubricated by high vacuum silicone grease.

The high vacuum systems was mainly used for drying of glassware, degassing, transferring liquids by distillation and preparation of sodium mirrors.

3.2.2. Purification of Reagents

Tetrohydrofuran (THF) (BDH,AR grade reagent stabilized with 0.1% quinol).

THF was prepared by refluxing over calcium hydride and lithium aluminium hydride for 24 hours before transferring to a flask containing

sodium benzophenone. THF was refluxed again for another 24 hours with sodium benzophenone to give a fresh blue colour of the complex. In presence of excess sodium benzophenone, the colour changed to the purple radical di-anion. The THF was collected and thoroughly degassed before distilling under high vacuum onto sodium mirrors and benzophenone for storage.

Sodium mirrors, which act as a drying agent for THF and the initiator solution, were prepared by the following method. Pieces of dry sodium metal were placed in one finger and benzophenone in another finger of a flask (Fig. 3.1). The stopcock between the flask and the vacuum system was opened to reduce the pressure and vaporize impurities (e.g., carbon dioxide, water, etc.) adhering to the wall of the flask. The sodium was then heated under vacuum with the soft yellow flame of a hand torch until it melted. The sodium vapor spread quickly and condensed on the cool wall of the flask to form a mirror, and benzophenone was subsequently vaporized by heating. When the THF was distilled in the blue colour of the sodium benzophenone - THF complex appeared instantaneously.

Toluene (BDH, AR grade)

The same purifying procedure was undertaken for toluene.

Methyl methacrylate (MMA) (BDH, AR grade stabilized with 0.1% quinol).

MMA was washed with 10% (W/V) caustic soda solution to remove quinol and subsequently washed with water until neutral to litmus. The MMA was then dried with anhydrous magnesium sulphate and transferred onto fresh calcium hydride. It was stored in a freezer for at least 24 hours to allow the complete evolution of hydrogen gas. This sample was further purified by distilling under vacuum onto a sodium mirror and benzil (1,2 - diphenyl - 1,2 - ethandione). This complex gave a purple colour in MMA. Because sodium benzil is a weak initiator for MMA, long contact must be avoided. A suitable contact time enough to destroy impurities in MMA without any undesired polymerization would

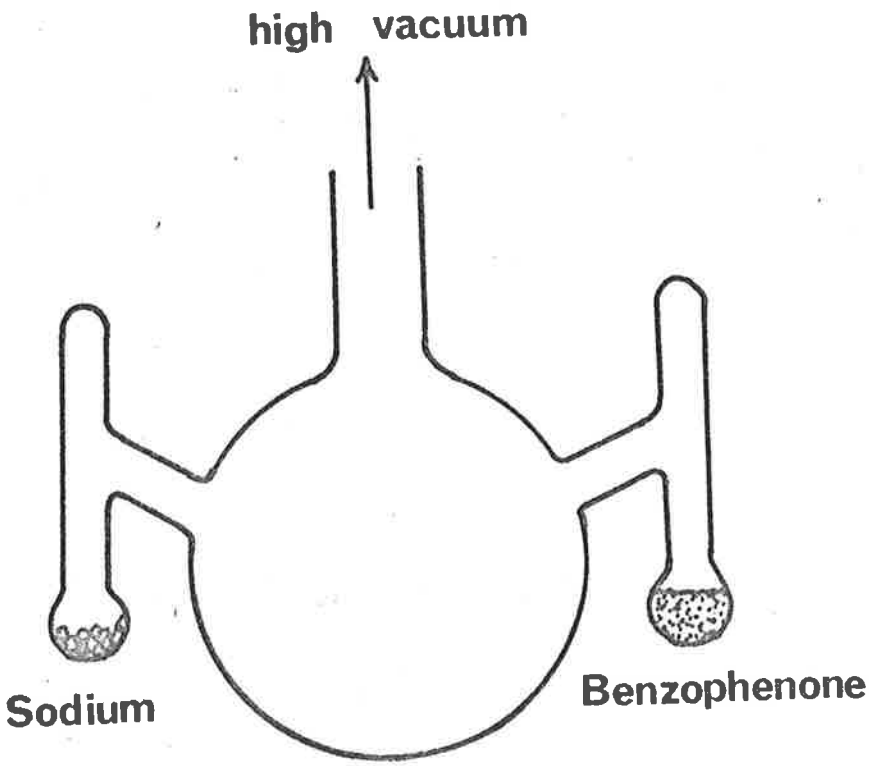

Fig.3.1 Apparatus for preparation of sodium benzophenone.

be about 30 minutes. The MMA was then distilled into an impurity-free flask and stored in a freezer.

Alkyl Halides (Fluka AG)

Phenyl bromide and t-butyl bromide used for the preparation of Grignard reagents were refluxed over calcium hydride.

3.2.3 Preparation of Initiator Solutions

Sodium Biphenyl Initiator

Sodium biphenyl complex was used as initiator and purifying reagent for THF before polymerization. Details of preparation will be described in Section 3.2.4.

Grignard Reagents (45)

(a) Tert-butylmagnesium Bromide

Grignard reagents were prepared in the apparatus shown in Fig. 3.2. A flat bottomed flask A was charged with oven dried magnesium turnings (7.0g) and flame dried while being purged with dry nitrogen. When the flask had cooled, it was charged with freshly distilled THF (200ml). A solution of dry t-butylbromide (27.4g) in dry THF (80ml) was introduced into the reaction vessel through the dropping funnel B while the reaction mixture was stirred vigorously.

After the addition of 10ml of t-butylbromide solution, the reaction mixture was heated by hot air to initiate the Grignard reaction. Because the reaction was highly exothermic, the remainder of the t-butyl-bromide solution was added dropwise to maintain the reaction at reflux temperature. When the addition of the t-butylbromide solution was completed, the reaction mixture was heated under reflux for a further hour and then cooled to room temperature before filtering through glass sinter funnel. If the solution was filtered when it was still hot, the filtrate would contain a large amount of magnesium bromide which would effect the initiation conditions and leads to low molecular weight polymers (46).

The filtrate was degassed prior to its use in polymerization.

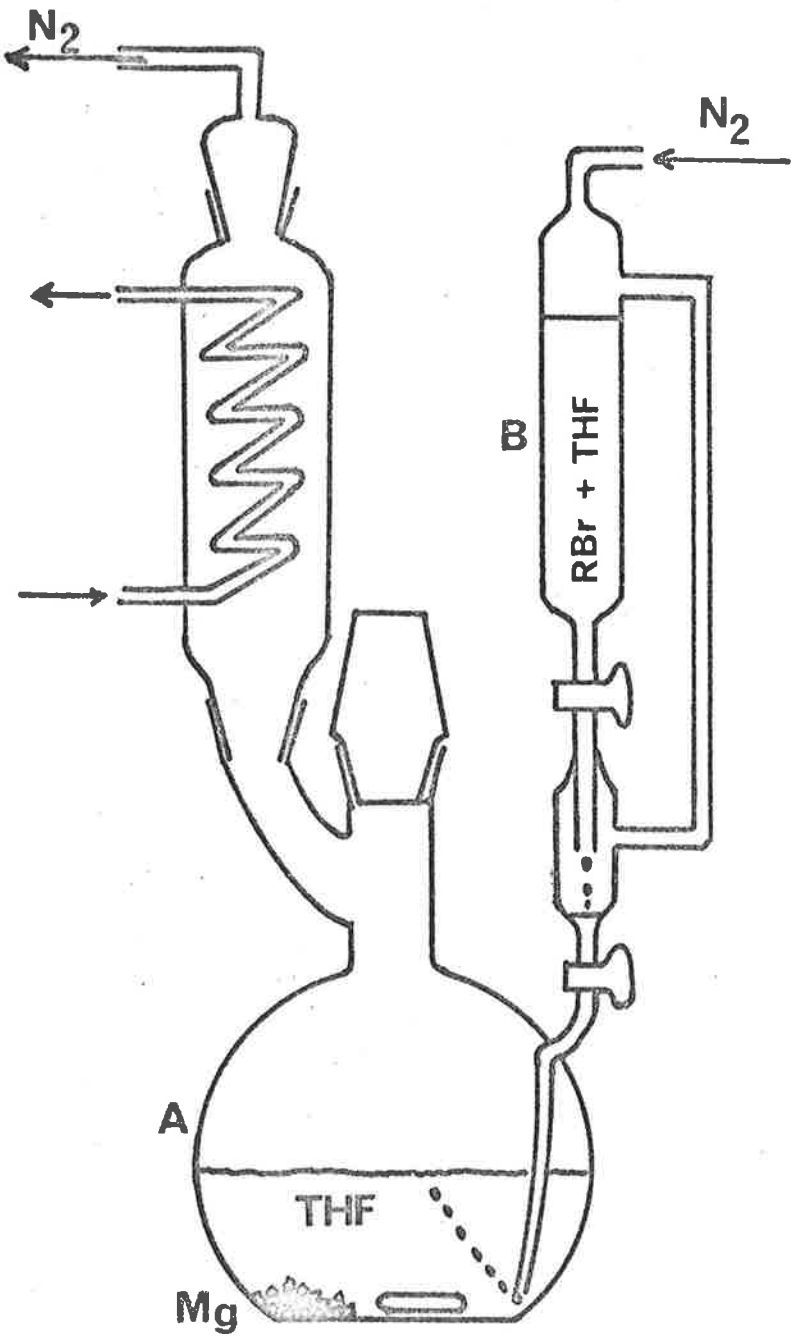

Fig.3.2 Apparatus for preparation of Grignard reagents.

(b) Diphenylmagnesium

There were two steps in preparation of diphenylmagnesium. In the first step, the preparation of phenylmagnesium bromide was carried out similarly to the preparation of t-butylmagnesium bomide but with the following quantities: magnesium 7.4g, bromobenzene 38.4g and a total of THF volume of 240ml. In the second step, 250ml of about 1M of phenylmagnesium bromide in THF was added to 2.2 equivalents (26.4g) of 1,4 - dioxan. The solution was then allowed to stand for 48 hours with periodic shaking before filtering under vacuum to remove the precipitate of $MgBr_2$.2 dioxan. The filtrate was found to contain (Ph_2Mg) = 0.045M (determined as (Ph^-) = 0.09M and (Br^-) = 0.01M).

(c) Determination of Organo - magnesium and Bromide Groups Concentration (45)

The concentration of Br^- in the initiator solutions was determined by Volhard's method.

The concentration of organo-magnesium group was estimated as the concentration of base in the solutions. Hydrochloric acid (0.1M) was added to a measured quantity of initiator solution in 10ml aliquots until the solution was acidic to methyl orange. This solution was then titrated with 0.1M soldium hydroxide solution to neutralize the excess acid. Then the number of moles of H^+ required to destroy R-Mg groups present in solution could be calculated.

3.2.4. Polymerization Procedure

Anionic Polymerization

This method was used to produce narrow MWD and controlled mean MW polymers.

Prior to the addition of solvent to the apparatus (Fig. 3.3) was carefully degassed by heating with the yellow flame of a hand torch under vacuum. The purified MMA (~20ml) was further purified twice with sodium benzil in a separate purification flask before being distilled into the calibrated monomer ampoule E. This ampoule was then isolated from the

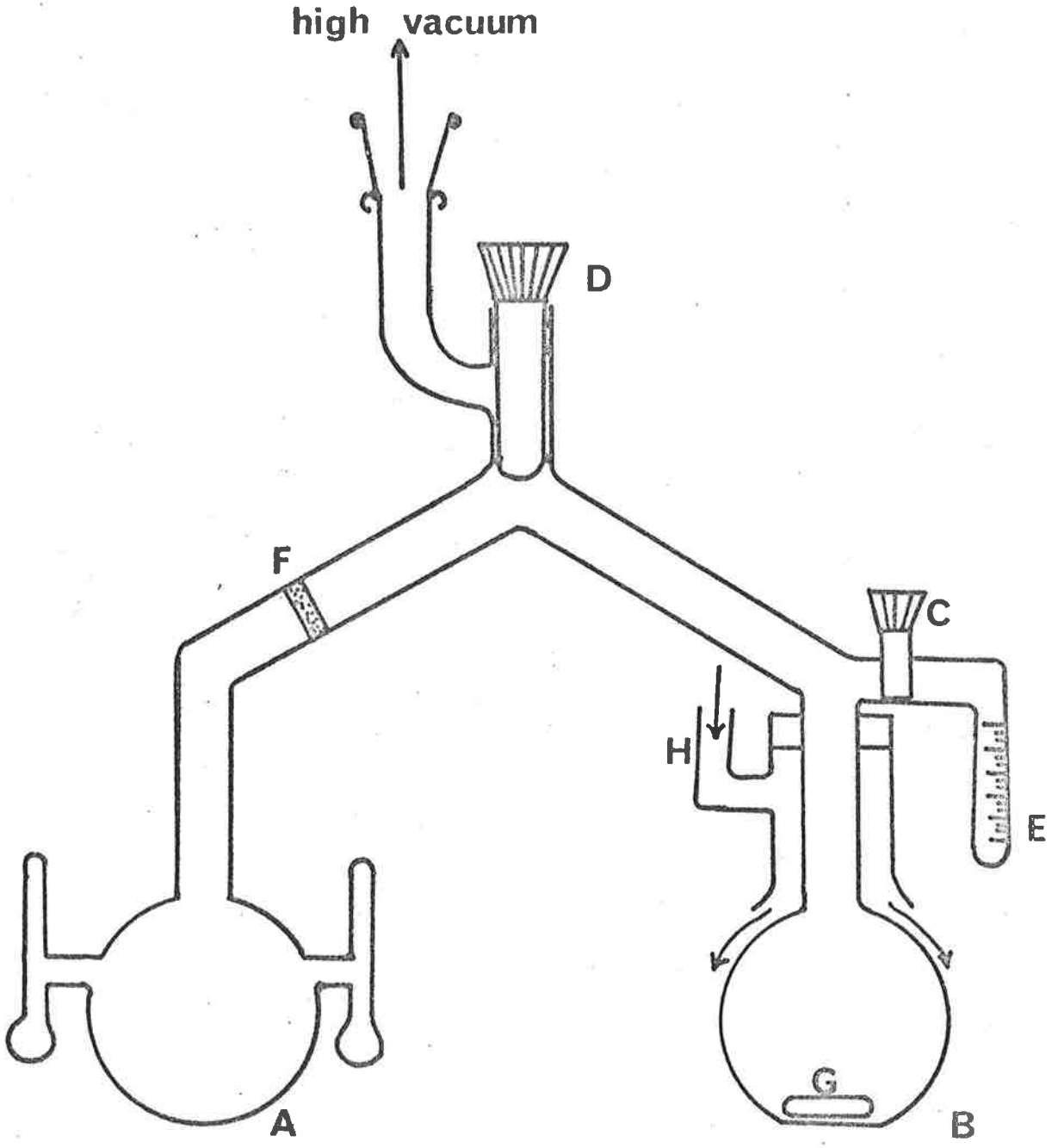

Fig.3.3 Apparatus for anionic polymerization.

rest of vessel by closing the valve C and frozen in liquid nitrogen prior to polymerization.

In second step, sodium biphenyl was prepared in initiator solution vessel A in a similar way with sodium benzopheonone (Section 3.2.2). The purified THF (500ml) was then distilled into vessel A (1000ml capacity), and on contact with sodium biphenyl, the initiator blue colour developed immediately. This solution was degassed twice before the whole apparatus was isolated from the vacuum system by closing the valve D.

MW of the product was controlled by concentration of the initiator ($MW = [monomer]/\frac{1}{2}[initiator]$) = a value adjusted by experience to give the desired MW. The adjustment of the initiator concentration was carried out by distilling the fresh THF from vessel A to vessel B, then the remaining complex solution was filtered from A to B to a desired concentration. The concentration of the initiator solution was judged by the darkness of the solution colour. When the adjustment of the concentration had been completed, the contents of vessel B was introduced into a methanol kept at $-78^{\circ}C$. By opening the valve C, the monomer vaporized into the sodium biphenyl/THF solution. To avoid the condensation of the monomer vapor on the wall, the connecting passage was kept warm by a hot air heated jacket H. On vaporization of the monomer, the initiator blue colour disappeared instantaneously, indicating a rapid initiation step. The solution was stirred vigorously by a magnetic stirrer. The polymerization was completed in approximately 30 minutes and the "living" polymers were terminated by the introduction of degassed butylchloride.

The polymer solution was poured into an excess of methanol/water mixture (1:1 V/V) to precipitate the PMMA. After filtering and washing, the polymer was dried in a vacuum oven at $60^{\circ}C$. The yield was larger than 90%.

The above polymerization procedure produced 10 to 20g of required MW PMMA. However, because of the larger size of the polymerization apparatus, the amount of THF was reduced to make the apparatus less bulky at the expense of a broader MWD (see Section 3.4).

Pseudo-anionic Polymerization

The polymerization procedure developed by Fisher and Mair (46) was adopted to scale up the amount of products. This procedure, however, involved some difficulties such as the irreproducibility and the sensitivity to the minor variation in experimental technique and in the preparation of initiator solution. The polymerization sometimes gave a very low yield of low MW polymers in contrast to the products of Fisher and Mair. The main reason is that the type of active centres for polymerization, which are created at the initiation step, is effected by the experimental conditions and/or the initiator preparation. The irreproducibilities in this step subsequently result in the different nature of product (44). This problem is still under investigation in our laboratory.

The following polymerizations were carried out to prepare highly syndiotactic and isotactic PMMA.

(a) Polymerization of S.73h(73% syndiotacticity)

The most important experimental parameters controlling the tacticity of PMMA are temperature and mole fractions of monomer, solvents and Grignard initiator. In this case, the mole ratios were χ (MMA/THF)=0.08 and χ (Initiator/MMA)=0.04. The polymerization apparatus (Fig. 3.4) consisted of two round-bottom flasks of 100ml (C) and 250ml (D). The purified THF was first allowed to flow into D from a burette attached to the vacuum manifolds. The predetermined volume of a solution of diphenyl magnesium (Ph_2Mg) was dispensed by a calibrated tilt meter mixed with more THF in flask D. The flask D was isolated from the flask C by closing valve B, and the known amount of monomer was then introduced into C from another burette attached to the manifolds. Finally, the whole reaction apparatus

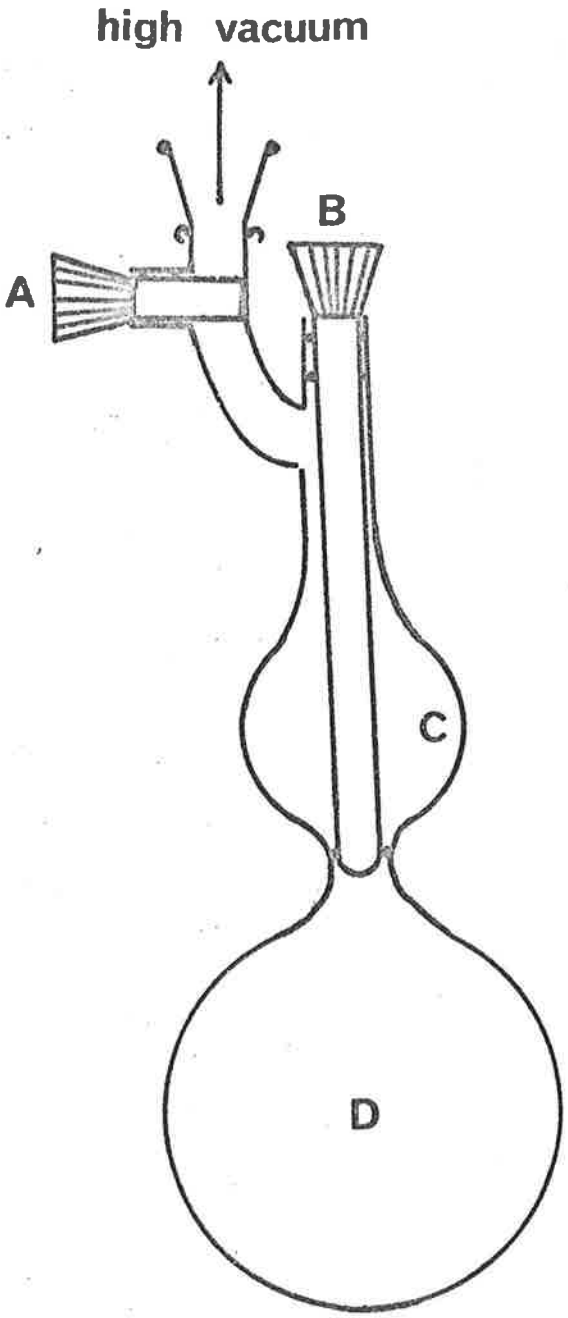

Fig.3.4 Apparatus for pseudo-anionic polymerization.

was separated from the vacuum system and kept under high vacuum by closing valve A. The apparatus was transferred to a methanol bath (T = -23°C). When the temperature of the solvent was in equilibrium with the bath (after 15 minutes), valve B was opened and polymerization commenced by mixing the monomer with THF/initiator. The apparatus was kept in the bath at constant temperature (T = -23°C) in 16 hours to complete the polymerization. Degassed methanol was used to terminate the reaction and the product was precipitated in an excess of methanol. The yield was 50%.

(b) Polymerization of I.74 (74% isotacticity)

The Grignard compound of t-butylmagnesium bromide was used as initiator. Initiator solution (0.1M in THF) of original weight 10.1g was fed into flask D and then vaporized all THF to reduce to the dryness of 0.2g. This procedure is described as "ether-free" or "de-etherated" of the initiator solution. According to Allen et al.(44), the "de-etherated" initiators have been shown from the NMR spectra to retain co-ordinated THF in mole rations (THF)/(t-BuMg)≥1. The monomer (12.1g) was polymerized without supporting solvents on the dry initiator at -40°C for 3 hours. The yield was 62%.

(c) Polymerization of I.100 (100% isotacticity)

Prior to polymerization, the Grignard compound of t-butyl-magnesium bromide was de-etherated to dryness and heated gently under high vacuum, then re-dissolved in toluene to give a desired concentration. This solution was used to initiate the I.100 series. The extent of heating and pumping determines the amount of THF in excess of that co-ordinated in the [THF]/[t-BuMg]=1 mole ratio. The most efficient initiation of isotactic polymerization occurs when [THF]/[t-BuMg] is slightly in excess of the ratio (46). From experience, under these conditions the solid initiator shows a grey colour. Furthermore, it was known that the concentration ratio of the co-ordinating THF and toluene as checked by gas chromatography would effect the MW of product. A detailed analysis of this effect is still under investigation.

The initiator solution was added with more toluene in chamber D (Fig. 3.4). Monomer was stored in chamber C before mixing with the initiator/toluene mixture in D to commence polymerization. The reaction conditions for different I.100 are listed in Table 3.1.

TABLE 3.1 Polymerization Conditions for I.100 Series

Sample	MMA (g)	Toluene (g)	Initiator (g)	$\frac{[MMA]}{[Toluene]}$	$\frac{[Initiator]}{[MMA]}$	Time (h)	T (^{o}C)	Yield (%)
I.100(1)	15.7	73.9	0.140	0.177	6.69×10^{-3}	4	-23	20
I.100(2)	10.0	74.5	0.140	0.110	12.6×10^{-3}	10	-23	35
I.100(3)	8.4	48.8	0.140	0.136	13.5×10^{-3}	10	-23	53

The products show mono-, bi- and trimodal on gel pemeation chromatograms, but at this stage it is still unknown what factors effect the MW and MWD of these polymers.

3.3 Characterization of Polymers

3.3.1. Molecular Weight and Molecular Weight Distribution

Gel permeation chromatograph (GPC) is an effective technique which allows a rapid determination of the MW and the MWD of polymers. Since its introduction (47), it has been widely accepted as a simple and reproducible method of polymer characterization. The GPC gives directly a MWD cure from which ratio of weight-average MW, M_n, and number-average MW, M_w, expressing the MW dipersity can be calculated.

The generalized treatment of the GPC may be attributed to Tung et al.(48). However, their phenomenological theory including a broad and multimodal MWD, is too complicated for application into simpler cases. Many attempts of calibration of the GPC from narrow MWD and known MW "standard" polymer have been made to develop a "universal" calibration curve for all polymer. The most common methods were suggested by Grubisic et al. (49) and by Dawkins (50). Grubisic et al. suggested that plot of log $((\eta)M)$ vs. V_e, where (η) is viscosity, M is molecular weight and V_e

is evolution volume, is universal for a narrow MWD as well as for a broad MWD (49). Dawkins proposed a simpler calibration method by using the unperturbed end-to-end distance $\langle \bar{r}_o^2 \rangle^{\frac{1}{2}}$ related with MW by a constant (50).

A plot of log M vs. V_e for narrow MWD (M_w/M_n = 1.10 to 1.06) polystyrene using Dawkins' method is shown in Fig.3.5. The plot is used as a calibration curve for PMMA samples.

TABLE 3.2: Calibration curve for GPC analysis.

Machine	:	GPC (Waters Associates)
Samples	:	Polystyrene (Water Associates)
Temperature	:	30°C
Solvent	:	Dichloromethane
Solution concentration	:	0.2 ~ 0.5%
Columns	:	μ-Stygel 10^5nm, 10^4nm, 10^3nm, 10^2nm

M_p*	log M_p	V_e**
2,700,000	6.43	81.25
451,000	5.65	87.75
200,000	5.30	92.00
110,000	5.04	98.50
35,000	4.54	104.25
17,500	4.24	112.25
8,500	3.93	118.00
3,600	3.56	124.00
2,900	3.46	125.00

* M_p = molecular weight at the GPC peak

** V_e = evolution volume in evolution count.

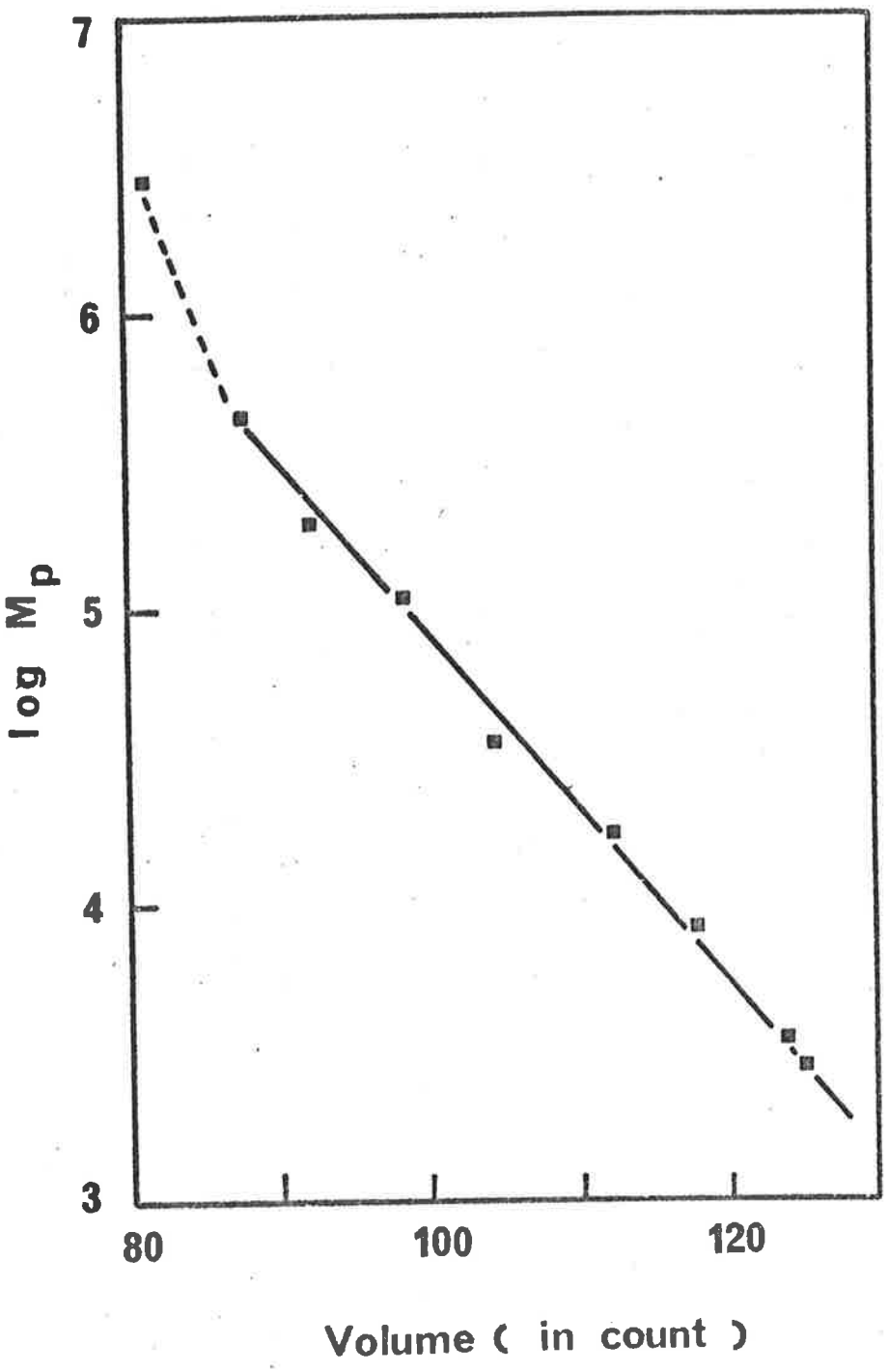

Fig.3.5 Calibration curve for GPC analysis.

Samples of synthesized or commercial PMMA were run with the same conditions as the standard polystyrene samples. The ratio of M_w/M_n and M_w are obtained from the following relations (51)

$$M_w = M_p \exp\left(\frac{1}{2}\sigma_D^2\right) \tag{3.1}$$

$$M_w/M_n = \exp \sigma_D^2 \tag{3.2}$$

where σ_D is the standard deviation in normal distribution and M_p is the MW at the peak of GPC curve (the geometric mean MW).

Another simple method has been proposed by Bly (54) for monomodal distribution to evaluate the ration $M_w/M_n = d$ which obeys the relation

$$\frac{w_o}{d_o} = \frac{w}{d} \tag{3.3}$$

where w_o is the width of the base line cut by two tangents to the point of inflection of the bell shaped distribution, d_o is the known ratio M_w/M_n of a standard sample. Thus w can be calculated if d is known from the GPC. By combination Eqs. 3.1 - 3.3, M_w/M_n, M_w and M_n can be obtained. This method of calculation of these parameters is simple and accurate for monomodal polymers. The combining method Eqs. 3.1 - 3.33 also shows an improvement over a tedious calculation of conventional way given by

$$M_n = \frac{\Sigma_i h_i}{\Sigma_i h_i/M_i} \tag{3.4}$$

$$M_w = \frac{\Sigma_i h_i M_i}{\Sigma_i h_i} \tag{3.5}$$

where h_i is the height in the chromatogram of i component and M_i is the corresponding MW obtained from calibration curve. The results of two methods are shown in Table 3.3.

TABLE 3.3

Sample	Conventional Method (Eqs. 3.4-3.3)			Combining Method (Eqs. 3.1-3.3)		
	M_w	M_n	M_w/M_n	M_w	M_n	M_w/M_n
MH*	156,000	92,000	1.70	136,400	70,300	1.94
MG*	113,000	59,000	1.91	90,000	46,300	1.94

*Commercial Samples

The results obtained from the two methods shows a reasonable agreement. However, using the calibration curve of standard narrow MWD polystyrene samples, neither of these methods is totally credible because the properties of polymer solution are dependent on the characteristics of polymer, especially the chain configuration. These methods are well established for atactic PMMA, but they are not known to any degree of confidence, "universal" calibration cannot be applied to any polymer solution of different stereoregularity. It was therefore essential to check M_w values by viscometry, particularly in the case of highly tacticity PMMA.

The following results for MWD, M_w and M_n were obtained from the combining method (Eqs. 3.1-3.2) and listed in Table 3.4. Because of the broad MWD or multimodality, the MW of pseudo-anionic PMMA were obtained by comparing with GPC of polystyrene standard samples. The gel permeation chromatograms for anionic and pseudo-anionic polymerized samples are shown in Fig. 3.6.

TABLE 3.4 Molecular Weight and Molecular Weight Distribution

(1) Anionic Polymerization*

Sample	M_w	M_w/M_n
A1	550,000	1.25
A1a	450,000	1.20
A2	500,000	1.25
A3	380,000	1.20
A4	150,000	1.20
A4a	120,000	1.20
A5	97,000	1.20
A6	84,000	1.20
A7	71,000	1.20
A8	36,000	1.20
A9	31,000	1.25
A10	23,500	1.25

(2) Commercial*

Sample	M_w	M_w/M_n
MH (Diakon)	149,000	1.90
MG (Diakon)	75,000	1.90
HMW (Polyscience)	787,000	2.10
MMW (Polyscience)	220,000	2.10
LMW (Polyscience)	160,000	2.10

(3) Pseudoanionic Polymerization

Sample	MW at peak (M_p)			MWD	Ratio of Area
	Peak 1	Peak 2	Peak 3		
S.73h	2,700,000	200,000	-	bimodal	1:1
S.73l	-	-	30,000	monomodal	-
I.74	2,000,000	110,000	35,000	trimodal	1.0:1.4:1.8
I.100(1)	3,500,000	400,000	100,000	trimodal	1.0:2.2:1.6
I.100(2)	-	-	35,000	broad monomodal	-
I.100(3)	2,700,000	400,000	-	bimodal	1:2

*Calculated by the combining method

Fig.3.6 Gel permeation chromatograms of synthesized PMMA. I.74 (Curve 1), I.100 (1) (Curve 2), I.100 (2) (Curve 3), I.100 (3) (Curve 4), S.73h (Curve 5) and narrow MWD sample (Curve 6).

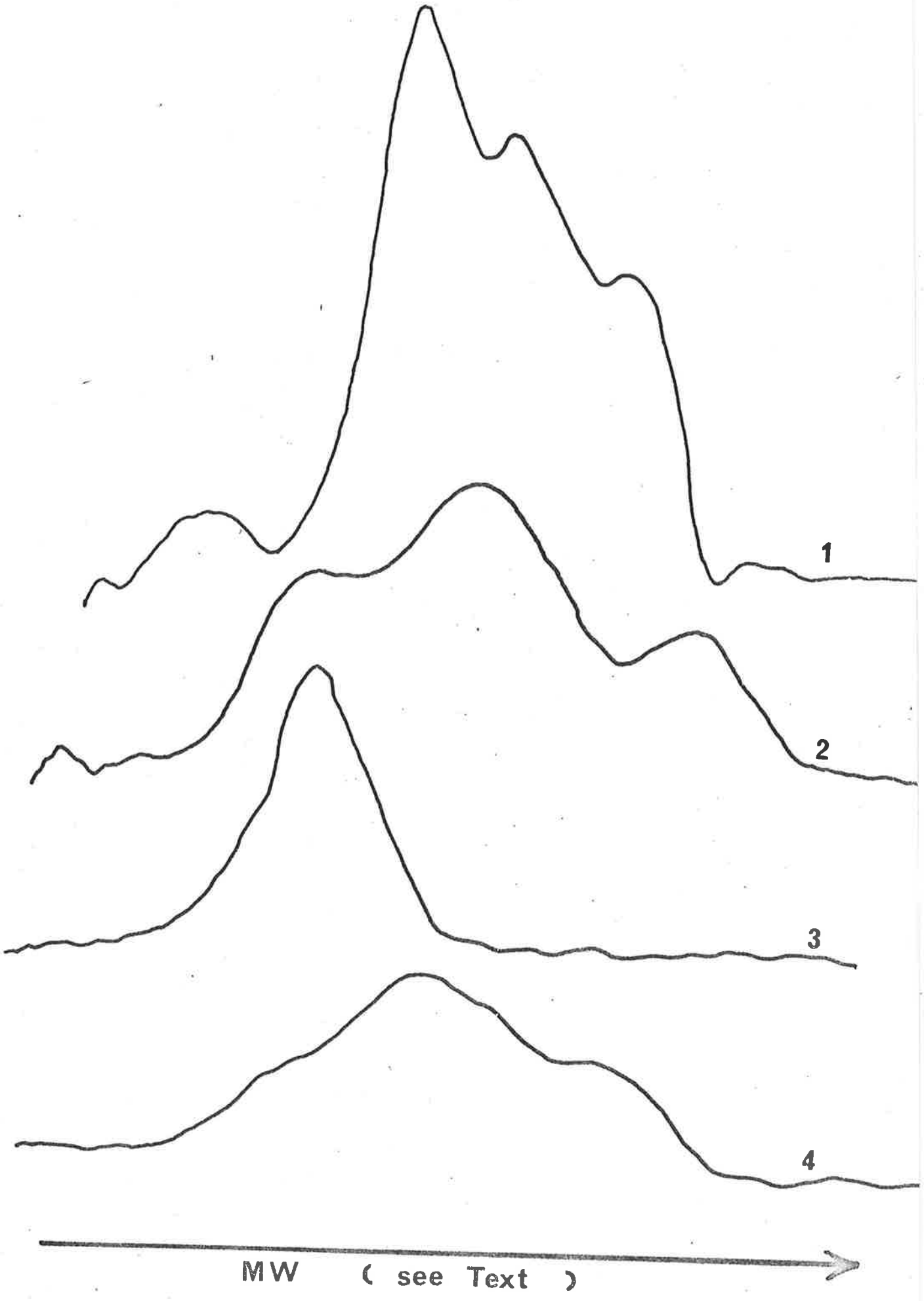
1
2
3
4
MW (see Text)

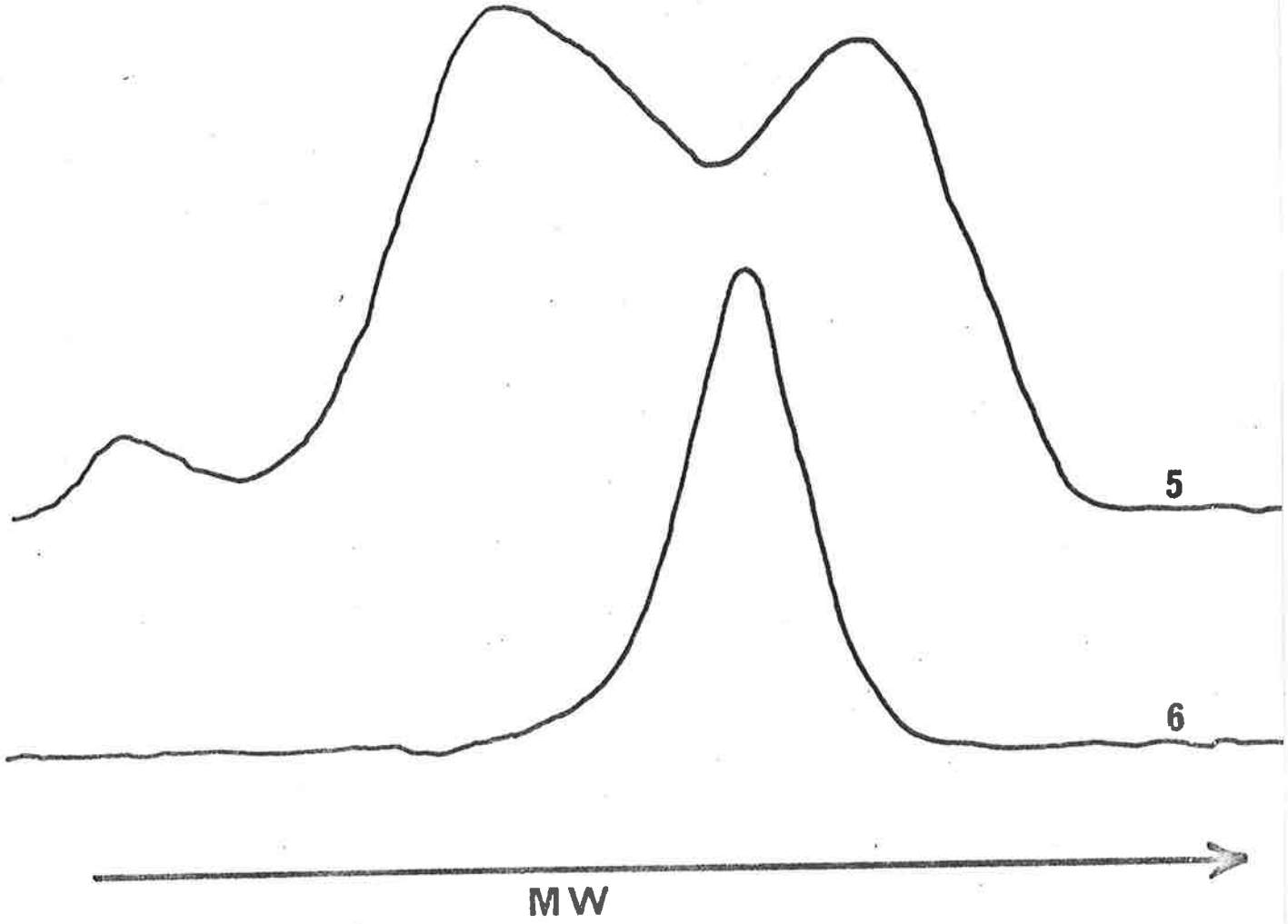
5
6
MW

3.3.2 Determination of Weight - Average Molecular Weight by Viscometry (52)

Relationship of viscosity and concentration, c, can be expressed by Huggins' equation,

$$\frac{\eta_{sp}}{c} = (\eta) + k' (\eta)^2 c \qquad (3.6)$$

or by Kraemer's equation

$$\frac{\ell n \eta_r}{c} = (\eta) - k' (\eta)^2 c \qquad (3.7)$$

where η_{sp} = the specific viscosity, η_r = the reduced viscosity, (η) = the intrinsic viscosity and k', k" = constants with

$$k' + k" = 0.5$$

Plots of η_{sp}/c vs. c and $\ell n \eta_r/c$ vs. c. will give the same intercept, (η). Typical plots for sample MG is shown in Fig. 3.7.

Molecular weight can be determined by Mark-Houwink equation,

$$(\eta) = K_\eta M^a \qquad (3.8)$$

The constants, K_η and a, are 7.1×10^{-5} and 0.72, respectively, for butanol at 25°C (53), and MW was weight-average MW, M_w, i.e. $M = M_w$. The measurements were made with an Ubbelohde viscometer. The experimental procedure was described in Appendix 2. The results are shown in Table 3.5 in comparison with the results obtained from GPC.

TABLE 3.5 Comparison of the MW obtained from GPC and Viscometry.

Polymer	M_w by GPC*	M_w by Viscometry
MG	75,000	90,000
MH	149,000	136,400
Sample 1**	165,000	206,000
Sample 2**	380,000	342,000
Sample 3**	580,000	609,000

*Calculated from Eqs. 3.1-3.3

**Anionic polymerized samples

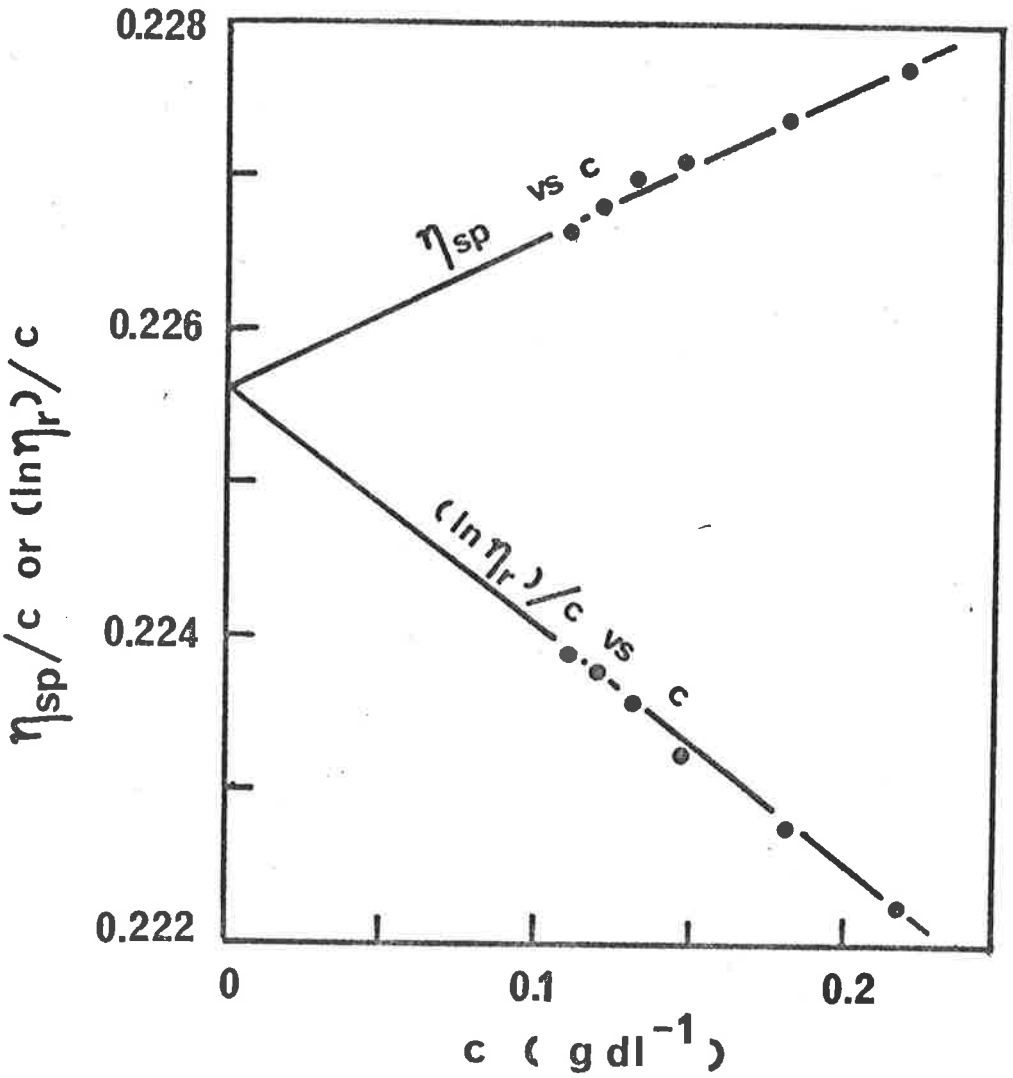

Fig.3.7 Measurement of MW by viscosity method.

A good agreement between the results from GPC and that from viscometry method suggest the combining method (Eqs. 3.1-3.3) is a suitable method to give a rapid calculation of M_w/M_n, M_w and M_n.

3.3.3 Determination of Stereoregularity

Chain configuration was determined by NMR spectrometry (90 MHz, ^1H, Bruker HX90E Spectrometer) using a 10% solution of polymer in a d_6 - dimethylsulphoxide/dischlorobenzene (1:9) solvent mixture. Bovey's nomenclature and assignments (55) were followed.

There are two kinds of dyads: meso (m) and recamic (r),

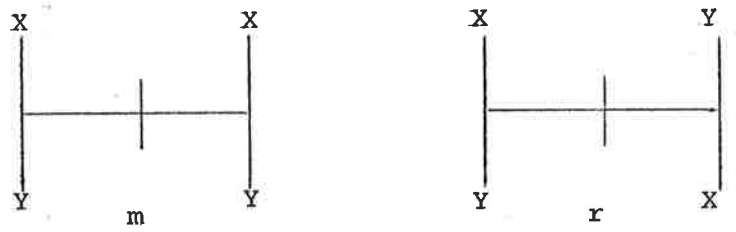

and three kinds of triads: isotactic (i), syndiotactic (s) and heterotactic (h),

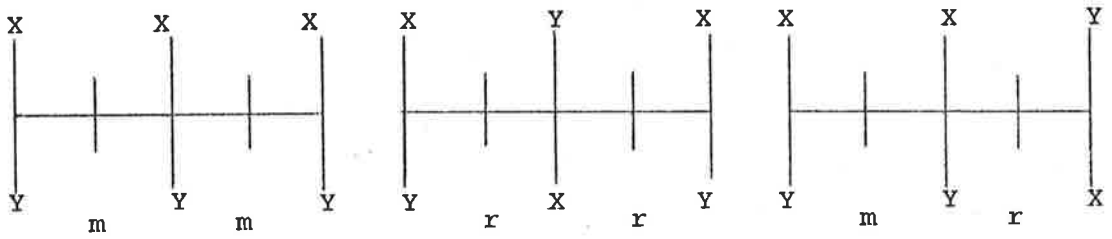

i=mm s=rr h=mr

The proportion of isotactic, heterotactic and syndiotactic triads are given by

$$i = mm = P_m^2 \qquad (3.9)$$

$$h = mr + rm = 2P_m(1-P_m) \qquad (3.10)$$

$$s = rr = P_r^2 = (1-P_m)^2 \qquad (3.11)$$

and $$i + h + s = 1 \qquad (3.12)$$

In the extreme cases, isotactic polymer forms when $P_m \to 1$ and syndiotactic if $P_m \to 0$.

However, if the addition of a monomer is affected by the previous additions, the statistics will obey multi-order Markov chain statistics.

In the simplest case, the first order Markov chain general statistical parameters are given by,

$$P_{mr} = \frac{h}{2i + h} \tag{3.13}$$

$$P_{rm} = \frac{h}{2s + h}$$

so that isotactic polymer forms when $P_{mr} \to 0$ and $P_{rm} \to 1$; syndiotactic if $P_{mr} \to 1$ and $P_{rm} \to 0$. Two other non-Bernoullian types are heterotactic when $P_{mr} + P_{rm} \neq 1$ (both larger than 0.5), and stereoblock when $P_{mr} < 0.5$, $P_{rm} < 0.5$; that is $P_{rm} + P_{mr} < 1$. In a special casewhere $P_{mr} + P_{rm} = 1$, the chain propagation will obey the Bernoulli trial statistics. Bovey also classified polymer type (e.g. syndiotactic-like, stereoblock) by calculation of number-average length of tactic block given by,

$$\bar{n}_r = 1 + 2s/h \tag{3.15}$$

$$\bar{n}_m = 1 + 2i/h \tag{3.16}$$

$$\bar{n} = 1/h \tag{3.17}$$

where $\bar{n}_r$ is number-average length of syndiotactic block

$\bar{n}_m$ is number-average length of isotactic block

$\bar{n}$ is number-average stereoblock length.

Other non-Bernoullian distribution can occur. One which is very plausible in systems where stereoblock polymers arise, is the Coleman-Fox multistate growth distribution which cannot be distinguished from first order Markov on triad data (57).

The results of various synthesized and commercial polymers are listed in Table 3.6 and NMR spectra are shown in Fig.3.8.

Fig.3.8 NMR spectra of PMMA. Commercial PMMA (MMW) (Curve 1), anionic polymerized narrow MWD PMMA (Curve 2), I.100 (Curve 3) and S.73 (Curve 4).

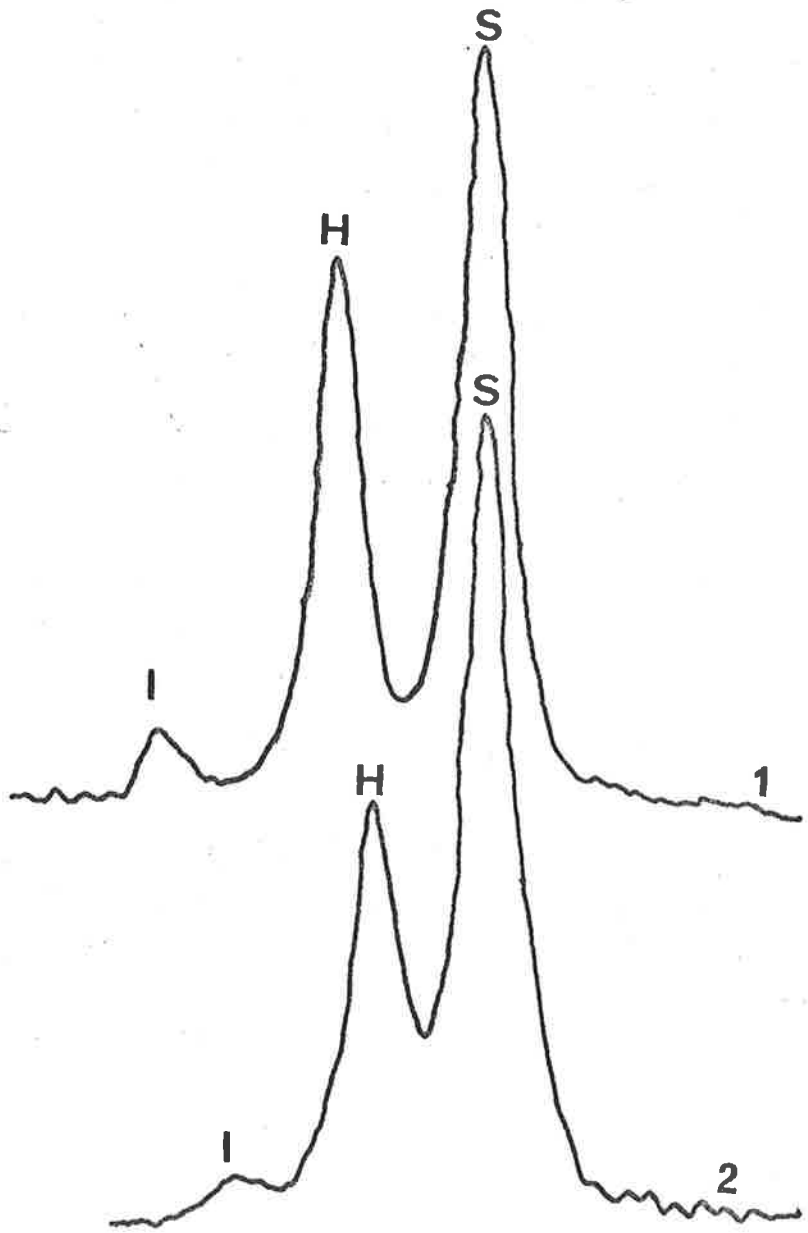
S
H
S
I
1
H
I
2

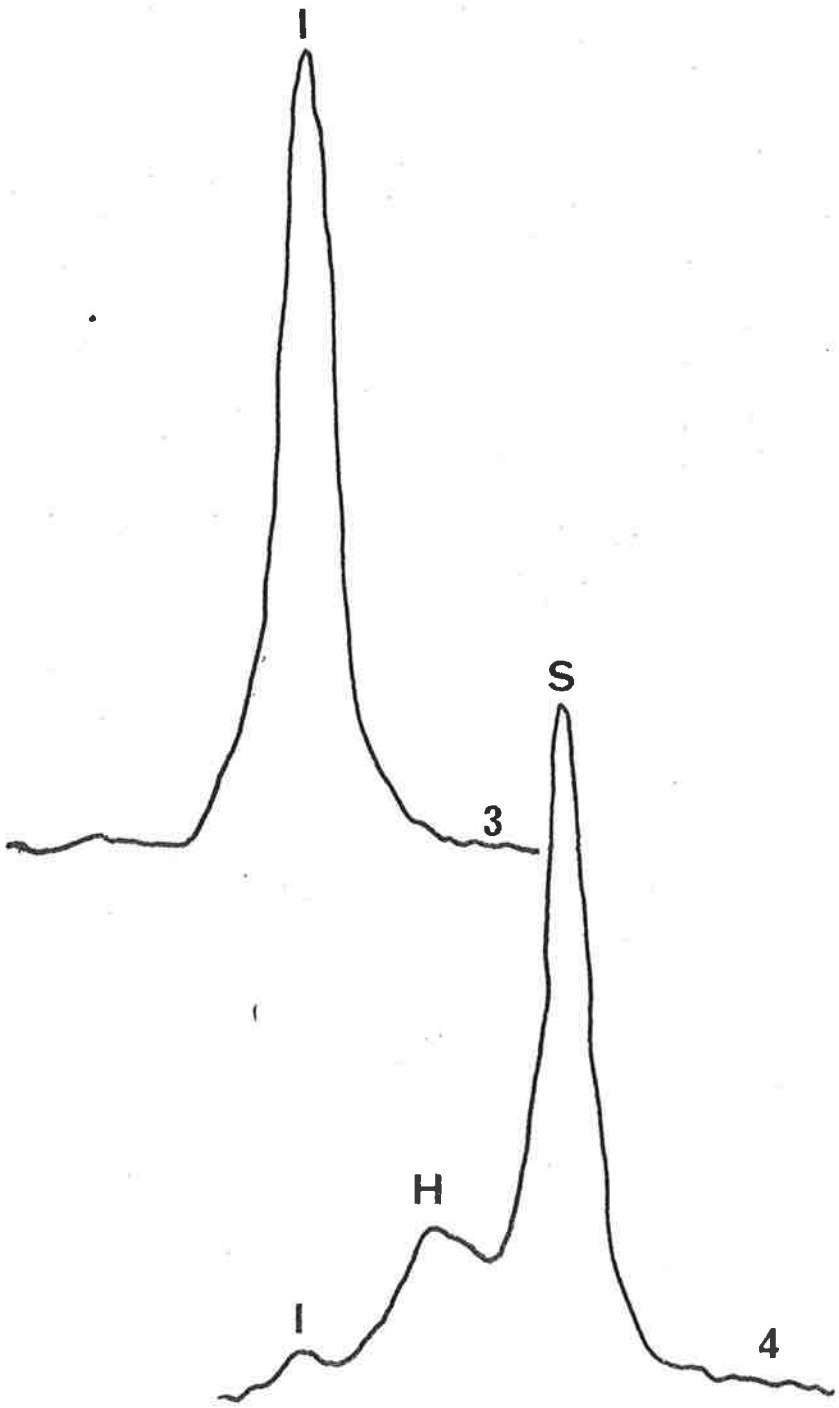
I
S
3
H
I
4

TABLE 3.6 Stereoregularity

Samples	Triads fraction			Dyads fraction		P_{mr}	P_{rm}	$P_{mr}+P_{rm}$	$\bar{n}_m$	$\bar{n}_r$
	i	h	s	m=i+h/2	r=s+h/2					
A*	0.035	0.327	0.638	0.198	0.801	0.824	0.204	1.028	1.214	4.902
S.73	0.03	0.24	0.73	0.15	0.85	0.889	0.247	1.135	1.25	7.08
I.74	0.74	0.10	0.16	0.79	0.21	0.063	0.238	0.301	15.8	4.2
I.100	1.0	0	0	1.0	0	0	1	-	∞	0
Commercial										
MH	0.056	0.413	0.531	0.262	0.737	0.787	0.280	1.067	1.27	3.57
MMW	0.07	0.38	0.55	0.26	0.74	0.731	0.257	0.988	1.37	3.89

*A = anionic polymerized samples

3.3.4. Determination of the Glass Transition Temperature, T_g

The glass transition temperature T_g (Table 3.7) was determined by differential scanning calorimeter (DSC) (Perkin Elmer Model II). The specimen was moulded to a thickness of 0.5mm and approximately 15mg was loaded into the DSC cell. Heating rate of 20 degree/min was adopted throughout the measurement. The T_g was determined at C, the midpoint of A B on the tangent of the sloping portion of the curve. (A, B are the intersections between the upper and lower base lines and the tangent, Fig. 3.9). It was observed that the cooling rate affected the shape of the curve, but the T_g in the measurement remained unchanged (Fig. 3.9). The T_g of each sample was measured at least twice with the same cooling rate (320 degree min^{-1}) used for all samples. Prior to the measurement the instrument was calibrated using lead and indium as standards.

3.4 Concluding Remarks

Some technical difficulties were encountered in the scaling up of pseudo-anionic polymerization, but the anionic polymerizations were carried out successfully with a compromising step of reduction of the amount of THF to make the apparatus less bulky. The main problem of the pseudo-anionic polymerization was the irreproducible yield and MW of products and this has been currently investigated in our laboratory. Especially, the de-etheration procedures which seem to be the main factor in the polymerization of isotactic PMMA influences the yield and MW of product through the concentration ratio of THF/toluene. Hitherto, the de-etheration procedures have been based on working experience and a more quantitiative specification is necessary to produce efficient and reproducible experimental conditions.

Comparing with the pseudo-anionic polymerization, the anionic polymerization requires a more rigid control of high-vacuum and more

TABLE 3.7 Glass transition temperature, T_g, from DSC.

(1) Anionic Polymerized Samples

M_w	$1/M_w \times 10^6$	T_g(K)
580,000	1.72	397.5
530,000	1.89	397.5
510,000	1.96	399.0
380,000	2.63	398.5
165,000	6.06	394.0
160,000	6.25	393.5
97,000	10.31	393.0
84,000	11.90	395.0
71,000	14.08	390.5
36,000	27.78	383.0
31,000	32.26	377.0
23,500	42.55	357.5

(2) Pseudo-anionic Polymerized Samples

Sample	T_g(K)
I.74	331
I.100(1)	331
I.100(2)	310
I.100(3)	331
S.73h	399

(3) Commercial Samples

Sample	T_g(K)
MH (Diakon)	385
MG (Diakon)	384
HMW (Polyscience)	376
MMW (Polyscience)	376
LMW (Polyscience)	376

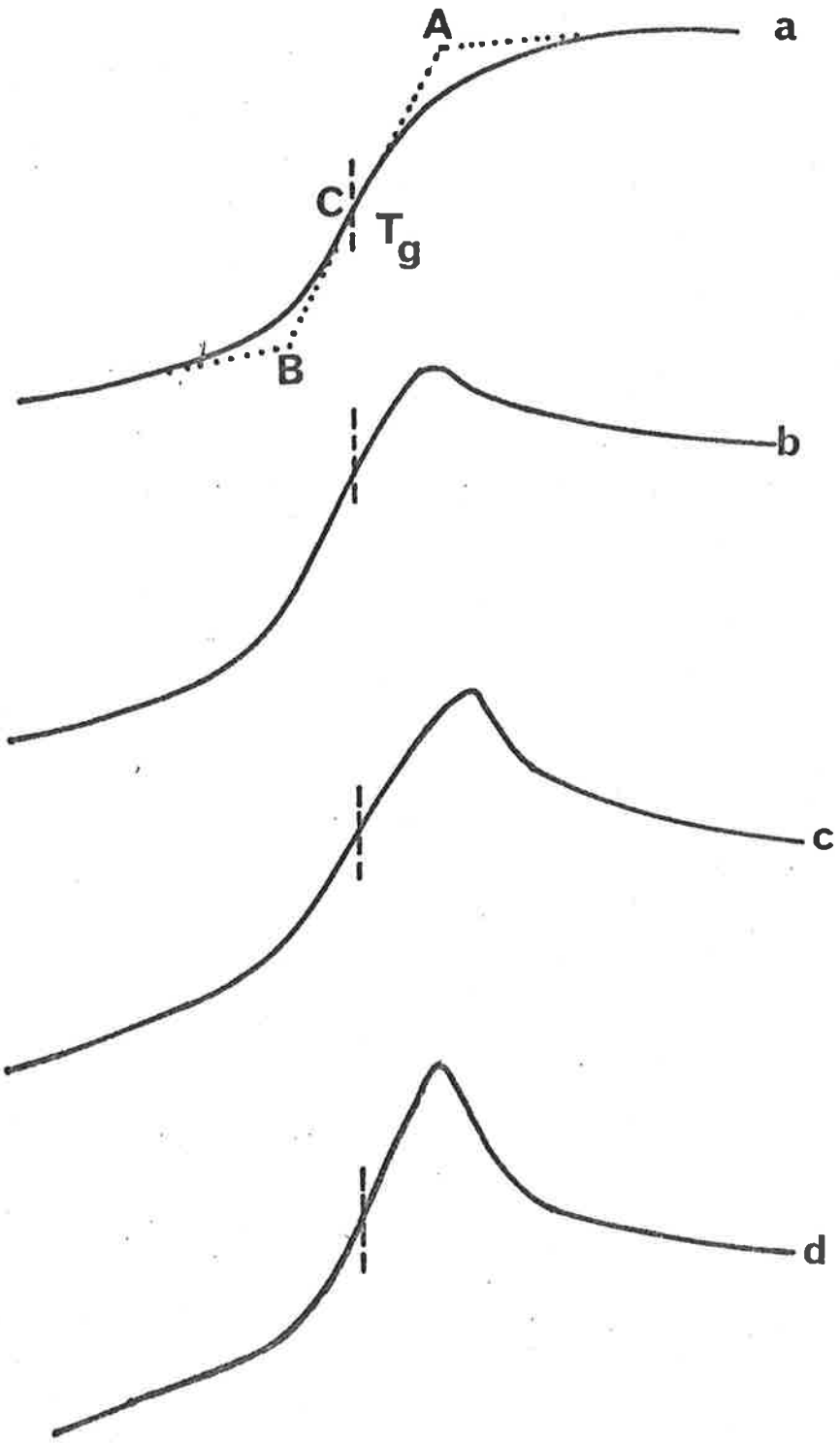

Fig.3.9 Determination of the glass transition temperature, T_g, at various cooling rates. (a) 320°/min, (b) 80°/min, (c) 20°/min and (d) 5°/min.

purified solvents, but the simple preparation of initiators and the unsophisticated initiation step sufficed to give a reproducible reaction. Consequently, the reaction was successfully scaled up, but because of the bulky polymerization apparatus, the volume of THF had to be reduced. This reduction led to an unfavourable equilibrium of the propagating species for a narrow MWD products. The propagating species in anionic polymerization is a free or paired anion (56), the abundance of ethereal solvent will enhance solvation of contact ion pairs, producing solvated ion pairs which because of their reactivity and high concentration play an important part in propagating mechanism. Although the concentration of the free ion is small, the free ion is more active than the ion pair and this enables the polymerization to occur via the free ions.

In the large scale, THF was reduced to the ration 1:25 (MMA/THF by weight) compared with 1:100 in small scale polymerization (40,42), this would give less solvated ion pairs in the reaction and thus caused a broadening of MWD to M_w/M_n = 1.2 (cf. the reported value M_w/M_n = 1.06 for small scale polymerization (42)). As an attempt to narrow the MWD, few grams of sodium tetraphenylborate was added to encourage the solvated ion pairs - free ions equilibrium shift to the left thus suppressing the existance of the reactive free ions and increasing the concentration of the ion pairs. The attempt, unfortunately, did not achieve its goal due to the low concentration of the free ion (i.e. the low dissociation constant), particularly at low temperature - 195K ($-78^{o}C$)

From the monomodal MWD shown by the GPC, however, it can be concluded that side reactions can be neglected and that the sodium biphenyl initiated a bifunctional propagating mechanism which was well maintained during the reaction as long as the solvents and monomer were kept at a maximum purified condition.

In summary, the two polymerization methods have proved to be a supplementary to each other to produce the required molecular properties of polymers: the MW, the MWD and stereoregularity. The MWD can be controlled by blending the narrow MWD of high and low MW at different weight ratio . The pseudo-anionic polymerization initiated by various Grignard compound provides a wide range of different stereo-regularity, especially the stereoblock and isotactic polymers. However, this process needs to be developed to be able to produce controlled MW and stereoregularity polymers simultaneously in a more reproducible manner.

CHAPTER 4

GLASS TRANSITION TEMPERATURE AND STRESS RELAXATION OF METHANOL EQUILIBRATED POLY(METHYLMETHACRYLATE)

4.1 Introduction

A knowledge of the glass transition temperature, T_{sg}, of methanol - equilibrated PMMA and the diffusion rate of methanol into PMMA is necessary to understand the condition of the bulk polymer in the vicinity of a solvent plasticized crack tip. Unfortunately, measurement of the T_{sg} by the normal methods of differential scanning calorimetry (DSC) or the use of a torsion pendulum do not give reproducible results (58-59) because large amounts of solvent will escape as the temperature is slowly increased to the glass transition temperature.

To overcome these difficulties, a stress relaxation method of measuring T_{sg} was developed. The test required the immersion of PMMA sample in methanol to produce methanol-equilibrated PMMA. At the same time, the diffusion coefficient of the mass flux of methanol was deduced from the weight gain data. Quantitative information on other aspects of behaviour such as the MW between the entanglement loci, M_e, the glass transition depression in plasticized PMMA from the stress relaxation data are discussed.

4.2 Experimental

4.2.1 Preparation of Sheet Polymer

Synthesized narrow MWD polymers and commercial polymers were moulded in a hydraulic press at 200°C to produce sheet specimens of thickness 1.2mm. Prior to moulding, polymers were vacuum dried at 50°C for several days. To avoid unnecessary thermal degradation during moulding, the sheets were rapidly cooled from 200°C to 150°C followed by slow cooling to room temperature over a period of 45 minutes. Using

this cooling program, the residual stresses could be reduced to an undetectable amount as observed under crossed polarized light*. Sheets of low MW polymer tended to crack on cooling. The problem was generally overcome by cooling to 150°C in a hydraulic press and then transferring the mould to a vacuum oven where the cooling was continued down to room temperature over a period of 3 hours. Measurement of the MW of the polymer by GPC before and after moulding at 200°C revealed no change in MW and MWD.

4.2.2 Methanol Uptake Measurements

The sheet specimens were immersed in methanol (LR grade) bath at a temperature of 20±1°C and at successive time intervals, specimens were removed, quickly wiped with tissue paper and weighed. After a period of 3-4 weeks, all specimens saturated with methanol and the percentage uptake did not change by more than 0.1% by weight over a 24 hour period.

4.2.3 Stress Relaxation and Glass Transition Temperature Measurements for Methanol Equilibrated PMMA.

As already mentioned in Section 4.1, the stress relaxation method of measuring the T_{sg} of methanol - equilibrated PMMA is the accurate and simple method. Prior to a description of the method of measurement, it is well to point out the shortcomings in other methods.

Krenz et al. (59) heated solvent swollen film over a hot plate and determined the T_{sg} by observing the first sagging of the specimen - an attempt to measure the temperature coinciding with the abrupt change in elastic modulus at the glass transition temperature. The method of Andrews et al. (60) was to measure the tensile yield stress as a function of temperature and by extrapolating back,

* The author is aware that the absence of visible photoelasticity is not necessarily an indication of the absence of residual stress, but alternative more sensitive methods of detecting the residual stress are, at the moment, extremely tedious and open to question.

determine the temperature at which the yield stress became zero; this temperature was assumed to be T_g. The method of Krenz et al. would give incorrect results with volatile solvents, especially at temperatures higher than the boiling point of the solvent and furthermore the observation of the "first" sagging of specimen is a rather subjective measurement. Andrews' method gave reproducible results but the measurement required a considerable amount of polymer to allow testing to destruction of numerous specimens.

In this work, however, the stress relaxation measurement only required a small methanol equilibrated specimen(10x5mm of 1.2mm thickness). The specimen was placed between platens A and B and immersed in methanol at a temperature controlled by water circulating in the external jacket (Fig.4.1). The specimen was compressed to a constant strain ε ($\varepsilon < 0.05$) and the relaxation in the load recorded as a function of time on the Instron recorder. The test was conducted at temperatures between 0°C and 50°C. Change in weight of the specimen due to loss or gain of methanol did not exceed 5% of the total equilibrium uptake. This low value is attributed to (a) the platens covering 95% of the area of the specimen, (b) the short elapsed time of the experiment.

The T_{sg} is determined as the temperature at which the stress relaxation curve show the steepest slope. Details of the determination will be described in Section 4.3.2. The determined glass transition temperature by the stress relaxation curve for various polymers has been reported to be close to the glass transition temperature as measured by DSC (61-62).

4.3 Results

4.3.1 The Diffusion Coefficient of the Mass Flux of Methanol in PMMA

The weight gain data are presented as a plot of the ratio of

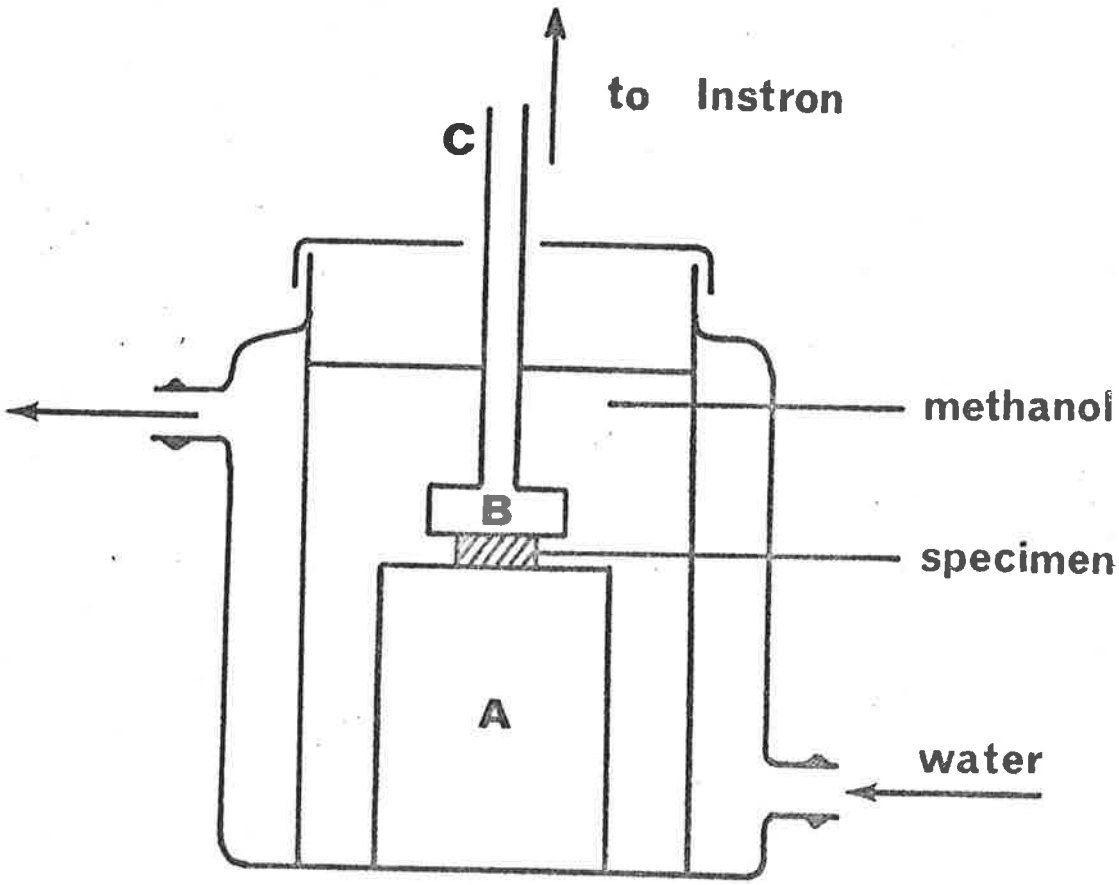

Fig.4.1 The stress relaxation testing vessel.

weight gain W_1/W_2 (W_1 = weight gain at time t, W_2 = original weight) against $t^{\frac{1}{2}}/\ell$ (ℓ = thickness of specimen). From Fig.4.2 it can be seen that the equilibrium methanol uptake is almost independent of molecular weight in the range $30,000 \lesssim M_w \lesssim 500,000$ and has an average W_1/W_2 value of 0.22. It was noticed that specimens of low MW ($M_w \lesssim 84,000$) became white at approximately 75% of the equilibrium uptake of methanol while specimens of higher MW remained translucent. These unusual features of the absorption of methanol were examined in more detail in some concurrent work in this laboratory by Williams (63). The available evidence suggested that the whitening of low MW PMMA ($M_w \lesssim 84,000$) was due to the formation of a methanol rich phase which scattered visible light and thus caused the specimens to become opaque. Removal of methanol from these specimens by slow drying gave a fracture surface* containing a large number of evenly sized spherical cavities (Fig.4.3). The suggestion therefore arises that the high equilibrium uptake of specimen of M_w = 23,500 is partly due to the formation of a methanol rich phase. Further investigations of the MW effect on the formation of the methanol rich phase is being undertaken.

The diffusion of organic liquids in glassy polymers can be described in terms of a Fickian mechanism, or a Case II mechanism or "anomalous" behaviour lying between the first two extreme cases. A generalised diffusion equation which embodied the three mechanisms was derived by Kwei et al. (64). By combining the Fickian and Case II mechanisms, they developed the following equation for the "anomalous" mechanism.

$$\frac{\partial C}{\partial t} = \frac{\partial}{\partial x}\left(D \frac{\partial C}{\partial x} - v_D C\right) \qquad (4.1)$$

* Specimen fractured at room temperature.

Fig.4.2 The methanol uptake for narrow MWD PMMA of various MW: M_w = 23,500 (○), M_w = 31,000 (●), M_w = 36,000 (■), M_w = 71,000 (▼), M_w = 84,000 (□), M_w = 97,000 (▲), M_w = 380,000 (△), M_w = 550,000 (▽).

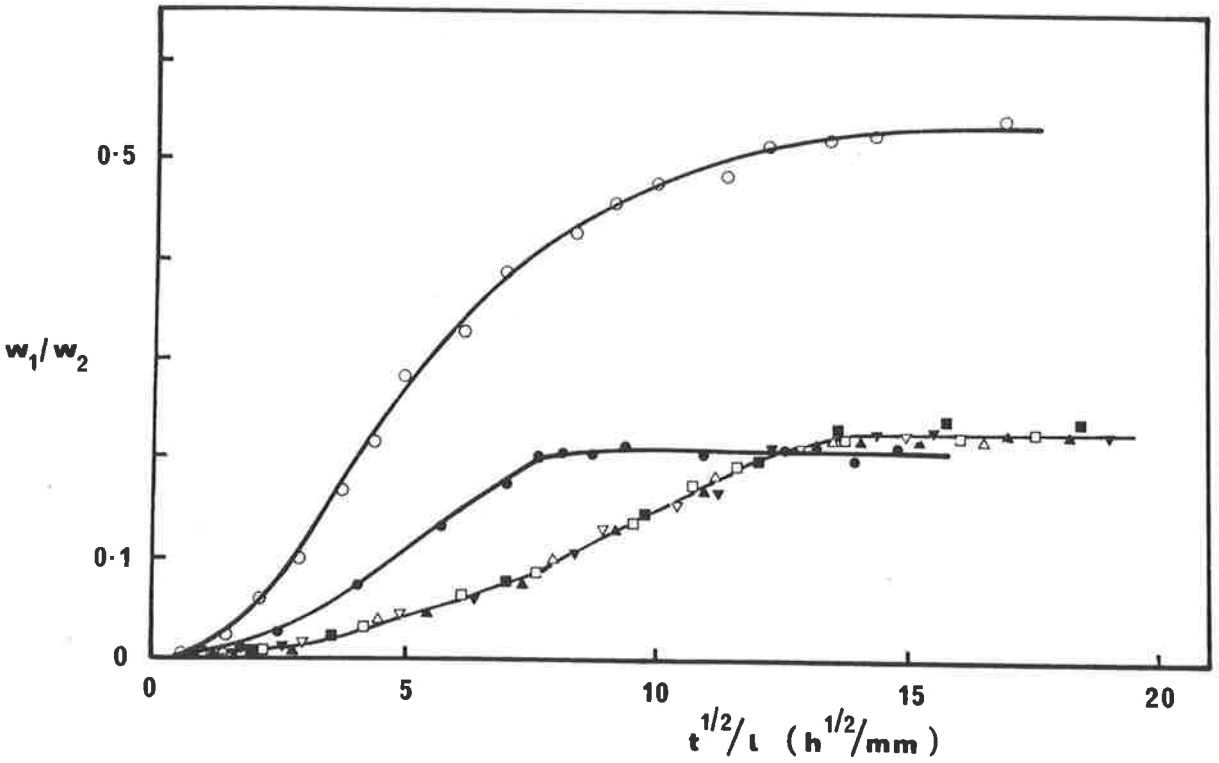
0·5
0·1
0
w_1/w_2
0
5
10
15
20
$t^{1/2}/l$ ($h^{1/2}/mm$)

Fig.4.3 Formation of spherical cavities in fracture surface of PMMA after equilibrated in methanol. 500x.

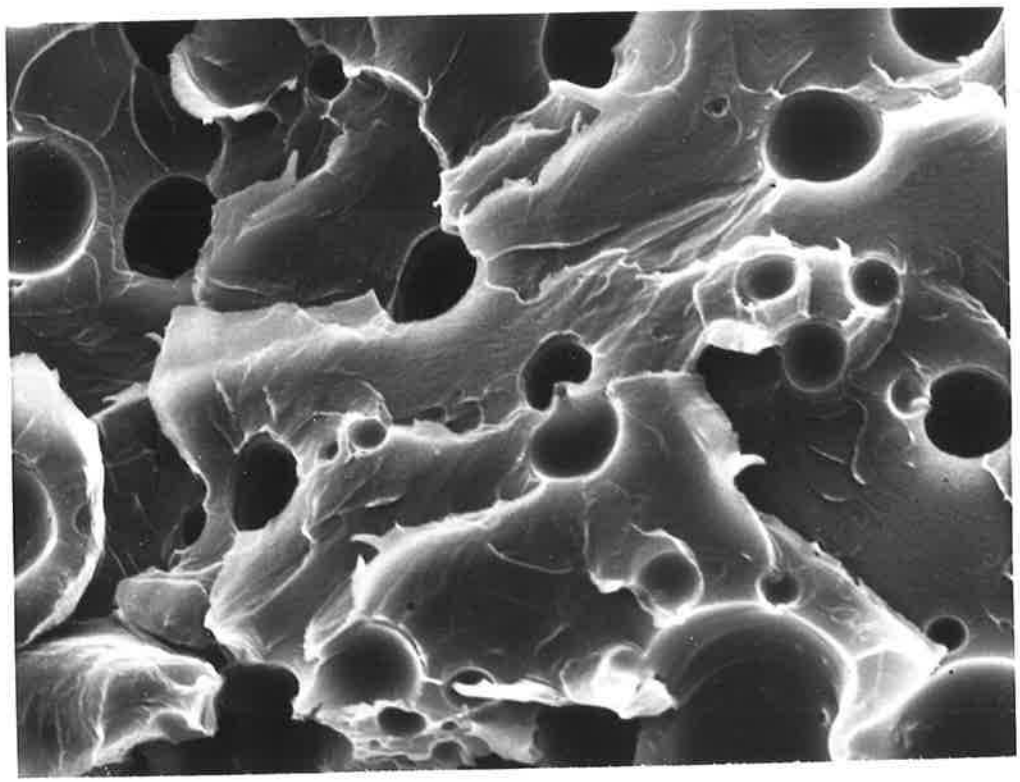

Where C is concentration at time t and at distance x; D the diffusion coefficient and v_D velocity of the solvent front in Case II mechanism. Transport of methanol in PMMA was reported to obey Case II behaviour at low temperature and approach a Fickian mechanism when temperature was increased to the methanol boiling point (65). Ware and Cohen (66) have applied Eq.4.1 to the PMMA-methanol system at 42°C to investigate the effect of specimen thickness on the diffusional behaviour of methanol. Application of Eq.4.1 enables the diffusion coefficient, D, to be obtained and the details of the calculation will now be discussed.

At long times, Kwei et al. (64) derived the following relationship between the mass M_t of methanol absorbed per unit surface area of specimen and time t,

$$M_t = C_o \left(\frac{D}{v_D} + v_D t \right) \qquad (4.2)$$

where

$$M_t = \frac{W_1}{W_2} \rho_p \ell \qquad (4.3)$$

The density of the polymer, ρ_p, was measured by liquid displacement methanol and found to be equal to 1.18 g cm^{-3}. The surface concentration, C_o, is taken as the equilibrium concentration of methanol in the swollen PMMA, that is

$$C_o = \left(\frac{W_1}{W_2}\right)_{equilibrium} \cdot \rho_p \qquad (4.4)$$

where $(W_1/W_2)_{equilibrium}$ is obtained from equilibrium weight gain (Fig.4.2).

A linear relationship was observed between M_t and t at intermediate to long times and from the slope and intercept of this linear region (Fig.4.4), v_D and D were calculated by linear regression (Table 4.1).

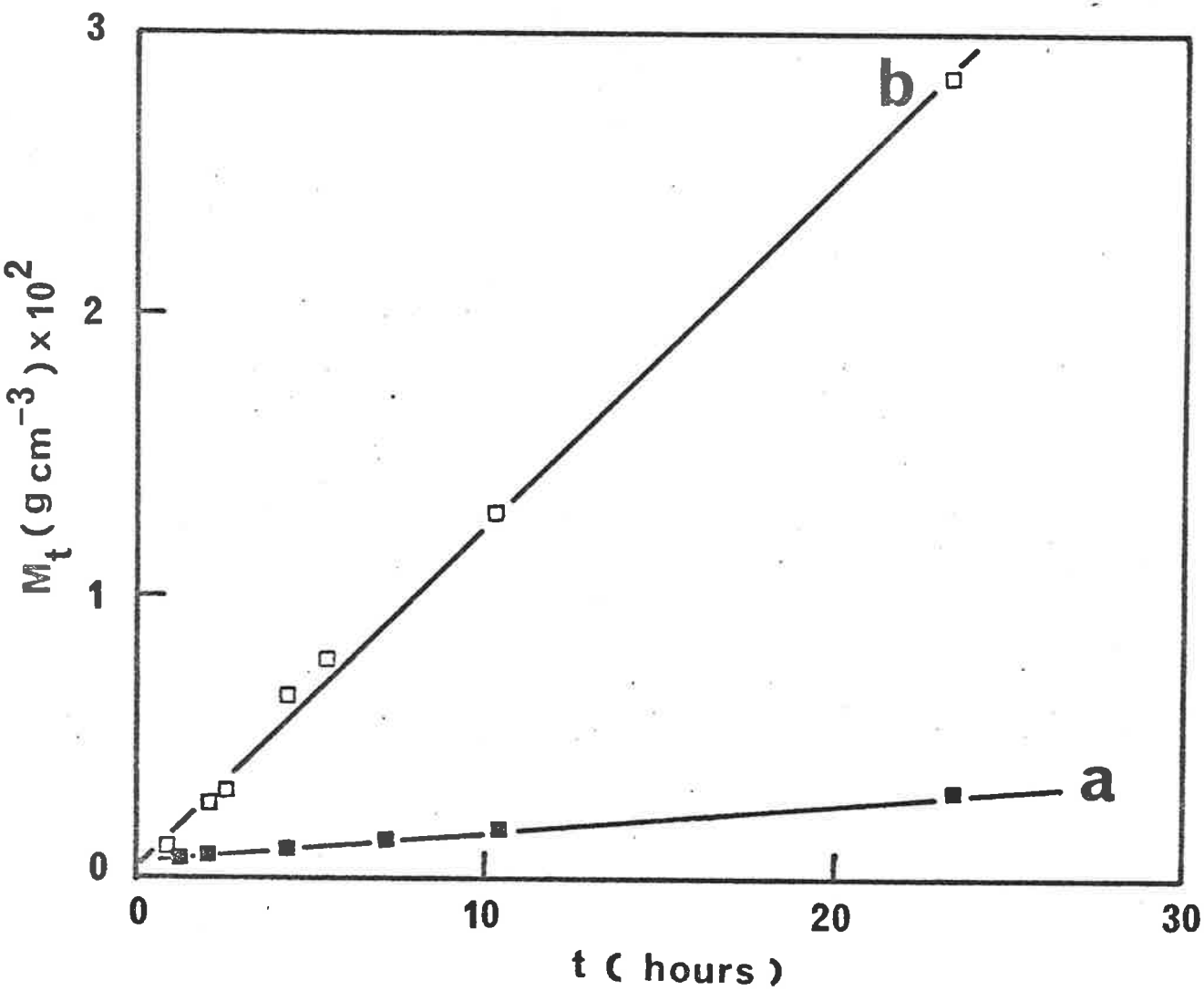

Fig.4.4 Plot of the mass of methanol absorbed per unit area, M_t, vs. the time, t, for narrow MWD PMMA, (a) sample A3 (M_w = 380,000) and (b) sample A10 (M_w = 23,500).

TABLE 4.1: Relationship between C_o, D, v_D and MW, MWD.

M_w	M W D	C_o (g cm^{-3})	D (cm^2 sec^{-1})	v_D (cm sec^{-1})
23,500	1.2	0.703	4.55×10^{-10}	4.52×10^{-7}
31,000	1.2	0.242	6.40×10^{-10}	5.00×10^{-7}
36,000	1.2	0.259	0.88×10^{-10}	2.07×10^{-7}
71,000	1.2	0.257	1.00×10^{-10}	1.91×10^{-7}
84,000	1.2	0.285	0.72×10^{-10}	1.77×10^{-7}
97,000	1.2	0.257	1.46×10^{-10}	2.01×10^{-7}
380,000	1.2	0.306	1.43×10^{-10}	1.57×10^{-7}
550,000	1.2	0.271	2.42×10^{-10}	1.71×10^{-7}
160,000 (LMW)	2.1	0.309	7.77×10^{-10}	5.73×10^{-7}
220,000 (MMW)	2.1	0.319	1.36×10^{-9}	6.16×10^{-7}
787,000 (HMW)	2.1	0.217	2.67×10^{-10}	9.75×10^{-7}

It can be noted that the magnitude of v_D and D do not show any trend with MW and MWD, and are of the order of $v_D \simeq 10^{-7}$ cm sec^{-1} and $D \simeq 10^{-10} cm^2$ sec^{-1}. This suggests that the MW and MWD do not have any effect on the methanol diffusity under zero external stress. The values of D will be again deduced from data of crack propagation of PMMA in the presence of methanol. Using the values of D listed in Table 4.1 as reference, the comparison of the value of D obtained from cracking data with the reference value will provide a basic information on the role of the methanol diffusion in the cracking mechanism of PMMA.

4.3.2 Stress Relaxation and Glass Transition Temperature

Typical stress relaxation curves at various temperatures are shown in Fig.4.5 for a narrow MWD sample, A4 (M_w = 84,000). The stress relaxation curves can be superposed to form a master curve using the time-temperature superposition principle. This procedure requires the determination of a shift factor a_T which can be expressed

Fig.4.5 Time dependence of modulus E for narrow MWD PMMA at various temperatures (Sample A4, M_w = 84,000).

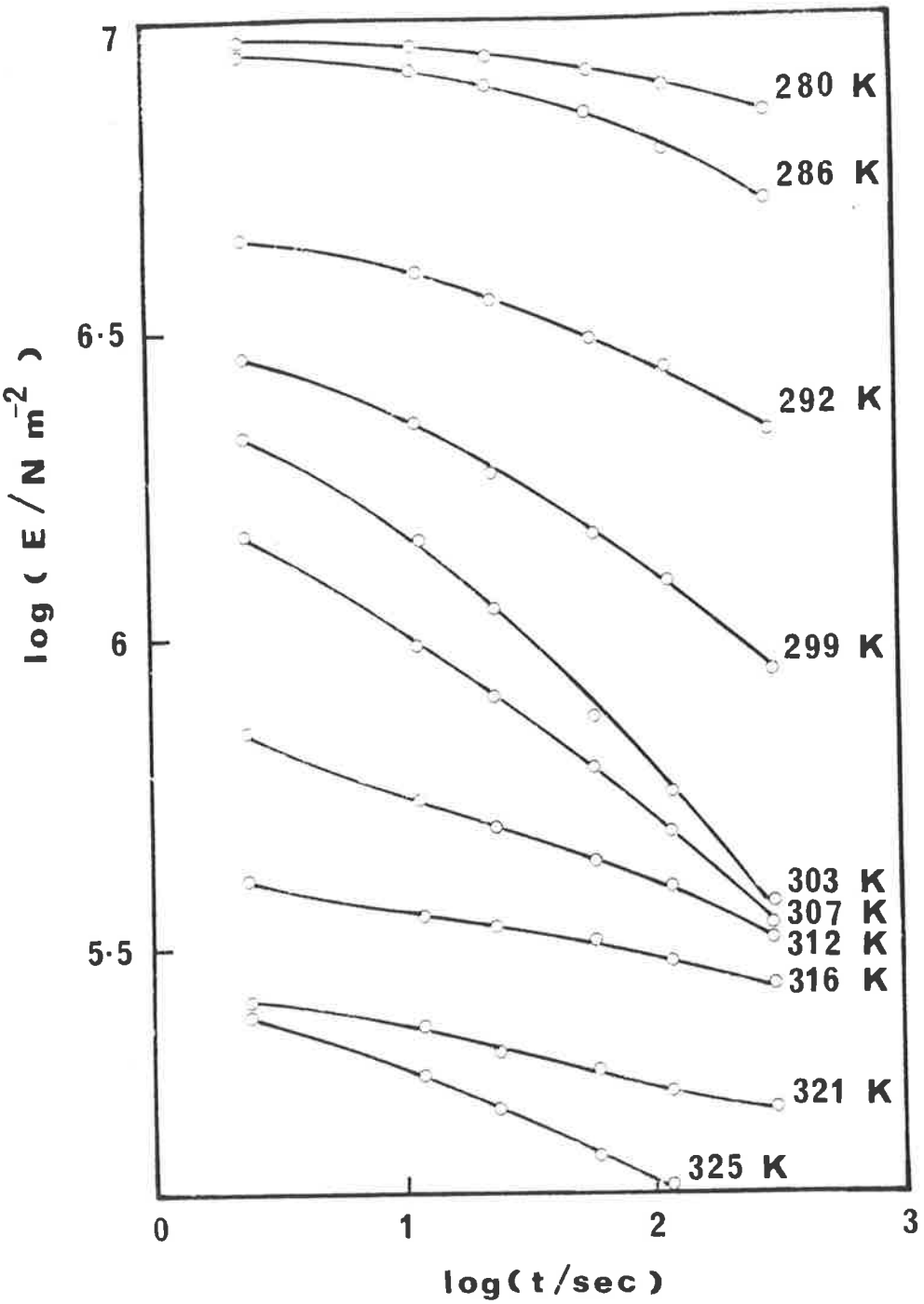
7
6·5
6
5·5
0
1
2
3
log (E / N m^{-2})
log(t /sec)
280 K
286 K
292 K
299 K
303 K
307 K
312 K
316 K
321 K
325 K

by the following WLF equation (67)

$$\log a_T = \frac{-c_1^r (T - T_r)}{c_2^r + (T - T_r)} \qquad (4.5)$$

where c_1^r and c_2^r are positive constants and T_r is the reference temperature.

Eq.4.5 implies that a plot of $-(T - T_r)/\log a_T$ versus $(T - T_r)$ should give a straight line with the constants c_1^r, c_2^r evaluated from the slope and intercept, respectively. The shift factor a_T can then be determined from Eq.4.5 at temperature T with T_r = 412 K as the reference temperature. The values of c_1^r and c_2^r are listed in Table 4.2 and $\log a_T$ in Table 4.3 for samples A1, A3, A5, A6 and A7.

TABLE 4.2: Values of c_1^r and c_2^r with T_r = 412 K

Sample	M_w	c_1^r	c_2^r
A1	550,000	17.71	82.59
A3	380,000	14.14	79.00
A5	97,000	18.17	116.35
A6	84,000	12.08	93.47
A7	71,000	7.05	53.58

TABLE 4.3: Values of the shift factor $\log a_T$

Samples	T - 412 (K)								
	-30	-25	-20	-15	-10	-5	5	10	10
A1	10.10	7.69	5.66	3.93	2.44	1.14	-1.01	-1.91	-2.72
A3	8.66	6.55	4.79	3.32	2.05	0.96	-0.84	-1.59	-2.26
A5	6.31	4.97	3.77	2.69	1.71	0.82	-0.75	-1.44	-2.08
A6	5.71	4.41	3.29	2.31	1.45	0.68	-0.61	-1.45	-1.67
A7	8.97	6.17	4.20	2.74	1.62	0.73	-0.60	-1.11	-1.54
Average $\log a_T$	7.95	5.96	4.34	3.00	1.85	0.87	-0.76	-1.50	-2.05

As observed by Onogi and co-workers (68-69) for polystyrene and PMMA, there is an obvious trend in a_T if we regard Sample A7 as an exception. It is possible the result for A7 may be due to experimental error, but without evidence to the contrary, it was decided to include the values for A7 in the calculation of c_1^r and c_2^r by taking the mean of the log a_T values.

TABLE 4.4: Mean value $\overline{\log a_T}$ versus $-(T - T_r)/\overline{\log a_T}$ with T_r = 412 K

$(T - T_r)$(K)	$\overline{\log a_T}$	$-(T - T_r)/\overline{\log a_T}$
-30	7.95	3.77
-25	5.96	4.19
-20	4.34	4.61
-15	3.00	5.00
-10	1.85	5.40
- 5	0.87	5.75
0		
5	-0.76	6.58
10	-1.50	6.67
15	-2.50	7.32

The plot of $-(T - T_r)/\overline{\log a_T}$ vs. $(T - T_r)$ gave a straight line (Fig. 4.6) from which the constant c_1^r and c_2^r were found by linear regression to be 13.35 and 81.31, respectively.

The master curves (log-log plots of modulus E vs. reduced time t/a_T) are shown in Fig.4.7 for narrow MWD PMMA of various MW and Fig.4.8 for commercial PMMA. Considering the master curve of narrow MW PMMA, a glassy zone, a transition zone and a rubbery zone for high MW ($M_w \geq 71{,}000$) are observed. A flow zone is observed in the curve of low MW ($M_w \leq 36{,}000$) PMMA. The technique was unable to detect a flow zone for high MW because the test became inappropriate as the temperature approached the methanol boiling point (T_b=64.56°C).

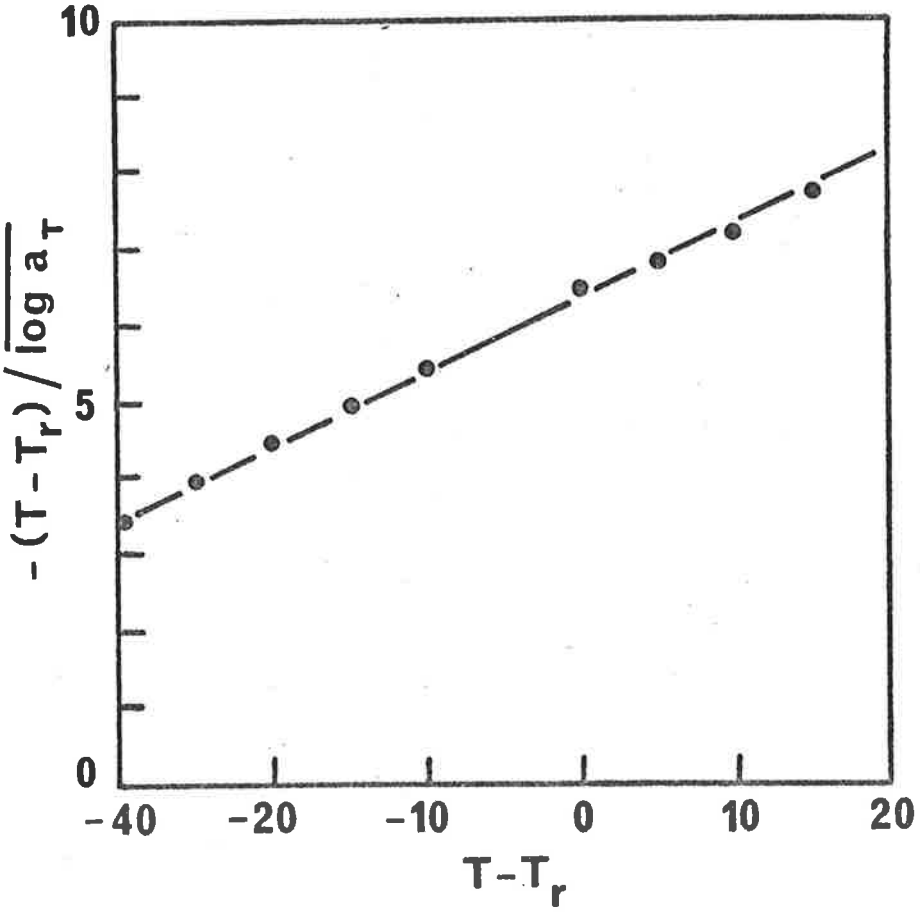

Fig.4.6 Plot of $-(T-T_r)/\overline{\log a_T}$ vs. $(T-T_r)$ for narrow MWD PMMA.

Fig.4.7 Stress relaxation master curves of narrow MWD PMMA with the reference temperature, T_r = 412 K.
M_w = 550,000 (1), M_w = 380,000 (2),
M_w = 94,000 (3), M_w = 84,000 (4),
M_w = 71,000 (5), M_w = 36,000 (6),
M_w = 31,000 (7) and M_w = 23,500 (8).

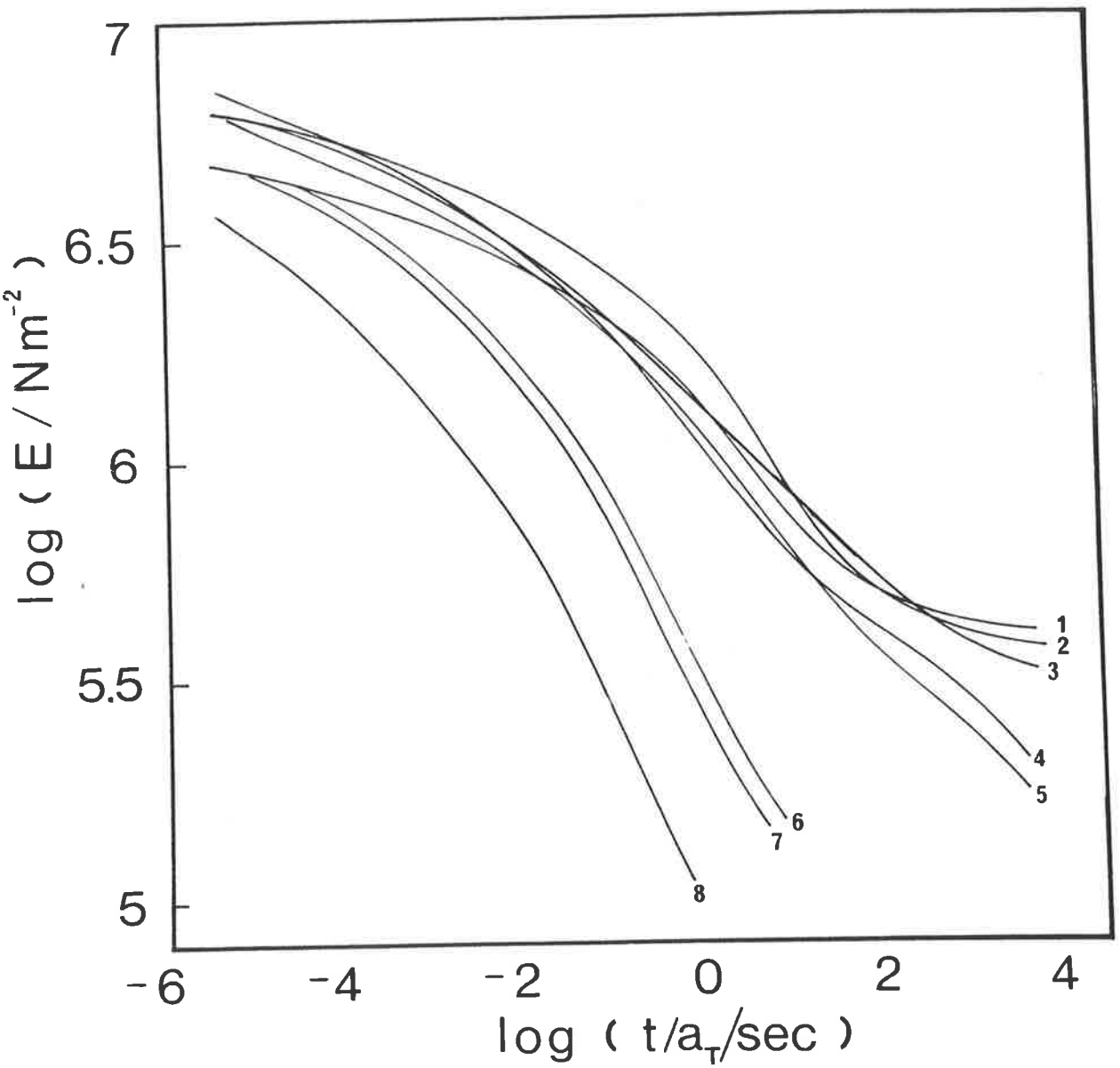
7
6.5
6
5.5
5
log (E / Nm^{-2})
-6
-4
-2
0
2
4
log (t/a$_T$/sec)
1
2
3
4
5
6
7
8

Fig.4.8 Stress relaxation master curves of broad MWD commercial PMMA with the reference temperature, T_r = 412 K. Sample HMW(1), sample MMW(2) and sample LMW(3).

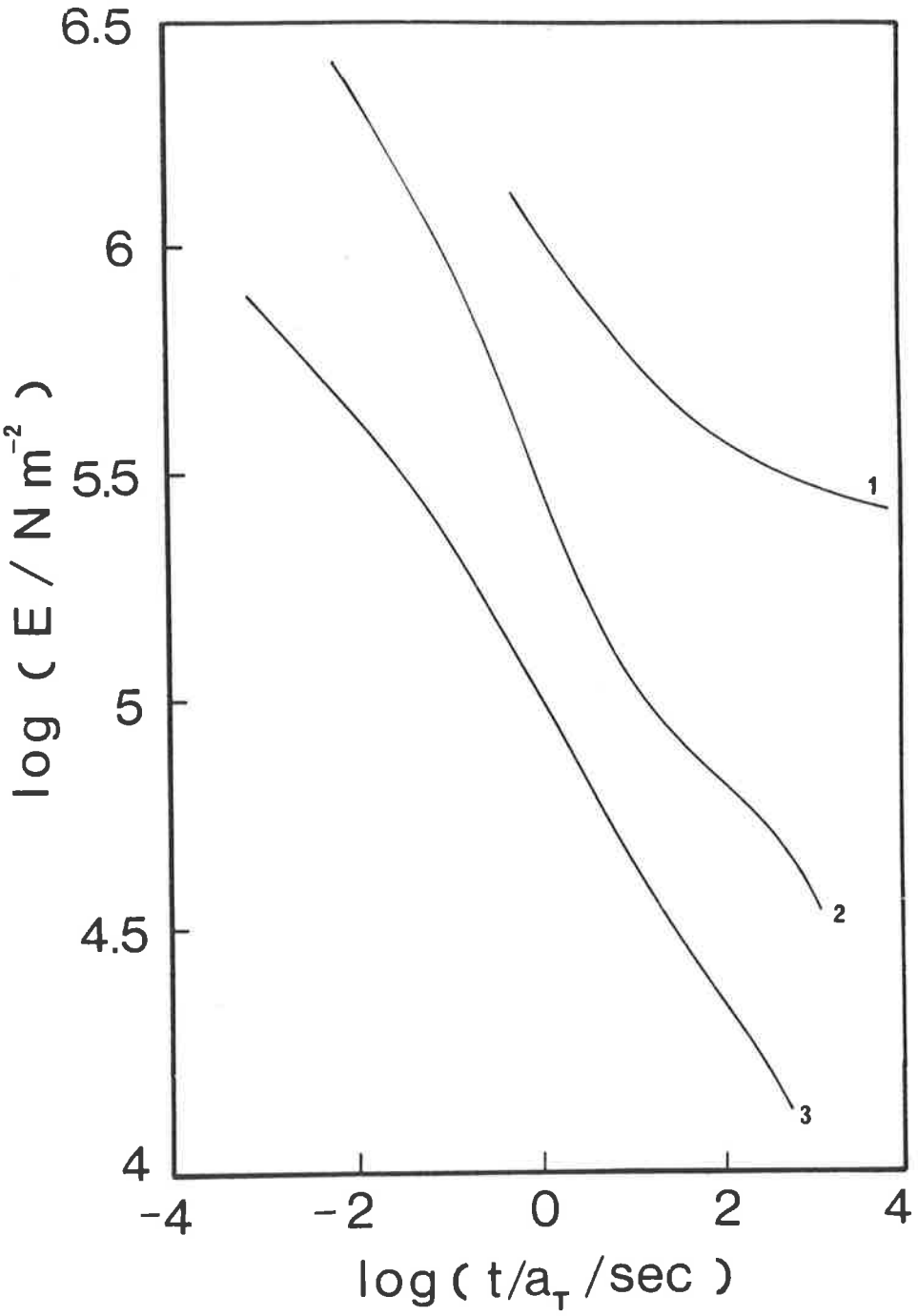
6.5
6
5.5
5
4.5
4
log (E / N m^{-2})
-4
-2
0
2
4
log (t/a$_T$ /sec)
1
2
3

The glass transition temperature of methanol equilibrated PMMA, T_{sg}, was determined by plotting the tangent of the stress relaxation curves at each temperature and defining the T_{sg} as the temperature where the slope of the tangent reaches a maximum (Fig.4.9). The T_{sg}'s determined by this method are shown in Table 4.5.

TABLE 4.5: The glass transition temperatures, T_{sg}, of methanol-equilibrated narrow MWD PMMA of various MW.

Sample	M_w	T_{sg}(K)
A1	550,000	303
A2	380,000	303
A5	97,000	303
A6	84,000	300
A7	71,000	303
A8	36,000	298
A9	31,000	298
A10	23,500	293

The T_{sg} of high MW specimens are in good agreement with the zero-yield stress method adopted by Andrews et al. (60), providing the T_{sg} are compared at the same equilibrium methanol absorption concentration.

4.4 Discussion

4.4.1 The Glass Transition Temperature T_{sg} of Narrow MWD PMMA.

Before embarking on the discussion of the glass transition temperature of methanol-equilibrated PMMA, it is of interest to consider the effect of MW on the T_{og} of the narrow MWD PMMA (containing 0% methanol) and to compare the results with published data. Follow-

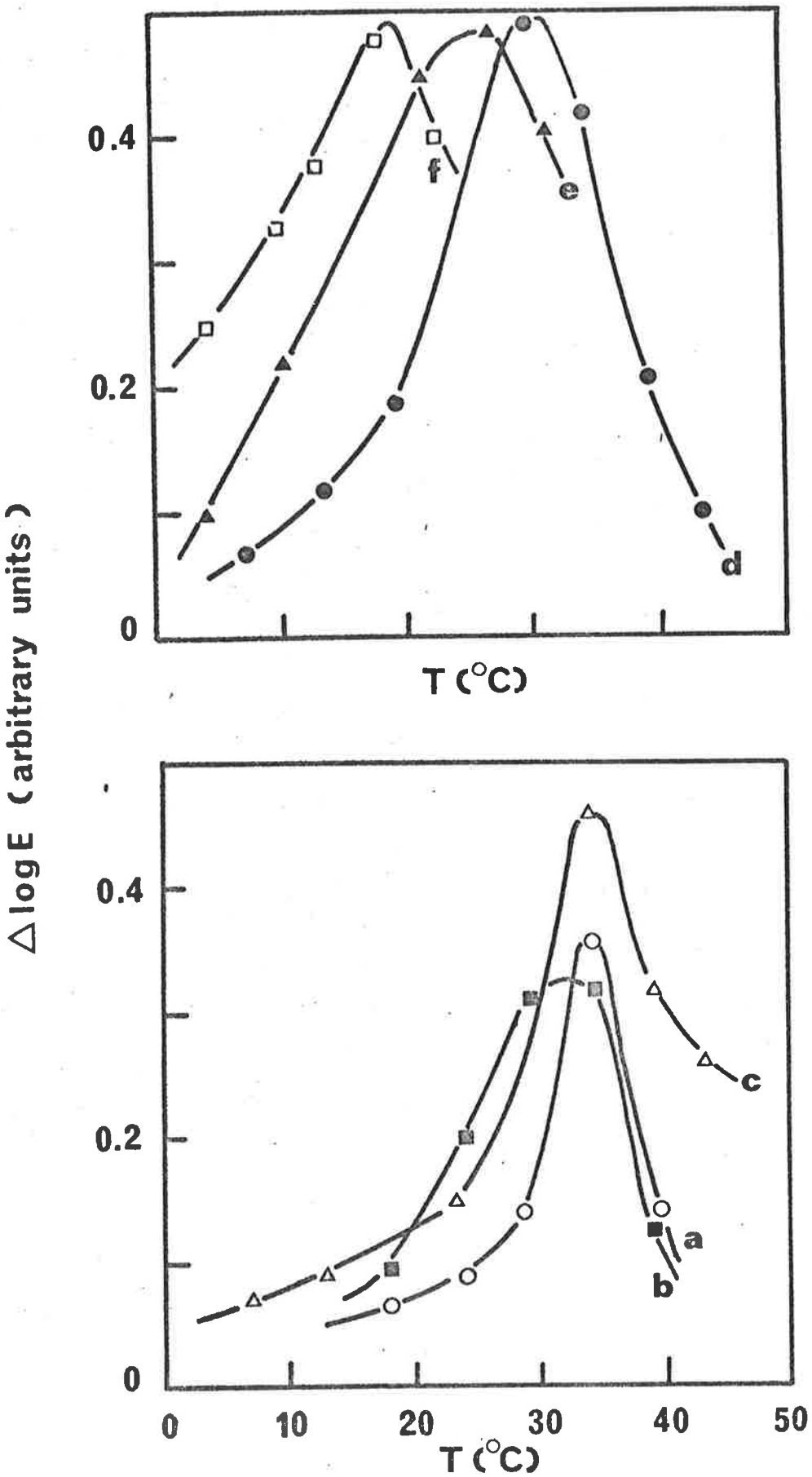

Fig.4.9 The slope of tangent of the stress relaxation curves vs. temperature. Δ log E is the difference of log E at log (t/sec) = 2 and log (t/sec) = 0.5 being the two extremes of the stress relaxation curves. The temperature at the maxima is determined as the glass transition temperature, T_{sg}.

ing the original work of Fox and Flory (70), the MW dependence T_{og}, is expressed by the following empirical equation

$$T_{og} = T_{og}(\infty) \quad K_{og} \, M_n^{-1} \tag{4.6}$$

where $T_{og}(\infty)$ = glass transition temperature, T_g, of dry polymer (containing 0% methanol) of infinite MW, $T_{og} = T_g$ of dry polymer and K_{og} = constant K_g for dry polymer.

According to Bueche (71), the constant K_g is proportional to the free volume created by the chain ends. Further development of molecular nature of K_g was contributed by Turner (72). This problem will be reviewed and discussed in Section 4.4.3.2.

The experimental data fitted a straight line (Fig.4.10) and using linear regression, $K_{og} = 6.5 \times 10^5$ and $T_{og}(\infty) = 399.34$ K. Values of K_{og} and $T_{og}(\infty)$ reported by the other workers are listed in Table 4.6.

TABLE 4.6: Values of K_{og} and $T_{og}(\infty)$ for PMMA

$K_{og} \times 10^{-5}$	$T_{og}(\infty)$ (K)	MWD	Syndiotactic diad fraction	Source	Reference
2.1	387	Broad	Atactic	Bulk polymer	(74)
2.9	387	"	0.75	irradiated	(75)
3.3	-	"	-	"	(72)
3.4	399	"	0.82	"	
4.3*	433*	-	1	-	(75)
6.4	399	$\frac{M_w}{M_n} = 1.2$	0.80	Bulk polymer	This work

* Extrapolated value

For a wide range of common polymers, Boyer (73) has found that a non-linear relationship exists between K_{og} and $T_{og}(\infty)$ and that the $T_{og}(\infty)$ increases with K_{og}. Although there has been no rigorous theoretical treatment to provide an insight into this relationship, there have been various attempted empirical interpretations. Boyer suggested that K_{og} might be proportional to $[T_{og}(\infty)]^n$

Fig.4.10 Plot of the glass transition temperature vs. M_n^{-1} (a) narrow MWD PMMA (0% methanol) (T_{og}) and (b) methanol -equilibrated narrow MWD PMMA (T_{sg}).

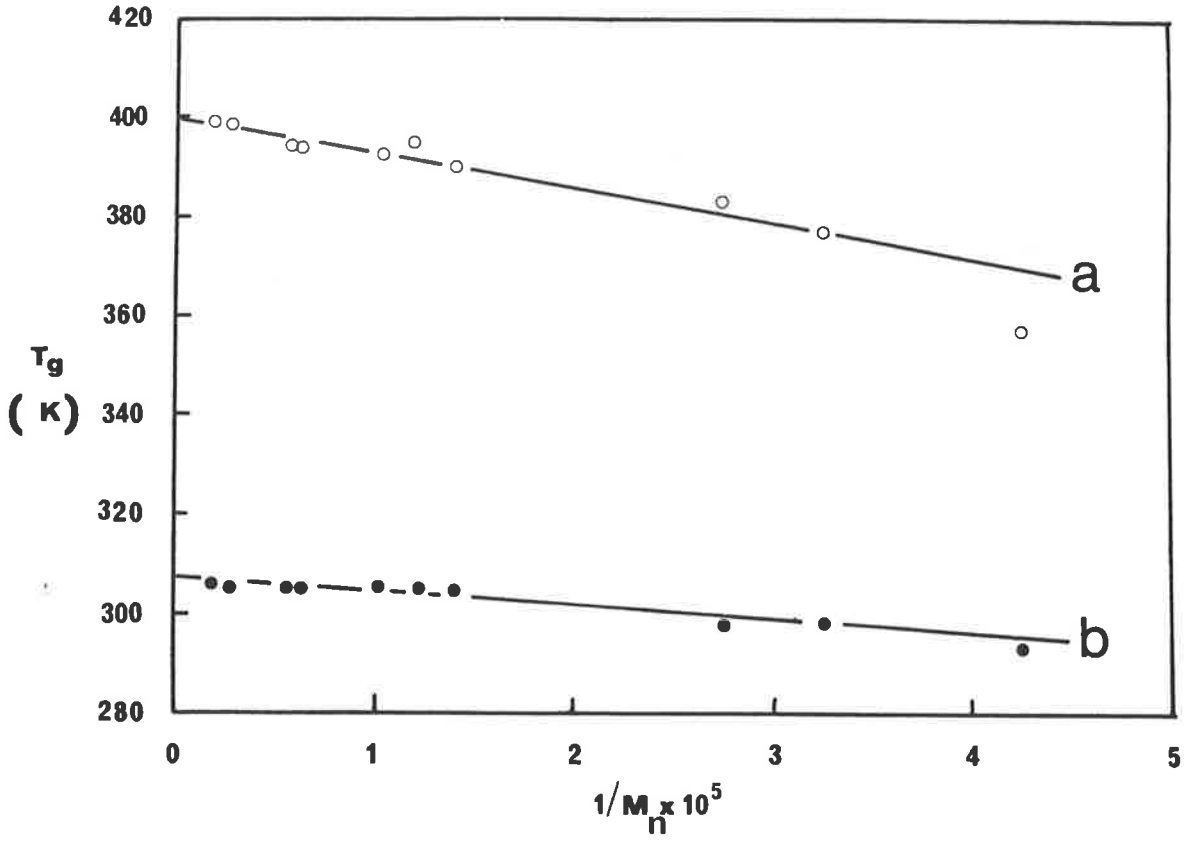
420
400
380
360
340
320
300
280
T_g
(K)
0
1
2
3
4
5
$1/M_n \times 10^5$
a
b

where n = 2 to 4, but was unwilling to comment on the significance of n.

It is reasonable to suggest that the unusually high value of K_{og} in this work, 6.4×10^5 with $T_{og}(\infty)$ = 399 K, corresponds to high power of n in the K_{og} vs. $T_{og}(\infty)$ relationship, whereas Thompson's result (75) for irradiated PMMA of the same syndiotacticity, $K_{og} = 3.4 \times 10^5$ and $T_{og}(\infty)$ = 398 K (Table 4.6), corresponds to low power of n. The high value of n for our specimens may be due to the narrow MWD. Because of the empirical nature of Boyer's K_{og} vs. $T_{og}(\infty)$ relationship, however, the influence of MWD on the value of n, at this moment, can not be clarified.

Another explanation of the high value of K_{og} can be based on Cowie's treatment (76). Cowie found that a plot of T_{og} vs. x_s, the number of mainchain segment , gave a straight line at lower values of x_s, i.e. $x_s < x_{si}$, where x_{si} is a characteristic value of x_s. If an asymtote indicated by $T_{og}(\infty)$, is drawn through the data at high values of x_s, i.e. $x_s > x_{si}$, Cowie found that the value at the point at intersection, x_{si}, was related to $T_{og}(\infty)$ by

$$T_{og}(\infty) = a \log x_{si} + b \qquad (4.7)$$

where a,b = constants (Fig.4.11).

The characteristic MW, M_i*, for the narrow MWD PMMA in this work is compared to the corresponding results for poly(α-methyl styrene) (PαMS) and other PMMA (74,76).

From Table 4.7, high values of M_i correspond to high values of T_{og} and K_{og}. Again, because of the empirical nature of the T_{og} vs. M_i (or x_{si}) relationship, the molecular properties represented by M_i which effect the value of K_{og} are still not revealed.

* M_i corresponds to the characteristic number of main chain segment, x_{si}. For PMMA and PαMS, each monomer unit consists of two segments, therefore $M_i = x_{si} M_u/2$, where M_u is MW of monomer.

Fig.4.11 Plot of the glass transition temperature, T_{og}, vs. the number of mainchain segment, x_s, for various PMMA. This work (●), Cowie's data (76) (Δ) and Beever and White's data (74) (▼).

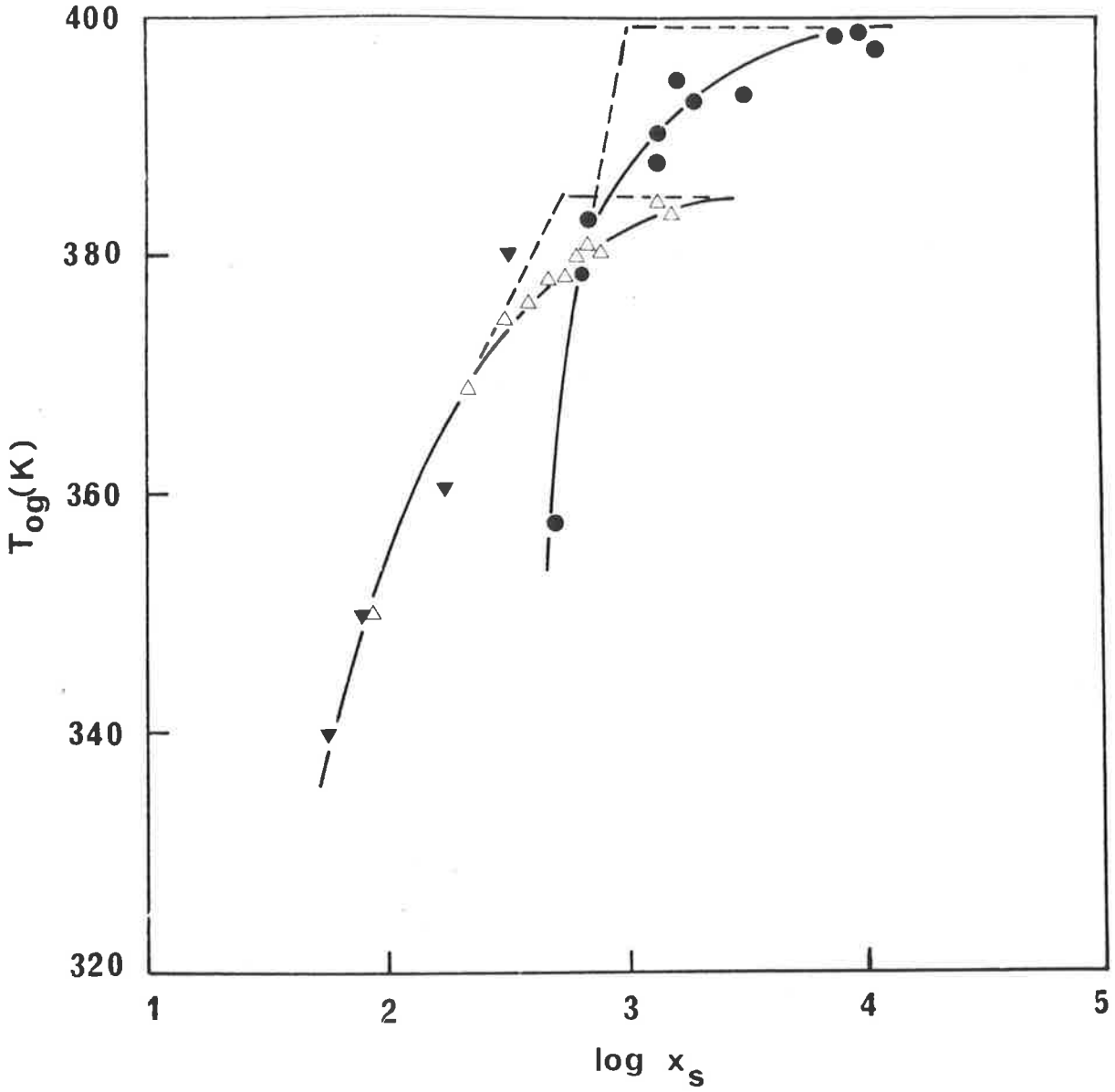
400
380
360
340
320
T_{og}(K)
1
2
3
4
5
log x_s

TABLE 4.7: Relationship of K_{og} and M_i according to Cowie (76)

Polymer	$T_{og}(\infty)$ (K)	M_i	$K_{og} \times 10^5$	Reference
PαMS	440	4.7	35,400	(76)
PMMA	385	2.4	21,340	(76)
PMMA	387	2.1	28,000	(74)
PMMA	899	6.5	50,000	this work

4.4.2 Calculation of Molecular Weight between Entanglement Loci

The effect of absorbed solvent on the MW between entanglement loci, M_e, or the critical MW, M_c is an important factor to predict the solvent cracking or crazing behaviour of polymers. As will be discussed in later Chapters, a criterion for cracking or crazing of polymers developed on the basis of the entanglement density requires determination of M_c. In this Section, a method of M_c calculation is proposed and the value of M_{sc}, the critical MW of plasticized PMMA, will be estimated.

The critical MW of entanglement M_c defined from zero shear viscosity, η_o, measurements (77) is understood to indicate the onset of chain entanglement. The ratio of M_c/M_e varies from 2 in polystyrene and PMMA of $M_w \gtrsim 200{,}000$ to 6 in PMMA of $M_w = 45{,}200$ (68,69). Now, the value of M_{sc} for solvent-equilibrated polymers can be related to M_{oc} of non-solvent containing polymers and the volume fraction of polymer ϕ_p by the empirical relation

$$M_{sc} = M_{oc}/\phi_p$$

Although the equation can simply show how M_{sc} varies with ϕ_p as a first approximation, the equation has been found to be correct only over a limited range of ϕ_p and it will be more direct to calculate M_e from the height of the rubbery plateau modulus E^o_{eN}.

Kamei and Onogi (78) have used this approach to investigate the concentration dependence of M_{sc} for concentrated solutions of polystyrene.

Using a similar method of calculation to that employed in the estimation of permanent crosslinks in rubbers, the height of the rubbery plateau E^o_{eN} can be related to the average MW, M_e, between entanglement loci by

$$E^o_{eN} = 3g_N \rho_p RT/M_e \qquad (4.8)$$

where g_N = a constant near unity, ρ_p = the density of polymer and R = the gas constant (67). In methanol, ρ_p is replaced by $\rho_s W_p$, where ρ_s = the density of methanol-equilibrated polymers and W_p = the weight ratio of original polymer to methanol-equilibrated polymer. Substituting the following stress relaxation data obtained from the rubbery region of narrow MWD PMMA (high MW) $E^o_{eN} = 3.72 \times 10^6$ dyne cm^{-2} at T = 316 K and $\rho_s W_p = 0.89$ g cm^{-3} (see Appendix 2) into Eq.4.6, we obtain

$$M_e = 19{,}000$$

In this case, as M_e was determined in the high MW range, it was found that $M_{sc}/M_e = 2$ (68-69) or $M_{sc} = 38{,}000$. The corresponding value for narrow MWD PMMA, M_{oc} is reported to be 27,500 to 31,500 by various workers (77) and accordingly it can be seen that the presence of solvent has the effect of increasing the MW between entanglement loci.

The value of M_{sc} has been calculated from Eq.4.8 using the modulus corresponding to the height of the rubbery plateau (Fig.4.7). It can also be seen from Fig.4.7 that the master curves of high MW PMMA join in the glass transition zone. As the MW decreases to values smaller than M_{sc}, the curves shift to lower times on $\log(t/a_T)$ scale and the rubbery zone disappears. However, this is not unique to solvent-PMMA system, similar phenomena were also

observed by Onogi et al. (68-69) for polystyrene and PMMA.

While the narrow MWD PMMA show the existence of the rubbery zone in the stress relaxation curves in the range of MW, $M_w \lesssim 71,000$ (Fig.4.7), the minimum MW possessing the rubbery zone in broad MWD commercial PMMA is limited at higher MW, i.e. sample MMW of $M_w = 220,000$ (Fig.4.8), compared with $M_w = 71,000$ of narrow MWD PMMA. Further examination of the master curve of MMW reveals that although the methanol uptake in this sample at equilibrium is close to narrow MWD PMMA of high MW ($W_1/W_2 = 0.22$, Fig.4.2), the height E^o_{eN} of the rubbery zone for MMW is lower than that for narrow MWD PMMA. From Fig.4.8, E^o_{eN} for MMW is 7.94×10^5 dyne cm^{-2}, and thus M_{sc} is calculated to be equal to 178,000 for this commercial PMMA sample. The high value of M_{sc} implies that in the presence of solvent the entanglement density is so low that the entanglement networks cannot be formed in MMW so easily as in narrow MWD samples.

The existence of the rubbery zone, i.e. the capacity of forming the entanglement networks, playing a crucial role in understanding fracture process, will be discussed in relating to cracking and crazing behaviours in later Chapters.

4.4.3 The Glass Transition Temperature, T_{sg}, of Methanol Equilibrated PMMA

4.4.3.1 The Effect of Temperature on the Free Volume

Before commencing the discussion of the T_{sg} of methanol-equilibrated PMMA, it is worthwhile introducing the concept of iso-free volume to facilitate the evaluation of some parameter relevant to the solvent-induced depression of T_g. This iso-volume concept was initially used by Fox and Flory (70) to explain MW dependence of T_g for polystyrene. Later, Doolittle (79) developed the empirical relation between viscosity, η, and fractional free volume, f,

$$\ell n\ \eta = A + B/f \qquad (4.9)$$

where $f = (\nu - \nu_o)/\nu_o$

and A,B = constants

ν = specific real volume of liquid

ν_o = specific occupied volume of liquid

Using the Doolittle equation, one can modify the WLF theory of time-temperature superposition and express the shift factor a_T as

$$\log a_T = \frac{(-B/2.303\ f_r)(T - T_r)}{f_r/\alpha_f + (T - T_r)} \qquad (4.10)$$

where f_r = fractional free volume at T_r and α_f = free volume temperature coefficient. Comparison of Eq.4.10 with Eq.4.5 yields $c_1^r = -B/2.303\ f_r$ and $c_2^r = f_r/\alpha_f$. The effect of temperature on the fractional free volume, f, is expressed by

$$f = f_g + \alpha_f (T - T_g) = \alpha_f (T - T_o) \quad T \geq T_g \qquad (4.11)$$

where f_g = the fractional free volume at T_g, T_o = the zero-free-volume temperature known as the Vogel temperature and α_f = the free volume coefficient. From the previous results of $c_1^{412} = 13.32$ and $c_2^{412} = 81.31$ (at $T_r = 412$ K) (Section 4.3.2), $T_g \equiv T_{sg} = 303$ K (Section 4.3.2) and by assuming B = 1, the following values were obtained

$$\alpha_f = 4.00 \times 10^{-4}\ \text{deg}^{-1}$$

$$f_{412} = 0.0325$$

$$T_o = 231\ \text{K}$$

$$f_g = 0.032$$

The calculated value of f_g at $T_{sg} = 303$ K is fairly consistent with the universal value $f_g = 0.026$. The value of α_f, although determined from mean data on a range of methanol-equilibrated narrow MWD polymers, has the same magnitude reported by Masuda et al. (69) for narrow MWD PMMA and thus suggests that the presence of methanol

does not affect the magnitude of f_g and α_f. In other words, the solvent translationally shifts the curve of f vs. T for dry PMMA to the left hand side by a distance of $(T_{og} - T_{sg})$ where T_{og} is the glass transition temperature of dry PMMA (Fig.4.12).

4.4.3.2 The Depression of the Glass Transition Temperature. Free Volume Viewpoint.

According to the Simha-Boyer theory (80), the T_g and the temperature coefficient β of T_g are related by the following equation

$$(\beta_\ell - \beta_g)\, T_g = 0.113 \qquad (4.12)$$

where

$$(\beta_\ell - \beta_g) = \Delta\beta = \left(\frac{\partial v}{\partial T}\right)_{liquid} - \left(\frac{\partial v}{\partial T}\right)_{glass}$$

is an equation which is obeyed by all glass forming liquids. Although the "universal" value of 0.113 is open to criticism and modification (81-82), it has been found that for the majority of linear polymers, this relation is tolerably well obeyed (83-84). It is of interest to compare the constant 0.113 with that calculated from the experimental data. By definition

$$\Delta\beta = \alpha_f\, v_g$$

where v_g is the specific volume at T_g and will be equal to the inverse of the density ρ_s of methanol-equilibrated PMMA (ρ_s = 1.09, see Appendix 2). By utilizing $\alpha_f = 4 \times 10^{-4}$ deg^{-1}, T_g = 303K and v_g = 1/1.09, the calculated constant for Eq.4.12 is 0.112. This value is in agreement with Simha-Boyer's constant of 0.113 and suggests Eq.4.12 can also be applied to the PMMA-methanol system.

The plot of the T_{sg} of the methanol-equilibrated PMMA vs. M_n^{-1} is shown together with the T_{og} in Fig.4.10. The data are fitted to the Fox-Flory (FF) equation to give

$$T_{sg} = T_{sg}(\infty) - K_{sg}\, M_n^{-1} \qquad (4.13)$$

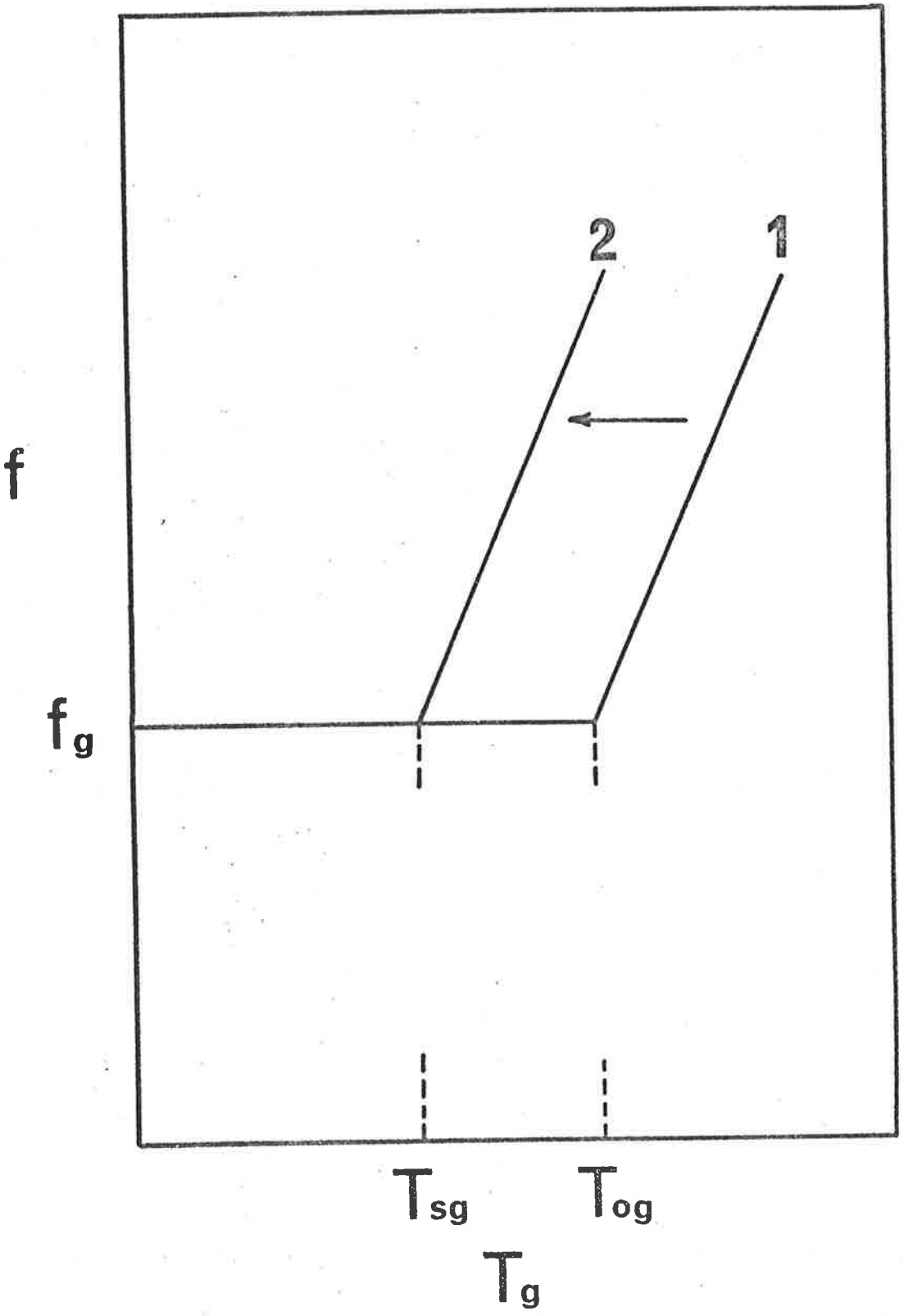

Fig.4.12 A schematic graph illustrating the shift of the fractional free volume f vs. temperature T curve to lower temperature by a distance of (T_{og}-T_{sg}) in the presence of solvent. (1) Dry polymer (0% solvent), (2) solvent-equilibrated polymer.

The physical meaning of K_{og} (Eq.4.6) and K_{sg} (Eq.4.13) will be referred later, but at this stage the analysis is restricted to an appreciation of why the addition of methanol to PMMA causes a reduction in the slope K_g (Fig.4.10). Qualitatively, K_{sg} and K_{og} can be understood by employing the concept of the flex energy, ΔE, a parameter of chain stiffness, proposed by Gibbs and Di Marzio (85). It was shown that $\Delta E/kT_g$ is equal to a constant and therefore

$$T_g \propto \frac{\Delta E}{k} \tag{4.14}$$

where k = Boltzmann's constant. This idea was related to the packing capability of the macromolecule chain (86). Polymers with stiffer chain backbones (high T_g) have less efficient packing capability than that of polymers with flexible chain backbone (low T_g). The flex energy, ΔE, can be related to the steric hindrance factor (87), $\sigma_r \equiv \langle \bar{r}_o^2 \rangle^{\frac{1}{2}} / \langle \bar{r}_o^2 \rangle_f^{\frac{1}{2}}$ ($\langle \bar{r}_o^2 \rangle^{\frac{1}{2}}$ = imperturbed end-to-end distance of the chain, $\langle \bar{r}_o^2 \rangle_f^{\frac{1}{2}}$ = the end-to-end distance at the state of free rotation), the higher σ_r, the more restricted the molecule chain and the larger is ΔE. Comparing the T_g of two given MW, say M_n^1 and M_n^2, gives,

$$K_{og} = \left(T_{og}^1 - T_{og}^2\right) \Big/ \left(\frac{1}{M_n^2} - \frac{1}{M_n^1}\right)$$

and

$$K_{sg} = \left(T_{sg}^1 - T_{sg}^2\right) \Big/ \left(\frac{1}{M_n^2} - \frac{1}{M_n^1}\right)$$

or

$$K_{og} \propto \Delta T_{og} \tag{4.15a}$$

$$K_{sg} \propto \Delta T_{sg} \tag{4.15b}$$

Combining Eq.4.14 gives

$$K_{og} \propto \Delta T_{og} \propto \frac{\Delta (\Delta E_o)}{k} \tag{4.16a}$$

and

$$K_{sg} \propto \Delta T_{sg} \propto \frac{\Delta (\Delta E_s)}{k} \tag{4.16b}$$

where M_n^i = number-average MW of sample i

T_g^i = T_g of sample i

ΔE_o, ΔE_s = flex energy of dry polymer (0% solvent) and solvent-equilibrated polymer, respectively.

Consequently, the lower value of K_{sg} compared with K_{og} suggests that the difference in the flex energy $\Delta(\Delta E_s)$ between high and low MW in methanol is smaller than the corresponding difference $\Delta(\Delta E_o)$ in absence of methanol. In other words, methanol improves the mobility of the long chain molecules to allow an increase in the packing capability close to that in the short chain molecules.

In quantitative terms, the decrease in K_g due to the presence of methanol can be explained by the combination of FF equation (Eq.4.6) and Kelley-Bueche (KB) equation (88) (Fig.4.13). The KB equation predicts the depression of T_g by an addition of diluent on the assumption that the free volumes of polymer and diluent are additive. The equation is expressed as

$$T_{sg} = \{(\alpha_p\phi_p T_{pg} + \alpha_d\phi_d T_{dg})/(\alpha_p\phi_p + \alpha_d\phi_d)\} \qquad (4.17)$$

where the subscripts d and p identify the diluent and polymer, and ϕ is the volume fraction.

T_{pg} is expressed by

$$T_{pg} \equiv T_{og} = T_{og}(\infty) - K_{og} M_n^{-1} \qquad (4.6)$$

can be substituted into Eq.4.13 to give

$$T_{sg} = \frac{\alpha_p\phi_p T_{og}(\infty) + \alpha_d\phi_d T_{dg}}{\alpha_p\phi_p + \alpha_d\phi_d} - \frac{\alpha_p\phi_p K_{og}}{\alpha_p\phi_p + \alpha_d\phi_d} \qquad (4.18)$$

and by comparison with Eq.4.13, we obtain

$$T_{sg}(\infty) = \frac{\alpha_p\phi_p T_{og}(\infty) + \alpha_d\phi_d T_{dg}}{\alpha_p\phi_p + \alpha_d\phi_d} \qquad (4.19)$$

and

$$K_{sg} = \frac{\alpha_p\phi_p K_{og}}{\alpha_p\phi_p + \alpha_d\phi_d} \qquad (4.20)$$

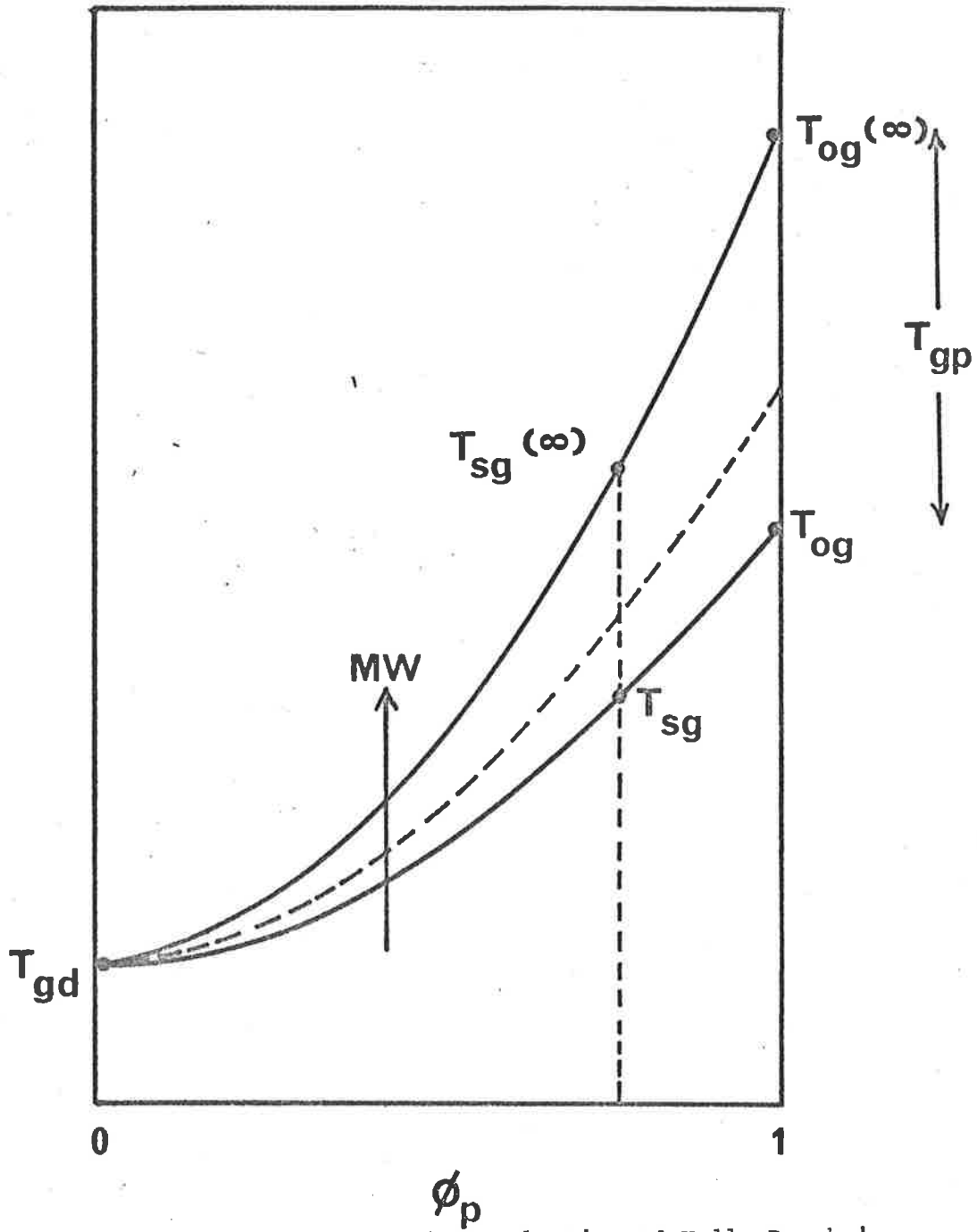

Fig.4.13 Schematic diagram of Fox-Flory's and Kelly-Bueche's equations. The upper curve represents the curve of infinity MW. Difference in (T_{og} (∞) - T_{og}) for dry polymer (ϕ_p = 1) is larger than the corresponding (T_{sg} (∞) - T_{sg}) for plasticized polymer.

Usually, in the application of KB equation, the temperature coefficient of expansion of diluent, α_d, is considered an adjustable parameter to fit the theoretical curve with experimental data (71). However, using the results from the stress relaxation tests, one can evaluate α_d and use this value to determine theoretical values of $T_{sg}(\infty)$ (Eq.4.19) and K_{sg} (Eq.4.20). The calculation of α_d is described below.

From stress relaxation results, the free volume fraction is expressed by

$$f = \alpha_f (T - T_o) \tag{4.11}$$

where $\alpha_f \equiv \alpha_p = 4 \times 10^{-4}$ deg^{-1} and $T_o = 231$ K (Section 4.4.3.1). By assuming that the free volume is additive in plasticized polymer, Kelly and Bueche (88) suggested that the free volume fraction of plasticized polymer can be expressed by

$$f = 0.025 + \alpha_p(T - T_{gp})\nu_p + \alpha_d(T - T_{gd})\nu_d \tag{4.21}$$

Equating Eq.4.11 with Eq.4.21 and substituting $\phi_p = 0.76$ (from absorption data), $T_{dg} = 106$ K (89-90) and assuming $T = T_{pg} = 400$ K, α_d was calculated to be 6×10^{-4} deg^{-1}. This value was substituted into Eqs.4.19 and 4.20 to give $T_{sg}(\infty)$ and K_{sg} (Table 4.8).

TABLE 4.8: Values of $T_{sg}(\infty)$ and ratio K_{og}/K_{sg} with $\alpha_p = 4\text{x}10^{-4}$ deg^{-1} and $\alpha_d = 6\text{x}10^{-4}$ deg^{-1}

	Experimental	Theoretical
$T_{sg}(\infty)$ (K)	303	300
K_{og}/K_{sg}	1.83	1.52

In contrast to previous studies (71) where the temperature coefficient of diluent, α_d, was adjusted so that the theoretical values fitted the experimental data, α_d of this work was determined directly from the results of the stress-relaxation test (Eq.4.11) and

from the Kelly and Bueche's assumption of additive free volume (Eq. 4.21) The calculation of $T_{sg}(\infty)$ and K_{og}/K_{sg} from α_d and α_p gave results in good agreement with the experimental values. This implies that the T_g depression and MW dependence of T_g can be predicted by the combination of the FF and KB equations (Eq.4.18).

Furthermore, Bueche (71) has re-expressed the FF equation in terms of the free volume contributed by chain ends. As the MW decreases the number of chain ends in a unit volume increase causing a depression of $T_g(\infty)$ by an amount of $[T_g(\infty) - T_g]$. If each end contributes θ cm^3 of free volume, the number of chain ends per cm^3 volume, $2\rho_p N_A/M$, contribute $\theta(2\rho_p N_A/M)$, that is

$$\theta(2\rho_p N_A/M) = \Delta\beta(T_g(\infty) - T_g) \qquad (4.23)$$

Rearranging the FF equation,

$$T_g(\infty) - T_g = K_g/M \qquad (4.24)$$

Comparing Eqs.4.23 and 4.24, K_g is expressed by

$$K_g = \rho_p N_A \theta/\Delta\beta \qquad (4.25)$$

According to Turner (72), however, for MW larger than M_c where entanglement networks exist, an entanglement will reduce free volume by an amount θ_1. Therefore, as the MW decreases, the free volume is increased by the formation of chain ends and by the "release" of entanglements. That is, θ cannot be considered as the free volume contributed by the chain ends only, but as the total free volume of the contribution from the chain ends, $2\theta_2$, and from the release of entanglement, θ_1. Thus for $M > M_c$ the free volume is given by

$$\theta = \theta_1 + 2\theta_2 \qquad (4.26)$$

Because the magnitude of θ_1 and θ_2 are of order of 10^{-2} nm^3 and 10^{-4} nm^3, respectively, for most amorphous polymers (including PMMA (72)), K_{og} and K_{sg} are not greatly influenced by the

free volume, $2\theta_1$, contributed by the chain ends. Consequently, the lower K_{sg} compared to K_{og} is mostly attributed to the reduction of θ_1 and it is plausible to assume the value θ_2 of 8×10^{-4} nm^3 (72) for PMMA to be the same in methanol equilibrated PMMA. The values of θ_1 can be calculated by using

$$K_{og} = 6.4 \times 10^5$$

$$K_{sg} = 3.5 \times 10^5$$

Density of methanol equilibrated PMMA $\rho_s = 1.09$ g cm^{-3}

$$\Delta\beta = 4 \times 10^{-4} \times 0.92 = 3.6 \times 10^{-4}$$

and $$\theta_2 = 8 \times 10^{-4} \text{ nm}^3$$

The results are listed in Table 4.9.

TABLE 4.9: Values of θ_1 for PMMA and methanol - equilibrated PMMA

	PMMA	PMMA + MeOH
$\theta_1(nm^3)$	2.30×10^{-2}	1.75×10^{-2}

The above results were calculated from the data of narrow MWD PMMA showing a constant equilibrium uptake, i.e. polymers in the range $35{,}000 \lesssim M_w \lesssim 550{,}000$. The data of sample A10, $M_w = 23{,}500$ was discounted because of the abnormally large uptake of methanol. The results in Table 4.9 show that there is a reduction in the free volume of the polymer chain in the presence of solvent.

On the whole, the free volume concept has changed the depression of T_g and the MW dependence of T_g via the combination of the FF and the KB equations. The smaller value of K_{sg} compared with K_{og} is attributed by the reduction of free volume in presence of methanol. Although the free volume concept was successfully applied to understand the problems, there are some deficiencies that need to be pointed out. Firstly, the KB equation is in agreement with experimen-

tal results only at low solvent equilibrium concentrations. Andrews et al. (60) have reported a considerable deviation from the theoretical curve at higher solvent uptake in various alcohols. These workers asserted that the theoretical curve would not fit the experimental data in the region of $\phi_p < 0.9$. However, it is difficult to determine from their data the value of ϕ_p at which the experimental curve deviates from the theoretical curve because the temperature coefficients α_d and α_p were not determined. The effect of different values of α_d and α_p on the curvature of the KB theoretical plot are shown in Fig.4.14. The T_g at the equilibrium uptake of $\phi_p = 0.76$ in this work is in agreement with the theoretical curve employing the values $\alpha_d = 6 \times 10^{-4} deg^{-1}$ and $\alpha_p = 4 \times 10^{-4} deg^{-1}$ (see calculated results in Table 4.8). The calculation of the T_g depression involving higher uptake of methanol must be treated with caution. Secondly, in contrast to the smooth T_g plot for the KB equation, Kovacs and co-workers (95) found that for some polymer-diluent systems, a discontinuity occurred in the T_g vs. ϕ plot.

The inability of the KB equation to accurately describe the T_g behaviour at higher solvent uptake and to explain the discontinuity in T_g vs. ϕ plot is probably due to the deficiency in the free volume concept. The free volume concept has been recently criticised because it fails to include the important intra- and intermolecular forces arising from polymer-polymer, polymer-diluent and diluent-diluent interactions (96).

4.4.3.3 The Depression of the Glass Transition Temperature. Thermodynamic Viewpoint.

Besides the free volume concept, the T_g has also been discussed in terms of the configurational entropy of the polymer chains. This concept was initially developed by Gibbs and DiMarzio (85,91) to predict the MW dependent T_g and the T_g depression in the presence of a plasticizer. Based on Gibbs and DiMarzio's idea of the glass tran-

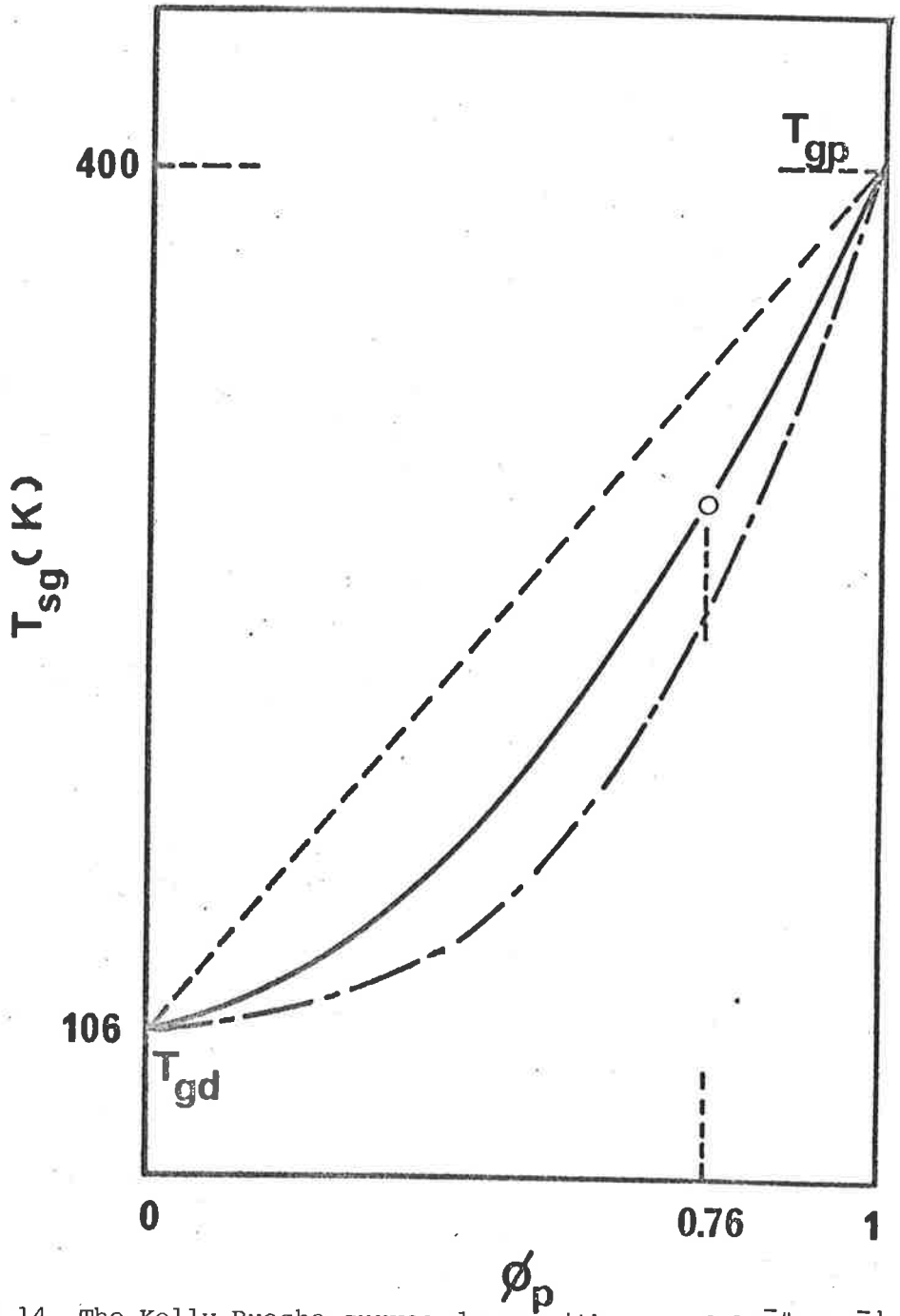

Fig.4.14 The Kelly-Bueche curves drawn with $\alpha_d = 6x10^{-4}$ deg^{-1} and $\alpha_p = 4x10^{-4}$ deg^{-1} (solid line), the straight line with $\alpha_d = \alpha_p = 4x10^{-4}$ deg^{-1} (---), and the curve with $\alpha_d > 6x10^{-4}$ deg^{-1} and $\alpha_p = 4x10^{-4}$ deg^{-1} (.-.-). The glass transition temperature ($\phi_p = 0.76$) (○) is in agreement with theoretical value.

sition temperature and the configurational entropy relationship, Chow (92) has proposed a simpler theory of the T_g depression by using the Bragg-Williams approximation (93) to calculate the configurational entropy. It is also noted that the configurational entropy is also the central part of the Flory-Huggins (FH) theory for concentrated polymer solutions. The configurational entropy resulted from the FH theory can be related to the T_g in the same way as done by Chow (92).

Although the experimental data are limited to one solvent (methanol) at one equilibrium uptake, it is of interest to compare the experimental results of the T_g depression with the theoretical values of Gibbs and DiMarzio (GD) theory, Chow's theory and FH theory. Furthermore, the effect of other factors such as the size and MW of penetrants, on the T_g depression is discussed to give an insight into the difference between these theories.

Before embarking on the discussion, it is worthwhile to review the background of the theories. According to the Gibbs-DiMarzio theory (85), there is a loss of configurational entropy at the glass transition expressed by

$$S_c = S_{liquid} - S_{glass} \tag{4.27}$$

The relation between S_c and the heat capacity at constant temperature C_p is

$$S_c(T) = \int_{T_g}^{T} \Delta C_p\,(T)\, d\,\ell n\, T \tag{4.28}$$

where ΔC_p is the difference in heat capacity between the supercooled liquid and glass. Chow developed his own theory on the assumption that the entropy of the polymer $S_{glass}\,(0,T)$ and that of the plasticized polymer $S_{glass}\,(N,T)$ were equal to zero. Chow derived the following equation

$$\ell n\left(\frac{T_{sg}}{T_{og}}\right) = -\frac{1}{\Delta C_p}\left[S_{liquid}\ (N,T) - S_{liquid}\ (0,T)\right] \qquad (4.29)$$

Using the Bragg-Williams approximation (93), Chow calculated the possible configuration of the diluent molecules randomly distributed in lattice sites and these evaluate the energy in Eq.4.22 to give

$$\ell n\left(\frac{T_{sg}}{T_{og}}\right) = \beta_c[\gamma(1-\gamma)\ \ell n(1-\gamma) + \gamma\,\ell n\,\gamma] \qquad (4.30)$$

and γ is expressed by

$$\gamma = \frac{V_u}{ZV_d}\ \frac{\phi_d}{1-\phi_d} \qquad (4.31)$$

where V_u, V_d = the molar volumes of monomer unit and diluent, respectively, ϕ_d = the volume fraction of the diluent and Z = the lattice coordinate number.

β_c is expressed by

$$\beta_c = Z\ R/m_u\Delta C_{pp} \qquad (4.32)$$

where R = gas constant and m_u = mass of monomer unit and ΔC_p = $m_p\Delta C_{pp}$ (m_p = mass of polymer), the excess transition isobaric specific heat of polymer.

The depression of the glass transition of PMMA by methanol can be evaluated from Eq.4.30 in terms of T_{sg}/T_{og} by substituting the following values: m_u = 100.12 g mol^{-1}, V_u = 106.51 $cm^3 mol^{-1}$, Z = 2, ΔC_p = 0.07 cal $g^{-1}deg^{-1}$ (53,94), ϕ_d = 0.24 and V_d = 40.56 cm^3 mol^{-1}. The results for two extreme MW, M_w = 500,000 and M_w = 31,000 are shown in Table 4.10.

The difference in entropy of Eq.4.27 can be expressed by the Flory-Huggins (FH) theory of the entropy of mixing.

$$S_{liquid}\ (N,T) - S_{liquid}\ (0,T) = \Delta S_{mix} = R[N_p\ell n\phi_p + N_d\ell n\phi_d] \qquad (4.33)$$

where N_p and N_d are the number of moles of polymer and diluent, respectively. Combining Eqs. 4.29 and 4.33 gives

$$\ln\left(\frac{T_{sg}}{T_{og}}\right) = \frac{R}{\Delta C_p}\left[N_p \ln\phi_p + N_d \ln\phi_d\right] \qquad (4.34)$$

Values of T_{sg}/T_{og} from the above equation (see Appendix 3 for detailed calculation) are compared with Chow's equation (Eq.4.30), DiMarzio-Gibbs (DG) theory and the experimental results in Table 4.10.

TABLE 4.10: Theoretical and experimental values of T_{sg}/T_{og} at $\phi_p = 0.76$

M_w	Experimental	Chow	DG	FH
500,000	0.763	0.680	0.600	0.757
31,000	0.790	0.680	0.600	0.757

From Table 4.10, the theoretical value of the modified FH theory shows a better agreement with the experimental results than the Chow and DG theories, but neither theory reveals the MW dependent nature of the glass transition depression. The theoretical value derived from the DG theory is based on the assumption that a methanol molecule occupies one lattice site, therefore if the methanol molecule is assumed to occupy more than one site, the theoretical value would have a larger value and be closer to the experimental result. However, from the magnitude of the MW or molar volume, the DG theory assumed that a styrene molecule unit occupies two lattice sites (MW = 100 g mol^{-1}) and therefore it is more logical to consider one lattice site for every methanol molecule (MW = 32.04 g mol^{-1}). The DG theory could show the general trend of the value T_{sg}/T_{og} with the volume fraction ϕ; but the theoretical value derived from the theory does not reveal a good agreement with experimental data. Furthermore, the MW dependent factor does not exist in the theory because it was developed on the assumption of infinite molecular weight.

Chow's and modified FH theories are essentially the same in nature; the only difference between the two lies in the manner of evaluating the configuration of arrangement. Chow used the Bragg-Williams approximation to calculate the possible configurations of solvent molecules on polymer lattice sites whereas the FH theory is concerned with the possible configurations of polymer molecules on the polymer-solvent mixture lattice sites. Although Chow suggested the Bragg-Williams approximation is most suitable approach to estimate the entropy of mixing in polymer-diluent system (Eq.4.27), the derived equation (Eq.4.30) is still dependent on a coordination number Z. This number is known to be dependent on the nature of the diluent in a polymer-diluent system (85,91). Furthermore, the calculated results are no closer to the experimental values than that from our modified FH theory.

As previously stated, the two equation (Chow's Eq.4.30 and FH's Eq.4.34) do not take into account the effect of MW because in the evaluation of the entropy of mixing by either the Bragg-Williams approximation or the FH theory it is implied that the process reaches a state of thermodynamic equilibrium whereas glass transition phenomena are known to possess some kinetic characters. Substitution of the MW in the range of $31{,}000 \lesssim M_w \lesssim 500{,}000$ did not change the value of T_{sg}/T_{og} by the third decimal place (Appendix 3). Again, as an attempt to reveal the MW dependence introduction of chain end effect into Eq.10 of Chow's paper (92) defining the number of lattice sites (NLS) did not give any substantial change in T_{sg}/T_{og} as shown in the following argument. According to Chow

$$NLS = Zm_p N_A n/M \qquad \text{(Eq.10 in (92))}$$

where m_p = mass of polymer

N_A = Avogadro's number

n = number of monomer units

M = MW of polymer

If the chain ends are taken into account

$$NLS = (nZ + 2)\frac{m_p N_A}{M}$$

because $nZ >> 2$, therefore

$$NLS \simeq Zm_p N_A n/M$$

Therefore, according to this approach, the effect of chain ends, i.e. the effect of MW, is almost negligible.

However, the thermodynamic approaches used in Chow's theory, the modified FH theory and the GD theory reveals a prediction, which the KB free volume theory failed to establish, that is, the size of solvent molecules affects the T_g depression. If the volume fraction and the density of solvent are held constant the larger the size of the solvent molecule, the less T_g is depressed. The T_g depression at constant $\phi_p = 0.76$ calculated by Chow's, the FH and the DG theory (with the DG theory, the theoretical values were taken from Fig.2 in Ref. (91) assuming that the flex energy of solvent molecules is equal to that of polymer molecules) with different sizes of plasticizer molecules are listed in Table 4.11 and shown in Fig.4.15. The size is described by the ratio of V/V_d, where V_d = the molar volume of methanol molecule and V = the molar volume of a given plasticizer

TABLE 4.11: The effect of the size of solvent molecule V/V_d on the glass transition depression T_{sg}/T_{og}

Size (V/V_d)	T_{sg}/T_{og} (Chow)	T_{sg}/T_{og} (DG)	T_{sg}/T_{og} (FH)
1	0.680	0.600	0.757
2	0.749	0.692	0.870
5	0.850	0.788	0.946
10	0.908	0.885	0.972

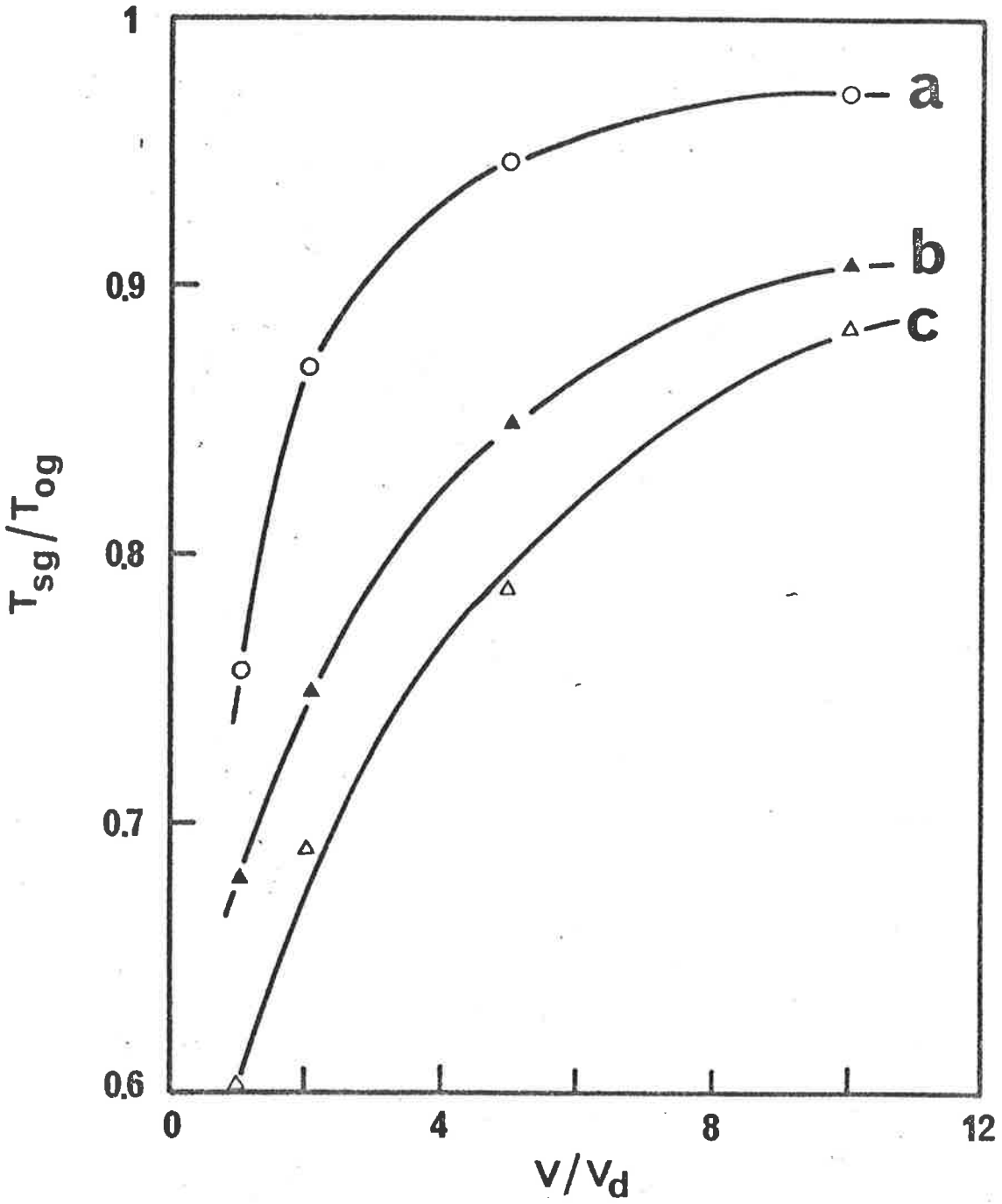

Fig.4.15 Effect of the molecular size of plasticizer on the glass temperature depression. (a) Flory-Huggins theory, (b) Chow's theory and (c) DiMarzio- Gibbs theory.

The effect of the size of penetrant molecule on the glass transition depression can be seen not only in alcohol-equilibrated polymer (60) but in the self-plasticization phenomena of polymer by oligomer or by blending high MW sample with low MW sample where oligomer or low MW sample acts as plasticizer. Nevertheless, a systematic experiment is required to clarify how the T_g is depressed and which theory is most applicable.

CHAPTER 5

MOLECULAR WEIGHT AND MOLECULAR WEIGHT DISTRIBUTION EFFECT ON FRACTURE TOUGHNESS IN AIR AND IN METHANOL

5.1 Introduction

The log K_c vs. log v diagrams of cracking in air, cracking and crazing in methanol will be established for various MW samples of narrow MWD PMMA and broad MWD PMMA. The effect of MW and MWD on the fracture toughness and the related analysis of fracture data will be discussed in this Chapter.

The discussion of experimental data is divided into two parts (a) the fracture process in air and (b) the fracture process in methanol. In each part, quantitative expressions are derived to describe the fracture toughness and the associated fracture mechanism in terms of the entanglement density. The analysis of the cracking data in air will involve calculation of the crack opening displacement (COD) as a function of MW and re-examination of the MW dependence of the fracture energy in comparison with data of previous reports. A theory for the relationship between the fracture energy and the number of entanglements is proposed to predict the effect of MW and MWD on the fracture energy in air. Data for fracture in methanol will be discussed in two parts (a) stress-cracking and (b) stress-crazing. Zhurkov's modified Rhee-Eyring theory will be used to calculate the potential energy of the cracking process. The LEFM concept will be also applied to the analysis of cracking and crazing in methanol to provide an understanding of the geometry of the craze, the energy absorbed by craze, and the time dependence of crazing behaviour.

Prior to the description of experimental procedures and discussion of results, a model of crack growth is proposed attempting to develop quantitative expressions between the crack tip velocity, v, and the strain rate, $\dot{\varepsilon}$, of craze fibrils along the craze.

5.2 A Model of Crack Growth

The Dugdale model of uniform stress distribution along the crack tip craze (35) has been applied successfully to the fracture of stressed polymers (100-102). The model has been developed further by Rice (103) and Riedel (104) to describe a distribution of plastic strain, i.e. the craze displacement profile within the craze zone. To provide more information about the character at the craze zone, an equation shall be derived for the strain rate in the zone as a function of the crack growth rate with the aid of a simple geometrical model (Fig.5.1).

Consider a craze zone of triangular geometry with a half-opening displacement of ℓ and length $(a - x_o)$ at time t. At time $(t + dt)$, ℓ increases a distance of $d\ell$ and the craze length $(a - x_o)$ increases da. Crack propagation occurs at a constant displacement, ℓ_o, and applied load relaxes with time. Considering the two similar triangles ACO, BCD, we obtain

$$\ell = \ell_o \left(\frac{a - x_o}{a}\right) \tag{5.1}$$

Similarly, the triangles AC'O and A'C'D give

$$\ell + d\ell = \ell_o \left(\frac{a + da - x_o}{a + da}\right) \tag{5.2}$$

From Eqs. (5.1) and (5.2), we obtain

$$\frac{\ell + d\ell}{\ell} = \left(\frac{a + da - x_o}{a + da}\right) \Big/ \left(\frac{a - x_o}{a}\right) \tag{5.3}$$

By assuming $da\, d\ell \simeq 0$, equation (5.3) becomes

$$\frac{d\ell}{\ell} = \frac{x_o}{a(a - x_o)}\, da \tag{5.4}$$

where $d\ell/\ell$ is the strain of the craze fibril.

According to Morgan and Ward (101), the real craze shape is not a distinct triangle, therefore in practice the straight edge AC is replaced by a curved edge AC'. The increase in craze length in time dt becomes da' instead of da (Fig.5.1) and the ratio da/da' is assumed to be

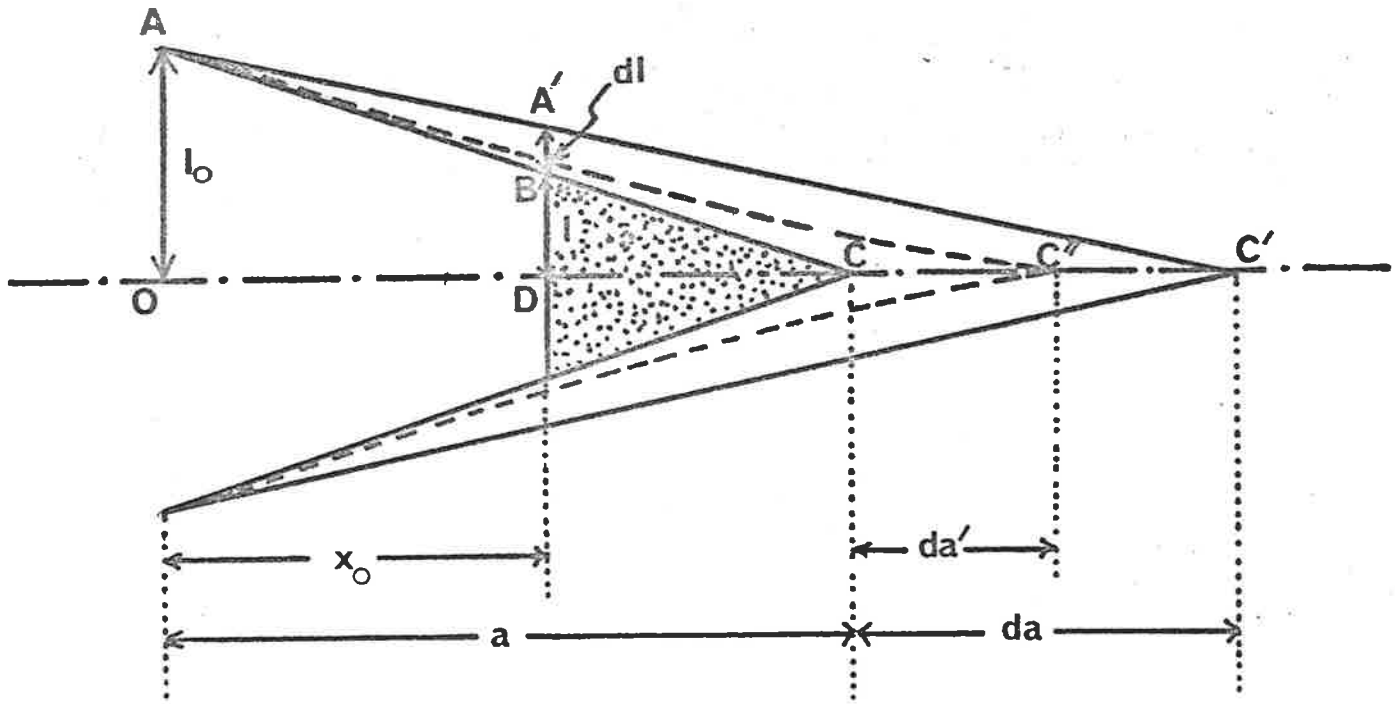

Fig.5.1 A model of crack growth. The shade area is craze matter.

$$da/da' = \alpha_g \tag{5.5}$$

where α_g is a constant. Using Eq.5.5, Eq.5.4 can be rewritten as

$$\frac{d\ell}{\ell} = \frac{x_o}{a(a - x_o)} \alpha_g \, da' \tag{5.6}$$

The strain rate, $\dot{\varepsilon}$, is obtained by dividing Eq.5.6 by dt

$$\dot{\varepsilon} = \frac{d\ell}{\ell dt} = \frac{x_o}{a(a - x_o)} \alpha_g \frac{da'}{dt}$$

$$= \frac{x_o \, \alpha_g}{a(a - x_o)} v \tag{5.7}$$

where v is the crack tip velocity.

Eq.5.7 can be developed for the strain rates at the front tip, the craze base* and the intermediate region between the tip and the base.

Application I: Relationship of $\dot{\varepsilon}$ and v at the front tip ($a \simeq x_o$)

Fracture in air is a typical example of this case where the crack is predominant in the breakdown process. Because $a \simeq x_o$, Eqs. 5.6 and 5.7 become

$$\frac{d\ell}{\ell} = \frac{\alpha_g}{\Delta} da' \tag{5.8}$$

where $\Delta = a - x_o$, is the craze length, and

$$\dot{\varepsilon} = \frac{\alpha_g}{\Delta} v \tag{5.9}$$

Based on Young and Beaumont's assumption that (105) at a period of time t, the bulk original material increases from zero strain to the yield strain, ε_y, while the crack propagates a distance of Δ. Integrating Eq.5.8 gives

$$\int_0^{\varepsilon_y} \frac{d\ell}{\ell} = \frac{\alpha_g}{\Delta} \int_0^{\Delta} da' \tag{5.10}$$

* Boundary between crack and craze matter.

Let $d\ell/\ell = d\varepsilon$ (ε is strain), Eq.5.10 becomes

$$\int_0^{\varepsilon_y} d\varepsilon = \frac{\alpha_g}{\Delta} \int_0^{\Delta} da'$$

or

$$\varepsilon_y = \alpha_g \tag{5.11}$$

where ε_y = 0.035 to 0.038 (97,105). Replacing α_g by ε_y and rewriting Eq.5.9 gives

$$\dot{\varepsilon} = \frac{\varepsilon_y}{\Delta} v \tag{5.12}$$

Fracture mechanics relates the craze length, Δ, with the COD, u_c, and the yield, ε_y, by the following expression (Chapter 2)

$$\Delta = \frac{\pi}{8} \frac{u_c}{\varepsilon_y} \tag{2.28}$$

Substituting this equation into Eq.5.12 gives

$$\dot{\varepsilon} = \frac{8}{\pi} \frac{\varepsilon_y^2}{u_c} v \tag{5.13}$$

The above equation gives exactly the same result as that derived by Young and Beautmont (105) and is close to Williams' result (97) based on viscoelastic analysis viz.,

$$\dot{\varepsilon} = \pi \frac{\varepsilon_y^2}{u_c} v$$

where the constant $8/\pi$ (Eq.5.13) was replaced by π.

Saito (106) determined $\alpha_g = 2$, but unfortunately this is much higher than the experimental values of 0.035 to 0.038 as reported by Williams (97) and Young and Beautmont (105).

Application II: Relationship of $\dot{\varepsilon}$ and v at the craze base of a long craze ($a >> x_o$)

Eq.5.7 can be written as the following for $a >> x_o$

$$\dot{\varepsilon} = \frac{\varepsilon_y x_o}{a^2} v \qquad a >> x_o \tag{5.14}$$

Application III: Relationship of $\dot{\varepsilon}$ and v in the region between the base and the tip.

This region is a general case where x_o is replaced by x in Eq.5.7 to give

$$\dot{\varepsilon} = \frac{\varepsilon_y x}{a(a - x)} v \qquad (5.15)$$

where x is the position of a particular craze fibril in the region of craze matter. From Eqs.5.13-5.15, the strain rate of the craze fibrils at a constant v is shown in Fig.5.2 a,b as a function of time, t, and craze length, Δ.

5.3 Experimental

5.3.1 Materials

Specimen sheets of narrow MWD PMMA and commercial PMMA polymer were prepared as described in Chapter 4. Sheets of dimension 6x6x1.2mm were used throughout the fracture test.

Blends:

Blending of high and low MW of narrow MWD PMMA at different ratios is an appropriate way to adjust the MWD. The components were dissolved in dichloromethane at a desired weight ratio and then precipitated in petroleum ether. Thereafter, the blend sheets were prepared in a manner described in Chapter 4. The components of the blends are high MW Ala (M_w = 450,000) and low MW A9 (M_w = 31,000). The low MW component was deliberately chosen as the MW close to the critical MW, M_c = 30,000 (70). Polymers of MW in this region, as will be seen later, show a much lower fracture toughness than that of high MW samples.

The MW of the blends can be calculated from the following formula, for weight average MW, M_w

$$M_w = \frac{\Sigma M_{wi} W_i}{\Sigma W_i}$$

for number average MW, M_n

$$M_n = \frac{\Sigma W_i}{\Sigma W_i / M_{ni}}$$

and W_i is the weight fraction of component i. Two blends, B1 (Ala: A9 = 9:1, by weight) and B3 (Ala: A9 = 7:3, by weight) were

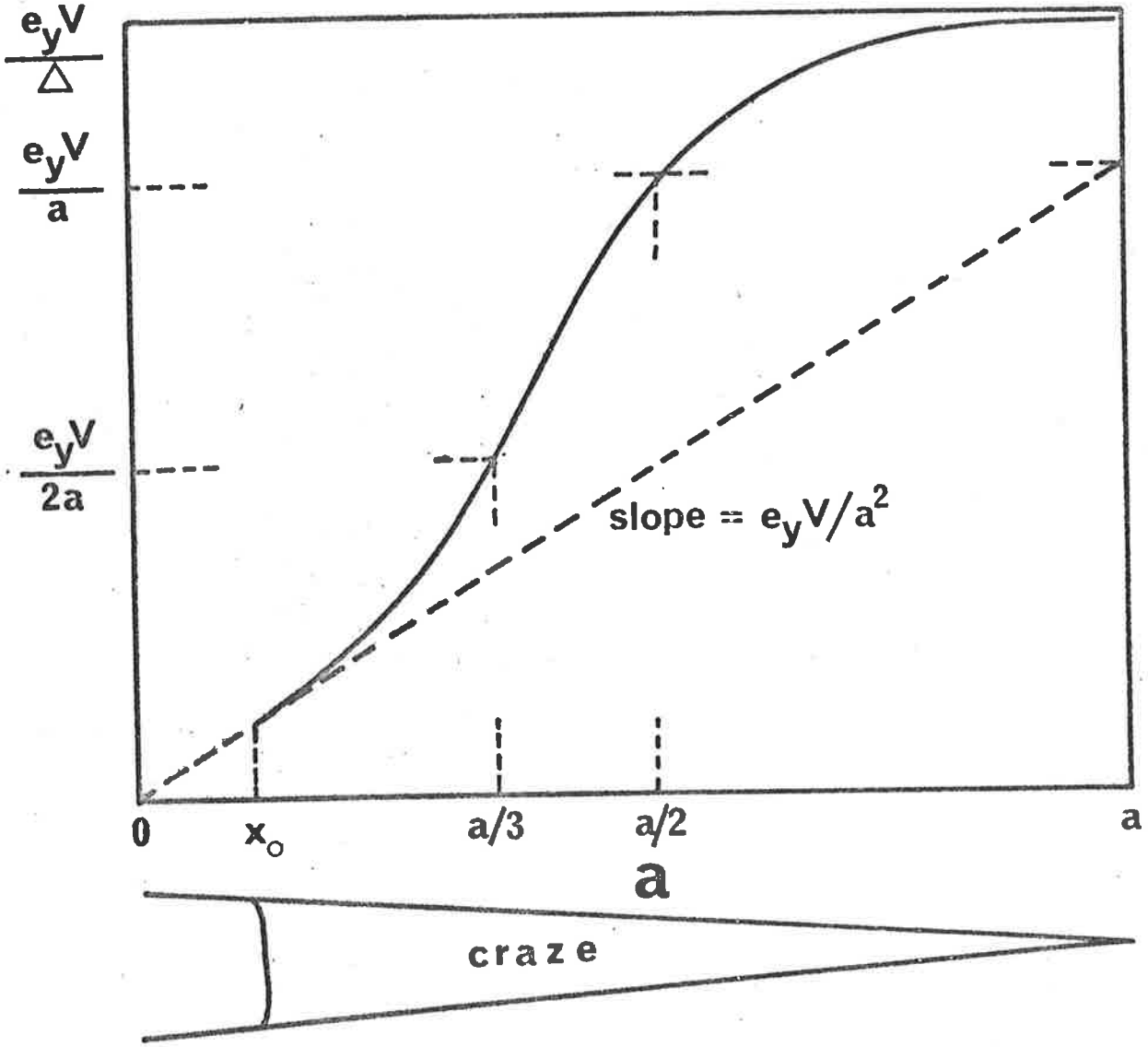

Fig.5.2a Profile of the strain rate, $\dot{\epsilon}$, as a function of craze length, Δ, at time t and crack tip velocity, v.

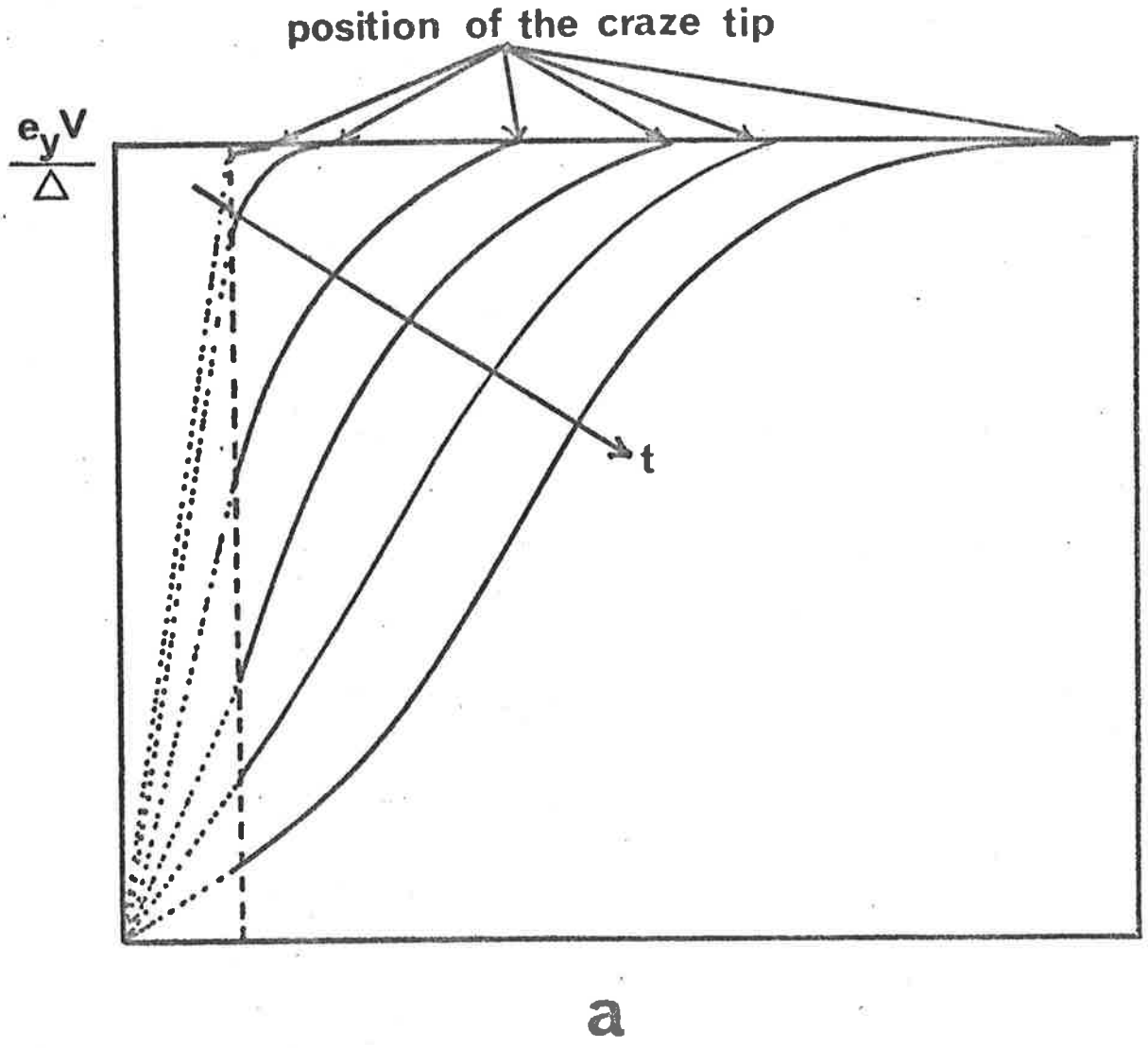

Fig.5.2b Profile of the strain rate, $\dot{\epsilon}$, varies with time as the front tip propagate at velocity, v.

prepared. Gel permeation chromatogram of the blends was shown in Fig.5.3 and Table 5.1 shows the MW and MWD of the components and the blends.

TABLE 5.1: MW and MWD of blends

	Component*		Blend	
	A1a	A9	B1	B3
M_w	450,000	31,000	408,100	324,300
M_n	375,000	25,800	159,000	74,100
M_w/M_n	1.2	1.2	2.6	4.4

* Syndiotactic-like polymers (64% syndiotactic triads)

5.3.2 Fracture Toughness Measurements

The test specimen configuration used in this work was double torsion (DT) geometry, an arrangement that has an advantage that the crack is not prone to wandering, and therefore has been widely used in fracture testing of metals as well as polymers (Fig.5.4). A pre-crack was introduced into the middle of one edge of the specimen by sawing a V-notch and forcing a razor blade into the notch to produce a sharp tip. The single edge-cracked specimen was supported on two parallel rollers and the load applied to the specimen via the cross bar of an Instron machine. The crack is encouraged to propagate along the axis of the specimen by prescribing a shallow groove on the bottom face of specimen I (Fig.5.4). The whole specimen could be immersed in a constant temperature bath of methanol.

The load relaxation (constant displacement) method was the main technique used in this work to evaluate the fracture toughness. A load in the range of 0.5 to 1.2 kg was applied to the pre-cracked specimen. It was found that with a specimen of 1.0 mm to 1.3 mm thickness, a load smaller than 0.5 kg cannot initiate crack propaga-

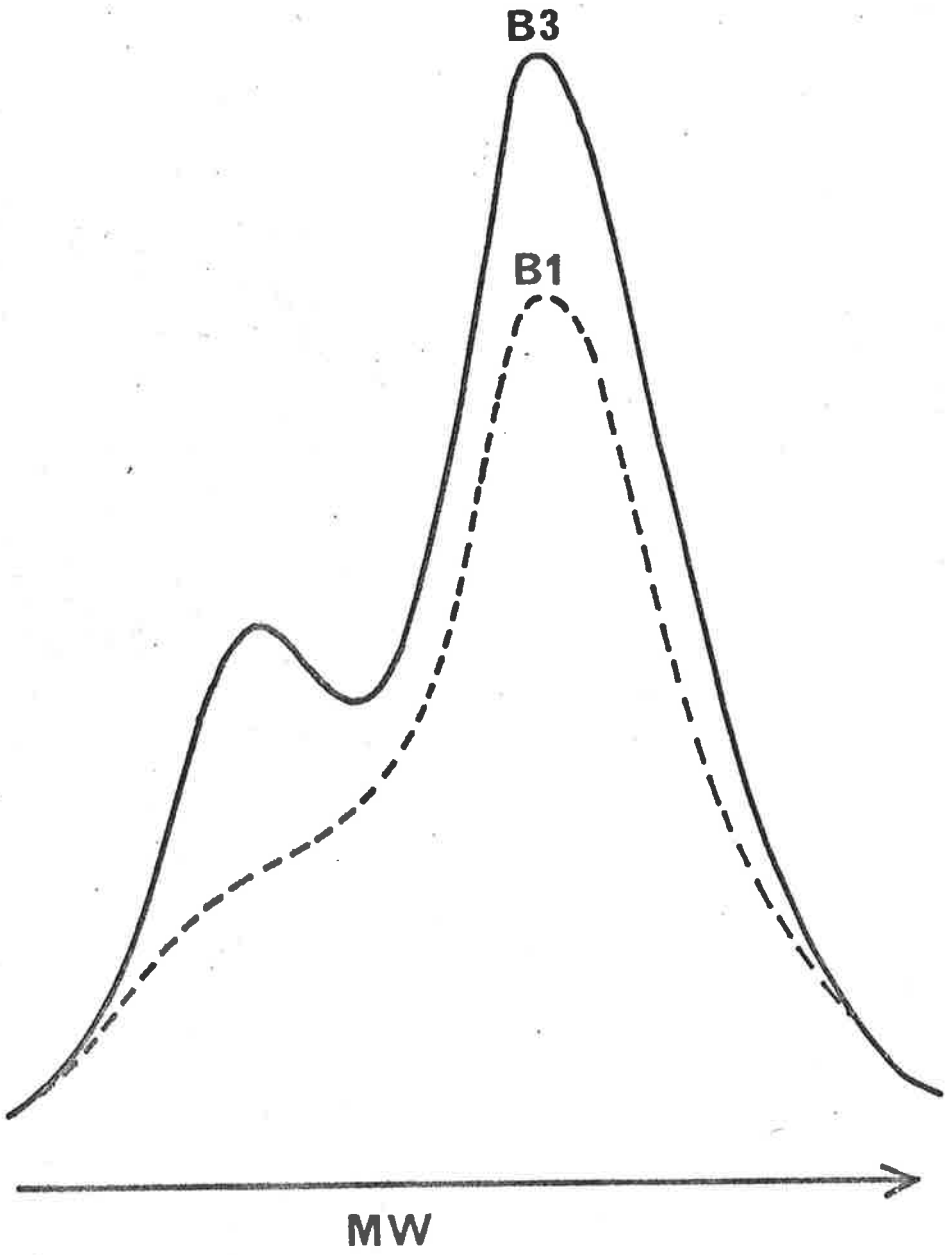

Fig.5.3 Gel permeation chromatograms of blends B1 and B3.

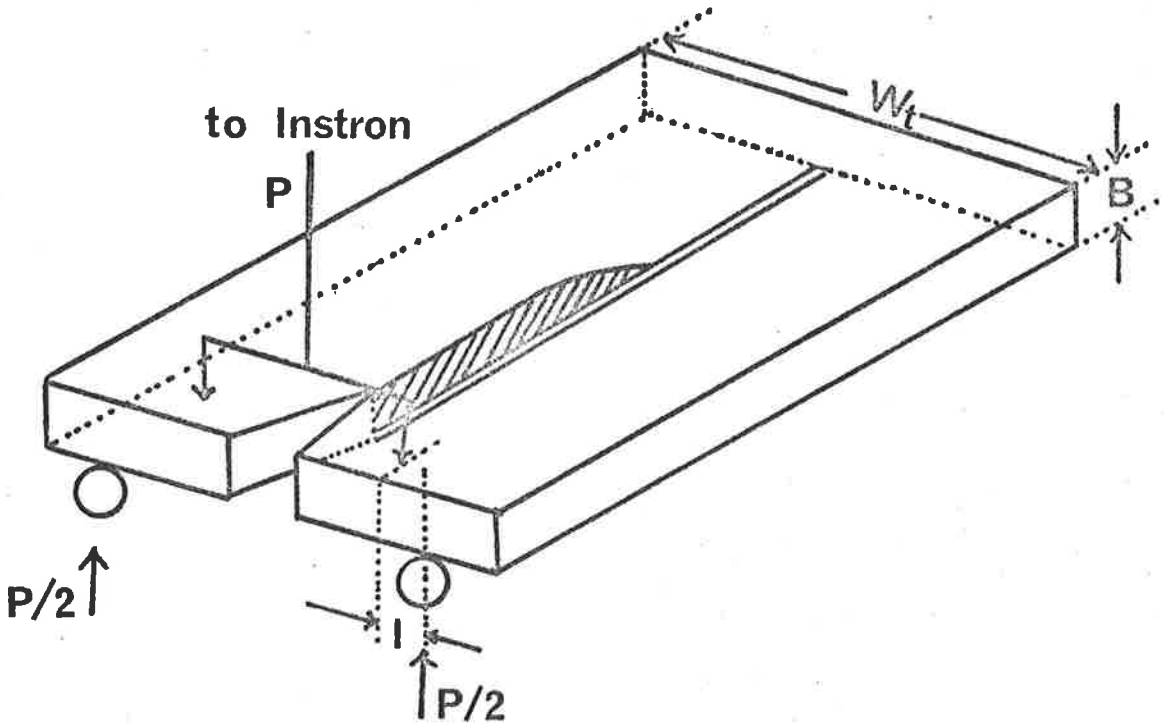

Fig.5.4 Double torsion geometry.

tion and a load larger than 1.2 kg causes the formation of multi-cracks especially in methanol. The specimen was loaded to a certain value in the range of 0.5 to 1.2 kg and then allowed to relax. This relaxation was attributed to plastic flow around the loading points. After approximately 15 minutes relaxing time the load become constant, indicating that the plastic flow had terminated. This constant value was taken as the initial load, P_i. Methanol was introduced into the bath to fully immerse the specimen. The temperature of methanol was controlled to within ±1°C over the range of 0 to 40°C.

For experiments conducted in air, the elimination of the plastic flow, i.e. the relaxation of the load P to a constant value, requires a stepwise increase of the load. The specimen was loaded to an initial value of 0.5 kg and loaded to relax until the load P become constant. Then P was increased by 0.05 kg and again allowed to relax. The same procedure was repeated with 0.05 kg increments until a crack commences.

The SIF at fracture, K_c, was determined utilizing the general compliance method (33)

$$K_c^2 = \frac{P^2}{2B_c} E \frac{dC}{dx_o} \qquad (5.16)$$

where C = specimen compliance, B_c = crack width (i.e. plate thickness, B, minus the centre groove). The compliance of the specimen in the DT geometry is given by

$$C = \left(\frac{(1 + \mu)\ \ell^2}{E\ W_t\ B^3} x_o \right) + C_o \qquad (5.17)$$

where C_o = the compliance at $x_o = 0$, ℓ = distance between loading points, W_t = plate width and μ = Poisson constant (Fig.5.4). By differentiating C with respect to x_o and substituting dC/dx_o into Eq.5.16, K_c at fracture is given by

$$K_c^2 = 3\ P^2 \frac{(1 + \mu)\ \ell^2}{W_t\ B_c\ B^3} \qquad (5.18)$$

Note that for DT geometry, K_c is independent of the crack length, x_o. Because the depth of the centre groove is small compared with the plate thickness, $B_c \simeq B$, Eq.5.18 becomes

$$K_c = 3 P^2 \frac{(1 + \mu)\ \ell^2}{W_t B^4} \tag{5.19}$$

or

$$K_c = A_g P \tag{5.20}$$

where A_g is a geometrical factor expressed by

$$A_g = \frac{\ell}{B^2} \sqrt{\frac{3(1+\mu)}{W_t}} \tag{5.21}$$

The linear relationship between the compliance, C, and the crack length, x_o, is shown experimentally in Fig.5.5.

The crack (craze) velocity, v, was determined by measuring the time elapsed for the crack to travel between prescribed 2mm incremental marks on the top surface. The corresponding average P can be found directly from the Instron recorder.

The crack velocity, v, could also be calculated from the rate of load relaxation dP/dt, the initial value of load and the initial crack length (107). However, it was often more convenient to find v by direct observation of the front tip propagation than from the dP/dt method. At $v \simeq 10^{-6}$ m sec^{-1} it was especially difficult to determine dP/dt as the change in slope approaches zero.

Loading the DT specimen in air produced the satisfactory propagation of a single crack but in methanol multi-cracks could be formed from the concentrated loading points. To avoid this problem, the methanol level was adjusted such that the bottom of centre pre-crack just touched the methanol while the loading points were still in the air. An adequate supply of methanol was directed to the vicinity of the pre-crack tip by a pipette to start crack propagation.

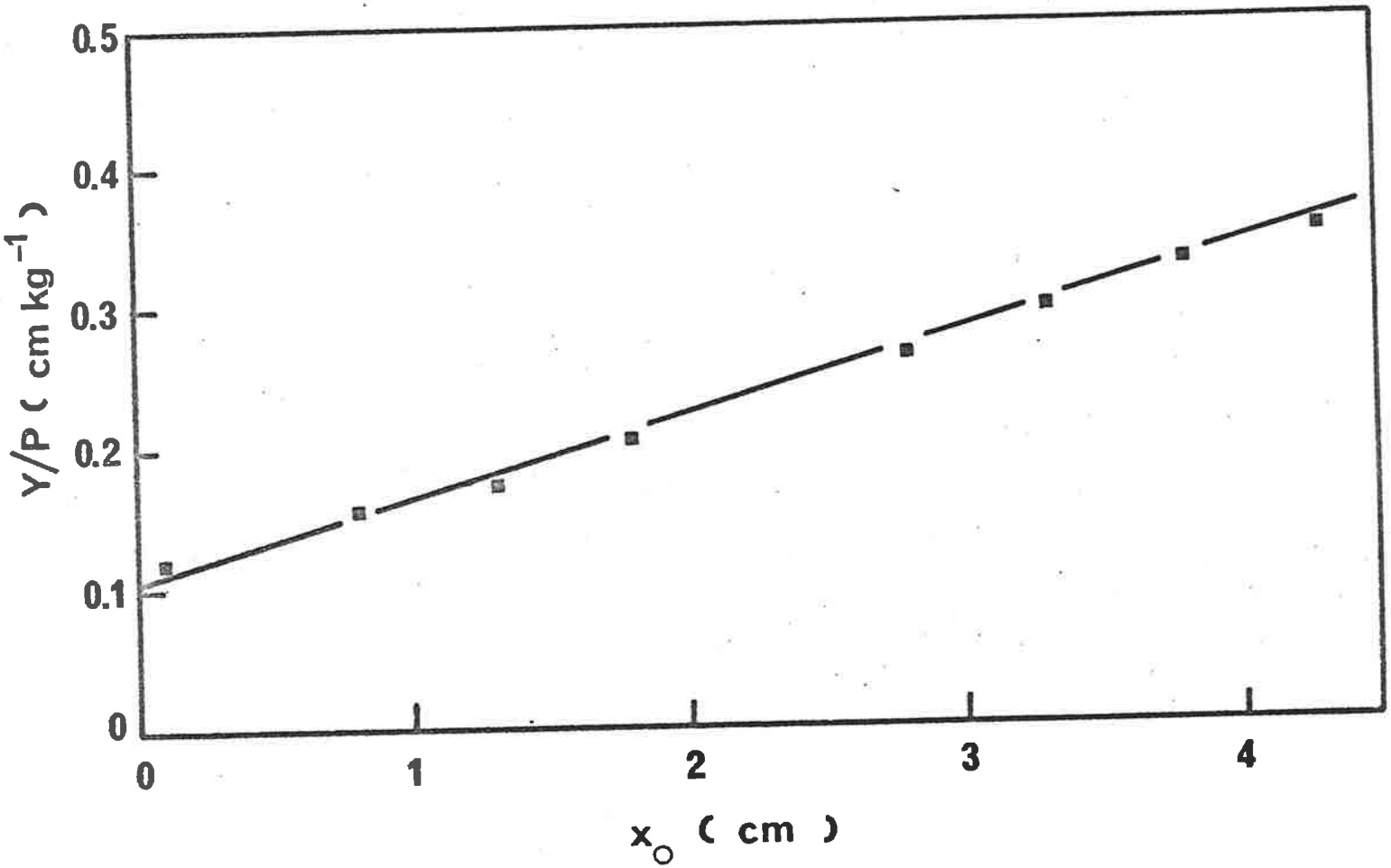

Fig.5.5 The linear relationship between the compliance, C = Y/P, and the crack length, x_o (commercial PMMA MG fractured in methanol at 20°C).

Specimen configuration used in the presence of methanol was the protected geometry (Fig.5.6), i.e. two sides of specimen were protected by silicone grease. Methanol entered the crack from the end but not the sides of the specimen and was termed by Marshall et al. as end flow (16). This configuration basically simplified the crazing kinetics by eliminating the complicating effects of methanol entering from the sides.

Although the range of measurable crack velocities was limited to the range of 10^{-6} to 10^{-3}m sec^{-1}this was sufficient to cover the stable crack propagation region (region AB in Fig.2.5). This range of velocities also included two Regions of behaviour (Regions I and II) for the cracking in methanol (Fig.2.6).

The major specific advantage of the DT geometry in the context of this study where polymerization of narrow MWD PMMA was tedious and difficult was that it was economical of material. Whereas most other testing methods capable of measuring K_c and v yield only single point data (16), the DT method was capable of providing from one specimen, values of K_c over a range of velocities.

Prior to discussing the main problem of the effect of MW and MWD on the fracture toughness, it is necessary to determine if the cooling rate of specimens during preparation effects the magnitude of K_c. The sample chosen for this test was a medium range MW commercial PMMA, sample MH of M_w = 149,000, M_w/M_n = 1.90. As shown in Fig.5.7, no obvious trend of the effect of the cooling rate could be detected. The scatter band of 10% can be attributed to the normal scatter associated with fracture testing.

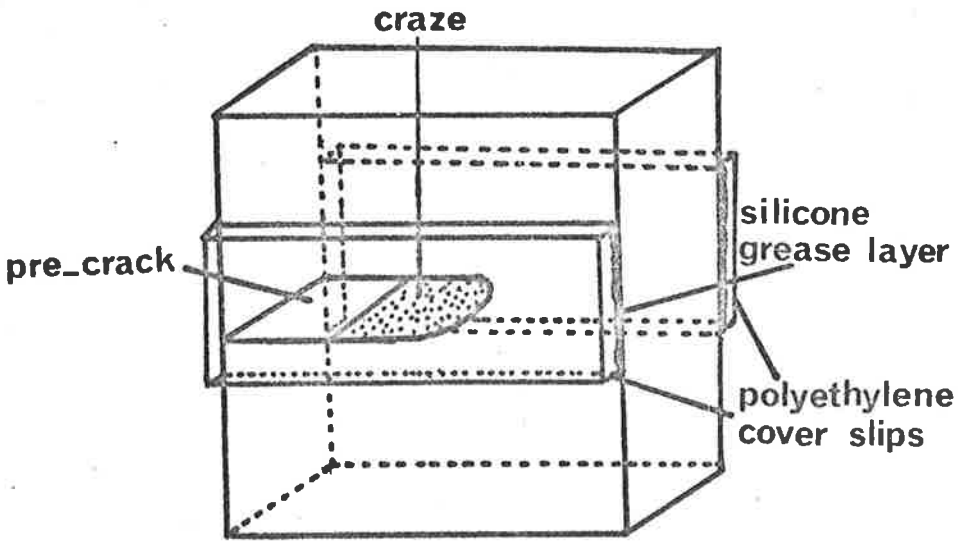

Fig.5.6 Protected geometry.

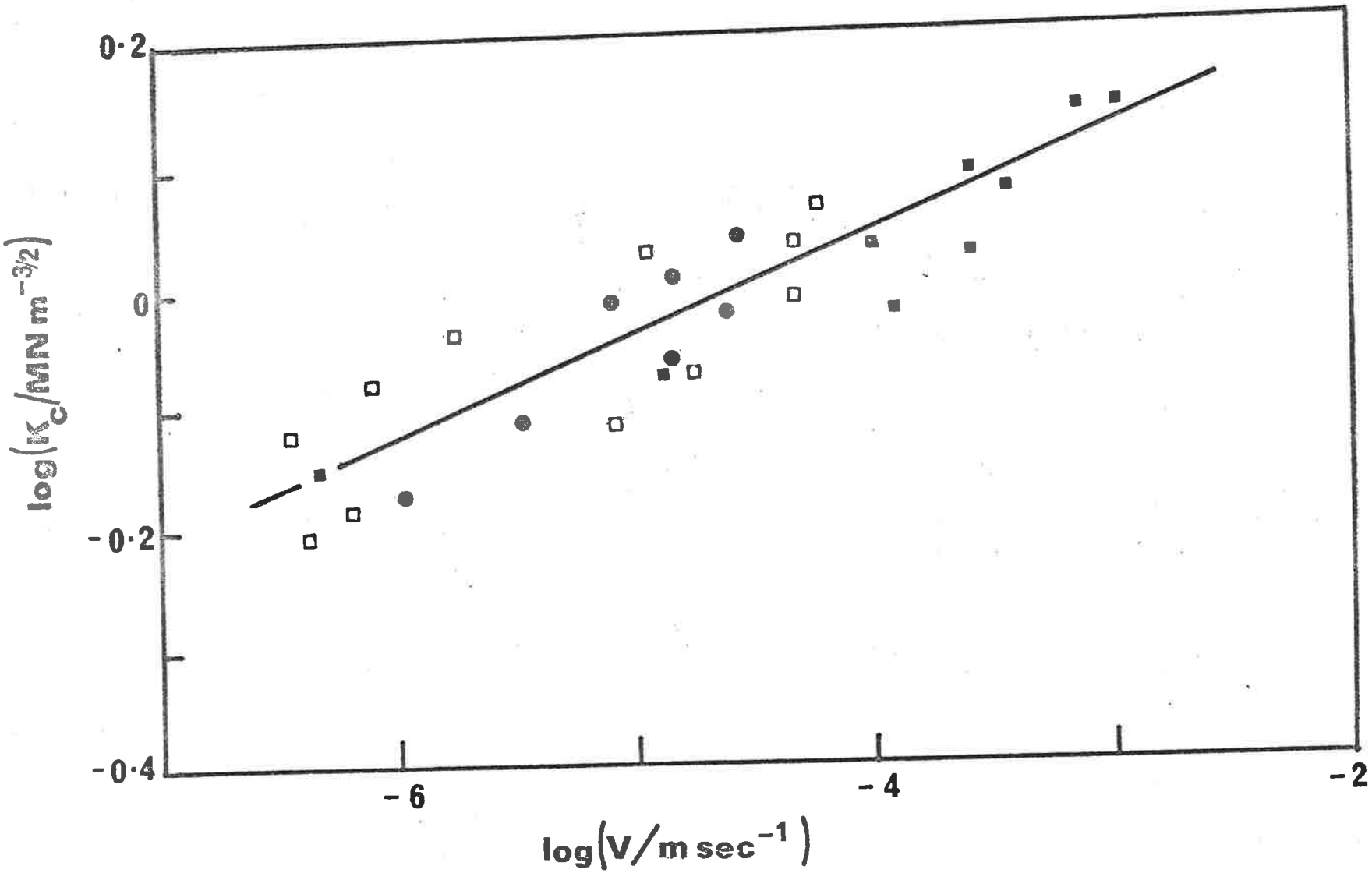

Fig.5.7 The log K_c vs. log v diagram of cracking in air (T=20°C) for samples MH prepared at different cooling rates: 200°min (●), 70°/min (■), 1°/min (○).

5.4 Results and Discussion

Molecular Weight and Molecular Weight Distribution Dependence of the Fracture Process in Air

5.4.1 A General Survey of Fracture Data in Air

The MW dependence of the fracture toughness shown in log K_c vs. log v diagrams for a series of commercial HMW, MMW, LMW and narrow MWD Ala, A4a, A7, A9 are illustrated in Figs.5.8 and 5.9. The plots of log K_c vs. log v approximately conform to a linear relationship in the range of experimental velocities (10^{-3} to 10^{-6} m sec^{-1}). Smaller values of the slope and higher values of K_c (at a particular v) indicate a higher toughness.

A comparison of K_c for various MW must be made at a particular crack velocity on the log K_c vs. v curve. An approximate value of v that allows determination of K_c for all specimens is $v = 5.62 \times 10^{-5}$ m sec^{-1} (log v = -4.25). The following Table shows values of K_c at log (v/m sec^{-1}) = -4.25 and values of slope of the log K_c vs. log v straight line.

TABLE 5.1: The slope of the log K_c vs. log v curves and the K_c values at $v = 5.62 \times 10^{-5}$ m sec^{-1} (log v = -4.25) for commercial and narrow MWD PMMA at 20°C.

Sample	M_w	M_w/M_n	Slope	K_c (MW $m^{-3/2}$)
HMW	787,000	2.1	0.07	1.122
MMW	220,000	2.1	0.07	1.122
LMW	180,000	2.1	0.10	0.871
Ala	450,000	1.2	0.10	1.122
A4a	120,000	1.2	0.10	0.933
A7	71,000	1.2	0.12	0.501
A9	31,000	1.2	0.18	0.234
Bl	408,000	2.6	0.10	1.318
B3	324,300	4.4	0.10	0.955

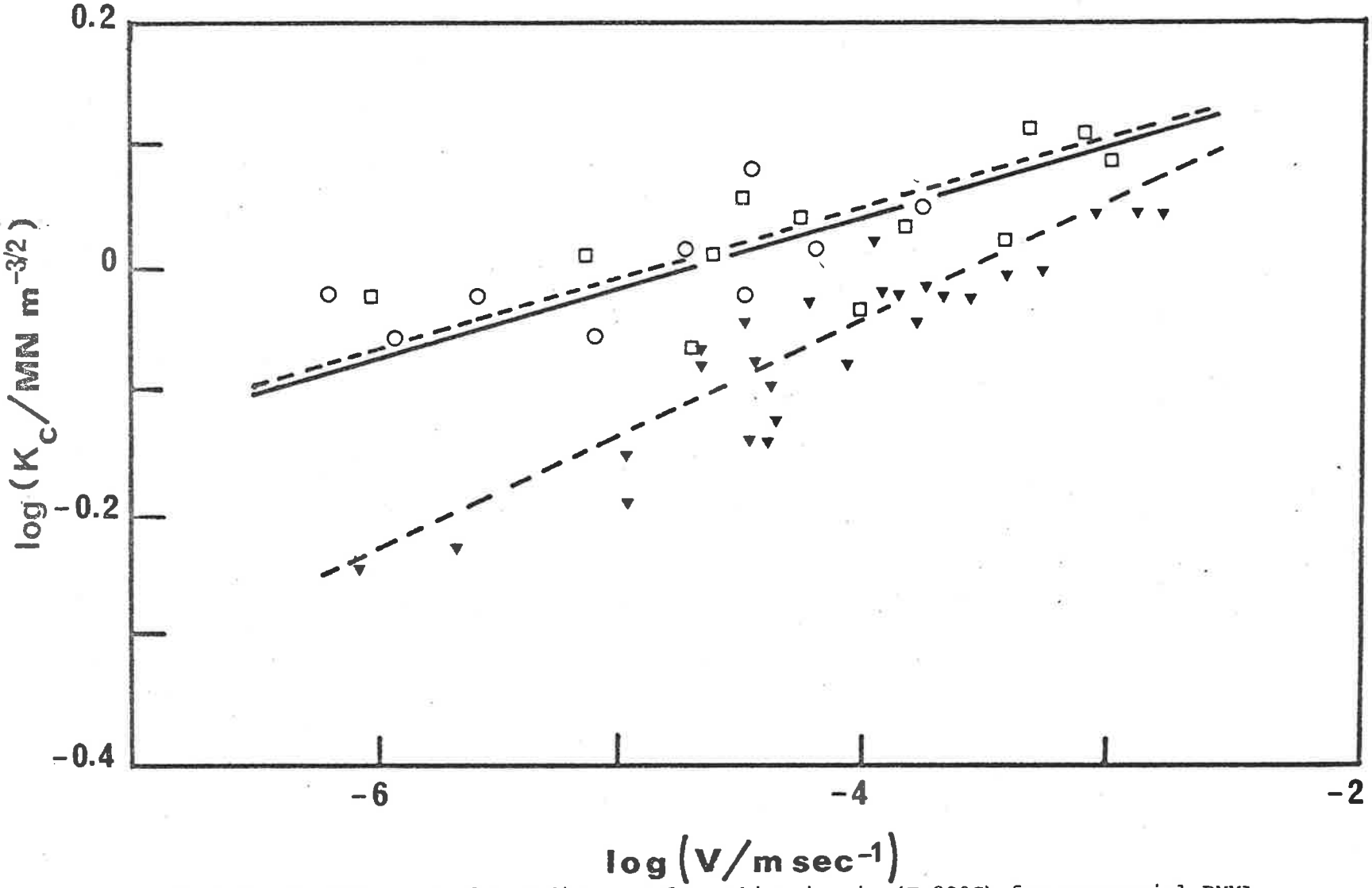

Fig.5.8 The log K_c vs. log v diagram of cracking in air (T=20°C) for commercial PMMA, HMW (□), MMW (○), LMW (▼). The solid line is Young and Beautmont's data (105).

Fig.5.9 The log K_c vs. log v diagram of cracking in air (T=20°C) for narrow MWD PMMA, A1a (M_w = 450,000, ●), A4a (M_w = 120,000, △), A7 (M_w = 71,000, ▲), A9 (M_w = 31,000, ■).

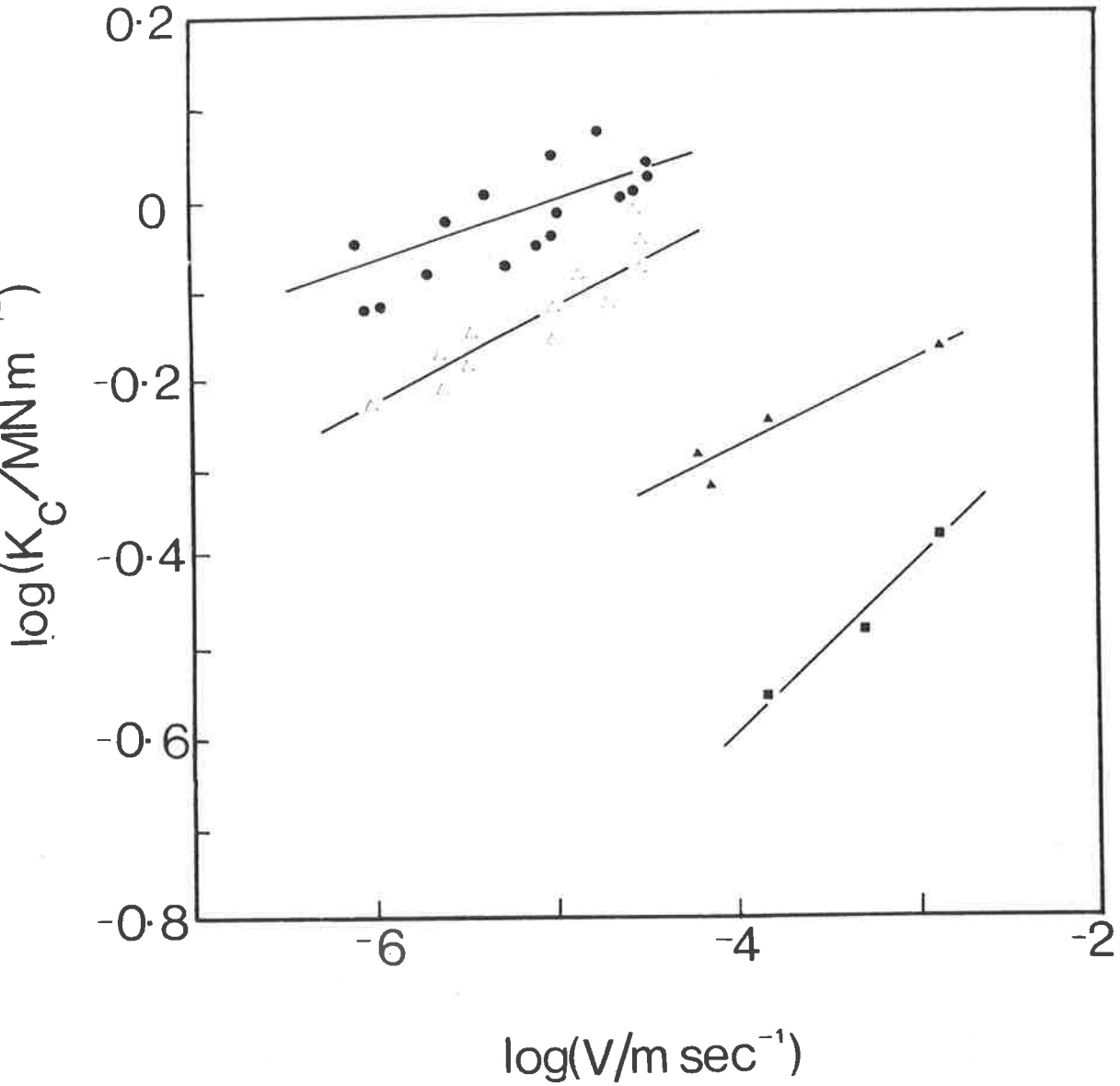
0·2
0
-0·2
-0·4
-0·6
-0·8
-6
-4
-2
log(K_C/MN m^-3/2)
log(V/m sec^-1)

The log K_c vs. log v data for HMW, MMW and Ala are consistent with Young and Beautmont's results (105) and Williams and co-workers' results (16-17) for commercial PMMA (stated by these authors as being high MW PMMA). Moreover, the effect of MW on K_c shown in Table 5.1 is obvious —K_c decreases with MW in both broad MWD commercial and narrow MWD PMMA. The MW dependence of K_c will be discussed in detail in Sections 5.4.2 and 5.4.3.

The effect on fracture toughness of adding low MW PMMA to high MW PMMA can be observed from log K_c vs. log v diagram of blends B1 and B3 (Fig.5.10). Addition of 10% low MW sample to high MW sample (blend B1) does not reduce the fracture toughness of high MW component whereas addition of 30% low MW leads to a decrease in K_c compared with that of the high MW component. The reduction of K_c by addition of low MW sample can be seen as the effect of MWD broadening and/or decrease in MW on the fracture toughness. These effects will be discussed in the following Section.

The log K_c vs. log v data will be analysed in the following Section using a LEFM approach to estimate the crack opening displacement (COD) and the fracture energy. On the basis of an entanglement concept, a model for plastic deformation and craze formation during the fracture process is suggested in an attempt to explain the molecular relationship between MW and fracture energy.

5.4.2 The Crack Opening Displacement (COD), u_c, and the Fracture Energy, γ_c.

Rewriting Eq.2.2.7, the SIF, K_c can be expressed by (see Chapter 2)

$$K_c = \sqrt{u_c \varepsilon_y}\, E\,(v) \qquad (5.22)$$

Fig.5.10 The log K_c vs. log v diagram of cracking in air (T=20°C) for blends. Blend B1 (●), Blend B3 (□). Curve(1): high MW component A1a, curve(2): low MW component A9.

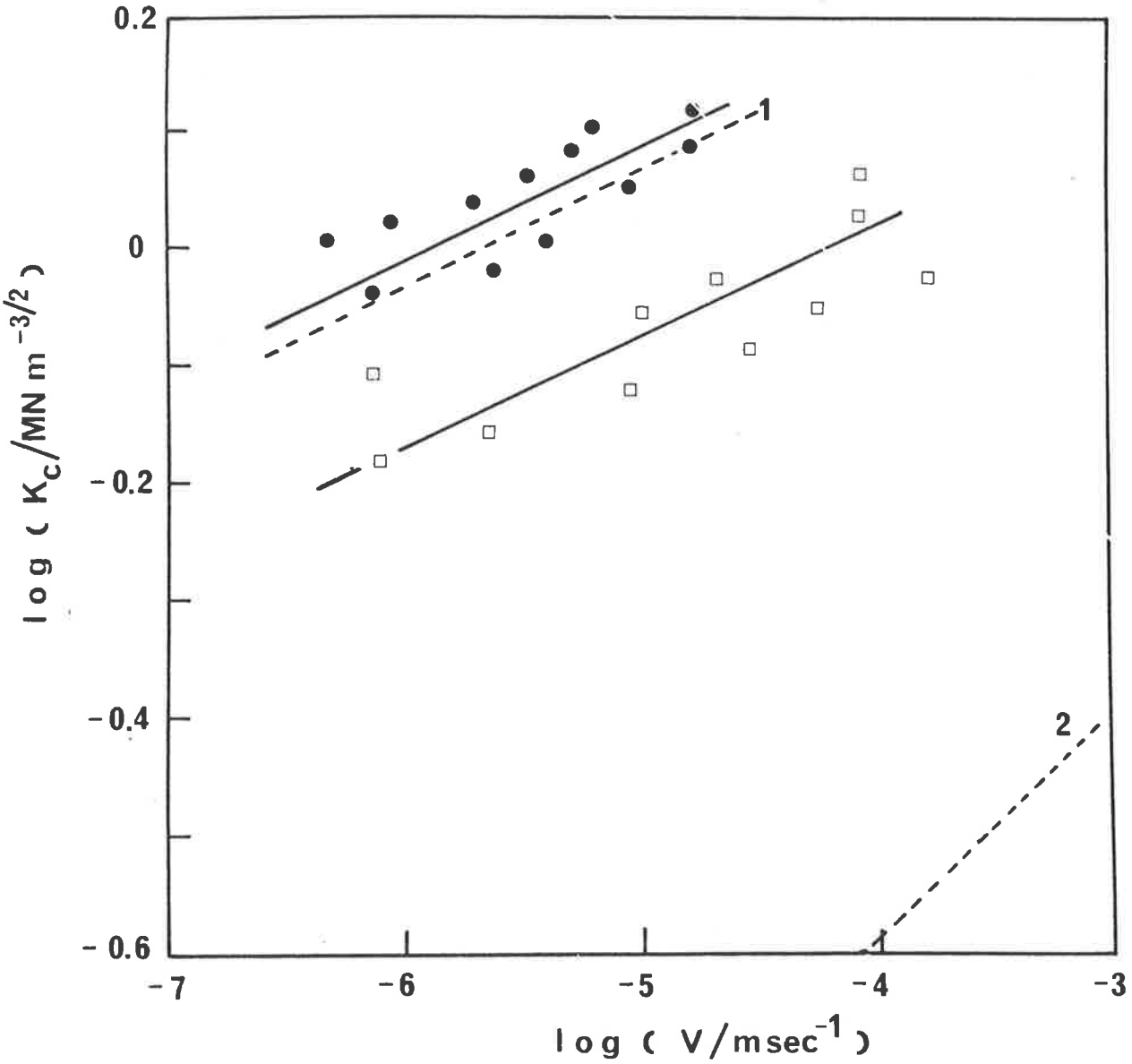
0.2
0
-0.2
-0.4
-0.6
-7
-6
-5
-4
-3
log (K_c/MN m$^{-3/2}$)
log (V/msec^{-1})
1
2

where E(v) is the modulus as a function of v (97,105). The fracture energy γ_c is expressed by

$$G_c = 2\gamma_c = K_c^2/E(v) = u_c\sigma_c \qquad (5.23)$$

The modulus E(v) of PMMA at 25°C was determined experimentally as a function of the strain rate $\dot{\varepsilon}$ by Williams (97).

$$E(\dot{\varepsilon}) = [655 + 2744\ (\dot{\varepsilon})^{0.109}] \quad MNm^{-2} \qquad (5.24)$$

According to the result of Section 5.2 the strain rate, $\dot{\varepsilon}$, and the crack velocity, v, are related by the equation

$$\dot{\varepsilon} = \frac{8}{\pi}\ \frac{\varepsilon_y^2}{u_c}\ v \qquad (5.13)$$

In air, $\varepsilon = 0.035$ and $u_c = 1.73 \times 10^{-6}$ m (97) so that

$$\dot{\varepsilon} = 1.28 \times 10^3\ v \qquad (5.25)$$

Substituting Eq.5.25 into Eq.5.24, we obtain

$$E(v) = [0.655 + 6.00\ v^{0.109}] \times 10^3 \quad MNm^{-2} \qquad (5.26)$$

It is seen from the above equation that the modulus E is not very sensitive to v and the average value of E in the experimental range of velocities 10^{-6} m $sec^{-1} < v < 10^{-4}$ m sec^{-1} can be taken as 3000 MNm^{-2}.

The COD, u_c, can also be calculated if the yield stress is known (Eq.5.22). Feller and Kee (108) found from experiment that the crazing stress, σ_c, in air (25°C) for polystyrene is independent of MW down to values approaching the critical MW, u_c. The constant σ_c implies a constant yield strain in this range of MW (MW $\geq M_c$), because σ_c relates to ε_y by $\sigma_c = E\ \varepsilon_y$. The values of u_c can be calculated for various PMMA from Eq.5.22 with $\varepsilon_y = 0.035$ (97,105). The calculated results of γ_c and u_c are listed in Table 5.2.

TABLE 5.2: The fracture energy, γ_c, and the COD, u_c, of PMMA as a function of MW [at log $(v/msec^{-1})$ = -4.25]

Sample	M_w	M_w/M_n	log (γ_c/Jm^{-2})	$u_c \times 10^6$ (m)	log u_c
A1a*	450,000	1.2	2.33	4.07	-5.39
A4a*	120,000	1.2	2.17	2.82	-5.55
A7 *	71,000	1.2	1.63	0.81	-6.09
A9 *	31,000	1.2	0.97	0.18	-6.79
HMW**	787,000	2.1	2.26	3.48	-5.46
MMW**	220,000	2.1	2.26	3.48	-5.46
LMW**	180,000	2.1	2.10	2.41	-5.62
B1	408,000	2.6	2.40	-	-
B3	324,300	4.4	2.18	-	-

* Syndiotactic-like (64% syndiotactic triads)
** Syndiotactic-like (55% syndiotactic triads)

Weidmann and Döll (109) obtained u_c by direct measurement for broad MWD atactic PMMA of various MW. The results are listed below.

TABLE 5.3: Weidmann and Döll's data of the COD of atactic PMMA at K_c = 0.63 $MNm^{-3/2}$ (109).

M_w	$u_c \times 10^6$ (m)	log u_c
110,000	1.2	-5.92
120,000	1.3	-5.88
163,000	1.9	-5.72
490,000	2.5	-5.60
850,000	2.6	-5.58
2,200,000	2.8	-5.55
8,000,000	2.9	-5.54

A plot of log u_c vs. log M_w is shown in Fig.5.11 where it is observed that the values of u_c in this work are slightly higher than Weidmann and Döll's. This is attributed to the fact that u_c was calculated at $K_c \simeq 1$ $MNm^{-3/2}$ (corresponding to log $(v/msec^{-1})$ = -4.25), whereas Weidmann and Doll's u_c were measured at K_c = 0.65

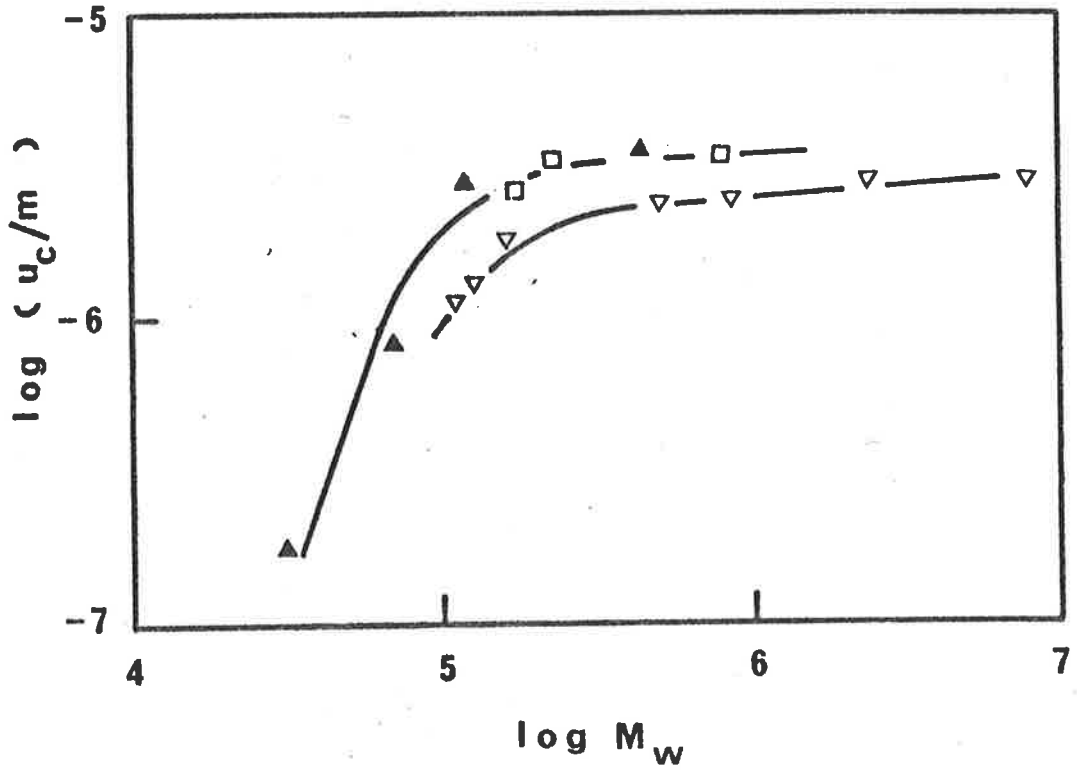

Fig.5.11 The relationship of the COD, u_c and M_w, Narrow MWD PMMA (▲), commercial PMMA (HMW, MMW and LMW) (□), and Weidnaann and Döll's data (▽) (109).

$MNm^{-3/2}$. The K_c dependence of the COD, u_c, was observed by Israel et al. (110), u_c increases with K_c and reaches a limit at K_c = 1 $MNm^{-3/2}$.

5.4.3 Theoretical Treatment

As mentioned in Chapter 2, the fracture energy γ_c comprises the surface energy expended in creating new surfaces by cleavage, γ_{c_1}, and the energy expended in localized plastic deformation at the crack tip, γ_{c_2}. That is

$$\gamma_c = \gamma_{c_1} + \gamma_{c_2} \tag{5.27a}$$

Similarly, as $G_c = u_c \sigma_c$ (Eq.5.23), the COD, u_c, can be expressed by

$$u_c = u_{c_1} + u_{c_2} \tag{5.27b}$$

where u_{c_1} and u_{c_2} correspond to γ_{c_1} and γ_{c_2}, respectively.

In the range of MW, $M \lesssim M_c$, plastic deformation does not exist, and the main contribution to γ_c is from the surface energy component, γ_{c_1}, that is

$$\gamma_c = \gamma_{c_1} \quad \text{for} \quad M \lesssim M_c \tag{5.28}$$

Based on the criterion for craze stability derived by Haward et al. (111), Kramer (112) developed quantitative expressions for γ_{c_1} and u_{c_1}. For the cracking of PMMA in air, using σ_c = 65 $MNm^{-3/2}$ (100, 109) the formula of G_c and u_c for PMMA according to Kramer's computation are obtained as the following

$$u_{c_1} = 0.210\ M_w^{\frac{1}{2}} \quad nm \tag{5.29a}$$

and

$$2\gamma_{c_1} = 0.0136\ M_w^{\frac{1}{2}} \quad Jm^{-2}$$

or

$$\gamma_{c_1} = 0.0068\ M_w^{\frac{1}{2}} \quad Jm^{-2} \tag{5.29b}$$

The fracture energy increases rapidly from value γ_{c_1} in most amorphous polymers such as polystyrene (3), polycarbonate (4) and PMMA (2,22) when the MW surpasses the critical MW, M_c, to the range of medium MW. This rapid increase is attributed to the energy required for plastic deformation, γ_{c_2} (Eq.5.27a). Thus, the experimental data of the relationship of the free energy and MW for amorphous polymers (2-4, 22) imply that only in the polymers of MW larger than M_c does the plastic deformation take place at the crack tip causing a larger fracture energy than γ_{c_1}.

On the basis of the experimental observation mentioned above, it is plausible to assume that

(a) only molecules of MW larger than M_c are able to participate in plastic deformation,

(b) the resulting craze zone consists of numerous craze fibrils which are spanned under stress and stabilized by the entanglement networks.

In addition to the experimental evidence established by the fracture energy vs. MW relationship, these assumptions are also justified by the work of Fellers and Kee (108) on the magnitude of the crazing stress and Wellinghoff and Baer (7) on the microscopic observation of craze formation in polystyrene of various MW. These workers came to the same conclusion that crazes essentially do not form if the MW is below M_c. It is also noted that assumptions (a) and (b) are related by the critical MW, M_c, that is a MW larger than M_c is a pre-requisite for the establishment of an entanglement network.

To derive an equation for the MW dependence of the fracture energy, γ_c, it is necessary to describe these above assumptions in quantitative terms. The assumption (a) can be expressed by the

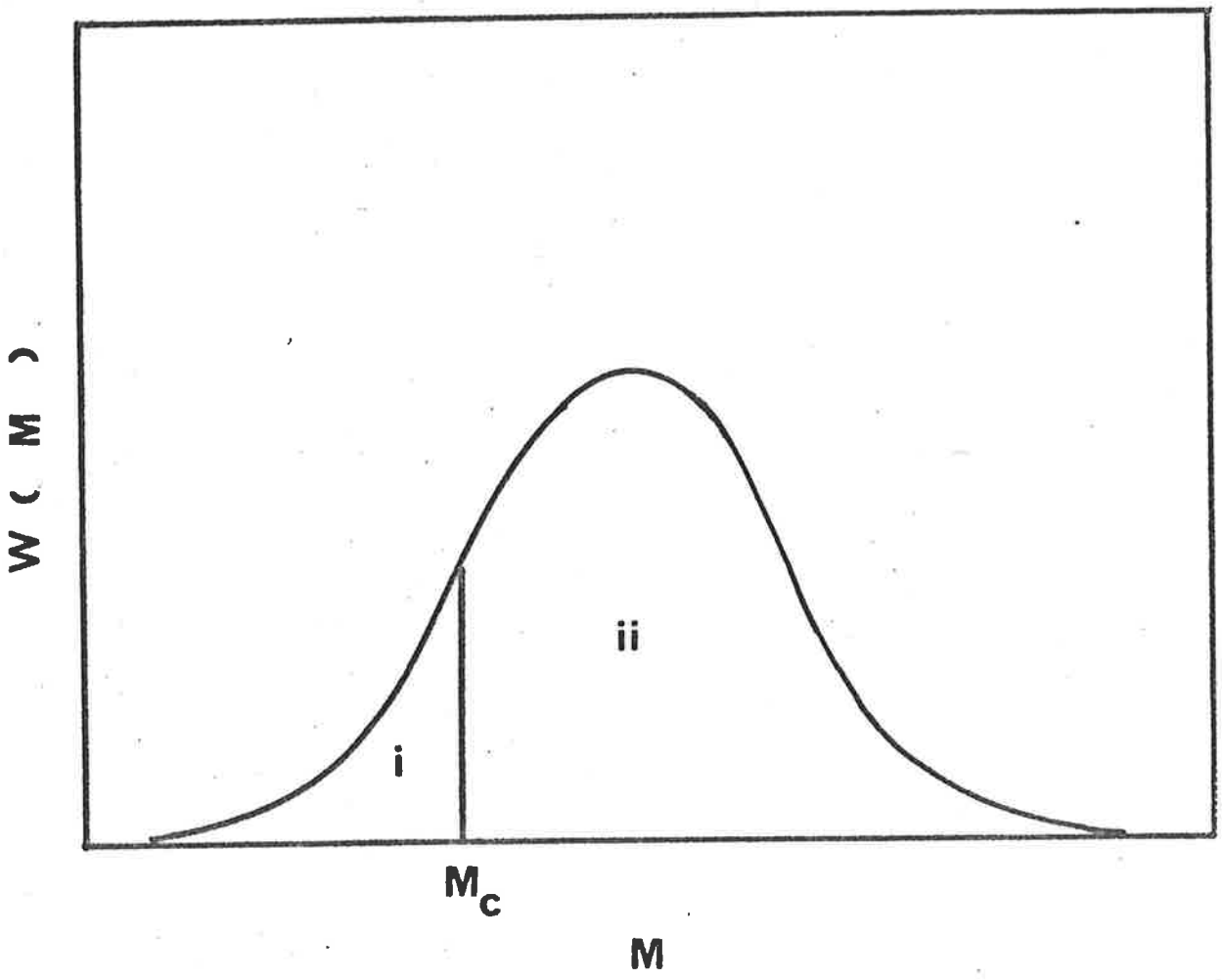

Fig.5.12 Schematic diagram showing the MWD curve, Region (i) containing molecules that do not contribute to plastic deformation and Region (ii) are capable of participating in plastic deformation.

weight fraction S of molecules having MW larger than M_c. Fig.5.12 shows the weight distribution curve of a polymer where the ratio S is equal to the area of region II to the total area under the curve. The assumption (a) is similar to Kusy and Turner's (2), but the characteristic MW which marks the boundary between region I and region II (Fig.5.12) is predetermined as M_c rather than an adjustable MW adopted by Kusy and Turner to fit the experimental data. This point will be discussed in detail in the next Section.

From the GPC results of the narrow MWD and commercial PMMA it was found that the MWD obeys a logarithmic normal weight distribution described by the following distribution function (Chapter 3)

$$W(\ell nM) = \frac{\exp[-(\ell nM - \ell nM_p)^2]/\ 2\sigma_D^2]}{\sqrt{2\pi}\ \sigma_D} \qquad (5.30)$$

and

$$M_n = M_p \exp(-\sigma_D^2/2) \qquad (5.31)$$

$$M_w = M_p \exp(\ \sigma_D^2/2) \qquad (5.32)$$

$$M_w/M_n = \exp \sigma_D^2 \qquad (5.33)$$

where σ_D = the standard deviation of the distribution and M_p = the peak MW of the distribution curve (113). Thus, the ratio S can be expressed as

$$S = \int_{\ell nM_c}^{\infty} W(\ell nM)\ d\ \ell nM \Big/ \int_{-\infty}^{\infty} W(\ell nM)\ d\ \ell nM \qquad (5.34)$$

where

$$\int_{-\infty}^{\infty} W(\ell nM)\ d\ \ell nM = 1$$

The entanglement networks of assumption (b) can be described quantitatively by the entanglement density. The density was originally developed for the case of permanent crosslinks in vulcanized rubber (114) and is expressed as

$$N_e = \frac{2\rho_p N_A}{M_c}\left(1 - \frac{M_c}{M}\right) \qquad (5.35)$$

where N_e is the density of entanglement and M is the MW. Although the entanglement network and the permanent crosslinks are different in nature, Eq.5.35 can be applied to the calculation of the number of the entanglements (or pseudo-crosslinks) in non-crosslinked polymers (115). If polydispersity is taken into account, the average density of entanglement, $\bar{N}_e$, is expressed by

$$\bar{N}_e = \int_0^\infty \frac{2\rho_p N_A}{M_c} \left(1 - \frac{M_c}{M}\right) W(M)\, dM \qquad (5.36)$$

where W(M) is a weight distribution function

Because

$$\int_0^\infty W(M)\, dM = 1 \qquad (5.37)$$

and by definition

$$M_n = \int_0^\infty \frac{1}{M} W(M)\, dM \qquad (5.38)$$

Eq.5.31 becomes

$$\bar{N}_e = \frac{2\rho_p N_A}{M_c} \left(1 - \frac{M_c}{M_n}\right) \qquad (5.39)$$

It is important to note from this equation that providing the MW is defined by M_n, $\bar{N}_e$ is independent of the MWD.

The average density of entanglements at infinite MW is

$$\bar{N}_e(\infty) = \frac{2\rho_p N_A}{M_c} \qquad (5.40)$$

Thus, Eq.5.39 can be rewritten as

$$\frac{\bar{N}_e}{\bar{N}_e(\infty)} = 1 - \frac{M_c}{M_n} \qquad (5.41)$$

Now, if the energy expended for plastic deformation, γ_{c_2}, of the infinite MW polymer is defined as $\gamma(\infty)$, then according to assumption (a) the plastic deformation work contributed by the molecules with $M_n > M_c$ of a polymer having number-average MW, M_n is described by

$$\gamma'_{c_2} = \gamma(\infty)\, S \qquad (5.42)$$

Also, using assumption (b) which takes into account the effect of entanglement density, γ_{c_2}, is given by

$$\gamma_{c_2} = \gamma'_{c_2} \frac{\bar{N}_e}{\bar{N}_e(\infty)} = \gamma(\infty)\, S\, \frac{\bar{N}_e}{\bar{N}_e(\infty)} \qquad (5.43)$$

Similarly, u_{c_2} is given by

$$u_{c_2} = u(\infty)\, S\, \frac{\bar{N}_e}{\bar{N}_e(\infty)} \qquad (5.44)$$

where $u(\infty)$ = the COD at infinite MW.

Hence, the fracture energy, γ_c, and the COD, u_c, become

$$\gamma_c = 0.0068\, M_w^{\frac{1}{2}} + \gamma(\infty)\, S \left(1 - \frac{M_c}{M_n}\right) \quad Jm^{-2} \qquad (5.45a)$$

and

$$u_c = 0.210\, M_w^{\frac{1}{2}} + u(\infty)\, S \left(1 - \frac{M_c}{M_n}\right) \quad nm \qquad (5.45b)$$

The second term on the RHS of Eq.5.45a can be calculated by substituting values of $\gamma(\infty)$ of 2×10^2 Jm^{-2} or 3×10^2 Jm^{-2} (suitable values obtained from a wide range of reported data falls in the range 1.1×10^2 to 4.9×10^2 Jm^{-2} for PMMA (1-2,22,116-118)). Similarly, u_c of Eq.5.45b can be estimated by using $u(\infty) = 4.09 \times 10^{-6}$m (this work). The calculated values of γ_c and u_c with $M_w/M_n = 1$ are listed in Tables 5.4 and 5.5 (see Appendix 4 for calculation).

TABLE 5.4 : Calculated values of γ_c with $M_w/M_n = 1$ and $\gamma(\infty) = 3 \times 10^2$ Jm^{-2}

M_n	log M_n	γ_{c_1} (Jm^{-2})	γ_{c_2} (Jm^{-2})	γ_c (Jm^{-2})	log γ_c
30,000	4.48	1.2	0	1.2	0.08
35,000	4.54	1.3	42.8	44.1	1.64
40,000	4.60	1.4	75	76.4	1.88
70,000	4.84	1.8	171.4	173.2	2.24
100,000	5.00	2.1	210	212.1	2.33
200,000	5.30	3.0	255	258	2.41
1,000,000	6.00	6.8	291	297.8	2.47

TABLE 5.5 : Calculated values of u_c with $M_w/M_n = 1$ and $u(\infty) = 4.09 \times 10^{-6}$m

M_n	log M_n	$u_{c_1} \times 10^6$ (m)	$u_{c_2} \times 10^6$ (m)	$u_c \times 10^6$ (m)	log u_c
30,000	4.48	0.039	0	0.039	-7.40
35,000	4.54	0.042	0.584	0.626	-6.20
40,000	4.60	0.045	1.022	1.067	-5.97
70,000	4.78	0.058	2.337	2.395	-5.62
100,000	5.00	0.068	2.863	2.931	-5.53

From these above tables, it can be seen that for $M_n >> M_c$ the contribution of γ_{c_1} to the total value of γ_c is only few percent of γ_{c_2}. Similar comments can be applied to the COD, u_c. Comparison of theoretical, experimental and published data are shown in Figs. 5.13 and 5.14 for commercial, narrow MWD and blends of PMMA. It is seen that the theoretical curves ($\gamma(\infty) = 2 \times 10^2$ Jm^{-2}) are in excellent agreement with experimental data. It is further noted that, Kusy and Turner proposed a theory for the fracture energy and MW relationship based on the Schulz type MW distribution function (2). A comparison of Kusy and Turner's curve and theoretical curves of this work is shown in Fig.5.15. Details of Kusy and Turner theory is discussed in the next Section.

It can be seen from a plot of the fracture energy against the number-average MW, M_n, that a very broad MWD (e.g. $M_w/M_n = 4$) has only a slight effect on the γ_c (Fig.5.16). That is, as the MWD becomes much broader it is predicted that there will be only a slight decrease in γ_c in the medium MW range.

This prediction is supported by a master log γ_c vs. M_n curve (commercial, synthesized narrow MWD PMMA and blends) compiled from experimental data of PMMA of various MWD (Fig.5.14). As a test on this prediction, a corresponding plot of log γ_c vs. log M_w

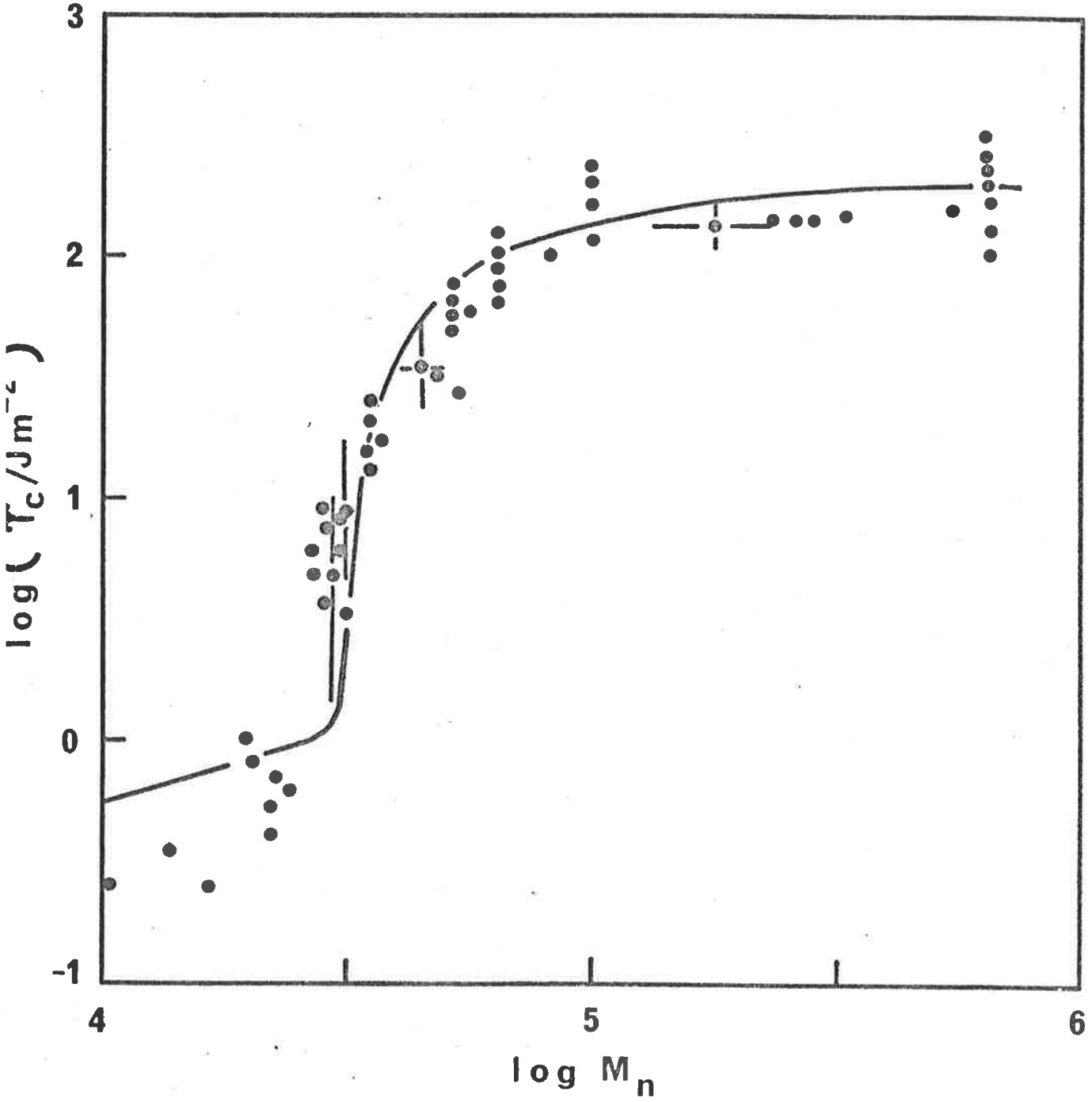

Fig.5.13 Published experimental data and theoretical curve of log γ_c vs. log M_n relationship for PMMA (●). Experimental data (1-2, 22,116-118). (——) Theoretical curve with $\gamma(\infty) = 2 \times 10^2$ Jm^{-2} and $M_w/M_n = 1$.

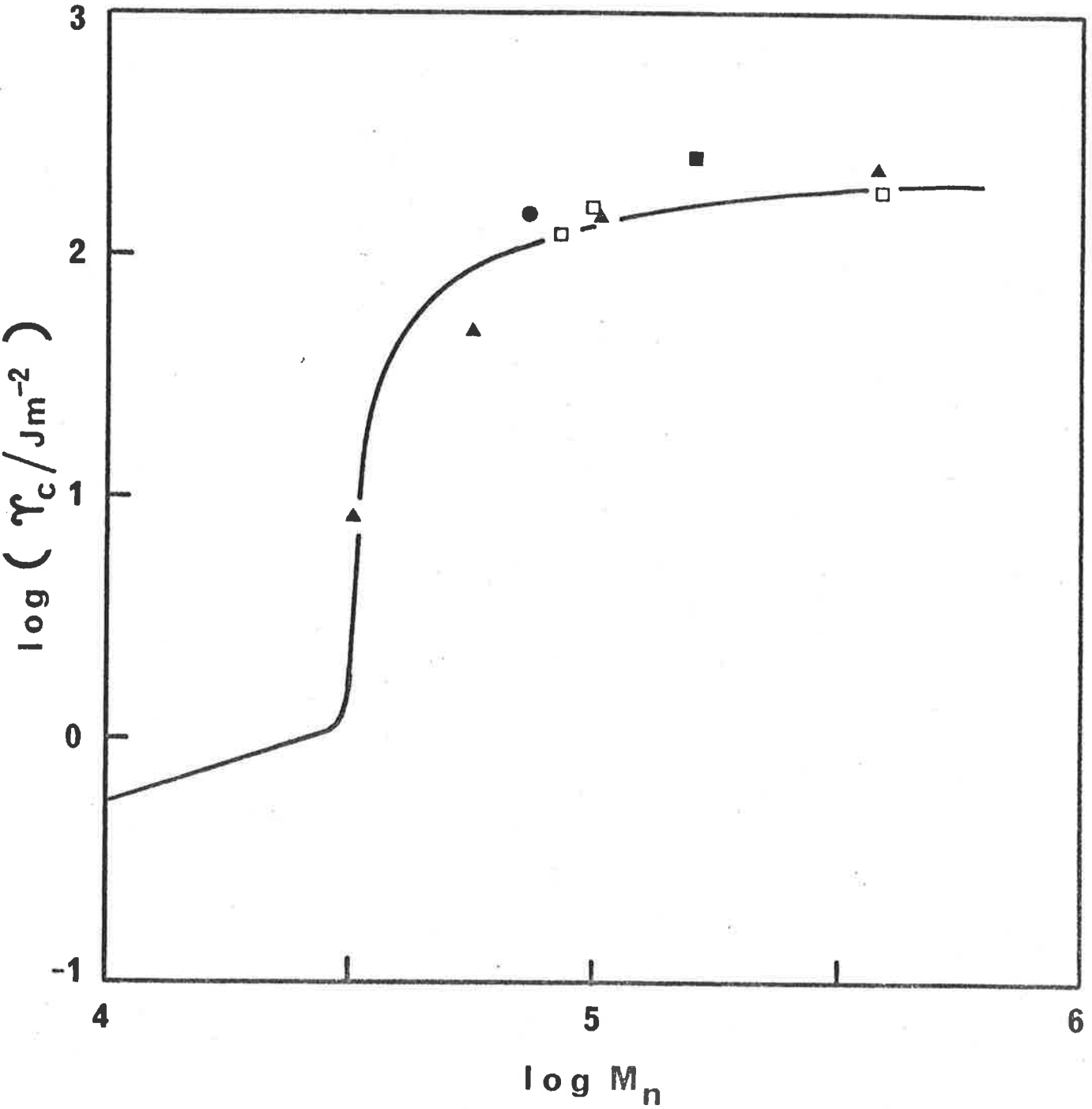

Fig.5.14 Experimental data and theoretical curve of log γ_c vs. log M_n relationship for PMMA. Narrow MWD PMMA (M_w/M_n = 1.2) (▲), commercial PMMA (M_w/M_n = 2.1) (□), blend B1 (M_w/M_n = 2.6) (■) and blend B3 (M_w/M_n = 4.4) (●).

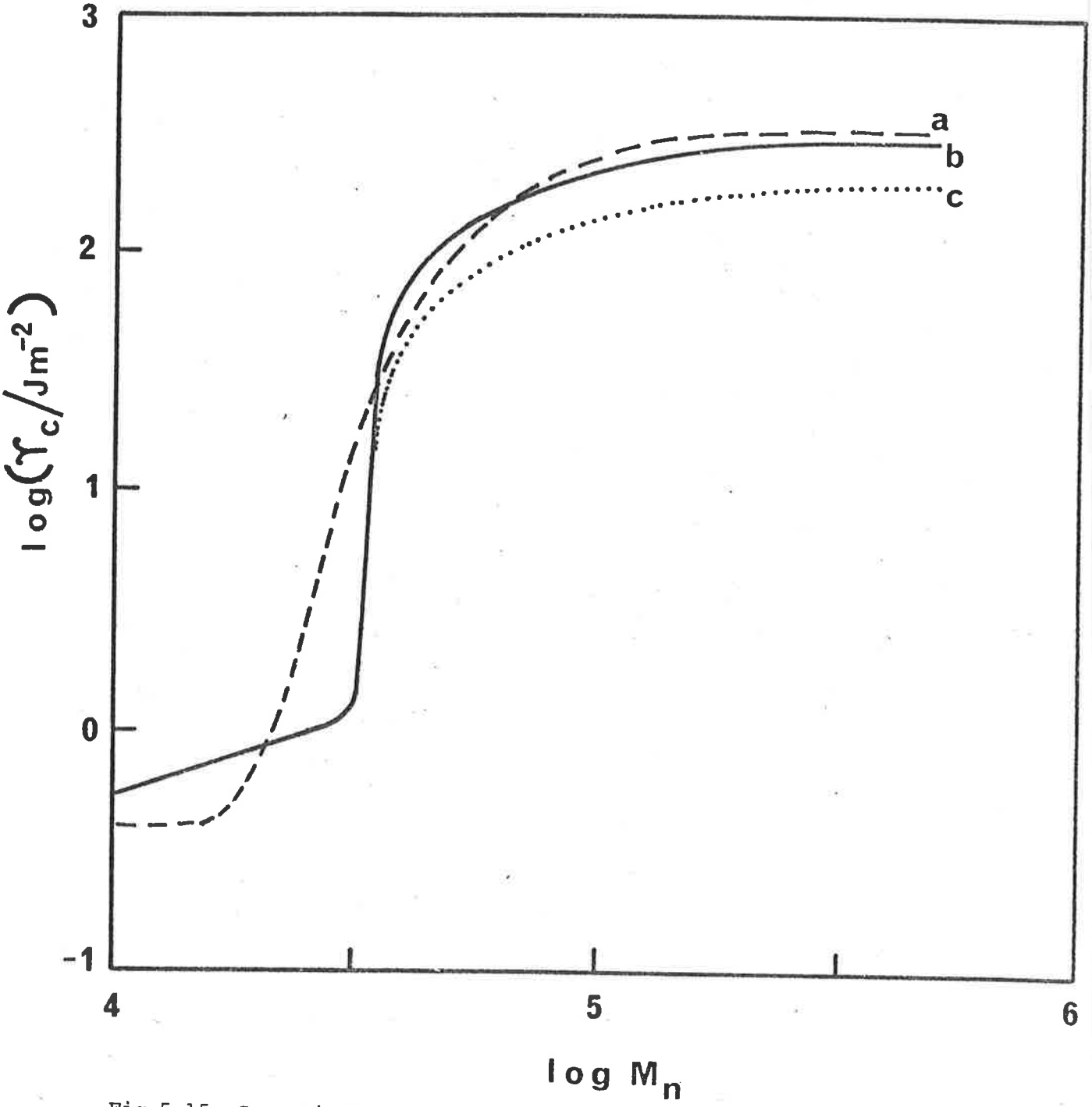

Fig.5.15 Comparison of Kusy and Turner's curve and theoretical curves of this work. (---) Kusy and Turner ($\gamma(\infty) = 3.5 \times 10^2$ Jm^{-2}). (——) This work ($\gamma(\infty) = 3.0 \times 10^2$ Jm^{-2}, $M_w/M_n = 1$). (....) This work ($\gamma(\infty) = 2.0 \times 10^2$ Jm^{-2}, $M_w/M_n = 1$).

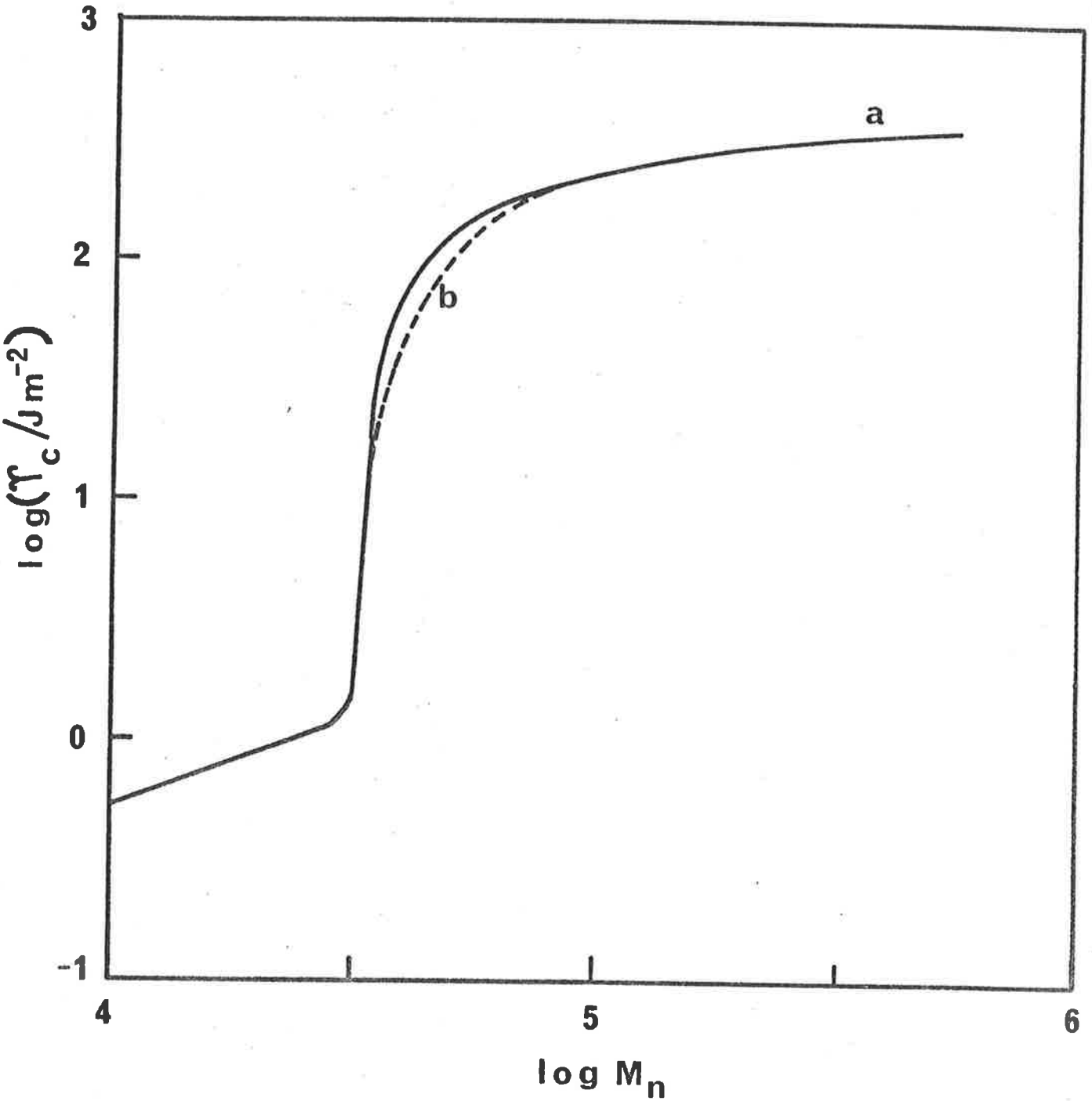

Fig.5.16 Effect of MWD on the fracture energy, (a) M_w/M_n = 1 and (b) M_w/M_n = 4.

is illustrated in Fig.5.17. It is obvious that no single correlation exists between log γ_c and M_w.

Furthermore, it is of interest to compare the theoretical values with the experimental values obtained by Pittman and Ward for polycarbonate (4). The critical MW, M_c, is known to be 4,800 (119) and therefore it can be assumed that the fracture energy at M_n = 4,800 is derived solely from a contribution of γ_{c_1} where Pittman and Ward's data indicate a value of $2\gamma_{c_1} \simeq 0.05$ kJ m^{-2}. To calculate theoretical values of γ_{c_2} (Eq.5.43), it is necessary to determine $\gamma(\infty)$. In Pittman and Ward's experiment, all specimens had low MW and the value of $\gamma(\infty)$ for infinite MW could not be determined. However, it is possible to calculate this value from the SIF, K_i, at crack initiation and this has been determined by Parvin and Williams (120) to be 2.2 MN $m^{-3/2}$. Thus $G(\infty) = 2\gamma(\infty)$ is determined by $G(\infty) = K_i^2/E$ where E = 2350 MN m^{-2} (121). That is

$$G(\infty) = 2.06 \text{ kJ } m^{-2}$$

Using Eqs.5.27a, 5.43 and $G_c = 2\gamma_c$, the theoretical values of G_c can be estimated from

$$G_c = 0.05 + 2.06 \left(1 - \frac{4800}{M_n}\right) S \quad \text{kJ } m^{-2} \qquad (5.45a)$$

As mentioned above, if M_n is used to calculate the G_c the MWD effect can be neglected, i.e. $S \simeq 1$ and Eq.5.45a is rewritten as

$$G_c = 0.05 + 2.06 \left(1 - \frac{4800}{M_n}\right) \text{ kJ } m^{-2} \qquad (5.45b)$$

The theoretical curve from Eq.5.45b shows an excellent agreement with Pittman and Ward's data (Fig.5.18). In their paper (4), Pittman and Ward posed two questions (a) Does the fracture energy depend on M_n or M_w, and (b) Why does the fracture energy depend strongly on MW in the region of MW just larger than M_c? The model suggested in this work provides answers to both of these questions. Firstly, because the effect of MWD can be neglected in

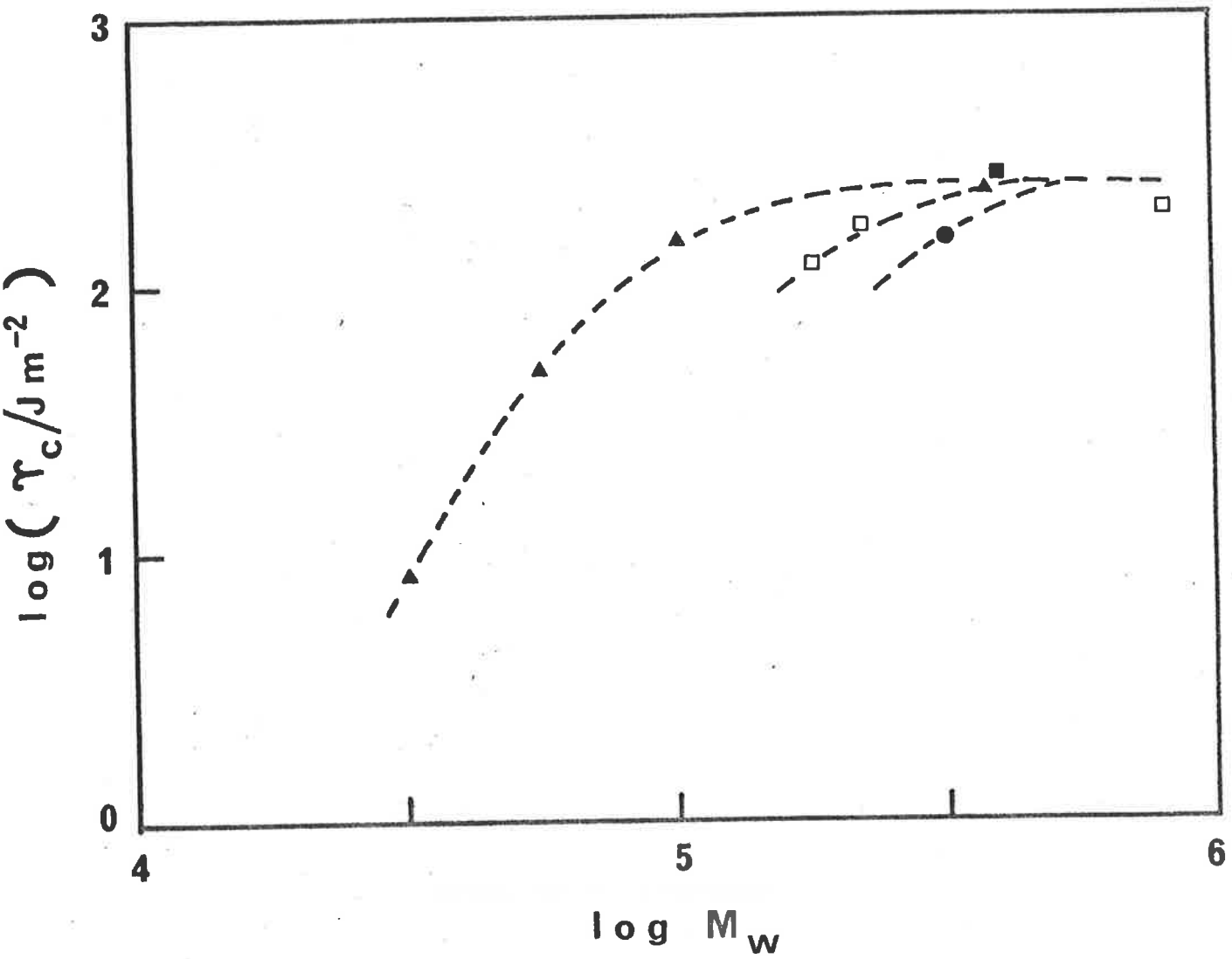

Fig.5.17 Plot of log γ_c vs. log M_w. Symbols as in Fig.5.14.

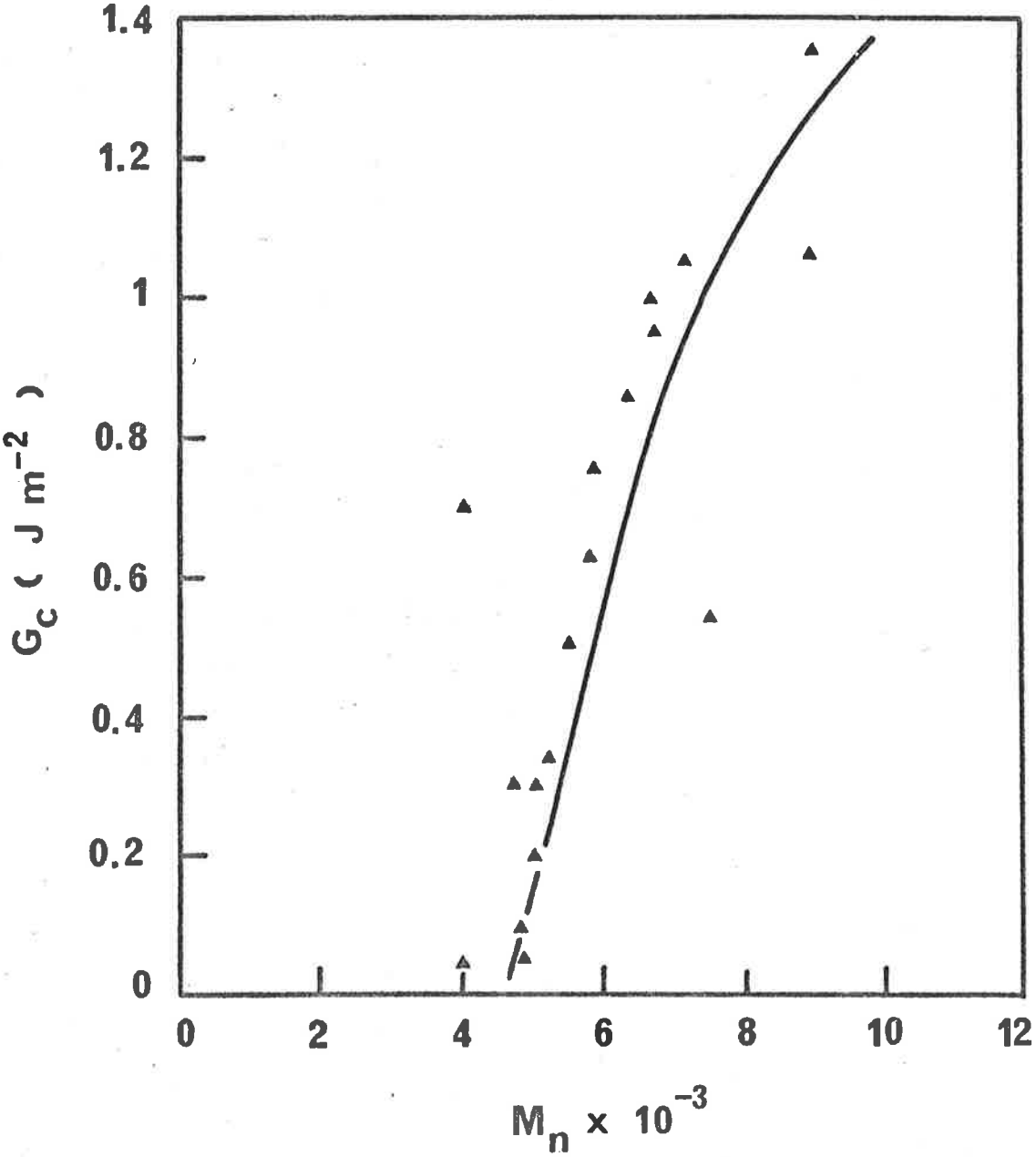

Fig.5.18 Theoretical curve of G_c vs. M_n (solid line) and experimental data for polycarbonate (▲). (4).

the log γ_c (or log G_c) vs. log M_n curve, the number-average MW, M_n, is the most suitable mean MW to relate to the fracture energy. Secondly, the drastic increase in the entanglement number when the MW increases from M_c to the medium MW range, is responsible for the strong dependence of the fracture energy on MW.

In brief, it is suggested that a relationship exists between the fracture toughness and MW based on the density of entanglements. The proposed theory has clearly pointed out the important fact that when the fracture energy is expressed in terms of M_n, the effect of MWD is negligible.

Recently, the entanglement network model has been utilized by Bersted (119) to interpret the tensile and impact strength of amorphous polymers. The agreement of the model with the experimental results leads to a conclusion similar to our theory in that a higher entanglement density will involve more molecular chains capable of supporting the stress. Feller and Huang (115) have proposed that the craze is a series of microvoids surrounded by entanglements and defined that probability of craze formation is probability of finding a microvoid surrounded by entanglements. The probability shows a sigmoidal dependence on MW, becomes zero at $M \leq M_c$ and reaches a limit at high MW.

Matveyev et al. (122) related the "durable time" of high density polyethylene (obtained from a creep test) with MW and MWD and discussed the results in terms of the number of tie chains, i.e. the number of molecular chains in the amorphous phase connecting crystalline phases. The experimental results suggest that the tie chain concept is analogous to the entanglement concept but further investigations are required to examine the effect of the MW and MWD and so understand the role of the tie chains in fracture process.

5.4.4 Criticism of Kusy and Turner's Theoretical Treatment (2)

A model of considerable relevance to this work is that proposed by Kusy and Turner (2). It represents the first attempt to establish the relationship between the fracture energy and MW. Kusy and Turner assumed that in the range of MW $\leq M_c$, the fracture energy, γ_c, is equal to the constant surface energy, γ_{c_1}, and in the range of MW > M_c the fracture energy, γ_c, is equal to the sum of $(\gamma_{c_1} + \gamma_{c_2})$, where γ_{c_2} is the plastic deformation work contributed by molecules having MW larger than a characteristic MW, M_{KT}. In contrast to our model, this characteristic MW, M_{KT}, is an adjustable parameter. Using the arguments previously developed (Section 5.4.3), the weight distribution curve of a polymer is divided into two regions, the region of MW > M_{KT} is the only region describing the molecules able to contribute to the plastic deformation. Kusy and Turner have chosen the Schulz-type distribution function, which is very similar to the logarithmic normal distribution function (113), as a suitable function to describe the MWD of their polymers. The Schulz-type distribution function is expressed by

$$W(M) = \left(\frac{k_s}{M_n}\right)^{k_s+1} \left(\frac{M^{k_s}}{k_s}\right) \exp\left(-\frac{k_s}{M_n}\right) \qquad (5.46)$$

and

$$M_w/M_n = (k_s + 1)/k_s \qquad (5.47)$$

where k_s is a parameter which characterizes the distribution.

The plastic deformation work γ_{c_2} is given by

$$\gamma_{c_2} = \gamma(\infty)\ S \qquad (5.48)$$

where

$$S = \int_{M_{KT}}^{\infty} W(M)\ dM$$

For $k_s = 1$, S becomes

$$S = \exp(-M_{KT}/M_n)\left(1 + \frac{M_{KT}}{M_n}\right) \qquad (5.49)$$

for $k_s = 2$,

$$S = \exp\left(-2M_{KT}/M_n\right)\left(1 + \frac{2M_{KT}}{M_n}\right)\left(1 + \frac{2M_{KT}^2}{M_n}\right) \qquad (5.50)$$

Then the fracture energy is expressed by

$$\gamma_c = \gamma_{c_1} + \gamma(\infty)\exp\left(-M_{KT}/M_n\right)\left(1 + \frac{M_{KT}}{M_n}\right) \quad ; \quad k_s = 1 \qquad (5.51)$$

and

$$\gamma_c = \gamma_{c_1} + \gamma(\infty)\exp\left(-2M_{KT}/M_n\right)\left(1 + \frac{2M_{KT}}{M_n} + \frac{2M_{KT}^2}{M_n}\right) \; ; \; k_s = 2 \qquad (5.52)$$

where γ_{c_1} is the surface energy. The variation of k_s from 1 to 2 which corresponds to the variation of the MWD from 2 to 1.5 (Eq. 5.47) has little effect on γ_c. In our model, the characteristic MW is assumed to be fixed at critical MW, M_c, while Kusy and Turner's M_{KT} is an adjustable parameter. The arbitrary selection of M_{KT} by Kusy and Turner is the focus of the present criticism.

Firstly, the parameter M_{KT} is ill-defined and lacks physical significance. Kusy and Turner realised that the craze could be regarded as an extended network of polymer molecules because in the medium MW range (M_n = 40,000 to 100,000 for PMMA) full extension of a molecule chain is smaller by a factor of three than the magnitude of the COD (2,123). In the framework of their treatment, the relationship of M_{KT} to entanglements was not explicitly established. To fit the theoretical curve to the experimental data for PMMA, Kusy and Turner adjusted the value of M_{KT} to 100,000, a value much larger than M_c (M_c = 30,000) (Fig.5.19). For the case of the fracture energy in polystyrene, M_{KT} is required to be as large as 500,000 to fit the theoretical curve compared to M_c = 70,000 (108). Therefore, although there is an implied notion that the entanglement network is a factor involved in craze information at the crack tip, the relationship between M_{KT} and M_c, or the physical significance of M_{KT}, was not established in Kusy and

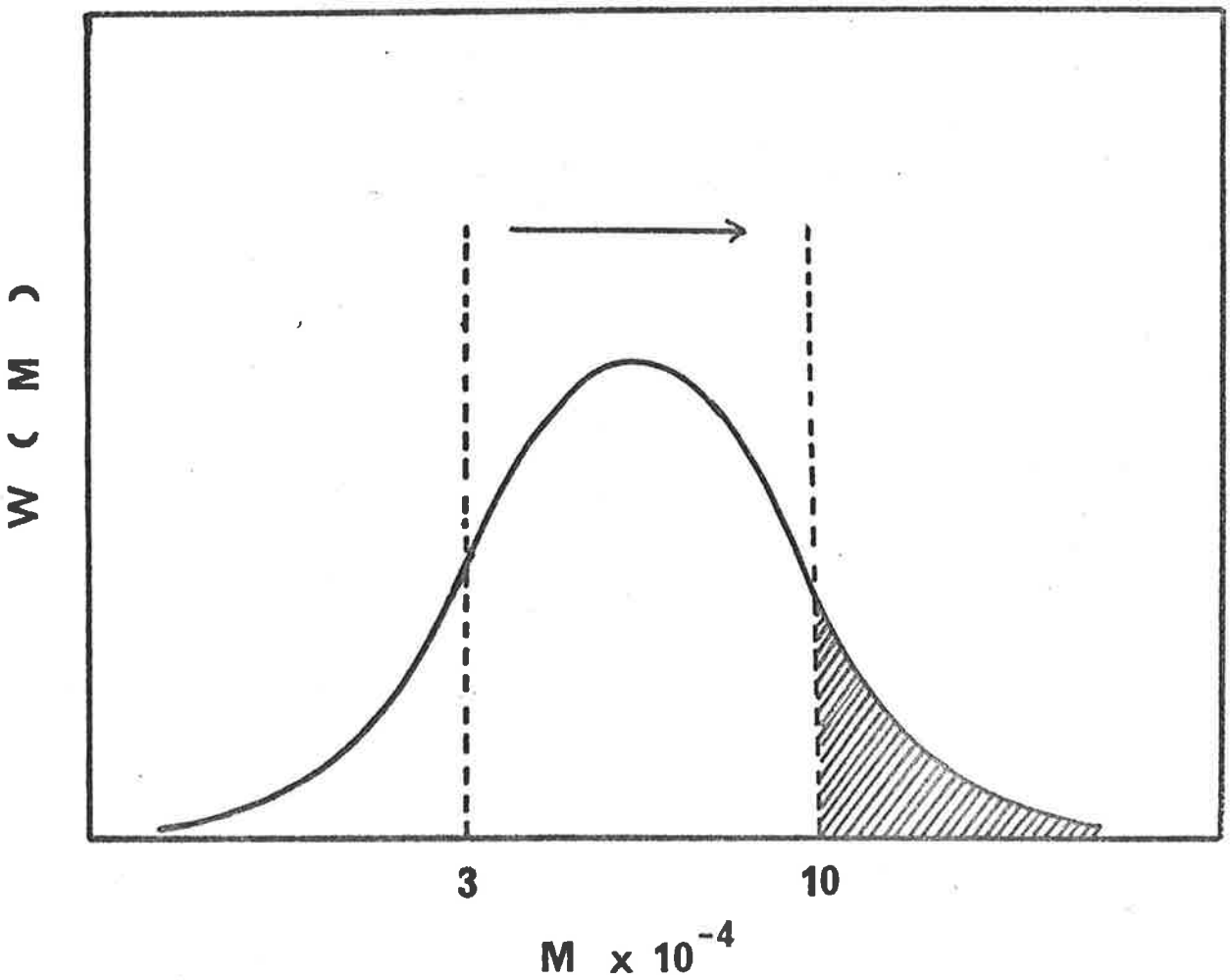

Fig.5.19 According to Kusy and Turner (2) the shaded area represents the weight fraction of molecules capable in participating plastic deformation.

Turner's theory.

Secondly, Kusy and Turner's model suggests that a step change in γ_c, that is an abrupt change from $\gamma_c = \gamma_{c_1} + \gamma_{c_2}$ to $\gamma_c = \gamma_{c_1}$, occurs at M_{KT} when the polymer is monodisperse. However, this suggestion is both contradictory and misleading. From the viewpoint of our model; there cannot be an abrupt change at M_{KT} as Kusy and Turner suggested; the entanglement density decreases sigmoidally from high MW range to M_c and so does the γ_c. These authors, however, did admit in their paper that the suggestion that there exists a unique boundary which determines an all-or-nothing contribution of γ_{c_2}, is an oversimplification. Examining the experimental curve of log γ_c vs. log M_n relationship (Figs.5.13-5.14) the sigmoid-like curve has a downturn in MW around M = 100,000 and an upturn in MW around M_c = 30,000. Kusy and Turner have defined M_{KT} as the MW corresponding to the plastic deformation. However, from our point of view if the M_{KT} has any physical significance at all, it may possibly designate the onset of <u>complete plastic deformation</u> where γ_c begins to approach the limiting value, $\gamma(\infty)$. Complete plastic deformation is associated with the formation of parabolic markings (Fig.5.20) and crazing interference colours on fracture surface of specimen subjected to unstable crack propagation ($v \simeq 10^{-2}$ msec^{-1}). It was observed that there was a lower density of parabolic markings and weaker interference colours in polymer of $M < M_{KT}$ (e.g. narrow MWD PMMA of M_w = 71,000) and these effects completely disappeared at MW close to M_c (e.g. narrow MWD PMMA of M_w = 31,000). The disappearance of the parabolic markings and interference colours suggests that plastic deformation has not occurred at the tip and the craze layer is too thin to be detected by interference fringes (20).

On the whole, because Kusy and Turner's theory failed to quantitatively include the entanglement concept, it could not explain

Fig.5.20 The parabolic markings created by nucleation under stress in narrow MWD PMMA of $M_w \geq 84,000$. Interference colours were observed indicating the presence of crazed material. 200x.

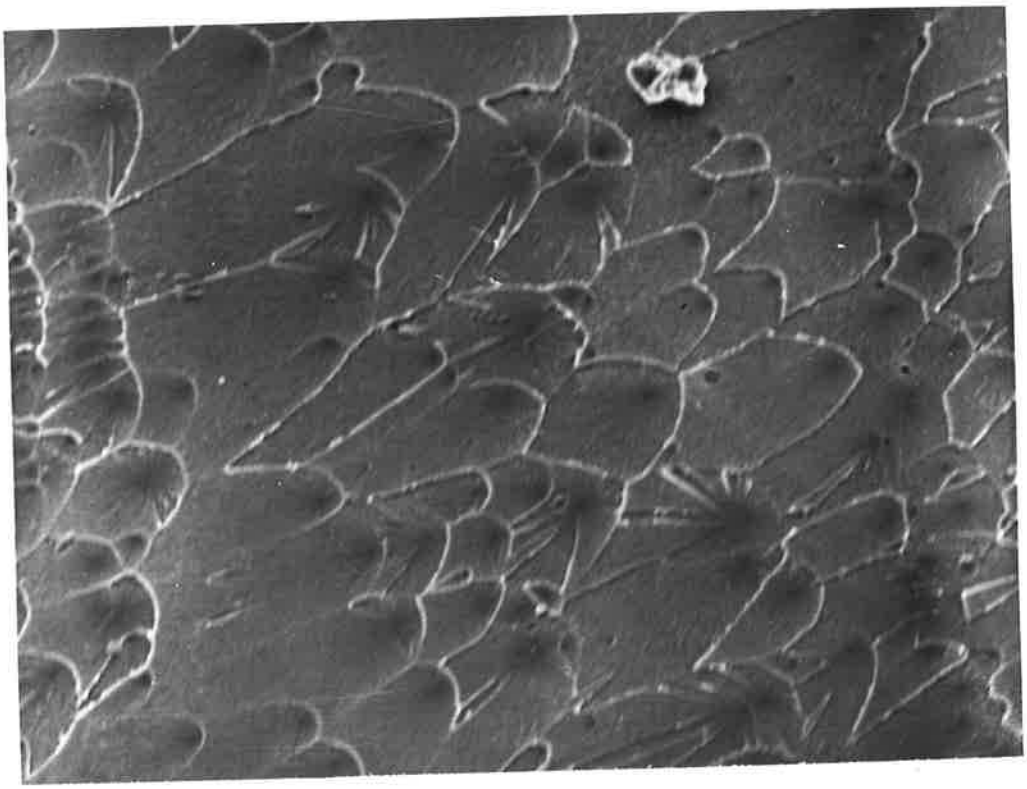

(a) the upturn in the log γ_c vs. log M_n curve occurring around the vicinity of M_c and (b) the strong dependence of fracture energy on MW as observed in amorphous polymers such as PMMA (2), polystyrene (3) and polycarbonate (4). The result was that Kusy and Turner found it necessary to position the characteristic MW, M_{KT}, at a higher MW than M_c (Fig.5.19) to reduce the relative area expressing the weight fraction of molecules capable of forming entanglement networks. Accordingly, the theoretical values γ_{c_2} were reduced to fit the experimental data but it was a procedure without physical basis and at the expense of M_{KT} possessing an ambiguous identity.

5.4.5 Conclusions

The following conclusions can be drawn from the above experimental results and discussion

(1) The DT geometry provides a simple and economical method to determine the SIF, K_c, as a function of the crack velocity, v.

(2) The log K_c vs. log v relationship is the most acceptable quantitative description of the effect of MW and MWD on the fracture toughness.

(3) An equation was derived to establish the relationship between the fracture energy, γ_c, and MW on the assumption that (a) only polymer molecules having MW > M_c are capable of participating in plastic deformation at the crack tip, and (b) resulting craze fibrils are stabilized by entanglement networks.

(4) The MWD has little effect on γ_c provided γ_c is expressed in terms of M_n.

(5) The entanglement networks account for a drastic increase in γ_c of polymers in the medium MW range.

(6) Kusy and Turner's theory lacks physical meaning through the use of the ill-defined and adjustable parameter M_{KT}.

Molecular Weight, Molecular Weight Distribution and Temperature Dependence of the Fracture Process in Methanol.

5.4.6 A General Survey of Fracture Data in Methanol

While the fracture process in air shows a crack predominant breakdown mechanism, the fracture process in methanol shows two distinct mechanisms that are strongly influenced by the MW — rapid crack propagation in low MW samples and long craze growth in high MW samples. Nevertheless, because the fracture behaviour in air or in methanol involves the stabilization of craze fibrils during crack or craze growth, the fracture process in air or in methanol can be understood through a common point — chain entanglement . As will be seen later in the experimental results, the role of the entanglement networks again is a key factor in understanding the effect of MW, MWD and temperature on fracture toughness.

The MW effect on the log K_c vs. log v behaviour in methanol at 20°C is shown in Fig.5.21 for narrow MWD PMMA. It can be seen from this figure that the log K_c vs. log v diagram naturally divides into three Regimes: Regime I, Transition Regime and Regime II.

Regime I ($84{,}000 \lesssim M_w \lesssim 550{,}000$) is a mature craze growth regime where a mature craze growth is defined as a fully developed craze (the morphology and scanning electron microscope (SEM) photographs will be discussed later). In this Regime, the log K_c vs. log v relationship is found to be linear where the high fracture toughness is characterised by a slow initial propagating velocity, v_i, and a small slope of the log K_c vs. log v straight line.

Regime II ($23{,}000 \lesssim M_w \lesssim 36{,}000$) is a crack propagation regime. The plot of log K_c vs. log v consists of two parts: (a) a limiting part of infinite slope characterised by the limiting velocity, v_o, and (b) a sloping part where $v < v_o$. As the MW is reduced, v_o will increase and the effect of MW on the sloping part

Fig.5.21 The effect of MW on fracture toughness in methanol (T=20°C) expressing in log K_c vs. log v diagram for narrow MWD PMMA.
(a) Regime I, A1 (M_w = 550,000, □), A3 (M_w = 380,000, ▲), A4 (M_w = 150,000, ○), A5 (M_w = 97,000, △) and A6 (M_w = 84,000, ●).
(b) Transition Regime, A7 (M_w = 71,000, ▽).
(c,d,e) Regime II, A8 (36,000, ▼), A9 (M_w = 31,000, ◊) and A10 (M_w = 23,500, ♦).

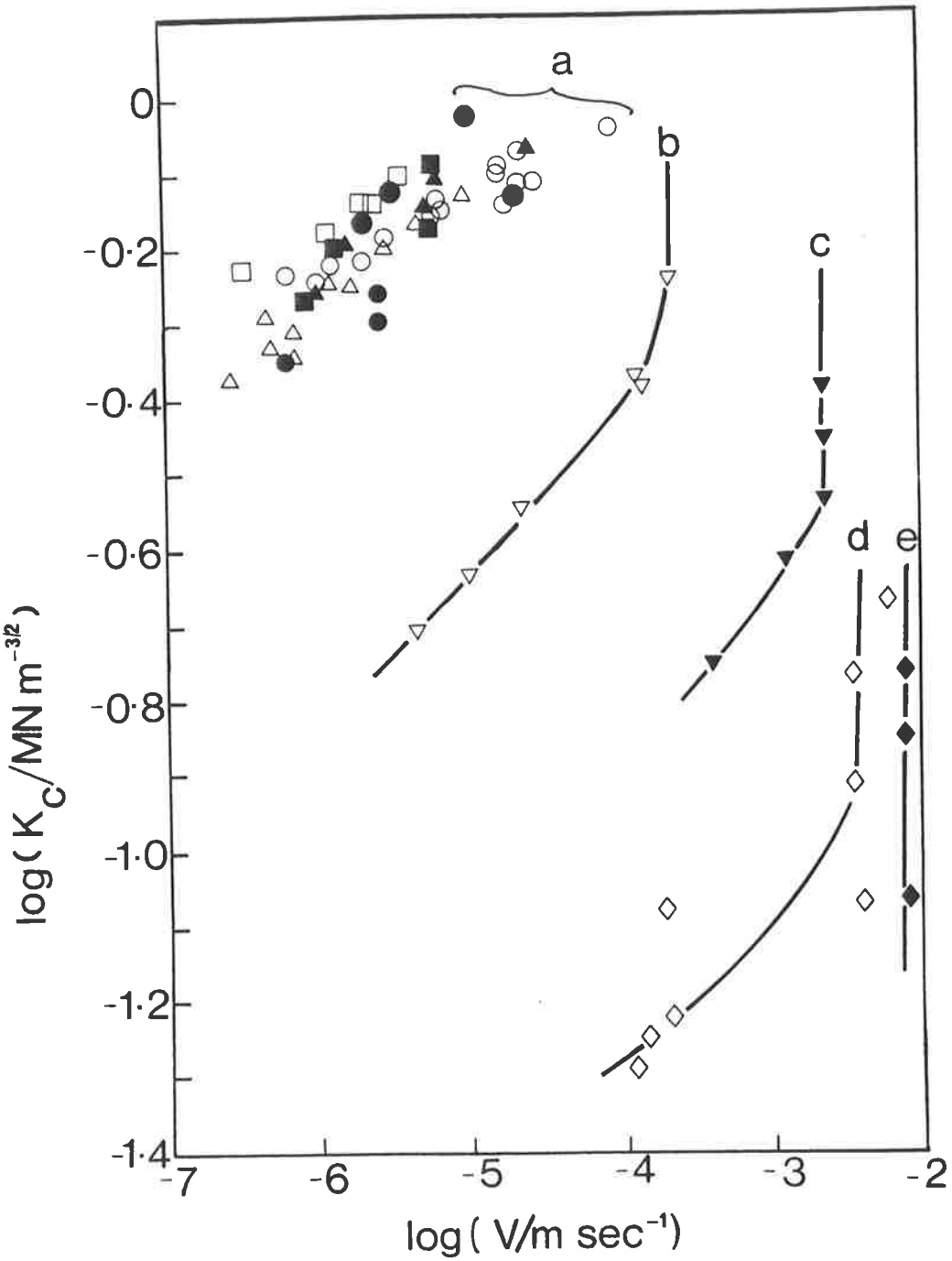
a
b
c
d
e
0
-0·2
-0·4
-0·6
-0·8
-1·0
-1·2
-1·4
-7
-6
-5
-4
-3
-2
log (K_C/MN m^-3/2)
log (V/m sec^-1)

becomes dramatic.

Polymer of M_w = 71,000 which exhibits Transition Regime behaviour shows premature craze growth. From SEM photographs, this Regime is a transition phase between the mature craze growth Regime I and the crack propagation Regime II.

Study of the cracking or crazing surface by SEM* suggests the nature of the fracture morphology is in agreement with the proposed characters of the Regimes in the log K_c vs. log v diagrams. The fracture surface of polymers in Regime I show honeycomb-like (Figs.5.22a,b) or tunnel-like craze matter (Fig.5.23) throughout the fracture surface, whereas the fracture surface of the polymers having low MW (M_w = 23,500 to 36,000) of Regime II show a surface devoid of features (Fig.5.24). Furthermore, it is interesting to note that one can observe a morphological transition zone between Regime I and Regime II that corresponds to the Transition Regime (M_w = 71,000). The SEM photograph of sample A7 (M_w = 71,000) shows a mixing of smooth area and "white" area (Fig.5.25). While the smooth area is typically cracking region, the "white" area is actually craze formation region, the size of the craze is about one tenth of that of the mature craze in Regime I (Fig.5.23). This implies the fact that deficiency of entanglement network support causes the premature breakdown of craze fibrils before the void can expand, also leading to a sudden separation of the log K_c vs. log v curve from Regime I when M_w decreases from 84,000 to 71,000.

The commercial samples HMW, MMW and LMW show different behaviour in log K_c vs. log v diagram (Fig.5.26). Examination of the fracture surfaces by SEM suggests that the fracture toughness

* The fracture surface was easily damaged by electron beam, even at low voltage and beam intensity. Therefore, a quick operation was required and sometimes slightly out-of-focus photographs were unavoidable over the time period required to take the photograph.

Fig.5.22 Honeycomb-like fracture surface of stress-crazing in methanol of narrow MWD PMMA (M_w = 550,000 at T=20°C). (a) 500x (b) 3000x.

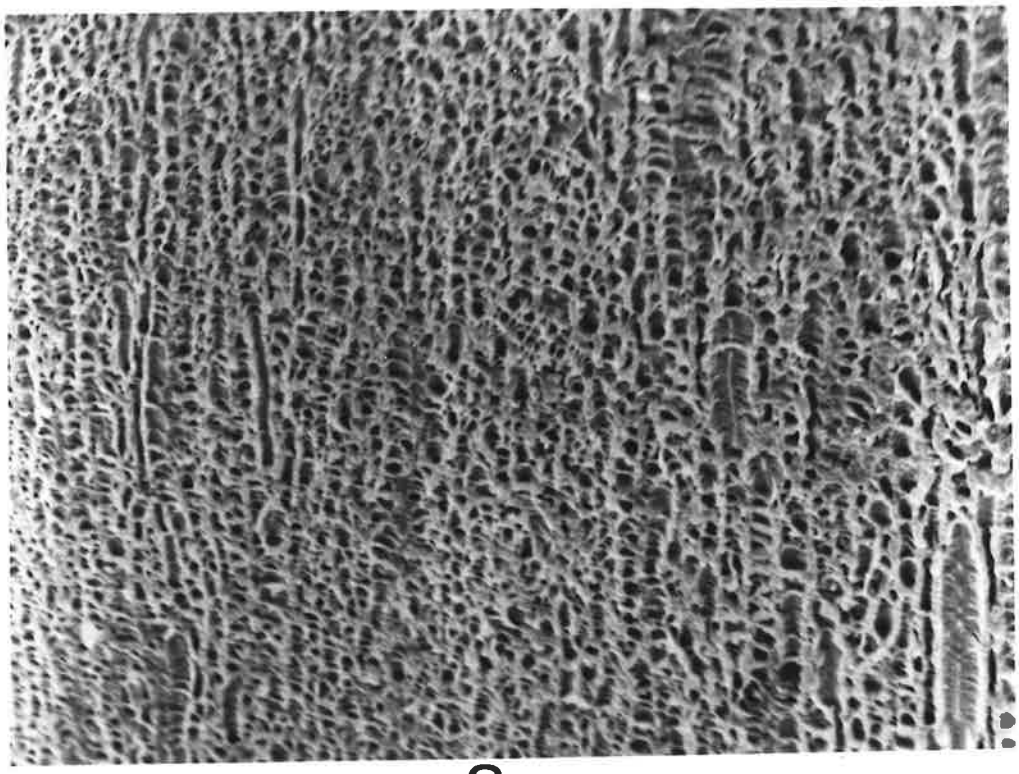

a

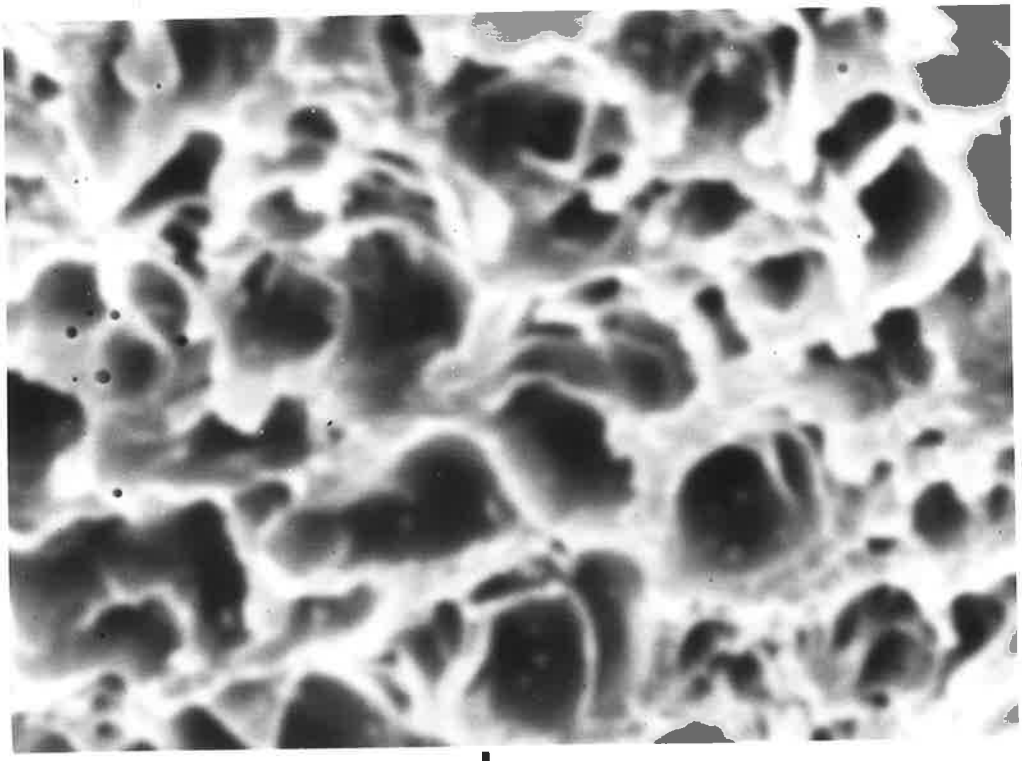

b

Fig.5.23 Tunnel-like fracture surface of stress-crazing in methanol of narrow MWD PMMA (M_w = 84,000 at T=20°C), 500x.

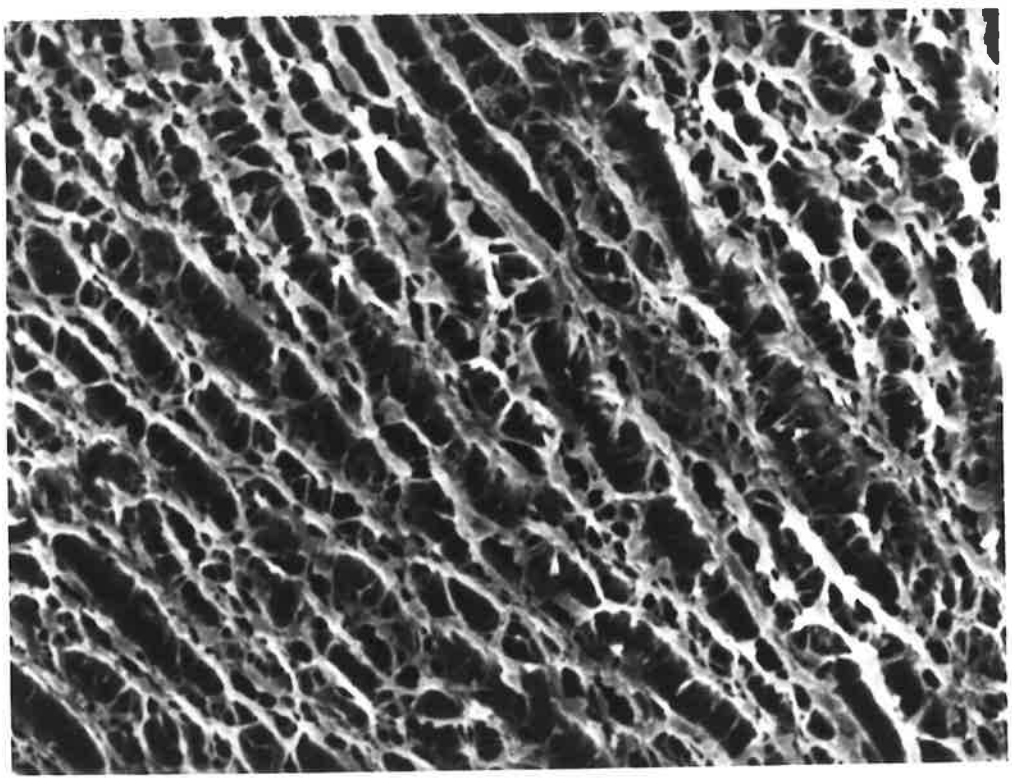

Fig.5.24 Fracture surface of stress-cracking in methanol of narrow MWD PMMA M_w = 36,000 at T=20°C, 500x.

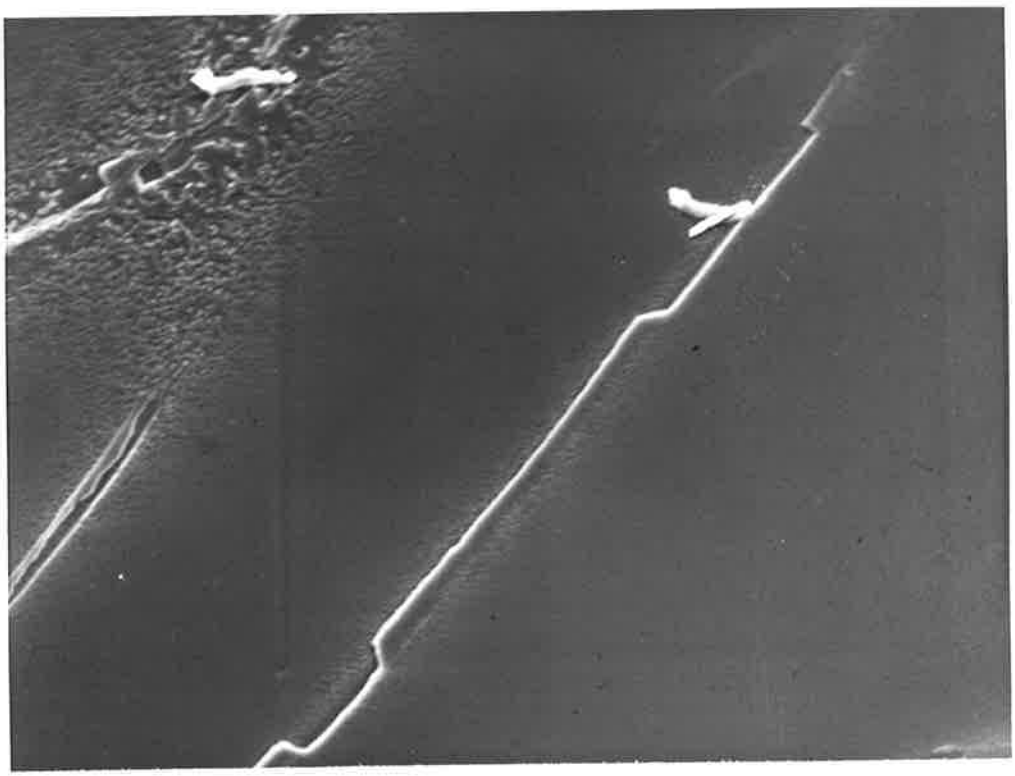

Fig.5.25 Fracture surface of stress-crazing in methanol of narrow MW PMMA (M_w = 71,000 at T=20°C). (a) "White" pattern is premature craze formation, 500x. (b) Enlarged area of premature craze, 3000x.

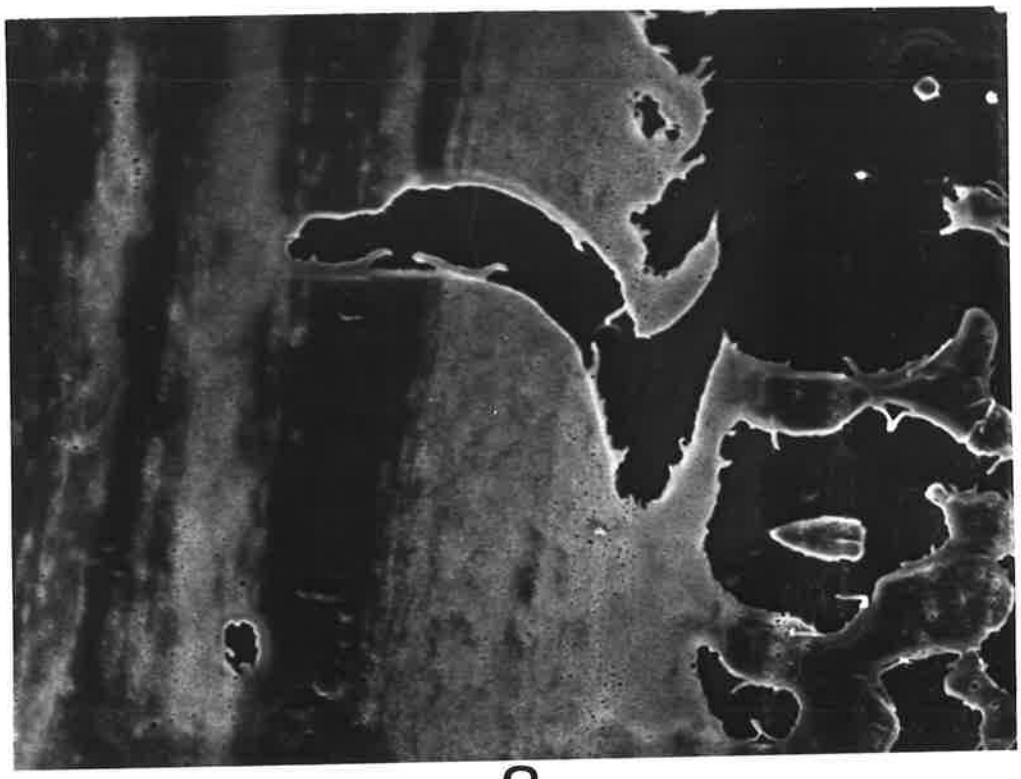

a

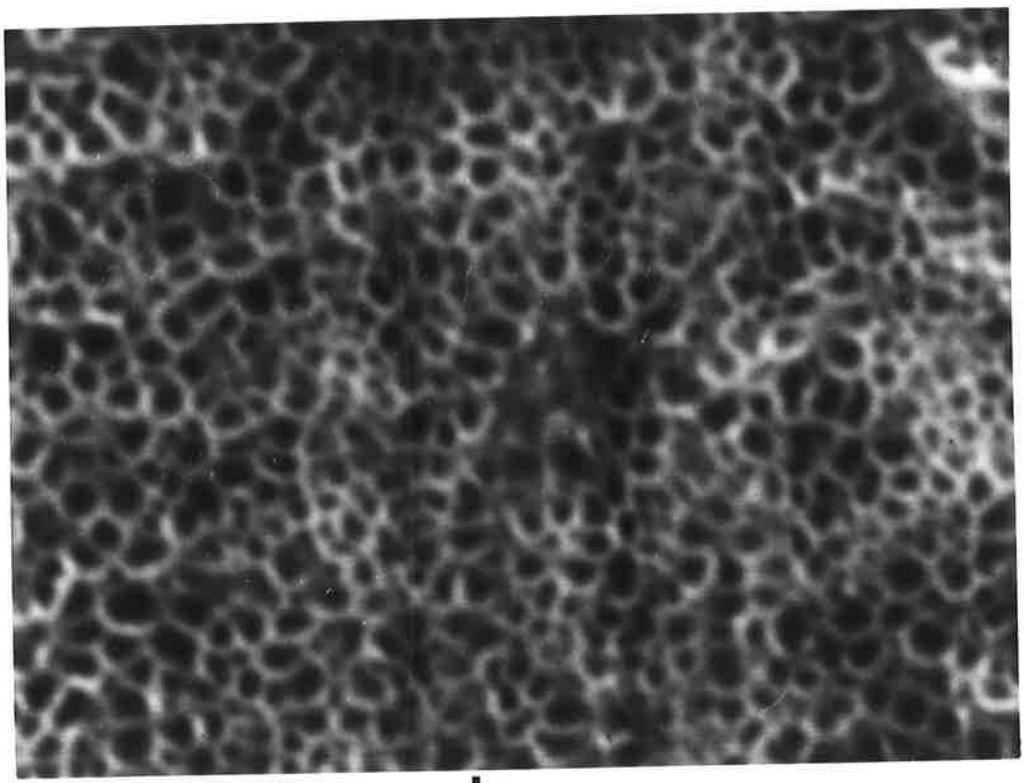

b

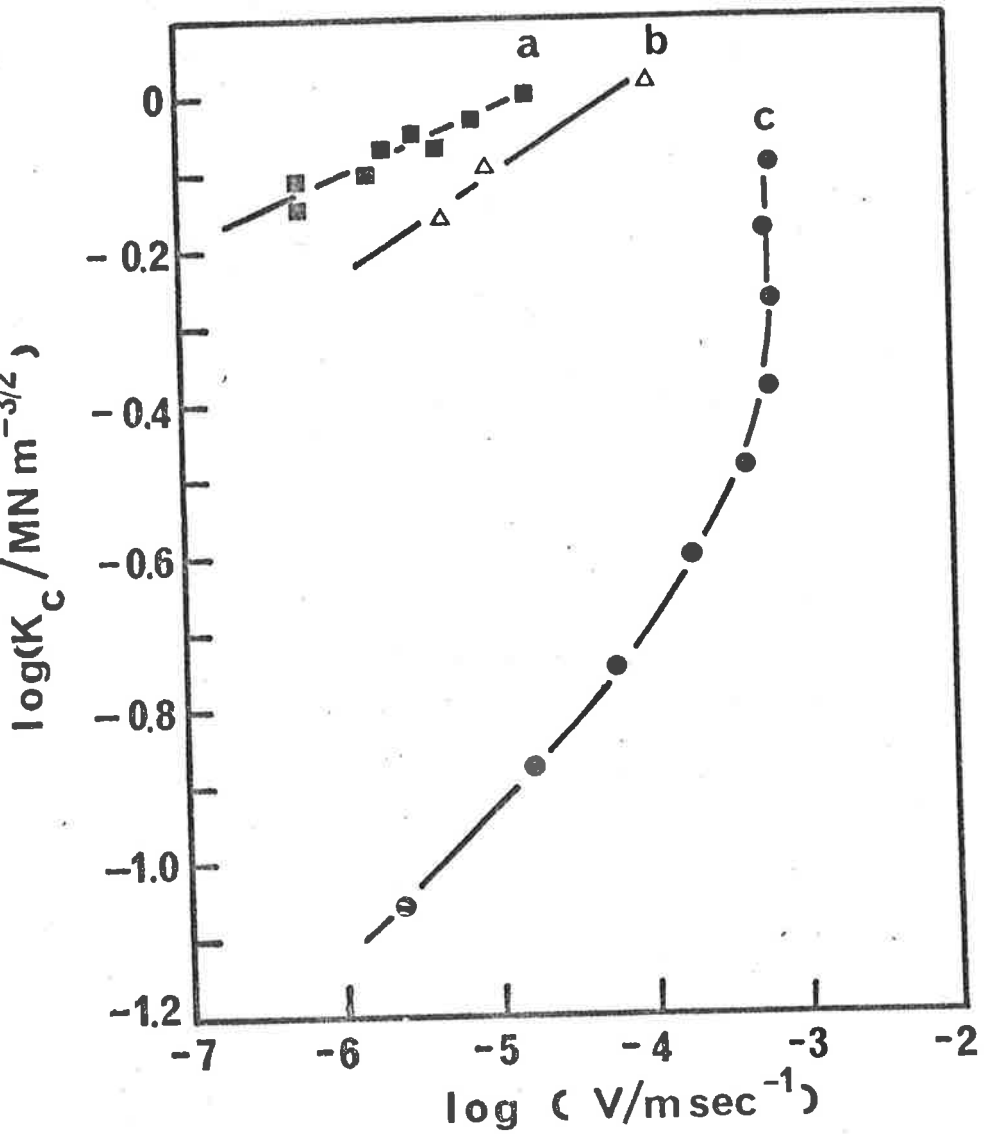

Fig.5.26 Plot of log K_c vs. log v for commercial PMMA fractured in methanol at T=20°C. (a) HMW (Regime I), (b) MMW (Transition Regime), (c) LMW (Regime II).

behaviour of HMW, MMW and LMW, respectively, belong to Regime I, Transition Regime and Regime II (HMW showed honeycomb-like fracture surfaces, MMW showed a mixing of crack and craze surfaces and LMW showed a mirror-like surface).

Addition of low MW polymer ($M \lesssim M_c$) to high MW polymer to produce a controlled MWD blend provided information on the effect of MWD and the effect of a low MW component on fracture toughness. Fig.5.27 shows the log K_c vs. log v diagram of blends B1 and B3 where the crack was started at the same initial SIF, K_i. The log K_c vs. log v behaviour of blend B1 is similar to that of the high MW component, that is 10% (by weight) of low MW component has negligible effect. In contrast, when the amount of the low MW component is increased to 30% (blend B3) a steeper slope in the log K_c vs. log v straight line suggest a lower toughness compared with B1. Examination of the fracture surface shows that B1 has a honeycomb craze pattern (similar to Fig.5.22a,b), whereas 30% of low MW in B3 is sufficient to create a weak craze by promoting a rapid coalescence of voids to result in a tunnel-like feature (Fig.5.28a,b).

The fracture morphology, however, only portrays the aftermath of the fracture process, therefore it cannot provide a full understanding of the effect of MW on the breakdown mechanism via crack propagation or craze growth. In a similar manner to the fracture process in air, the breakdown mechanism in methanol can be understood by adopting the concept of the entanglement networks. Based on the entanglement density, a quantitative criterion can be developed to understand how the MW influences the crack propagation or the craze growth in the presence of methanol.

Table 5.6 illustrates the interesting relationship between the cracking or crazing behaviour and the existence of rubbery zone in the stress relaxation curves of methanol equilibrated PMMA.

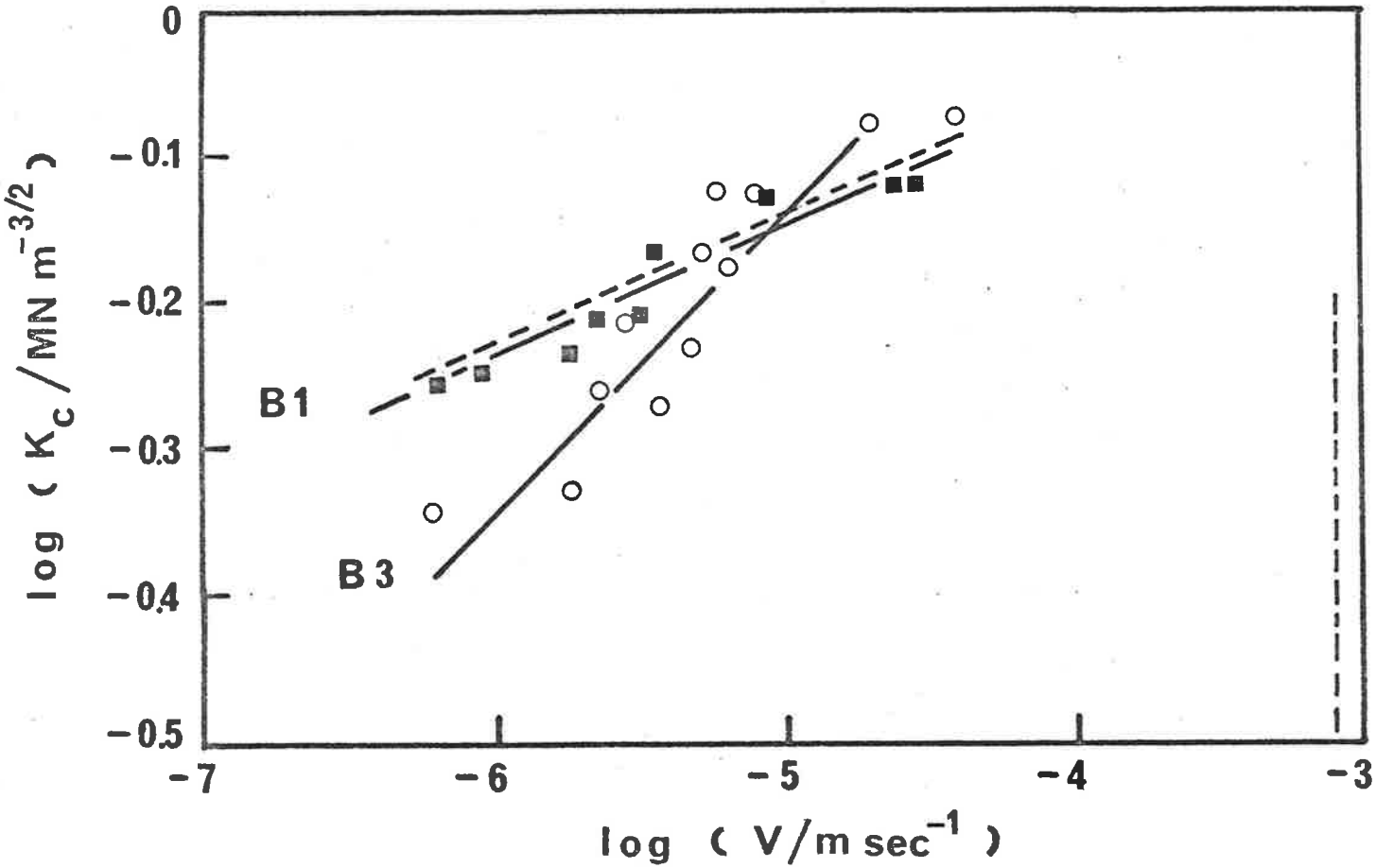

Fig.5.27 Plot of log K_c vs. log v for blends Bl and B3 fractured in methanol at T=20°C. The broken lines show the log K_c vs. log v relationship of the components.

Fig.5.28 Fracture surface of blend B3 in methanol at T=20°C, 500x.

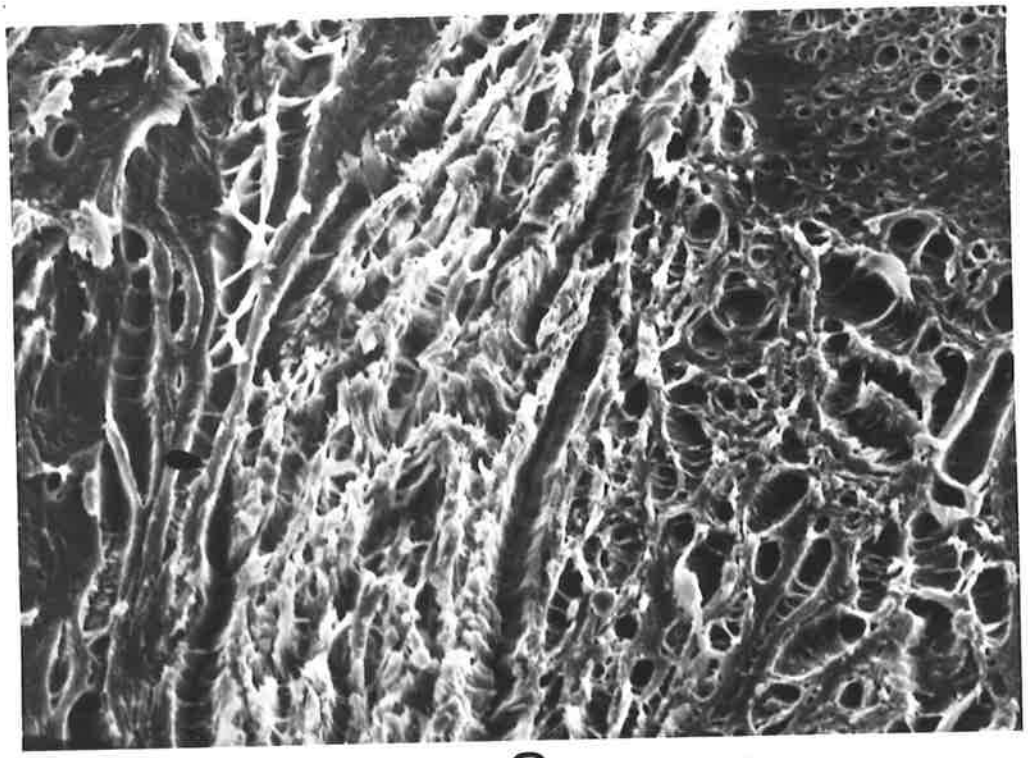

a

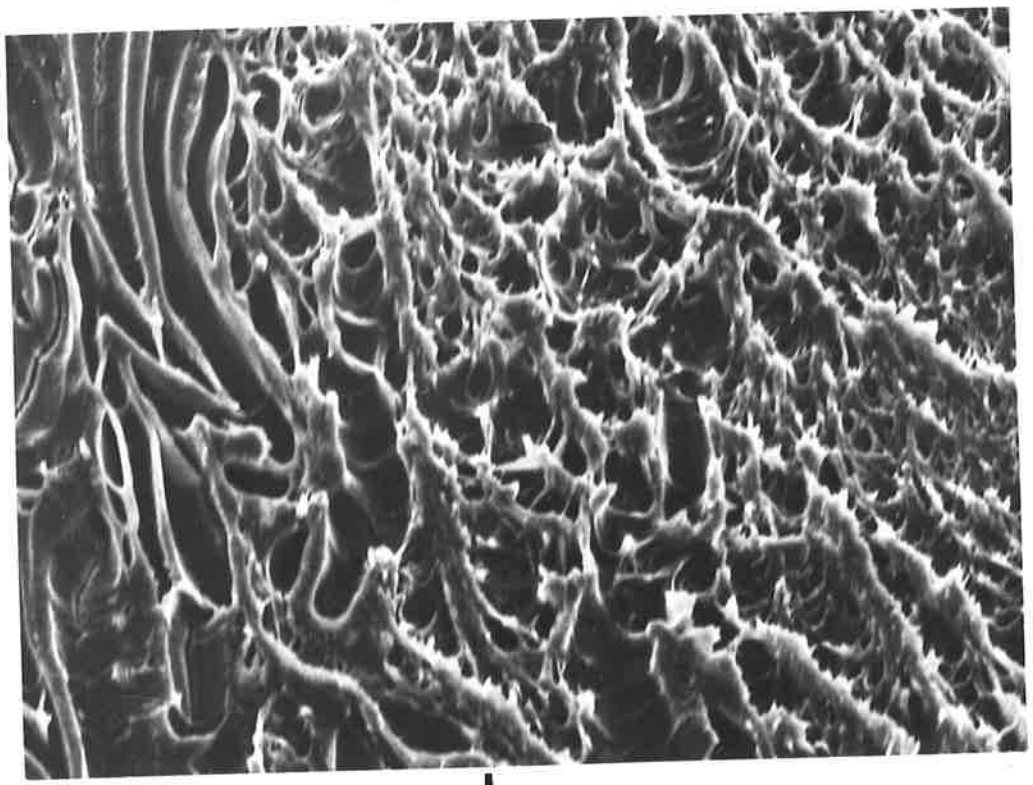

b

TABLE 5.6: Relationship between fracture behaviour and the existence of the rubbery zone of commercial and narrow MWD PMMA in the presence of methanol.

M_w	M_w/M_n	Behaviour on log K_c vs. log v diagram	Rubbery zone
$\geq$ 84,000	1.2	Regime I	Present
71,000	1.2	Transition Regime	↓
$\leq$ 36,000	1.2	Regime II	Absent
787,000	2.1	Regime I	Present
220,000	2.1	Transition Regime	↓
160,000	2.1	Regime II	Absent

As mentioned in Chapter 4, the presence of a rubbery zone implies the existence of entanglements. Table 5.6 clearly suggests that craze growth (Regime I) in methanol will only occur when entanglements exist and that cracks will propagate (Regime II) when the density of entanglements become zero (i.e. the rubbery zone is absent). Furthermore, the Transition Regime corresponds to the borderline of the presence and absence of the rubbery zone in the stress relaxation curve. This relationship confirms the important role of the entanglement network in determining whether the breakdown mechanism via crack propagation or craze growth. Rewriting Eq.5.35 for the density of entanglements of a plasticized polymer, we obtain

$$\bar{N}_e = \bar{N}_e^{(\infty)} \left(1 - \frac{M_{sc}}{M_n}\right) \tag{5.53}$$

In contrast to dry polymer (0% absorbed solvent) where the critical MW, M_c, is a MWD independent quantity, in the presence of methanol the broader MWD gives a higher M_{sc} (Chapter 4). The effect of MWD on the magnitude of M_{sc} foreshadows the influence of MWD on cracking and crazing behaviours of PMMA in methanol. That is, while the Transition Regime occurs at M_w = 71,000 for narrow MWD PMMA, it

occurs at M_w = 220,000 (MMW) for broad MWD samples. In other words, in the presence of methanol, crazing and high fracture toughness occurs above a higher limiting MW for broad MWD PMMA than for narrow MWD PMMA.

Another distinguishing feature of the MW effect on fracture toughness in the three Regimes can be seen from the log K_c vs. log v curves of various initial SIF, K_i (Fig.5.29), the log K_c vs. log v curves of craze growth Regimes (Regime I and Transition Regime) show a dependence of K_i, i.e. different log K_c vs. log v curves were initiated with different K_i (Figs.5.29-5.31). Consequently, for the case of crack growth (in methanol or in air), comparison of fracture toughness of various MW can be simply made from the magnitude of K_c at a particular v. However, for the case of craze growth, the fracture toughness of materials must be compared from log K_c vs. log v curves of the same initial SIF, K_i. Generally, the fracture toughness can be based on two criteria (a) the initial velocity, v_i, corresponding to K_i and (b) the magnitude of the slope of log K_c vs. log v straight line. Material possessing high fracture toughness, i.e. absorbing more energy, will show a slow initial velocity, v_i, and small slope of the log K_c vs. log v curve. For example, v_i and the slope of the log K_c vs. log v straight line has the value of 0.12 for HMW and 0.16 for MMW (Figs.5.30 and 5.31). Consequently, the mature craze of Regime I that is characterized by a slow initial velocity and small slope of the log K_c vs. log v straight line contains stronger craze matter capable of absorbing more energy than the premature craze of Regime II. The K_i dependence of log K_c vs. log v relationship will be discussed in Section 5.4.8.3.

An interesting phenomena that helps to distinguish a craze from a crack is craze healing. It was noticed that after the

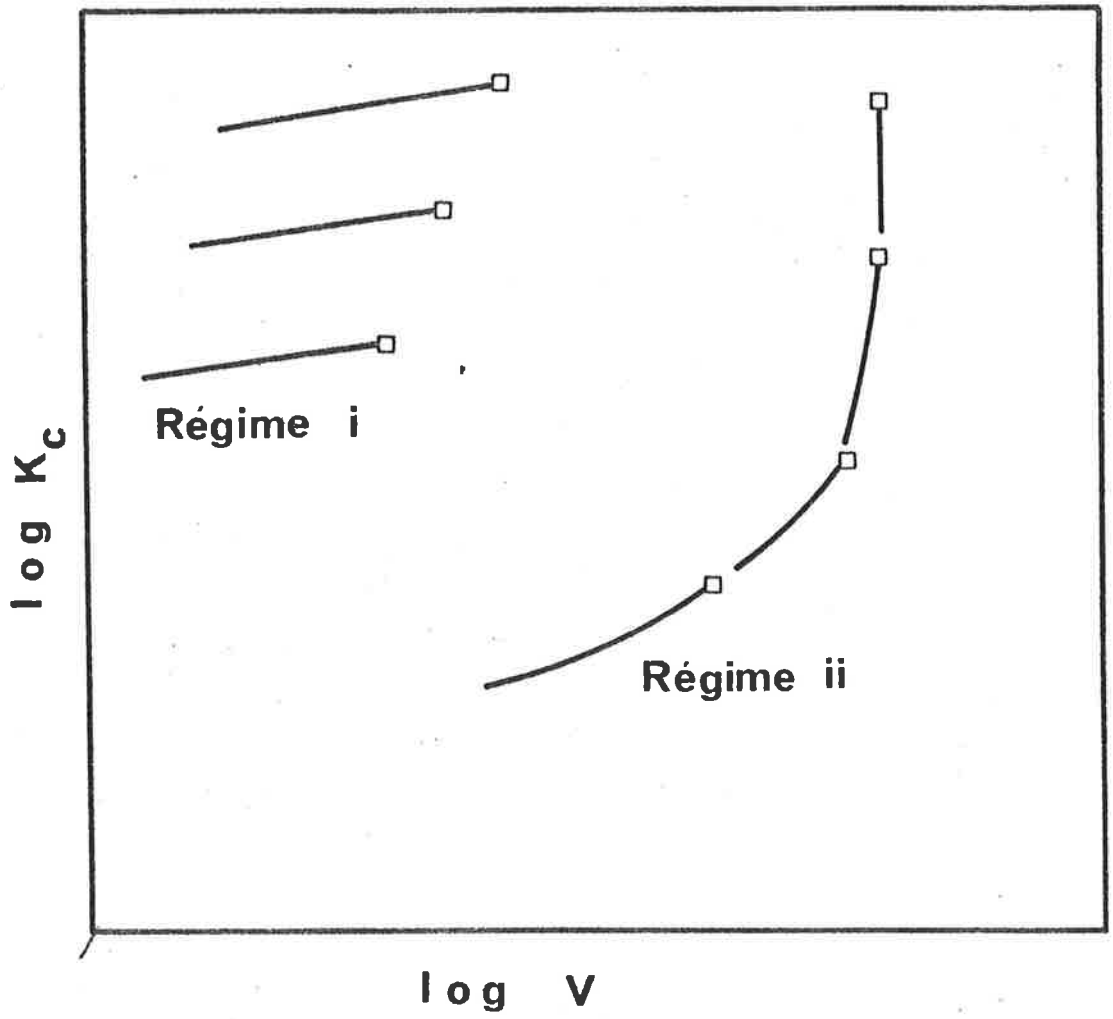

Fig.5.29 Schematic log K_c vs. log v diagram at various initial SIF, K_i (□) for stress-crazing (Regime I) and stress-cracking (Regime II) in methanol.

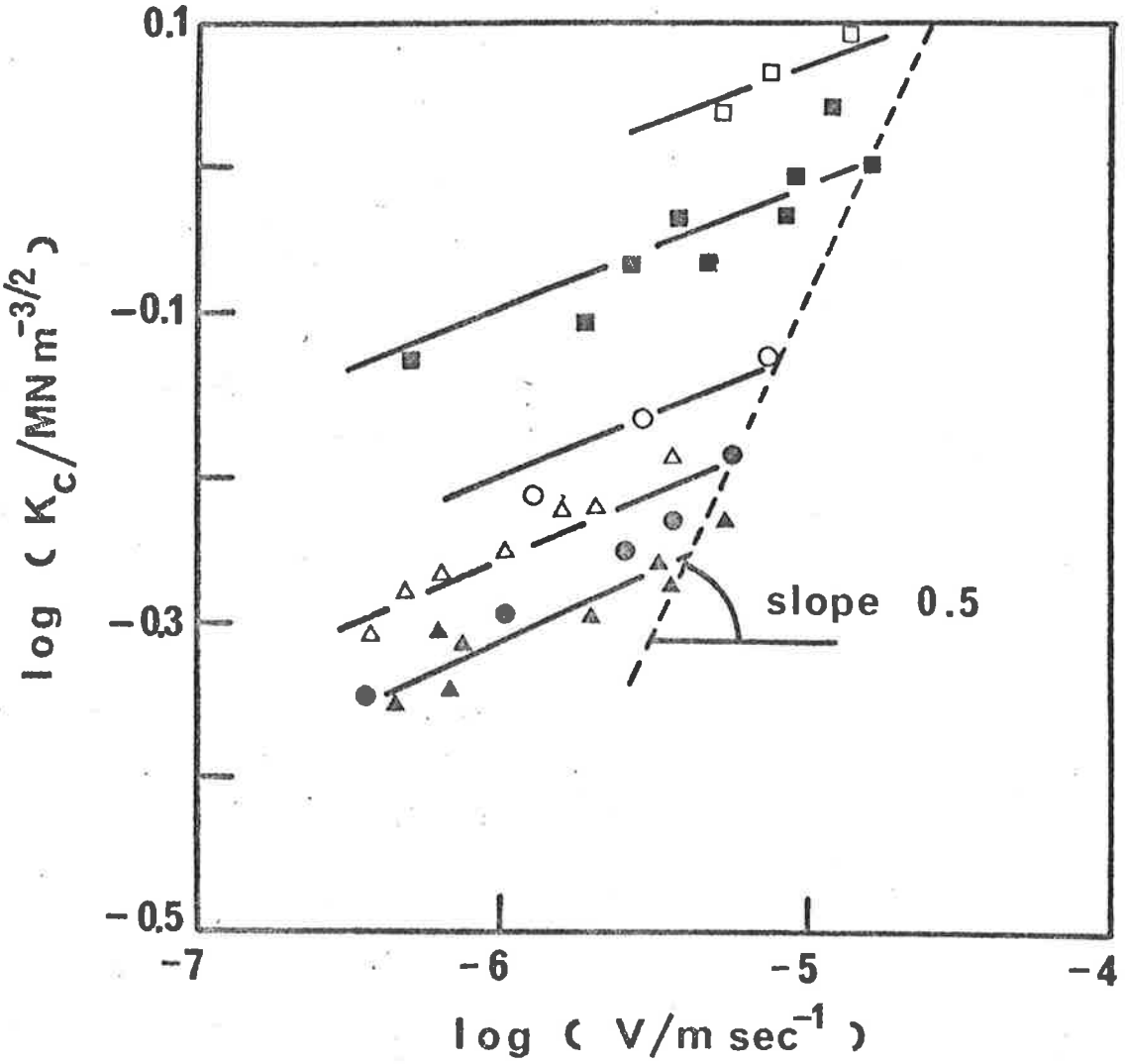

Fig.5.30 The log K_c vs. log v diagram of crazing in methanol at various initial SIF, K_i, for Sample HMW.

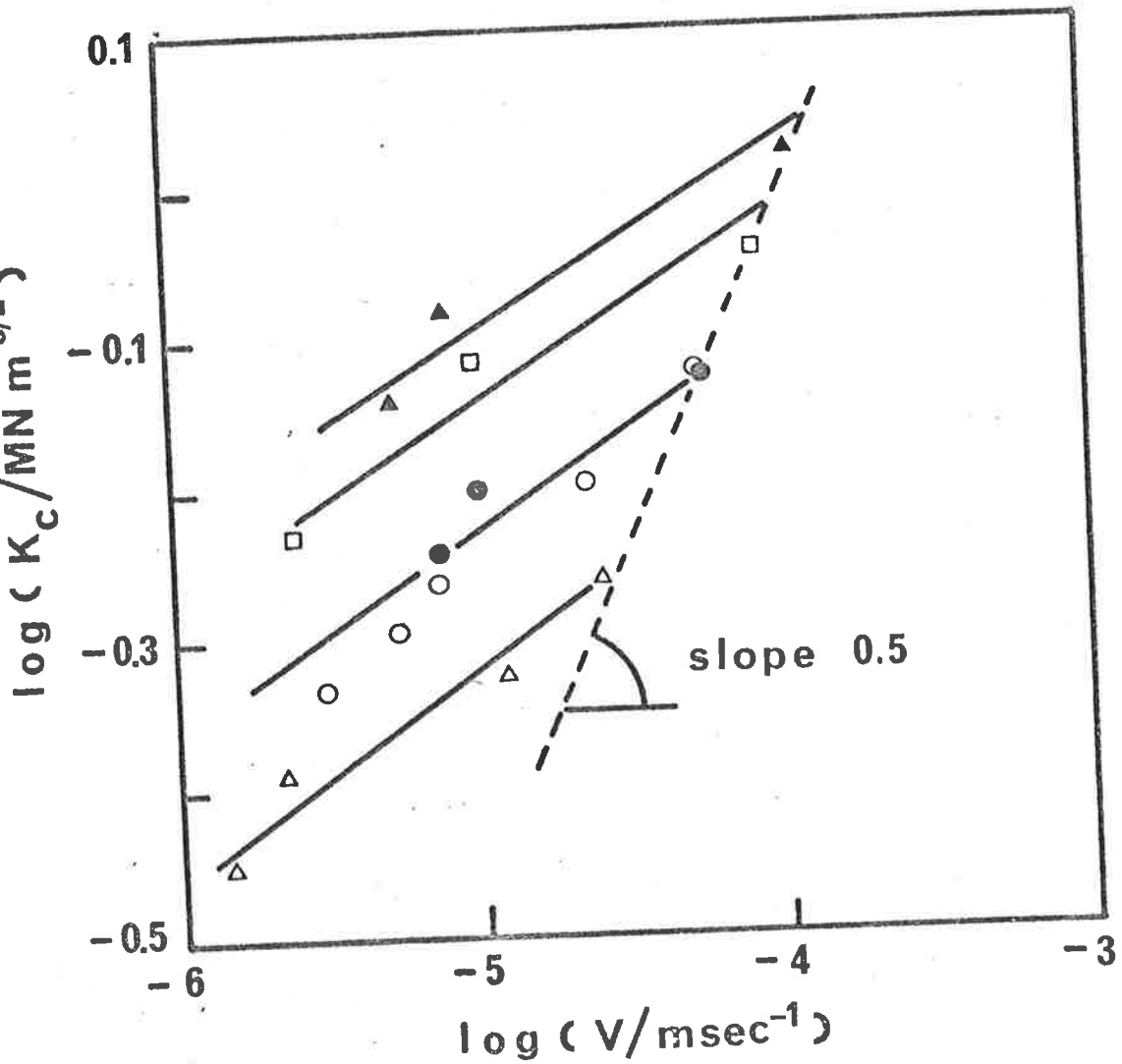

Fig.5.31 The log K_c vs. log v diagram of crazing in methanol at various initial SIF, K_i, for sample MMW.

test specimens were taken out of the methanol bath, the crazed specimens healed overnight and those specimens containing cracks did not heal. By healing, it is meant that the craze no longer reflects light. A simple test was carried out to verify this observation. A crack was forced to propagate in air and the cracked specimen was immersed in a methanol bath so that methanol was introduced into the crack. After the specimen was taken out of the bath and left overnight healing was not observed. Although the healing mechanism in the presence of a solvent has not fully developed, Kambour (20) believed that craze healing was caused by the residual methanol evaporating from craze to generate a contractile force within the craze matter that eventually closes the opposing forces.

The temperature dependence of craze growth or crack propagation provides further insight into the fracture process. The temperature influences the equilibrium uptake of methanol and thus the magnitude of the critical MW of methanol equilibrated PMMA (Chapter 4). Because the cracking or crazing behaviour is dependent on the density of entanglements, i.e. the magnitude of the critical MW (Eq.5.35), the temperature will show a profound effect on fracture behaviour of PMMA.

Figs.5.32 and 5.33 show the fracture behaviour in the temperature range of 0 to 40°C for LMW, MMW and HMW polymers. The effect of MW on the fracture toughness becomes more pronounced at elevated temperature, while the crack propagation was observed as a predominant breakdown process in LMW in this range of temperature, sample MMW showed crazing at 0°C and rapid cracking at 40°C (Fig.5.33). This interesting fracture behaviour is again attributed to temperature dependence of the entanglement density. As the critical MW of plasticized polymer, M_{sc}, increases with amount of solvent uptake (i.e. with increasing equilibrating temperature), the number of entanglements (Eq.5.34) will reduce with temperature. As illustrated

Fig.5.32 Plot of log K_c vs. log v for LMW at various temperatures, (a) T=0°C, (b) T=10°C, (c) T=20°C, (d) T=30°C (□) and T=40°C (♦).

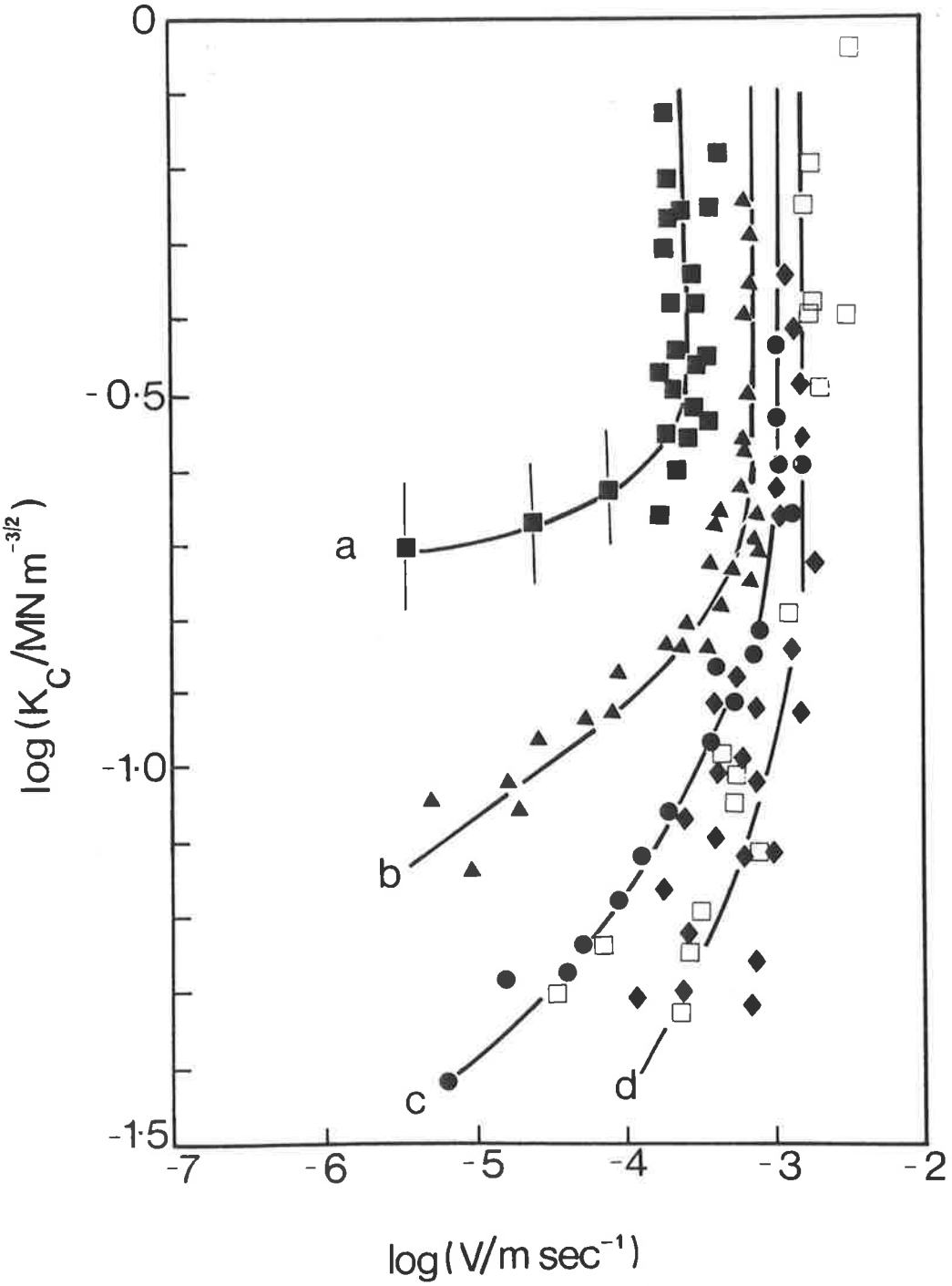
0
-0·5
-1·0
-1·5
-7
-6
-5
-4
-3
-2
a
b
c
d
log (K_C/MN m^-3/2)
log (V/m sec^-1)

Fig.5.33 Plots of log K_c vs. log v for HMW and MMW at various temperatures. Sample MMW (a) T=0°C, (b) T=30°C, (c) T=40°C. Sample HMW (1) T=0°C, (2) T=20°C.

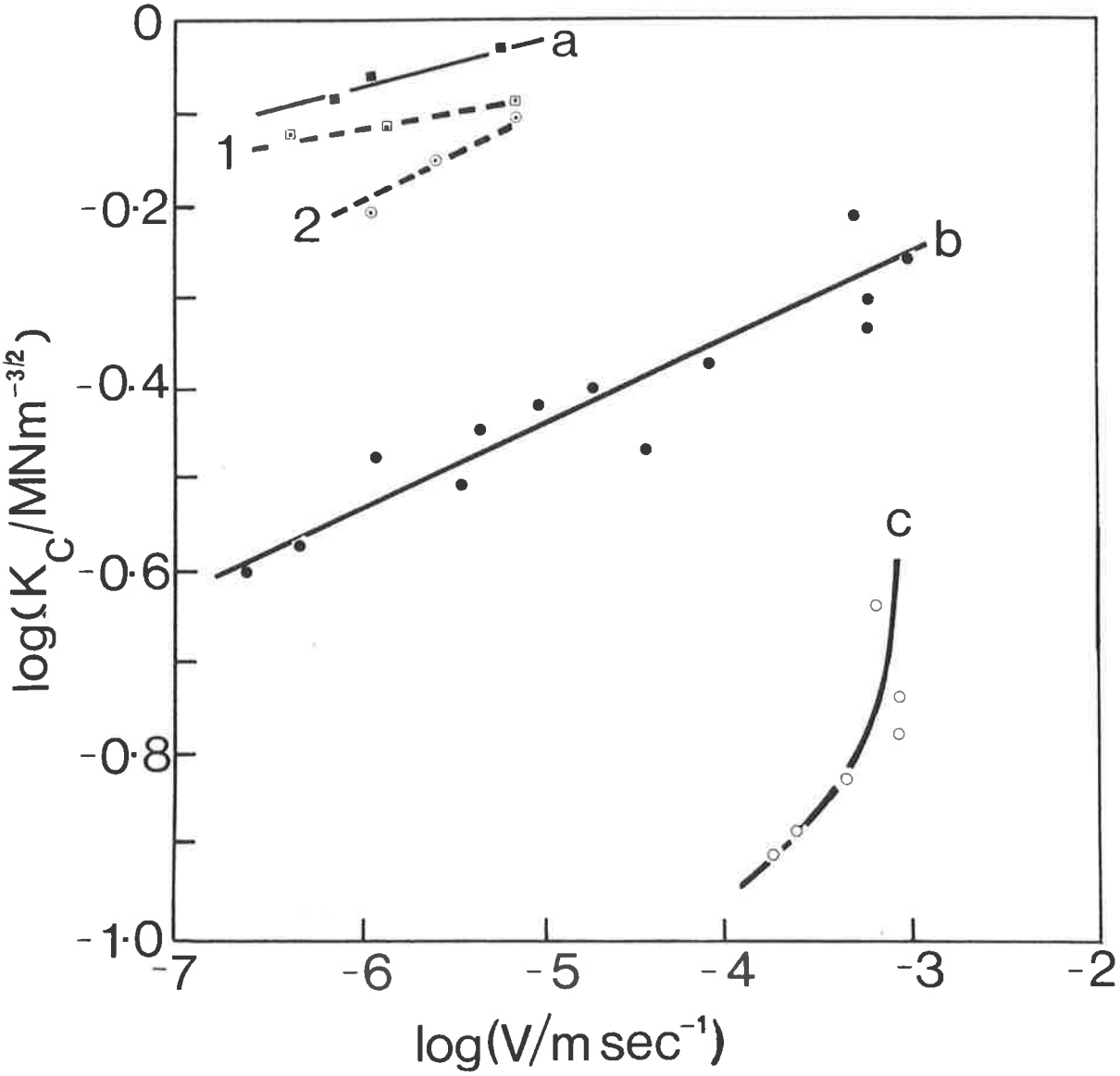
0
-0·2
-0·4
-0·6
-0·8
-1·0
-7
-6
-5
-4
-3
-2
a
1
2
b
c
log(K_c/MNm^-3/2)
log(V/m sec^-1)

in Fig.5.34, the number of the entanglements becomes very sensitive in the medium range, i.e. region of the MW just larger than M_c. The stress relaxation curve of methanol equilibrated MMW at 20°C (Chapter 4, Fig.4.8) indicated the borderline of entanglement existence. Therefore, at higher equilibration temperature (e.g. 35 to 40°C) it assumed that the magnitude of M_{sc} increases to a value higher than the MW of MMW sample leading to zero entanglement density at the plasticized crack tip, and consequently a rapid cracking in the fracture test at elevated temperature. In fact, the fracture morphology of MMW at 40°C observed by SEM was a smooth surface typical of cracking-predominant behaviour.

Sample HMW of high MW PMMA shows little effect of temperature on its fracture toughness as the density of entanglement becomes less sensitive with MW at high MW range. The sample becomes tougher at lower temperature because of less plasticization, i.e. higher crazing stress σ_c. At high temperature (T = 40°C), however, instead of a rapid crack propagation as in MMW or a long craze growth, homogeneous whitening of 2 mm diameter appeared at the initiation step and then arrested. Although the number of the entanglements is hardly influenced by temperature at high MW region, incapability of subsequent craze development required further investigation, for example, the direct measurement of the crazing stress profile would help to improve the understanding of this phenomena.

The least complicated fracture behaviour among three commercial samples is shown by sample LMW. The smooth fracture surface and non-healing behaviour of the crack confirm that the fracture test of LMW in methanol at T = 0 to 40°C occurred via a cracking mechanism rather than a crazing mechanism.

The behaviour of cracks and crazes is different in many aspects and requires separate treatment of data. The following discussion will be divided in two parts; Section 5.4.7 is concerned

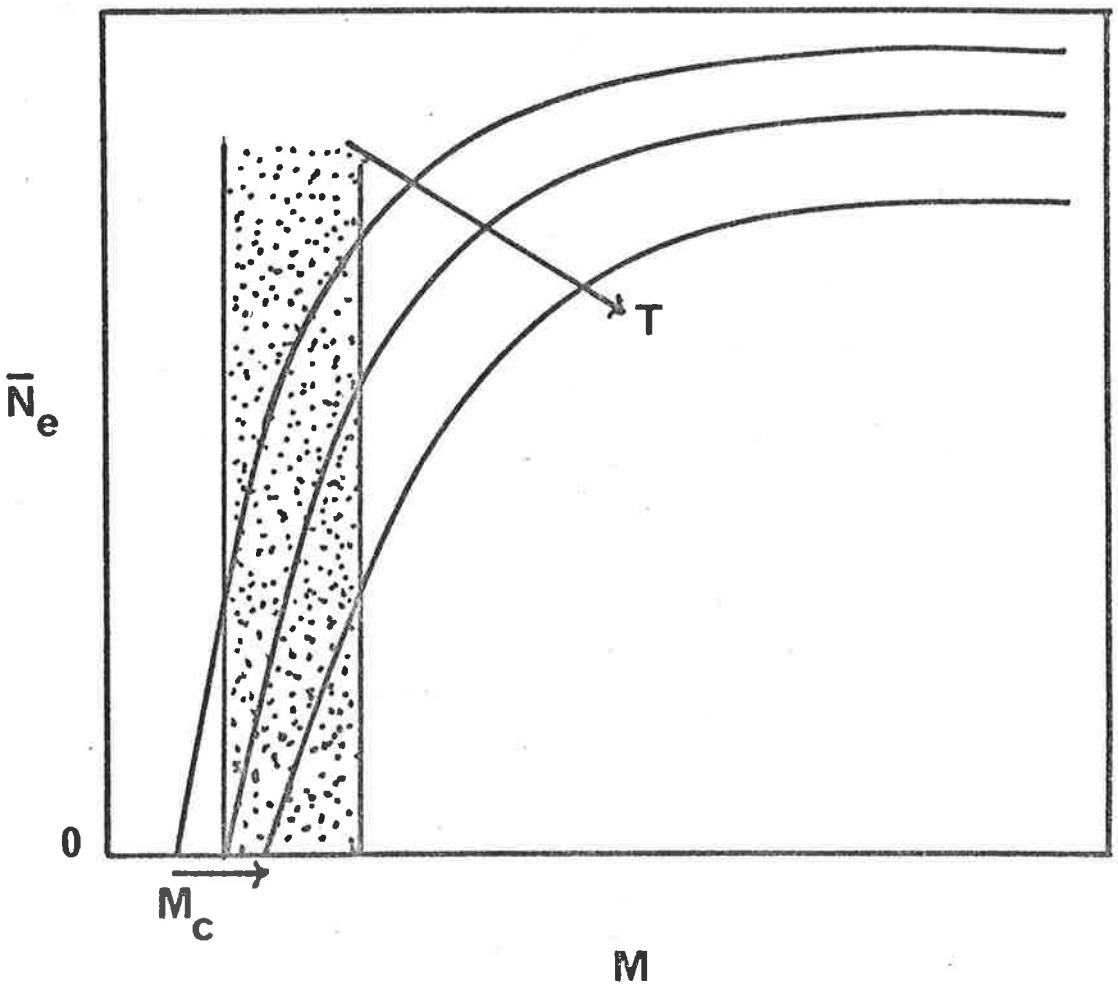

Fig.5.34 Schematic diagram shows variation in the entanglement density with temperature. The shaded area is the medium MW region.

with the cracking behaviour in Regime II and Section 5.4.8 deals with the crazing behaviour of Regime I and the Transition Regime.

5.4.7 Cracking Behaviour of Low Molecular Weight Poly(methylmethacrylate) in methanol (Regime II)

The fracture toughness of low MW (Fig.5.21 and 5.32) shows a strong dependence on MW and temperature, and it suggests that the log K_c vs. log v diagram can be divided into two sections: (a) a vertical section specified by the limiting velocity, v_o and (b) a sloping section at $v < v_o$. The similar effect of MW and temperature on the fracture toughness can be observed in (a) increase in the limiting velocity, v_o, and (b) decrease in K_c at a given $v < v_o$ in the sloping part, when the MW decreases or the temperature increases. The experimental data suggest an equivalence between the effect of MW and that of temperature in the cracking mechanism, but this requires further justification from polymers tested in various environments to establish the principle.

Nevertheless, the temperature dependent log K_c vs. log v relation can be analysed in terms of Zhurkov's theory to provide an understanding of the breakdown process via the magnitude of the activation energy (Section 5.4.7.1). Furthermore, application of LEFM to the analysis of experimental data gives an insight into the important variables such as the COD and the craze length in the presence of solvent (Section 5.4.7.2). The diffusion coefficient which can be deduced from the cracking data will be compared with the experimental values of the diffusion coefficient of methanol to clarify the effect of the rate of diffusion on the cracking mechanism. Because crack propagation is diffusion controlled, by comparing the stress and temperature dependence of the diffusion coefficient and that of the craze length, it is interesting to see how the rate of diffusion will effect the geometry of the crack tip (Section 5.4.7.3). Lastly, the WM theory will be applied to clarify the

time-dependent deformation process at the crack tip and the nature of the limiting velocity, v_o (Section 5.4.7.4).

5.4.7.1 Temperature Dependence from the Viewpoint of Zhurkov's theory

Zhurkov (26) carried out a rigorous study of the fracture kinetics of solids including metals and polymers and found that a wide range of materials followed as stress-biased Rhee-Eyring equation

$$t = t_o \exp\left(\frac{U_o - \gamma_F'\sigma_c}{RT}\right) \qquad (5.54a)$$

where t = the time to failure measured from the moment of loading, t_o = the limiting time, U_o = the activation energy, and γ_F' = constant (26,124). The crack velocity, v, is inversely proportional to the fracture time, t, and therefore

$$v = v_o \exp -\left(\frac{U_o - \gamma_F'\sigma_c}{RT}\right) \qquad (5.54b)$$

where v_o = the limiting crack velocity. According to Zhurkov (26) and also Schönert et al. (125) v_o can be expressed by

$$v_o = \frac{\lambda kT}{h} \qquad (5.54c)$$

where λ = average increase of crack length during the separation of a pair of atoms, h = Planck's constant and k = Boltzmann's constant, thus Eq.5.54b becomes

$$v = \frac{\lambda kT}{h} \exp -\left(\frac{U_o - \gamma_F'\sigma_c}{RT}\right) \qquad (5.55)$$

The energy release rate, G_c, is related to σ_c by $G_c = \sigma_c u_c$ and Eq.5.55 can be rewritten as

$$v = \frac{\lambda kT}{h} \exp -\left(\frac{U_o - \gamma_F G_c}{RT}\right) \qquad (5.56)$$

where $\gamma_F = \gamma_F'/u_c$. This equation has been applied successfully to the fracture process in air for glass by Schönert et al. (125), Kies and Clark (126), for PMMA by Atkins et al. (127) and for polystyrene by Mai and Atkins (128). Rewriting Eq.5.56 by substituting $G_c = K_c^2/E$,

we obtain

$$v = \frac{\lambda kT}{h} \exp - \left(\frac{U_o - \gamma_c (K_c^2/E)}{RT} \right) \qquad (5.57)$$

or

$$v = v_o \exp - \left(\frac{U_o - \gamma_F (K_c^2/E)}{RT} \right) \qquad (5.58)$$

As can be seen from Fig.5.32, the log K_c vs. log v curves for LMW at various temperatures approach a limiting velocity v_o, characterized by a vertical part of the curve. By applying Eq.5.58, the activation energy, U_o, and the constant, γ_F, can be evaluated. Eq.5.58 can be rewritten in the following expression

$$RT \ln \frac{v_o}{v} = U_o - \gamma_F \frac{K_c^2}{E} \qquad (5.59)$$

This equation suggests that RT ln v_o/v vs. K_c^2/E will give a straight line (Fig.5.35) where U_o is the intersection and γ_F is the slope. Modulus E is calculated according to Eq.5.26. The results are shown in Table 5.7.

TABLE 5.7: The calculated values of U_o and γ_F at T = 0 to 40°C for the cracking process in methanol.

T(°C)	U_o (kJ mol^{-1})	γ_F (m^2 mol^{-1})	γ_F^* (m^2) x 10^{21}
0	18.2	866	1.41
10	15.3	1912	3.19
20 to 40	11.4	2870	4.78

* Dimensions of γ_c is changed from m^2 mol^{-1} to m^2 by using Avogadro's number, N_A, γ_F (m^2 mol^{-1}) = γ_F (m^2) N_A.

As shown in Table 5.7, the activation energy, U_o, of crack propagation in the presence of methanol varies from 18.2 to 11.4 kJ mol^{-1} as the temperature increases from 0 to 40°C. The values of V_o are of the order of secondary bond energies and suggests that the breakdown does not occur by the rupture of the main-

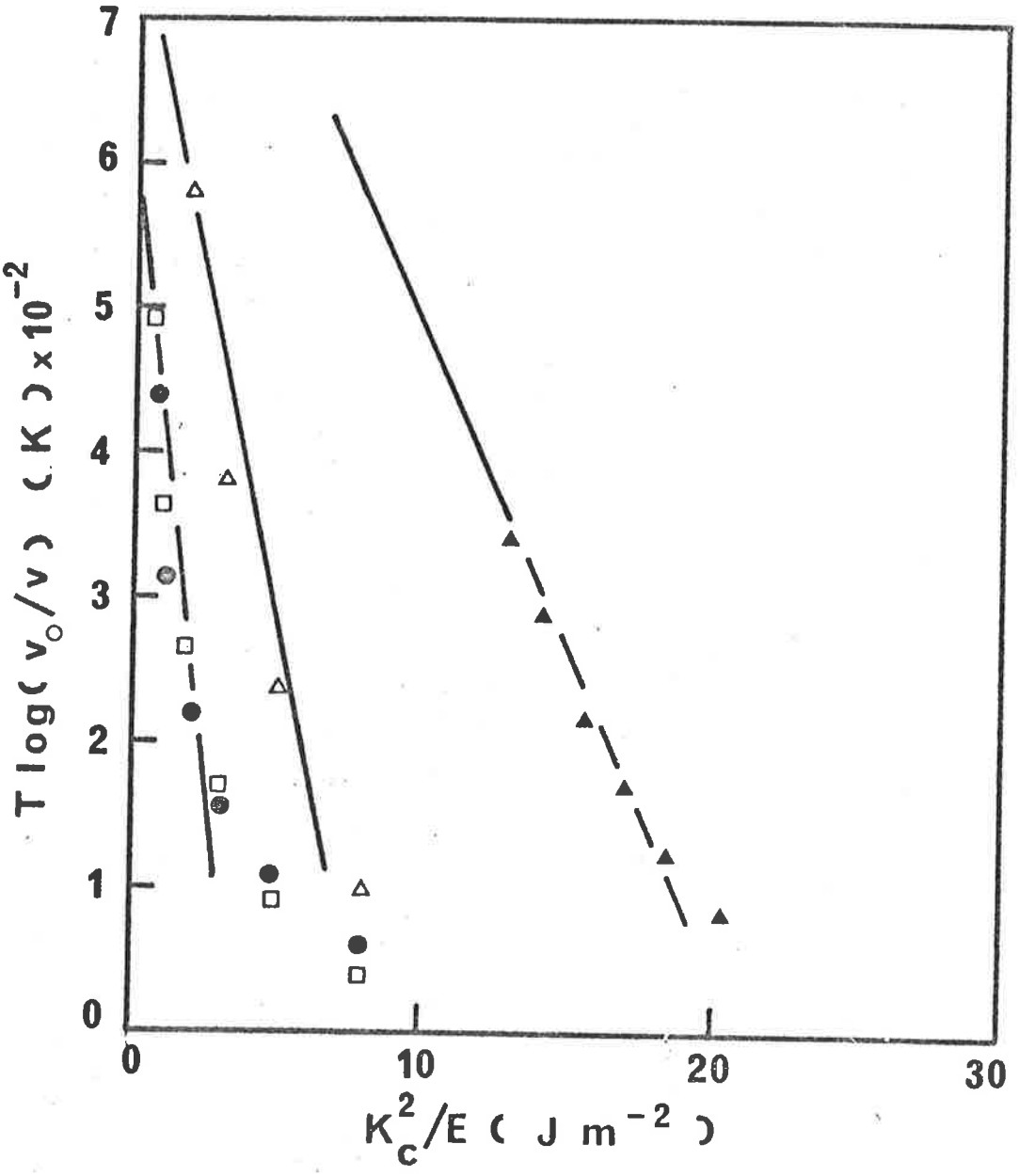

Fig.5.35 Plot of fracture toughness vs. velocity relationship for LMW in methanol in terms of Zhurkov's theory, [T log (v_o/v) vs. K_c^2/E]. The points deviating from the straight line have v close to the limiting velocity , v_o. T=0°C (▲), T=10°C (△), T=20°C (□), T=40°C (●).

chain but rather by the rupture of intermolecular secondary bonds. The temperature dependence of the activation energy also suggests the breakdown mechanism is governed by viscous flow processes (121). The magnitude of U_o is five to ten times smaller than that reported by Atkins et al. (127) and Marshall et al. (27) for the stable crack propagation of PMMA ($v < 10^{-1}$ m sec^{-1}) in air.

Furthermore, the magnitude of γ_F for the cracking of PMMA in methanol is larger by two decades (Table 5.7) than the γ_F for the cracking of PMMA in air ($\gamma_F = 8.9 \times 10^{-23}$ m^2) (127), and for the cracking of polystyrene and glass-filled polystyrene (γ_F = 1×10^{-23} to 6×10^{-23} m^2) (128). According to Zhurkov (26), the γ_F (or γ_F') describes the strength of solids and is senstive to the molecular orientation of the solids. Zhurkov believed that γ_F was inversely proportional to the fracture resistance of materials. In this sense, the γ_F values obviously suggests that PMMA is more prone to cracking in methanol than in air. This prediction can also be observed in log K_c vs. log v diagram where values of K_c in methanol cracking are always lower than K_c in air cracking at a given crack velocity, v.

However, Zhurkov's suggestion lacks theoretical background and molecular significance. On the other hand, Kies and Clark (126) suggested that

$$\gamma_F = \beta\lambda^2 \qquad (5.60)$$

where β = the fraction of the fracture energy required in breaking bonds to create surfaces and λ = the spacing distance for the intermolecular bond (λ = 0.7 nm). As defined in Chapter 2, the energy release rate at fracture, G_c, is twice the total of the plastic deformation energy, γ_{c2} and the surface energy, γ_{c1}, that is

$$G_c = 2\gamma_c$$
$$= 2(\gamma_{c_1} + \gamma_{c_2})$$

therefore

$$G_c\beta = 2\gamma_{c_1}$$

Evaluation of the product $G_c\beta$ requires calculation of G_c and β. The values of β can be calculated from Eq.5.60 and G_c is equal to K_c^2/E where K_c is the average value obtained from values of K_c in the sloping part of the log K_c vs. log v diagram (Fig.5.32). The results are shown in Table 5.8

TABLE 5.8: Values of G_c, β and $G_c\beta$

T(°C)	G_c (Jm^{-2})	$\beta \times 10^3$	$G_c\beta$ (Jm^{-2})	(G_c-$G_c\beta$) (Jm^{-2})
0	30	2.94	0.075	29.92
10	14	6.51	0.091	13.91
20 to 40	11	9.75	0.107	10.88

The $G_c\beta$ values are around 0.09 Jm^{-2} and are of the order of magnitude of the surface energy of PMMA/methanol ($2\gamma_{c_1}$ = 0.04 Jm^{-2}) (129). This agreement suggests that the van der Waals bonds are broken to create the new surface rather than by mainchain rupture. The remaining energy, i.e. the difference between G_c and $G_c\beta$, is expended by plastic deformation and void formation. Comparing with Atkins et al.'s data in air (127), the remaining energy of the fracture process in methanol is over ten times smaller and suggests that there is less craze formation in the presence of methanol than in air. On the other hand, as shown in Table 5.8, the remaining energy ($G_c - G_c\beta$) decreases with increasing temperature, i.e. less craze matter is formed at elevated temperature. Consequently, less energy is absorbed by the craze and the material becomes more vulnerable when exposed to stress.

From fracture mechanics, K_c can be expressed by

$$K_c = \sqrt{u_c \varepsilon_y}\, E \tag{5.22}$$

Substituting Eq.5.22 into Eq.5.59 gives

$$RT \ln \frac{v_o}{v} = U_o - \gamma_F \sqrt{u_c \varepsilon_y}\, K_c \tag{5.61}$$

Because the yield strain, ε_y, is independent of strain rate, if the COD, u_c, is assumed to be constant at a given temperature then the product $u_c \varepsilon_y$ is also a constant. Thus, plot RT ln v_o/v vs. K_c will give a straight line with the intersection U_o and slope $-\gamma_F \sqrt{u_c \varepsilon_y}$ (Fig.5.36). Values of U_o and $\sqrt{u_c \varepsilon_y}$ are shown in Table 5.9.

TABLE 5.9: Calculated values of $\sqrt{u_c \varepsilon_y}$ and U_o from Eq.5.61

T(°C)	$\gamma_F \sqrt{u_c \varepsilon_y}$ ($m^{5/2}$ mol^{-1})	$\sqrt{u_c \varepsilon_y}$ ($m^{\frac{1}{2}}$)	U_o ($kJmol^{-1}$)	U_o ($kJmol^{-1}$) (from Eq.5.59)
0	9.75×10^{-2}	1.12×10^{-4}	25.8	18.2
10	11.24×10^{-2}	5.88×10^{-5}	19.1	15.3
20 to 40	11.45×10^{-2}	4.00×10^{-5}	14.3	11.4

The U_o values determined from Eq.5.61 are approximately 20% larger than those determined by Eq.5.59. Although these values can be considered reasonably close to each other, the larger values of U_o from Eq.5.61 point to an obvious inadequacy of a constant COD assumption.

In air, Williams (97) estimated the value of u_c to be 2.56×10^{-6} m and ε_y to be 0.035 in the range of crack velocity $10^{-5} msec^{-1} \lesssim v \lesssim 10^{-3} m\ sec^{-1}$ so that $\sqrt{u_c \varepsilon_y} = 3.0 \times 10^{-4}\ m^{\frac{1}{2}}$. It is plausible that the corresponding $\sqrt{u_c \varepsilon_y}$ in methanol (Table 5.9) is smaller than in air. The result is either u_c or ε_y or both decrease in magnitude when the polymer is immersed in methanol.

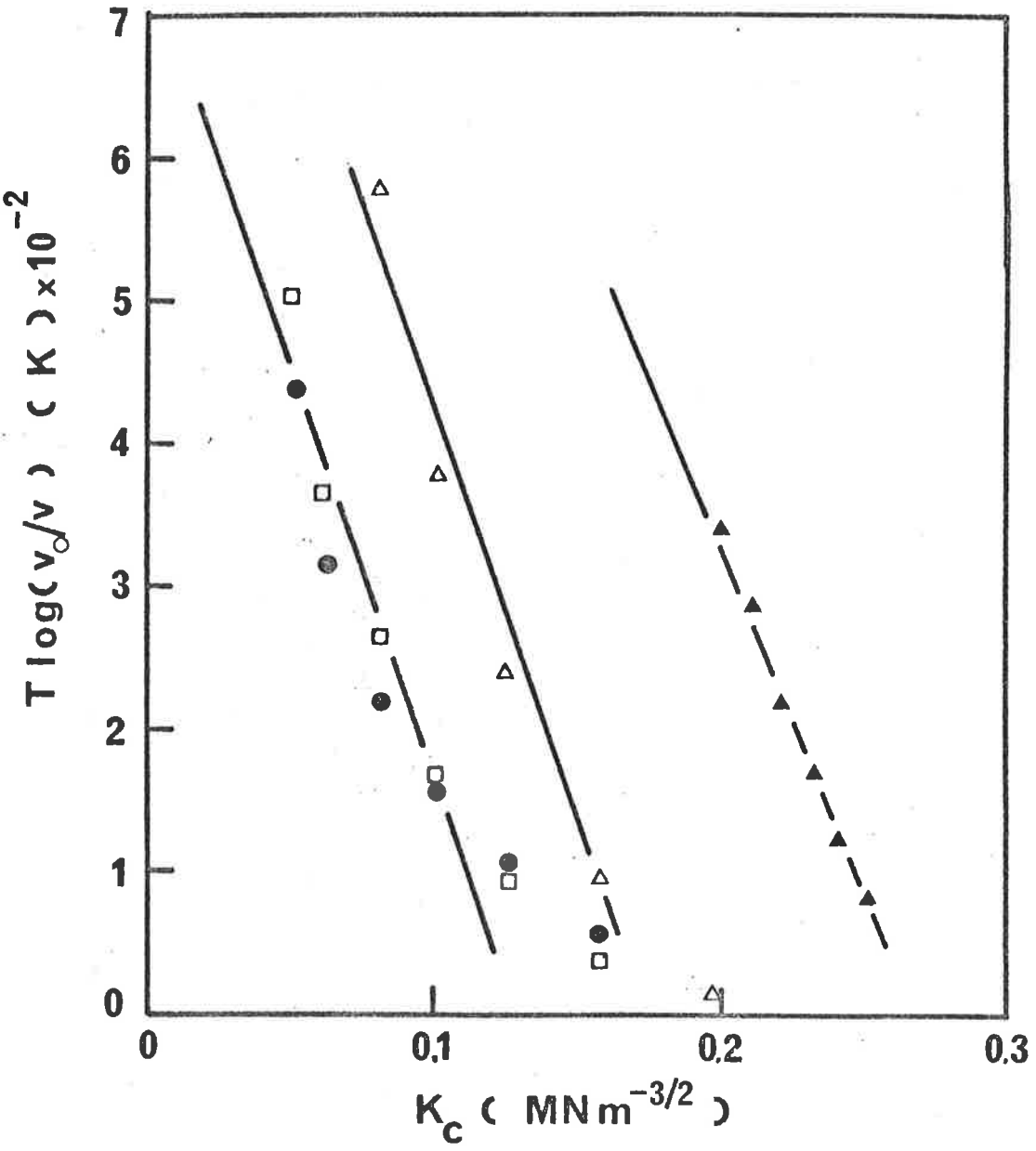

Fig.5.36 Plot of fracture toughness vs. velocity relationship for LMW in methanol in terms of Zhurkov theory, [T $\log(v_o/v)$ vs. K_c]. The points deviating from the straight line have v close to the limiting velocity, V_o. Symbols as in Fig.5.35.

The above analysis based on the Zhurkov modified Rhee-Eyring toughness-biased expression has provided useful information on the activation energy, U_o. However, the application of this expression to the experimental data did not yield reliable values for $\sqrt{u_c \varepsilon_y}$ because the assumption of a constant u_c at a particular temperature was not justified. Hitherto, it has been believed that the COD, u_c, for the cracking in air is a constant independent of K_c, but the recent work of Israel et al. (110) has suggested that the COD for air cracking increases with K_c and reaches a limit at $K_c \simeq 1$ MN $m^{-3/2}$. The magnitude of K_c may have the same effect on the COD of the methanol cracking as in air, and the possible K_c dependence of the values of u_c in methanol will be discussed from the LEFM viewpoint in the following Section.

5.4.7.2 Temperature Dependence of Crack Propagation from the Fracture Mechanics Viewpoint

The deficiency in the analysis of experimental data using the Zhurkov theory (Section 5.4.7.1) can be overcome by employing LEFM concepts. At the crack tip, the critical crazing stress, σ_c, ($\sigma_c = E\varepsilon_y$) is responsible for the load-carrying capacity of the material. In an aggressive environment, the craze at the tip, because of its porous nature, allows the fluid to diffuse through and eventually plasticize the craze fibrils. This process creates a drop in the critical stress from the value in air σ_c to $\alpha\sigma_c$, where α is the reduction factor for plasticization and $\alpha < 1$ (33). Because the bulk modulus E is not influenced by the environment, the drop of the critical stress to $\alpha\sigma_c$ is equivalent to the drop of the yield strain from the value in air ε_y to $\alpha\varepsilon_y$. In air, the SIF, K_c is given by

$$K_c = \sqrt{u_c \varepsilon_y}\ E \qquad (5.22)$$

In the aggressive environment, K_c becomes

$$K_c = \sqrt{u_c \varepsilon_y}\, E \sqrt{\alpha} \qquad (5.62)$$

where u_c and ε_c are the COD and the yield strain in air, respectively (33). The reduction factor, α, can be calculated by taking the ratio of K_c in air and K_c in methanol at a given velocity.

Young and Beautmont (105) suggested that the value of $\sqrt{u_c \varepsilon_y}$ in air is insensitive to temperature and therefore the reduction factor, α, can be evaluated from

$$\frac{K_{AIR}\ (T=20°C)}{K_{MeOH}\ (T)} = \frac{\sqrt{u_c \varepsilon_y}\ E(T=20°C)}{\sqrt{u_c \varepsilon_y}\ E(T)\ \sqrt{\alpha}}$$

or

$$\frac{K_{AIR}\ (T=20°C)}{K_{MeOH}\ (T)} = \frac{E(T=20°C)}{E(T)\ \sqrt{\alpha}} \qquad (5.63)$$

The LHS of Eq.5.63 can be evaluated from experimental data at a particular velocity (Fig. 5.37). For example, at $v = 3.16 \times 10^{-4}$ msec^{-1} ($\log v = -3.5$), $\log[K_{AIR}(T=20°C)/K_{MeOH}(T=0°C)] = 0.47$, from Williams' data (97) $E(T=20°C) = 3.5$ GNm^{-2} and $E(T=0°C) = 4$ GNm^{-2}. Thus α is calculated to be 0.090. Using the same method of calculation, the values of α at various temperatures are listed in Table 5.10.

TABLE 5.10: Effect of temperature of the reduction factor, α, at $v = 3.16 \times 10^{-4}$ msec^{-1} ($\log v = -3.5$)

T(°C)	$\log(K_{AIR}/K_{MeOH})$	$\log[E(T=20)/E(T)]$	α	α (from Zhurkov's theory.)
0	0.47	0.06	0.090	0.13
10	0.70	0.03	0.035	0.03
20	0.85	0	0.020	0.03
30 to 40	1.00	-0.04	0.012	0.03

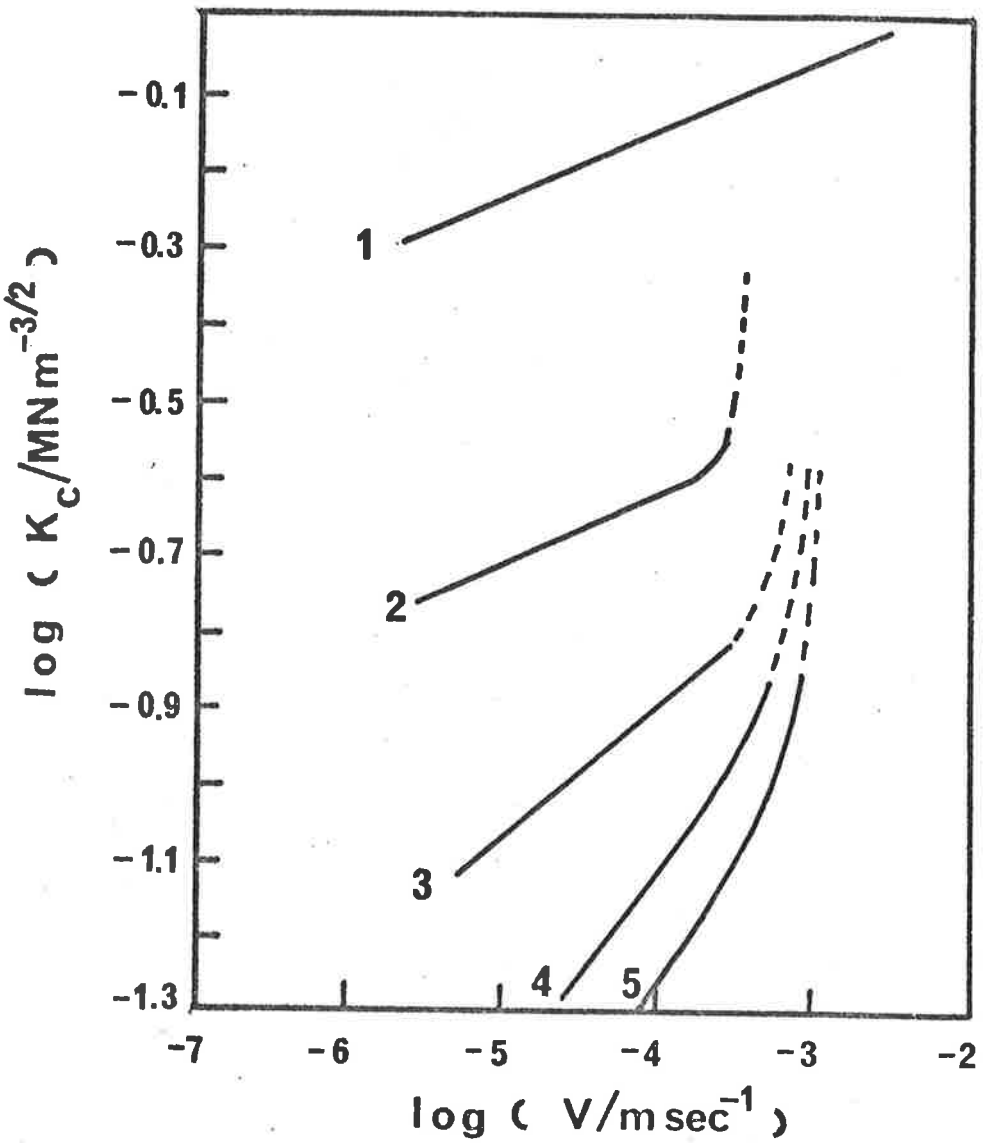

Fig.5.37 Comparison of fracture toughness in air and in methanol. (1) In air (T=20°C). (2) In methanol (T=0°C). (3) In methanol (T=10°C). (4) In methanol (T=20°C). (5) In methanol (T=30°C to 40°C).

Also listed in Table 5.10 are the values of α based on Zhurkov's theory, calculated as the ratio of $\sqrt{u_c \varepsilon_y}$ in methanol (Table 5.9) and in air. As seen in Table 5.10, calculated values from Zhurkov's theory are in reasonable agreement with those from LEFM theory. However, while the values of α from Zhurkov's theory remain constant from 10°C to 40°C, the values calculated by the LEFM show a systematic decrease with increasing temperature. Obviously, this indicates that as the temperature increases more methanol is absorbed (the volume fraction of absorbed methanol increases from 0.15 to 0.33 as temperature increases from 0°C to 40°C (60)) and the more plasticization will occur at the crack tip. As already mentioned, α is also the reduction factor of the yield strain, therefore the yield strain is reduced with increasing absorbed solvent. The effect of solvent on the reduction in yield strain was confirmed by Kamei and Onogi's experiments on the mixture of polystyrene and solvent at various ratios (78).

The values of α, for example at T = 20°C, can be obtained directly from experiment by measuring the yield stress of methanol equilibrated LMW at 20°C. The yield stress, which is the crazing stress in macroscopic sense, can be determined by simple tensile test with a "dog-bone" shape specimen. Because the magnitude of the yield stress is dependent on the strain rate, the measurements were made at predetermined rate of movement of the machine crosshead. This rate was chosen in the range of 50 cm sec^{-1} to 20 cm sec^{-1} so that the average strain rate, $\bar{\dot{\varepsilon}}$, would be of the order of 10^{-1} to 10^{-2} sec^{-1}*. The tensile tests of methanol equilibrated LMW at the velocities of crosshead travel will give an approximation of the

* $\bar{\dot{\varepsilon}}$ was calculated by $\bar{\dot{\varepsilon}} = \ln(\ell/\ell_o)/\Delta t$, where ℓ_o = original length of 2cm, ℓ = final length and Δt = 60 sec.

stretching of craze fibrils when the crack tip propagates at the velocities 10^{-4}msec$^{-1} \lesssim v \lesssim 10^{-3}$ msec^{-1} (corresponding to the strain rate of the fibril 10^{-1} sec$^{-1} < \varepsilon < 10^{-2}$ sec^{-1} from Eq.5.25). The yield stress was determined to be 1.7 MNm^{-2} and 3.1 MNm^{-2} at crosshead velocities of 20 cm sec^{-1} and 50 cm sec^{-1}, respectively. The value of σ_c in air was reported to be 65 MNm^{-2} (100), therefore experimental values of α vary from 0.026 to 0.047 compared with the theoretical value of 0.020 (Table 5.10), confirming the reasonable magnitude of calculated value of α at T = 20°C.

The decrease in fracture toughness in environmental stress-cracking is attributed not only by a drop in σ_c but also by a reduction in u_c. The reduction factor, α, therefore is contributed by the reduction of the crazing stress and the COD. Values of α as shown by experimental data decrease with the front tip velocity. For example, at T = 20°C we obtain

$$\alpha = 0.020 \quad \text{at} \quad \log(v/\text{msec}^{-1}) = -3.5 \quad (K_c = 0.112 \text{ MNm}^{-3/2})$$

and

$$\alpha = 0.008 \quad \text{at} \quad \log(v/\text{msec}^{-1}) = -4.5 \quad (K_c = 0.068 \text{NMm}^{-3/2})$$

Obviously, the smaller value of $\alpha = 0.008$ at $\log(v/\text{msec}^{-1}) = -4.5$ compared with $\alpha = 0.020$ at $\log(v/\text{msec}^{-1}) = -3.5$ indicate that the reduction factor, α, originates from two factors —— the COD and the crazing stress (the yield strain). In brief, in air cracking, the product of the COD and the yield strain is expressed by

$$u_c \varepsilon_y$$

and in methanol cracking,

$$(\alpha_u u_c)(\alpha_\varepsilon \varepsilon_y)$$

or

$$\alpha = \alpha_\varepsilon \alpha_u$$

where α_ε = the yield strain reduction factor

α_u = the COD reduction factor.

The results for other temperatures are listed in Table 5.11.

TABLE 5.11: Effect of temperature on the reduction factors α, α_ε, α_u and the craze length, Δ, at $v=3.14\times10^{-5}$ $msec^{-1}$, (log v = -4.5)

T(°C)	$\alpha=\alpha_\varepsilon\alpha_u$	α_ε *	α_u	u_c (μm)	** $\Delta=\frac{\pi}{8}\frac{u_c}{\varepsilon_y}$ (μm)
0	0.090	0.090	1	2.56	320
10	0.022	0.035	0.63	1.61	600
20	0.008	0.020	0.41	1.05	590
30 to 40	0.005	0.012	0.43	1.10	1020

* From Table 5.10 where $\alpha = \alpha_\varepsilon$

** Δ = 28 μm in air (97)

The above results have shown the temperature dependence of α_u is similar to that of α_ε. In other words, the effect of plasticization gives a smaller COD with increasing amount of solvent uptake at the crack tip (i.e. increasing temperature). At T = 10°C the COD still remains unchanged (α_u = 1), whereas at T = 20 to 40°C the COD reduces to less than half value at $\log(v/msec^{-1})$ = -3.5.

The effect of the SIF, K_c, on the magnitude of the COD, u_c, and the craze length, Δ, at a constant temperature can be seen in Table 5.12.

The relationship of K_c vs. u_c shows a straight line on a log-log plot (Fig.5.38) and was found that

$$u_c = 56.4\ K_c^{1.39} \quad (\mu m) \quad \text{at T = 20°C}$$

and

$$u_c = 15.9\ K_c \quad (\mu m) \quad \text{at T = 10°C}$$

whereas Israel et al. (110) found this relationship for air cracking to be

$$u_c \propto K_c^{2.14}$$

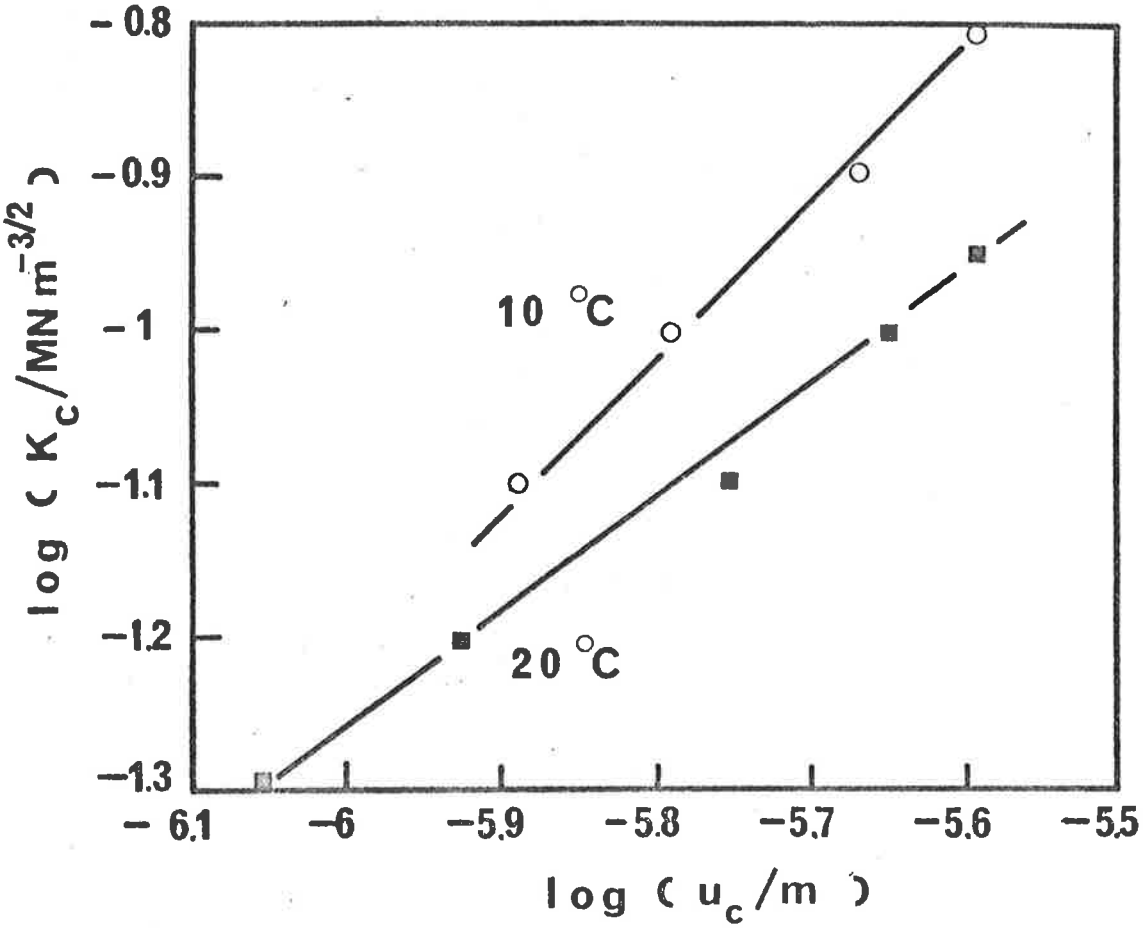

Fig.5.38 The effect of the SIF, K_c, on the COD, u_c.

TABLE 5.12: Effect of the SIF, K_c, on the reduction factors α, α_ε, α_u and the craze length, Δ, at T=20°C.

K_c ($MNm^{-3/2}$)	$\alpha=\alpha_\varepsilon\alpha_u$	α_ε	α_u	u_c (μm)	Δ (μm)
0.112	0.020	0.02	1	2.56	1436
0.100	0.017	0.02	0.87	2.23	1250
0.079	0.014	0.02	0.69	1.77	993
0.063	0.009	0.02	0.46	1.14	662
0.050	0.007	0.02	0.34	0.87	488

The temperature and the SIF, K_c, dependence of the craze length shown in Tables 5.11 and 5.12 reveal an interesting observation that the craze length increases with increasing temperature and SIF, K_c. The results can be understood in terms of the diffusion rate of methanol at various temperatures and stress at the crack tip. This problem will be discussed in the next Section.

5.4.7.3 Effects of Temperature and the SIF, K_c, on the Diffusion Behaviour of Methanol.

The basic factor which governs the plasticization and fracture mechanism in the aggressive environment is the diffusion of solvent molecules into bulk material at the crack tip. The plasticization of the crack tip of low MW PMMA is the only reason for a rapid crack propagation at low SIF, K_c, compared with the air cracking at the same velocity (Fig.5.37). Also, the faster diffusion rate at higher temperature results in the higher limiting velocity v_o (Fig.5.32).

According to the mechanism suggested by Brown and co-workers (130-132), the penetrant acts as a wedge to open the crack by jumping a distance J into a cavity smaller than itself — the cavity then expands under stress. This is an early stage of the craze nucleation and they have concluded that the rate of diffusion of penetrant into

the bulk material determines the velocity of crack propagation. Thus,

$$v = \frac{AD}{J} \tag{5.64}$$

where A = related to the surface coverage varies from zero to unity

D = the diffusion coefficient

J = the jump distance of a liquid molecule.

Because methanol wets PMMA completely, A is assumed to be unity representing full surface coverage of methanol on the PMMA surface (133), so that

$$v = \frac{D}{J} \tag{5.65}$$

Thus, Eq.5.56 can be rewritten as

$$v = \frac{D_o}{J} \exp\left(\frac{\gamma_F' \sigma_c - U_o}{RT}\right) \tag{5.66}$$

and

$$v_o = \frac{D_o}{J} \tag{5.67}$$

where $\gamma_F' = \gamma_F u_c$, the activation volume and D_o = the pre-exponential factor (130).

Brown (130) has suggested that the jump distance, J, can be estimated from the activation volume, where the product of J and the molecular cross-sectional area of the liquid molecule equals the activation volume. The molecular cross-sectional area calculated from

$$\text{molecular cross-sectional area} = \frac{(\text{molar volume})}{N_A \cdot (\text{length of the molecule})}$$

is 0.209 nm^2 for methanol and therefore the diffusion coefficient at zero stress can be calculated from

$$D(\sigma_c=0) = D_o \exp -\left(\frac{U_o}{RT}\right) \tag{5.68}$$

The calculated results are listed in Table 5.13, together with values of γ_F' and J at various temperatures. As previously stated, the COD, u_c, was assumed to have the value in air of 2.56 μm. Values

of γ_F and U_o were the results discussed in Section 5.4.7.1 (Table 5.9).

TABLE 5.13: Estimation of the diffusion coefficient at zero stress (σ_c=0) from solvent-cracking data of LMW.

T(°C)	$\gamma_F(m^2)x10^{21}$	$\gamma_F'=\gamma_F u_c(m^3)x10^{27}$	J(nm)	$D_o(cm^2sec^{-1})$	$D(cm^2sec^{-1})$
0	1.41	3.61	17.3	$4.3x10^{-8}$	$1.3x10^{-11}$
10	3.19	8.17	39.1	$2.7x10^{-7}$	$4.1x10^{-10}$
20	4.78	12.24	58.6	$5.9x10^{-7}$	$5.3x10^{-9}$
40	4.78	12.24	58.6	$1.0x10^{-6}$	$1.2x10^{-8}$

The calculated values of the diffusion coefficient, D, obtained from data for methanol stress-cracking of LMW and listed in Table 5.13 increase with temperature. The calculated values show excellent agreement with experimental data. For example, D has experimental values in the order of 10^{-10} cm^2 sec^{-1} at T=20°C (Section 4.3.1, Table 4.1) and of 10^{-8} cm^2 sec^{-1} at T=42°C (66), compared with the calculated values of $5.3x10^{-9}$ cm^2 sec^{-1} and $1.2x10^{-8}$ cm^2 sec^{-1} (Table 5.13), respectively, obtained from data for methanol stress-cracking of LMW.

In Section 5.4.7.1, the magnitude and temperature dependence of U_o suggests that the breakdown process is governed by a viscous flow process where secondary bond rupture occurs. Now, the agreement between the experimental values of D and the values of D calculated by Eq.5.65, reveal the other important point that the rate of solvent diffusion into bulk polymer is the basic factor controlling the breakdown mechanism (Eq.5.66).

Furthermore, the enhancement by stress of the diffusion coefficient D can be estimated from

$$D = D_o \exp\left(\frac{-U_o + \gamma_F(K_c^2/E)}{RT}\right) \qquad (5.68)$$

The effect of the SIF, K_c on the magnitude of D in methanol at T=20°C is shown in Table 5.14.

TABLE 5.14: The effect of K_c on the diffusion coefficient at T = 20°C.

K_c ($MNm^{-3/2}$)	α_u	J(nm)	D_o (cm^2sec^{-1})	D(cm^2sec^{-1})
0.112	1	17.3	$5.9x10^{-7}$	$3.6x10^{-7}$
0.100	0.87	15	$5.1x10^{-7}$	$1.3x10^{-7}$
0.079	0.069	11.9	$4.0x10^{-7}$	$3.0x10^{-8}$
0.063	0.46	7.9	$2.7x10^{-7}$	$9.2x10^{-9}$
0.05	0.34	5.9	$2.0x10^{-7}$	$4.2x10^{-9}$
0	(Table		5.13)	$5.3x10^{-9}$

The results clearly indicate a strong K_c dependence of the diffusion coefficient, D. The value of D increased two decades from $5.3x10^{-9}$ cm^2 sec^{-1} to $3.6x10^{-7}$ cm^2 sec^{-1} when K_c increased from 0 to 0.112 $MNm^{-3/2}$.

The diffusion coefficient, D, and the craze length, Δ, have the similar dependence on the temperature and the SIF, K_c —— they both increase with increasing temperature or K_c. This similarity confirms the role of the diffusion rate of solvent into bulk material at the crack tip as the controlling factor in environment cracking mechanism. That is, the enhancement of the diffusion coefficient by temperature or by K_c will lead to an increase in the size of plasticized zone, namely an increase in the craze length, Δ.

5.4.7.4 Analysis based on Williams-Marshall (WM) theory.

The WM theory developed from the LEFM has provided expressions for the time dependence of viscoelastic deformation at the crack tip (Chapter 2, Eqs.2.32-2.35). The values of m and n in Eqs.2.32, 2.33 are important factors for a quantitative understanding of the deformation process. In air, m and n were found to be approximately 0.1. The environment, n remains unchanged because viscoelastic effects of bulk material embodied in modulus E are not affected, but the value of m will increase by plasticization of the crack tip. Before embarking on the calculation of m, however, it is necessary to determine if the WM theory for relaxation controlled crack growth is applicable to the present experimental data. To this end, it requires to justify the assumption for the crack growth $1/\tau = v/\Delta$ (Eq.2.30) from experimental data in air and in methanol.

(a) The time scale, τ, of cracking in air and in methanol

As shown in Figs.5.39a,b and in Fig.5.40 for air and methanol cracking, the crack velocity, v, can be related to time, t, by

$$v = v_t \, t^{\Omega} \tag{5.69}$$

where v_t and Ω are constants. Substituting Eq.5.69 into Eq.2.29, we obtain

$$\frac{1}{\tau} = \frac{v}{\Delta} + \left(\frac{v}{v_t} \right)^{-1/\Omega}$$

Fig.5.39a Plot of log v vs. log t of cracking in air (T=20°C) for narrow MWD PMMA, A1a (M_w = 450,000, ●), A2a (M_w = 120,000, ○), A7 (M_w = 71,000, ▲) and Aa (M_w = 31,000, △). The slope Ω is -1.

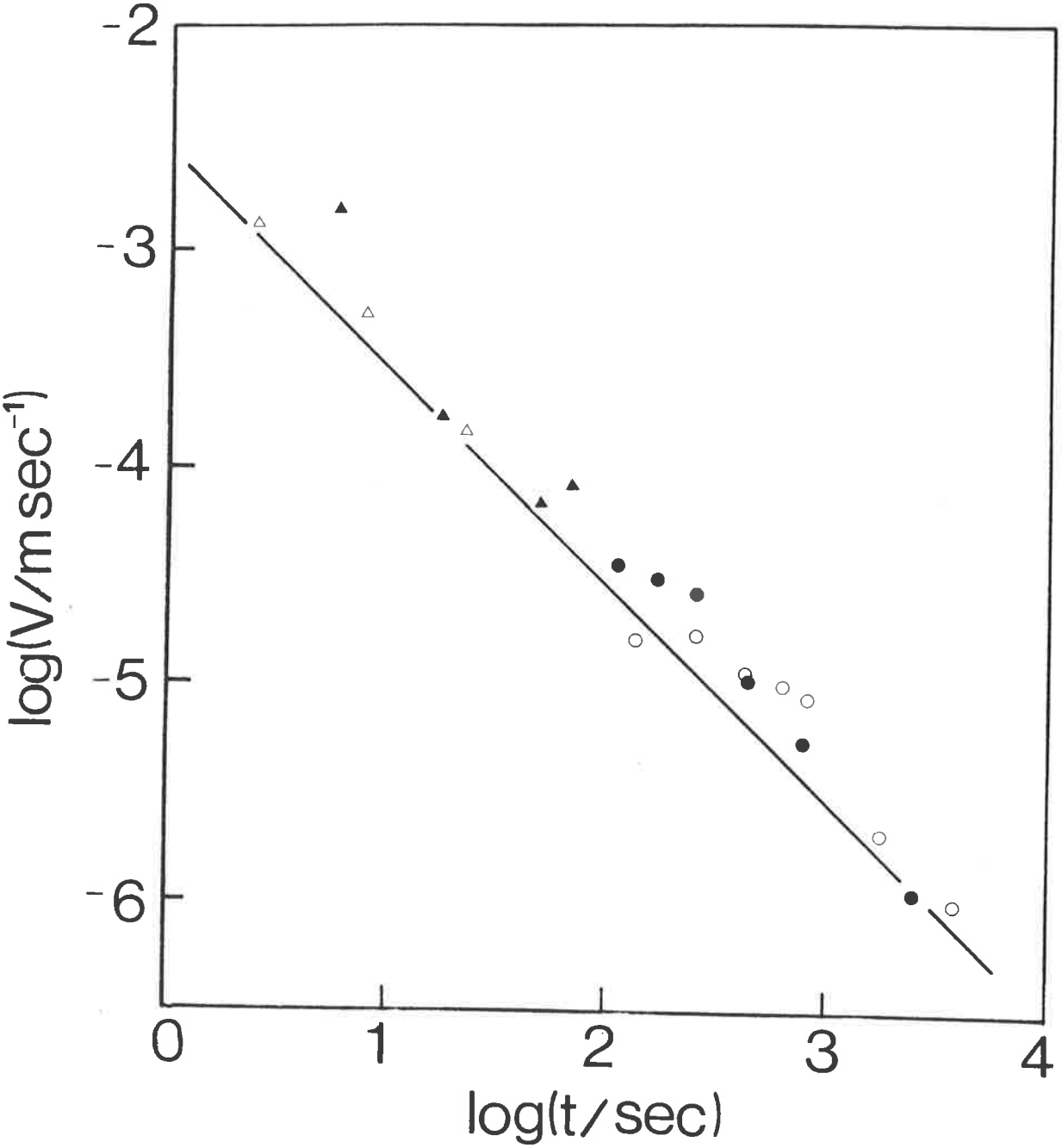
-2
-3
-4
-5
-6
log(V/m sec^{-1})
0
1
2
3
4
log(t/sec)

Fig.5.39b Plot of log v vs. log t of cracking in air (T=20°C) for commercial PMMA, HMW (▲, ▼, ■), MMW (△, ▽, □) and LMW (○, ●). The slope Ω is -1.

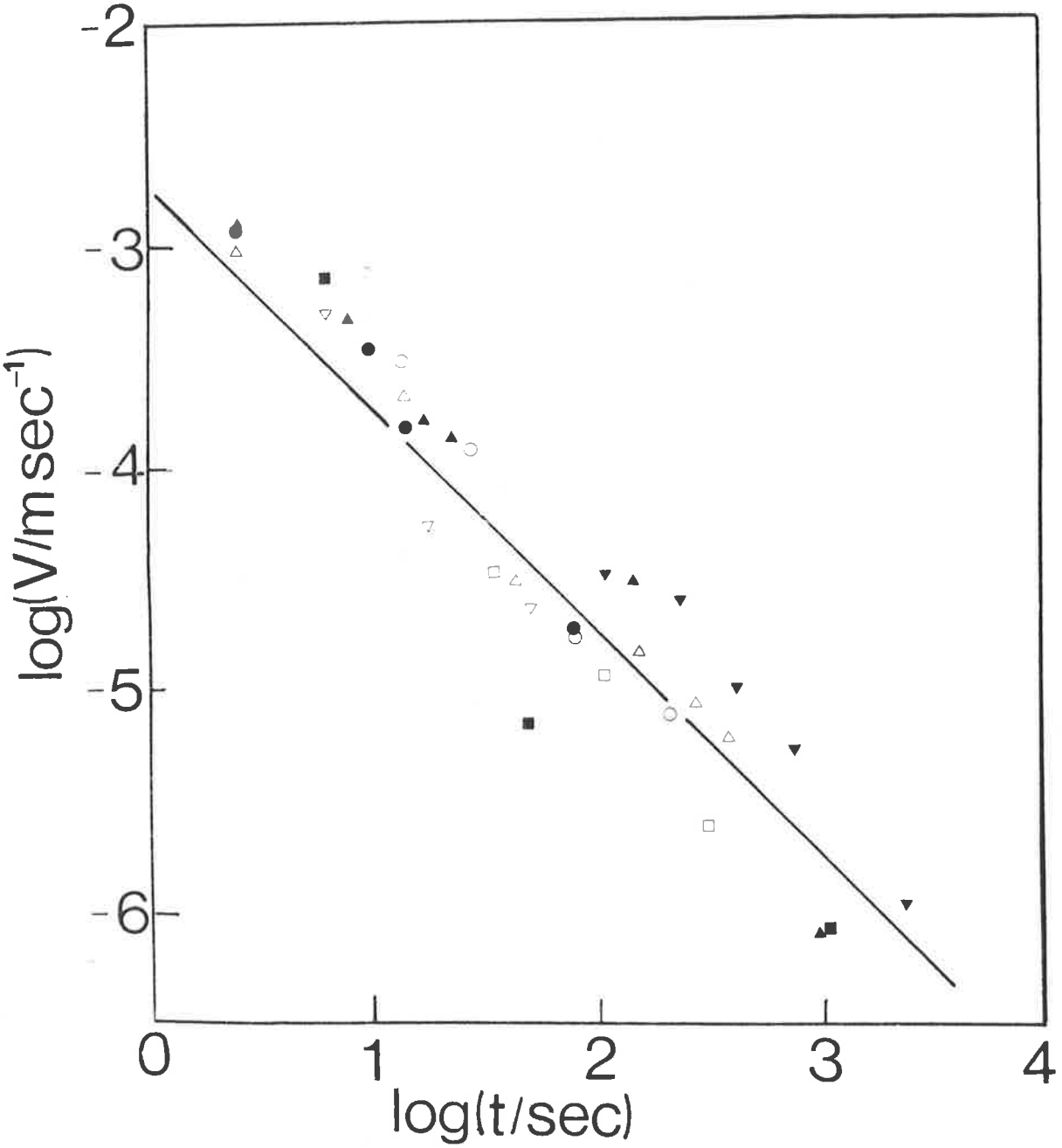
-2
-3
-4
-5
-6
log(V/m sec^{-1})
0
1
2
3
4
log(t/sec)

Fig.5.40 Plot of log v vs. log t of cracking in methanol for LMW (T=20°C). The slope Ω is -1.5. Symbols represent various initial SIF, K_i.

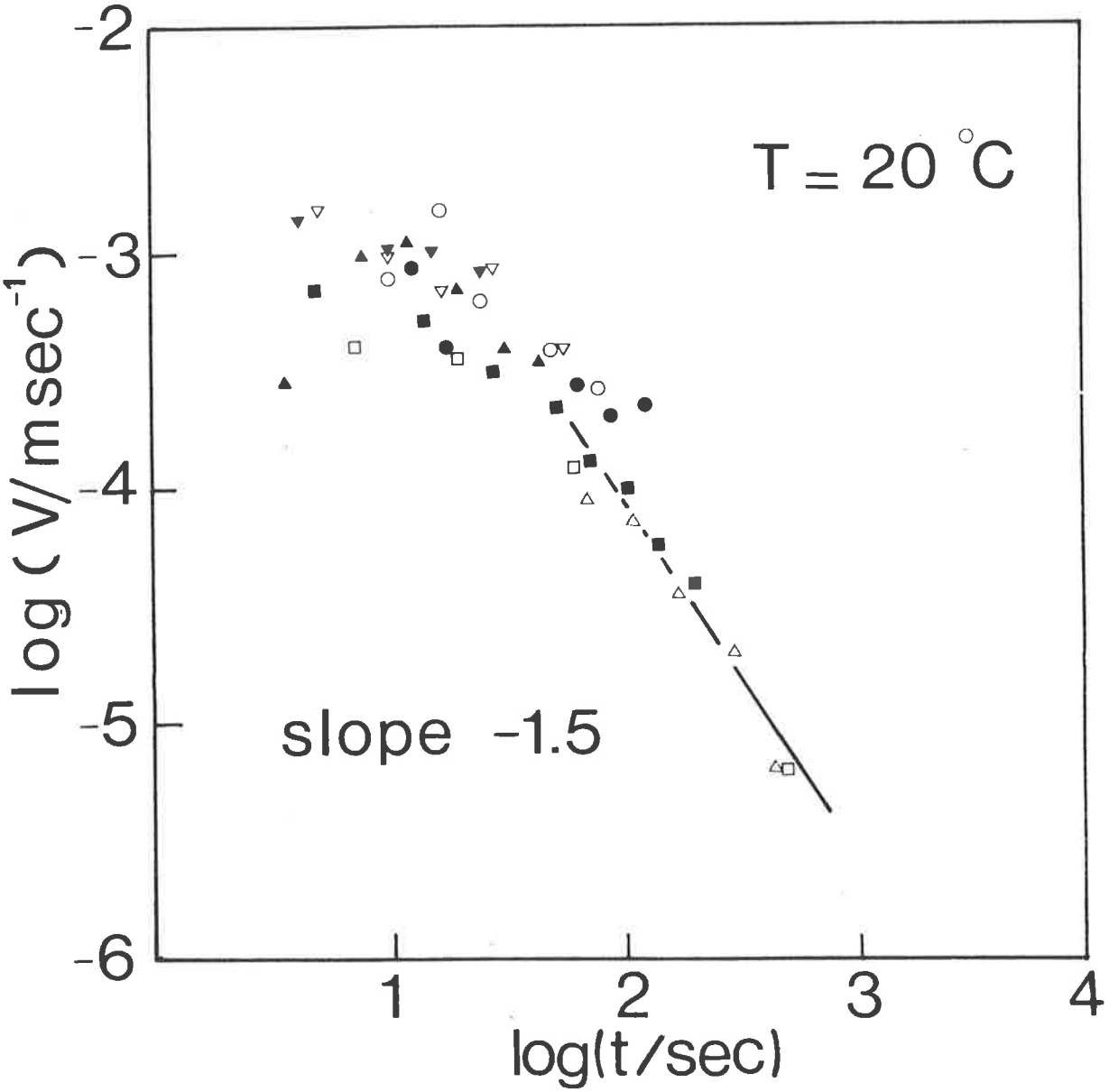
T = 20 °C
slope -1.5
log (V/msec^{-1})
log(t/sec)
-2
-3
-4
-5
-6
1
2
3
4

or
$$\frac{1}{\tau} = v\left(\frac{1}{\Delta} + \frac{v^{-(1/\Omega+1)}}{v_t^{-1/\Omega}}\right) \qquad (5.70)$$

At 20°C in air, the following values were obtained

$$\Omega = -1$$

$$\Delta = 28\ \mu m$$

and
$$v_t = 4.5\times10^{-3}\ msec^{-1}$$

Substituting these values into Eq.5.70 gives

$$\frac{1}{\tau} = v\left(\frac{1}{\Delta} + \frac{1}{v_t}\right)$$

$$= v\left(\frac{1}{2.8\times10^{-5}} + \frac{1}{4.5\times10^{-3}}\right) \simeq \frac{v}{2.8\times10^{-5}} \qquad (5.71)$$

At 20°C in methanol, the following values were obtained for the sloping part of log K_c vs. log v curve

$$\Omega = -1.5$$

$$\Delta = 488\ \mu m \text{ (at } v = 6\times10^{-6}\ msec^{-1})$$

$$\Delta = 1250\ \mu m \text{ (at } v = 3.16\times10^{-4}\ msec^{-1})$$

and
$$v_t = 0.10\ msec^{-1}$$

That is

$$\frac{1}{\tau} = v\left(\frac{1}{4.88\times10^{-4}} + 11\right) \simeq \frac{v}{4.88\times10^{-4}} \qquad (5.72a)$$

for $v = 6 \times 10^{-6}$ msec^{-1} and

$$\frac{1}{\tau} = v\left(\frac{1}{1.25\times10^{-3}} + 3\right) \simeq \frac{v}{1.25\times10^{-3}} \qquad (5.72b)$$

for $v = 3.16\times10^{-4}$ msec^{-1}

The second term on the RHS of 5.72a,b can be neglected with an error of less than 0.6% and therefore Williams and Marshall's formulae of stress-cracking (Eqs.2.34,2.35) are applicable for the analysis of experimental data of the crack propagation in methanol (restricted to the sloping part of log K_c vs. log v curve) and in air.

(b) Estimation of the time factor, m, of the crazing stress

The experimental time factor, m, can be determined from Eq.2.35. This equation can be rewritten in the following form

$$K_c = C\, v^{(m-n)/2(1-m+n)} \qquad (5.73)$$

where

$$C = \left(\frac{8}{\pi}\right)^{(m+n)/2(1-m+n)} (u_c E_o)^{(1-2m)/2(1-m+n)} \sigma_c^{(1+2n)/2(1-m+n)}$$

The relaxation of the load with time during the fracture test in methanol has the following form (Fig.5.41)

$$P \propto t^{-0.30}$$

Converting P into K_c by using $K_c = A_g P$ (A_g is geometrical factor of specimen), the relaxation of K_c with time at 20°C is expressed by

$$K_c = 0.25 t^{-0.30} \quad \text{MNm}^{-3/2} \qquad (5.74)$$

Also, the COD, u_c, is a function of K_c (Table 5.12) and a graphical plot indicates a relationship of the form (Fig.5.38).

$$K_c = 0.055\, u_c^{0.72} \quad \text{MNm}^{-3/2} \quad (T=20°C) \qquad (5.75)$$

or

$$u_c = 56.4\, K_c^{1.39} \quad \mu\text{m}$$

Fig.5.41 Relaxation of the load P with time at two different initial P_i for the cracking of LMW in methanol. The slope is -0.3.

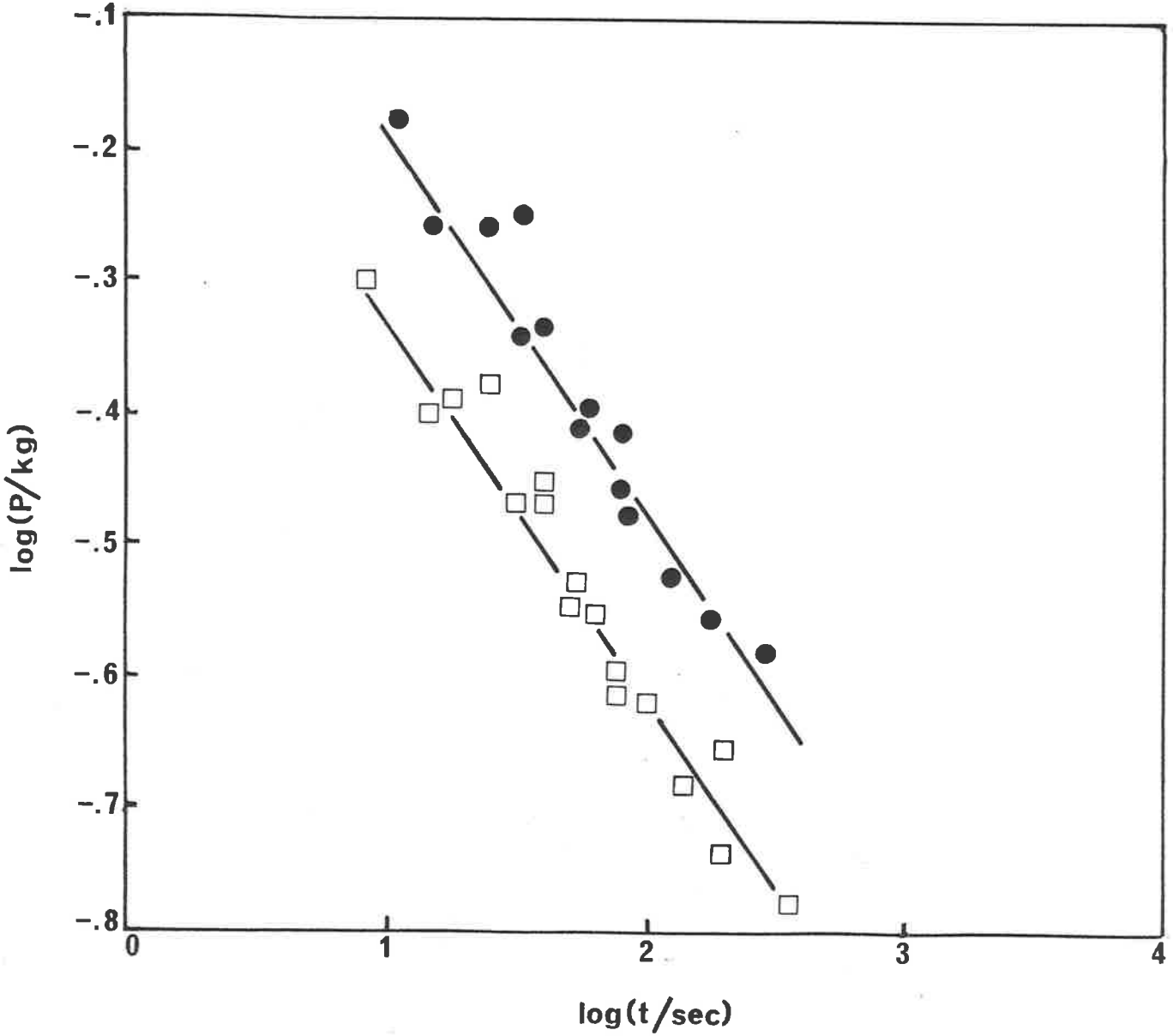
-.1
-.2
-.3
-.4
-.5
-.6
-.7
-.8
log(P/kg)
0
1
2
3
4
log(t/sec)

Combining Eqs.5.74 and 5.75 gives

$$u_c = 8.32\ t^{-0.42}\ \mu m \qquad (5.76)$$

Substituting Eq.5.76 into Eq.5.73, we obtain

$$K_c = C\ v^{(m+n)/2(1-m+n)}\ t^{-i}$$

or

$$K_c t^i = C\ v^{(m+n)/2(1-m+n)} \qquad (5.77)$$

where $i = 0.42\ (1-2m)/2(1-m+n)$. This equation indicates that because of the factor t^{-i}, the slope part of the log K_c vs. log v curve is not a straight line as expected. However, plot of log $(K_c t^i)$ vs. log v would give a linear relationship with the slope of $(m+n)/2(1-m+n)$.

The time factor, m, for σ_c can be calculated by the following method. Firstly, using a trial value of m (n = 0.1), a plot of log $(K_c t^i)$ vs. log v can be drawn (Eq.5.77). The value of the slope $(m+n)/2(1-m+n)$, found from the straight line of log $(K_c t^i)$ vs. log v can be used to calculate the value of m. The correct value of m is the value where trial m value is equal or close to calculated m.

The suitable trial value of m for crack propagation at 20°C is 0.18 and this value gives a slope of 0.14 (Fig.5.42). The calculated value of m from $(m+n)/2(1-m+n) = 0.14$, is found to be 0.16. Hence, it is reasonable to accept 0.18 as the value of m at 20°C. This trial method is sensitive to the chosen trial value, for example, if m is arbitrarily chosen at 0.3, then the calculated value will become 0.2.

At T=10°C, using the following data

$$K_c = 0.35\ t^{-0.25}\ \ MNm^{-3/2}$$

$$K_c = 0.063\ u_c\ \ MNm^{-3/2}$$

and

$$u_c = 5.55\ t^{-0.25}\ \ \mu m$$

m was determined to be 0.15 by the trial method.

The increase in the value of m with temperature (higher solvent uptake) implies that the stress will relax more rapidly

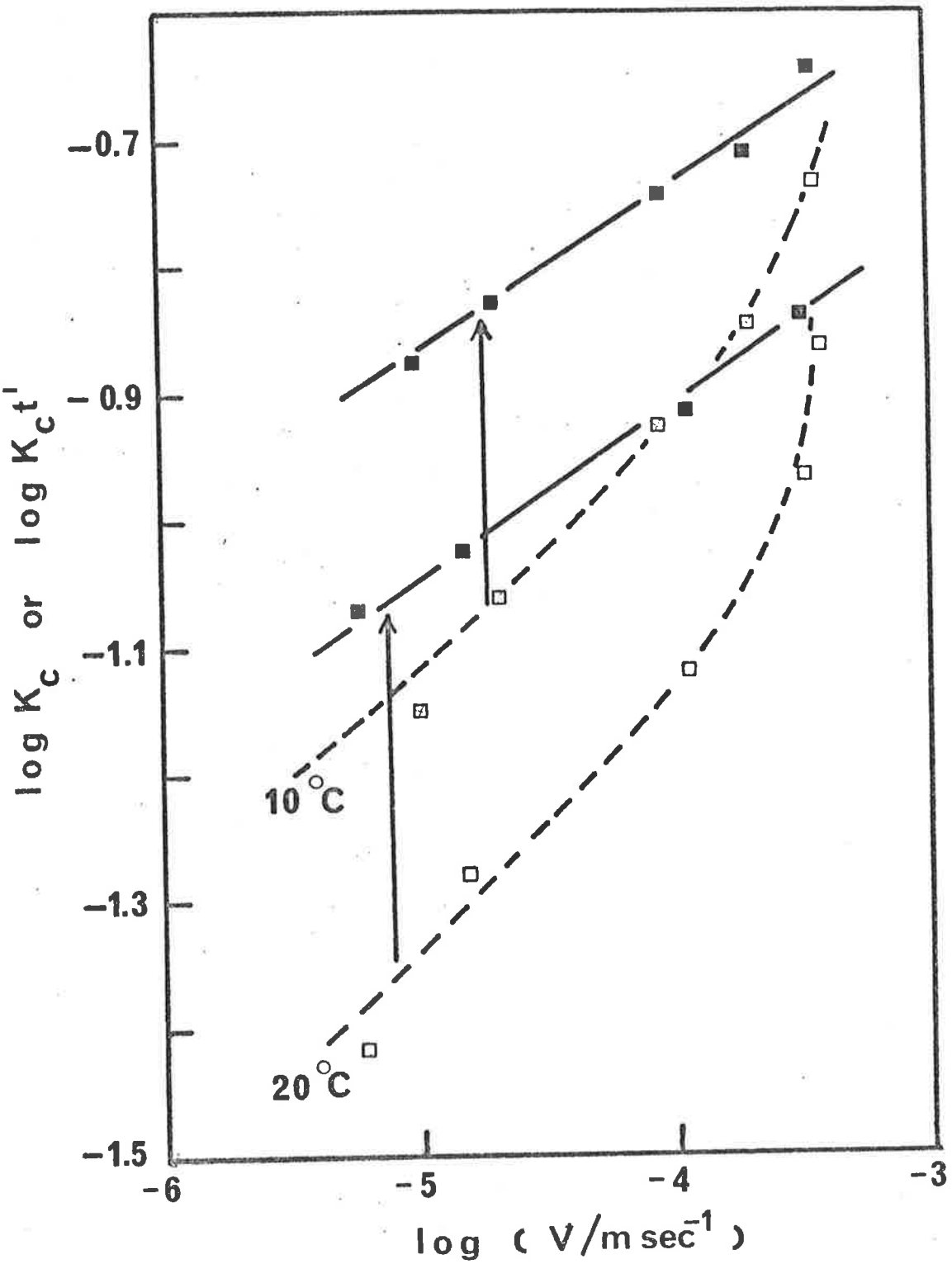

Fig.5.42 Plots of log K_c vs. log v (broken line) and log $K_c t^i$ vs. log v (solid line). Plots of log $K_c t^i$ vs. log v were drawn with m = 0.18 for T=20°C and m=0.15 for T=10°C.

with higher degrees of plasticization.

(c) The nature of the limiting crack velocity, v_o. Effect of temperature and MW

As stated in Chapter 2, except for the fracture process in inorganic glass, the transition from Region II to Region III of environmental stress cracking (Fig.2.6) has not previously been experimentally confirmed for polymers. Nevertheless, it is observed in Fig.5.43 that there exists a connection between the vertical part of log K_c vs. log v curve in methanol and the log K_c vs. log v straight line in air (cf. Fig.2.6). To confirm the transition from Region II to Region III (Region III corresponds to log K_c vs. log v curve in air) requires geometry other than DT geometry. This geometry yields undesirable multicracks at high K_c in methanol.

Williams and Marshall (17) suggested that the cracking mechanism in Region II is governed by d'Arcy's law that describes the liquid flow in a porous system. It is of interest to determine if the limiting velocity, v_o, obeys the d'Arcy's law. If this law is obeyed, v_o is given by

$$v_o = \frac{A}{2\eta}\left(\frac{dP}{dx}\right) \tag{5.78}$$

where the pore area, A, is expressed by

$$A = c\,u_c \tag{2.41}$$

let $$\frac{dP}{dt} = \frac{P}{\Delta}$$

where P = the pressure at the front tip. Eq.5.78 becomes

$$v_o = \frac{c\,u_c}{12\eta}\frac{P}{\Delta} \tag{5.79}$$

Substituting $\Delta = \frac{\pi}{8}\frac{u_c}{\varepsilon_y}$ (Eq.2.28) into Eq.5.79, v_o becomes

$$v_o = \frac{c\,u_c}{12\eta}\frac{8P\varepsilon_y}{\pi u_c}$$

$$= \left(\frac{2cP}{3\pi\eta}\right)\varepsilon_y \tag{5.80}$$

The first term on the RHS of Eq.5.80 can be considered as a constant,

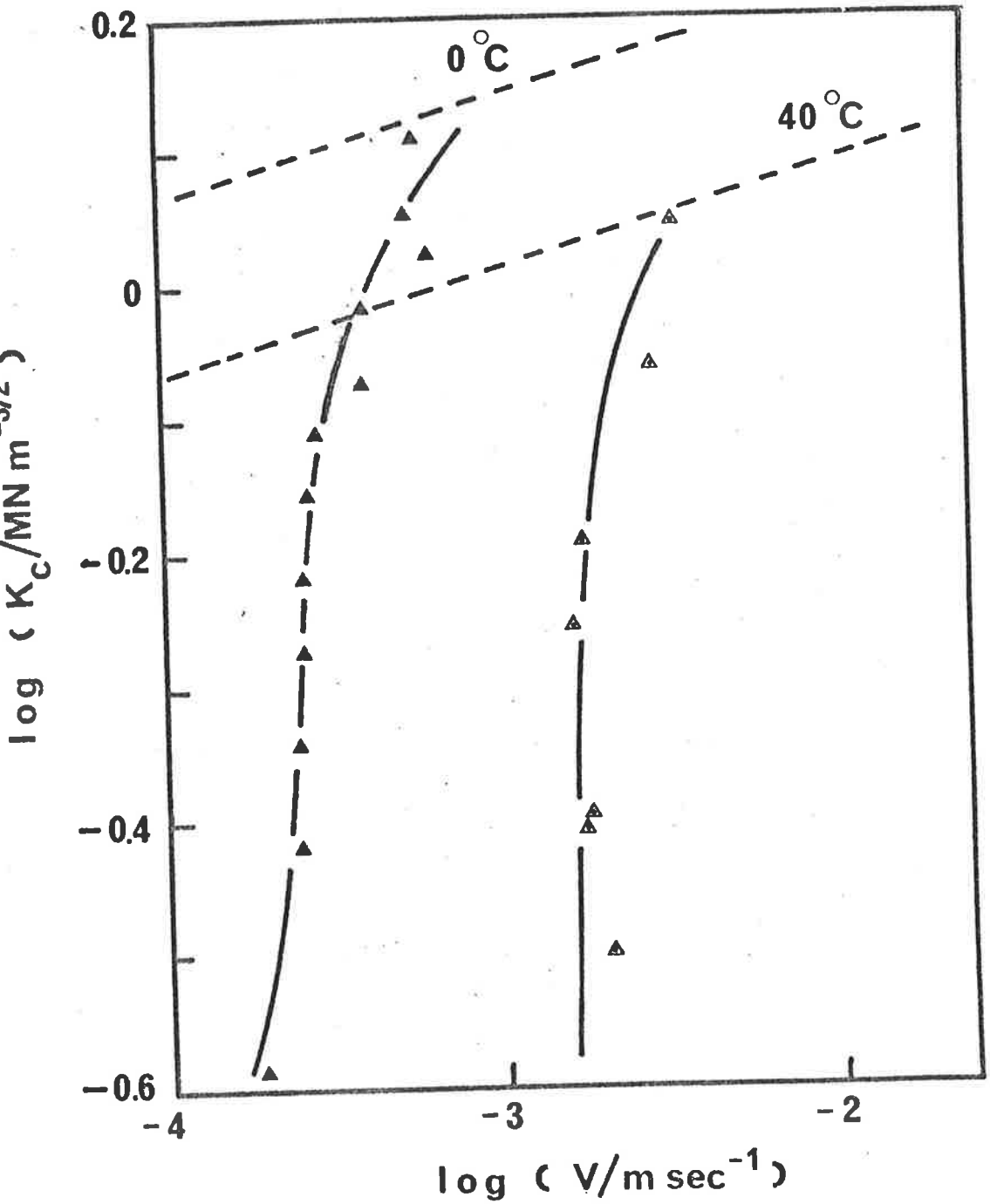

Fig.5.43 Plot of log K_c vs. log v of cracking in methanol for LMW. T=0°C (△), T=40°C (▲). The broken lines represent cracking in air.

because c, P are constants and the viscosity, η, of methanol does not show a large change in the range of the temperature $0°C \lesssim T \lesssim 40°C$. Therefore v_o depends only on the yield strain, ε_y. Unfortunately, the theoretical value of v_o expressed by d'Arcy's law (Eq.5.78) introduces a contradiction with the experimental data. From the cracking data of LMW in methanol, v_o increases with temperature whereas d'Arcy's law predict a decreasing v_o due to the decrease in ε_y with temperature (higher degree of plasticization).

Consequently, in contrast to Williams and Marshall's viewpoint, the evidence from this work suggests that the limiting velocity, v_o, is governed by the diffusion of liquid into bulk material at the crack tip rather than by the flow of liquid through the dry craze porous system.

It is observed from the plot of the limiting velocity, v_o versus temperature, that a linear relationship exists over a range of temperature from 0 to 40°C (Fig.5.44). However, this limiting velocity cannot be simply expressed as $v_o = \lambda kT/h$ (Eq.5.54c). This expression predicts successfully the limiting velocity in air by considering the bond rupture occurring in one vibration of the bond (frequency = kT/h). At room temperature, the bond frequency is approximately 10^{13} cycles per second and the bond length is of the order of 10^{-10} m, so that $v_o = 10^3$ msec^{-1} for most solids (26). It has been established by Zhurkov's group that it is chemical, or primary bonds that break under stress in the failure mechanism in air of polymers. However, from the magnitude of the activation energy calculated previously, the breaking of intermolecular bonds must be the main mechanism of the breakdown process in methanol. In other words, chain molecules rearrange their molecular conformation to slip past one another under stress. In this case the relaxation of chain molecules caused by the molecular rearrangement plays an important role in the determination of the limiting velocity. In

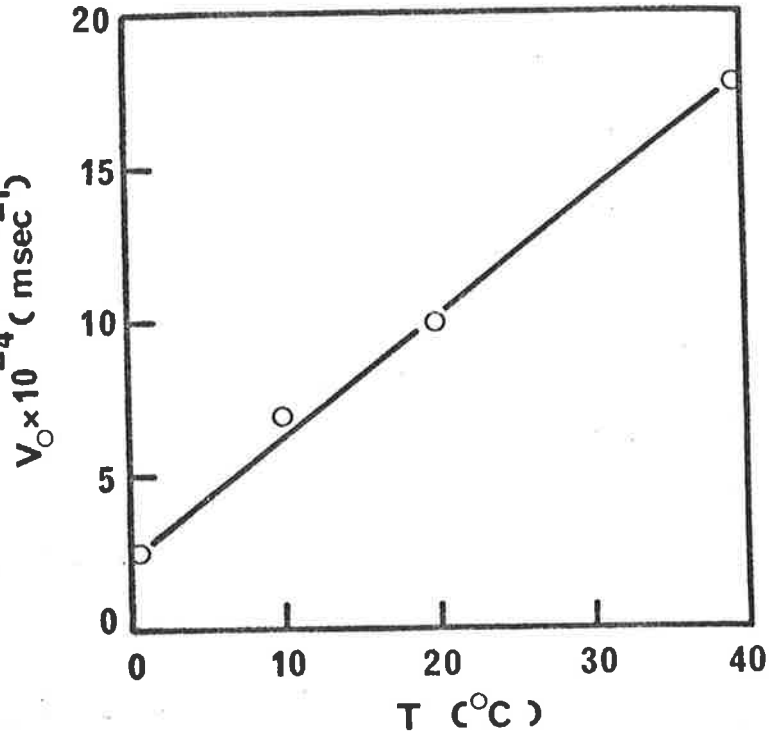

Fig.5.44 Effect of temperature on the limiting velocity, v_o.

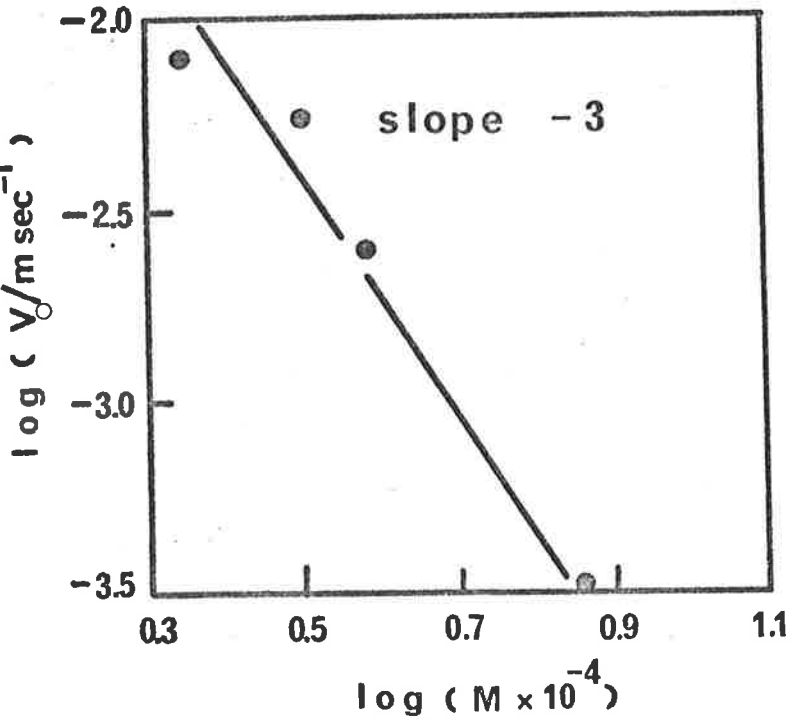

Fig.5.45 Effect of molecular weight on the limiting velocity, v_o.

more simple terms, a period of time of the order of the relaxation time, τ_r, is required to break an intermolecular bond, that is

$$v_o \simeq \frac{\lambda}{\tau_r} \tag{5.81}$$

The relaxation time, τ_r, can be written in the following general form

$$\tau_r = \frac{h}{kT} \exp\left(\frac{U_r}{kT}\right) \tag{5.82}$$

where U_r = the potential energy of the relaxation process (134-135), and can be assumed as the sum of the activation energy of the flow process, U_o, and the barrier energy, U_b, of the chain rearrangement. To fit the experimental values of v_o (10^{-3} to 10^{-1} $msec^{-1}$), the potential energy U_r must be in the range of $10\ kT < U_r < 100\ kT$ (i.e. $25\ kJ\ mol^{-1} < U_r < 250\ kJ\ mol^{-1}$ at $T = 300\ K$), so that the relaxation time, τ_r, required to break the intermolecular bond of spacing distance $\lambda = 10^{-10}$ m has the magnitude of 10^{-7} to 10^{-9} sec (Eq.5.82).

The MW dependence of v_o is another factor to support the relationship between v_o and τ_r (Eq.5.81). It was found that (Fig. 5.45)

$$v_o = 10^{11} M^{-3} \tag{5.83}$$

and therefore

$$\tau_r = 10^{-21} M^3 \tag{5.84}$$

The dependence on MW of τ_r is similar to that of maximum relaxation time, τ_m, of glassy polymers such as polystyrene (136) and poly(α-methystyrene) (137), that is

$$\tau_m \propto M^{3.4}$$

Although the above argument does not give a rigorous theoretical analysis of the nature of the limiting velocity, this

semi-quantitative treatment may initiate alternative thinking rather than the d'Arcy's law in improving the understanding of the limiting velocity in solvent stress-cracking.

5.4.8 Crazing Behaviour of High Molecular Weight and Medium Molecular Weight Poly(methylmethacrylate) in Methanol (Regime I and Transition Regime).

As mentioned in Section 5.4.6, one of the aspects which distinguishes craze from crack behaviour is the dependence of the initial SIF, K_i, of the log K_c vs. log v stress-crazing curves. Further to this observation, the initial SIF, K_i, and the initial velocity, v_i, in the log K_c vs. log v diagram of stress-crazing have a linear relationship on a log-log plot with the slope of 0.5, i.e. $K_i \propto v_i^{0.5}$ (Figs.5.30 and 5.31). Another characteristic of the log K_c vs. log v relationship shown in these Figures is that the slope of log K_c vs. log v straight line was observed to be unchanged at various K_i. The K_i independence of the slope will be clarified in Section 5.4.8.1.

The application of WM theory to craze growth needs justification, because the derivation of the WM theory is concerned with a crack with a small craze zone at the tip. To extend the theory to long crazes, a model for long craze growth is proposed and a theory based on the model is developed. The absorbed energy by craze matter and the COD, u_c, of the craze will be calculated by the developed theory, Section 5.4.6.2.

The relationship of K_i and v_i ($K_i \propto v_i^{0.5}$) at the craze initiation step, the time dependence of the crazing stress and the COD, and the craze propagation step (post-initiation step) will be discussed in the framework of the WM theory to give further insight into the crazing behaviour of PMMA in methanol, Section 5.4.8.3.

5.4.8.1 The Relationship between the Slope of log K_c vs. log v Straight line and the Initial SIF, K_i

It was found from experiments that the compliance y/P and the craze (or crack) length, a, for the major part of crack propagation or craze growth has a linear relationship

$$\frac{y}{P} = B\,a + C \tag{5.85}$$

where a is craze (or crack) length, B and C are constants. Differentiating the above equation with respect to t, we have

$$-\frac{y}{P^2}\left(\frac{dP}{dt}\right) = B\,v \tag{5.86}$$

Again, differentiating Eq.5.86 with respect to t

$$\begin{aligned} B\frac{dv}{dt} &= \frac{d}{dt}\left(-\frac{y}{P^2}\frac{dP}{dt}\right) \\ &= -\frac{y}{P^2}\frac{d^2P}{dt^2} + \frac{2y}{P^3}\left(\frac{dP}{dt}\right)^2 \\ &= \frac{y}{P^2}\left(-\frac{d^2P}{dt^2} + \frac{2}{P}\left(\frac{dP}{dt}\right)^2\right) \end{aligned} \tag{5.87}$$

Dividing both sides by dP/dt, we have

$$\frac{y}{P^2}\,\frac{\left(-\frac{d^2P}{dt^2} + \frac{2}{P}\left(\frac{dP}{dt}\right)^2\right)}{dP/dt} = B\frac{dv}{dP} \tag{5.88}$$

The relaxation of the applied load, P, during crack or craze propagation can be expressed in the form

$$P = P_i\,g(t) \tag{5.89}$$

Where P_i is the initial applied load corresponding to K_i and g(t) is a function of time. Combining Eqs.5.88 and 5.89 gives

$$\frac{v}{P_i^2\,[g(t)]^2}\,H(t) = B\frac{dv}{dP} \tag{5.90}$$

where $H(t) = -\frac{d^2[g(t)]}{dt^2} \Big/ \frac{dg(t)}{dt} + \frac{2}{g(t)}\frac{dg(t)}{dt}$, noting that

$$dv = v\, d\,(\ell n\ v)$$

and $$dP = P\, d\,(\ell n\ P)$$

or $$\frac{dv}{dP} = \frac{v}{P}\frac{d\,(\ell n\ v)}{d\,(\ell n\ P)} \tag{5.91}$$

Eq.5.90 may be rewritten in the form

$$\frac{y}{P_i}\frac{1}{vg(t)}H(t) = B\frac{d\ \ell n\ v}{d\ \ell n\ P} \tag{5.92}$$

Eq.5.85, $\frac{y}{P_i}$ is described by

$$\frac{y}{P_i} = B\ a_i + C \tag{5.93}$$

where a_i = initial crack length.

The load P is related with K_c by

$$K_c = A_g P \tag{5.20}$$

Substituting Eqs. 5.93 and 5.20 into Eq.5.92, we obtain

$$\frac{Ba_i + C}{v\ g(t)}H(t) = B\frac{d\ \ell n\ v}{d\ \ell n\ K_c}$$

or

$$\frac{d\ \log K_c}{d\ \log v} = \frac{B\ v\ g(t)}{(Ba_i + C)\ H(t)} \tag{5.94}$$

It is appropriate now to investigate the nature of the function g(t). The time function g(t) can be assumed to be

$$g(t) = t^{-q} \tag{5.95}$$

From experimental observation, v decreases with time, that is $\frac{dv}{dt} < 0$ and using Eq.5.90, we have

$$H(t) < 0$$

or

$$-\frac{d\ P}{dt} + \frac{2}{P}\left(\frac{dP}{dt}\right)^2 < 0 \tag{5.96}$$

Substituting Eq.5.95 into Eq.5.96, the inequality will be satisfied only when

$$q < 1$$

This prediction is verified by the relaxation of the load P with time having the form $P = P_i\, t^{-q}$, and q varies from 0.08 for HMW to 0.14 for MMW (Fig.5.46). Substituting Eq.5.95 into Eq.5.94 gives

$$\frac{d \log K_c}{d \log v} = \frac{B}{(Ba_i + C)(1 - q)}\, v\, t^{1-q} \qquad (5.97)$$

This equation clearly states that the slope ($d \log K_c / d \log v$) is independent of K_i. This prediction is supported by a family of parallel straight lines for craze growth of HMW and MMW (Figs.5.30, 5.31).

It is further noted that the slope is a time-dependent function, that is

$$\frac{d \log K_c}{d \log v} \propto v(t)\, t^{1-q}$$

Therefore, over a wide range of velocities log K_c vs. log v curve cannot be considered as a straight line. For example, for cracking in air, in the range of 10^{-6} msec^{-1} < v < 10^{-1} msec^{-1}, several authors have found that the slope decreases with decreasing velocity (17,105).

5.4.8.2 A model of Long Craze Growth.

In LEFM theory, the SIF, K_c, was determined as

$$K_c^2 = \sigma_c u_c E \qquad (2.27)$$

Also from geometrical analysis, K_c is expressed by

$$K_c = A_g P \qquad (5.20)$$

In crack propagation, these expressions are identical. However, for the case of a long craze, the equality of the above equations requires justification. A theory will be developed to re-examine the SIF, K_c, for the long craze growth. The derived theoretical K_c will be compared with $K_c = A_g P$ from geometrical analysis.

Fig.5.46 Relaxation of the load P with time at two different initial P_i for crazing of HMW and MMW in methanol. HMW (Δ), (slope = 0.08) and MMW (□) (slope = 0.14).

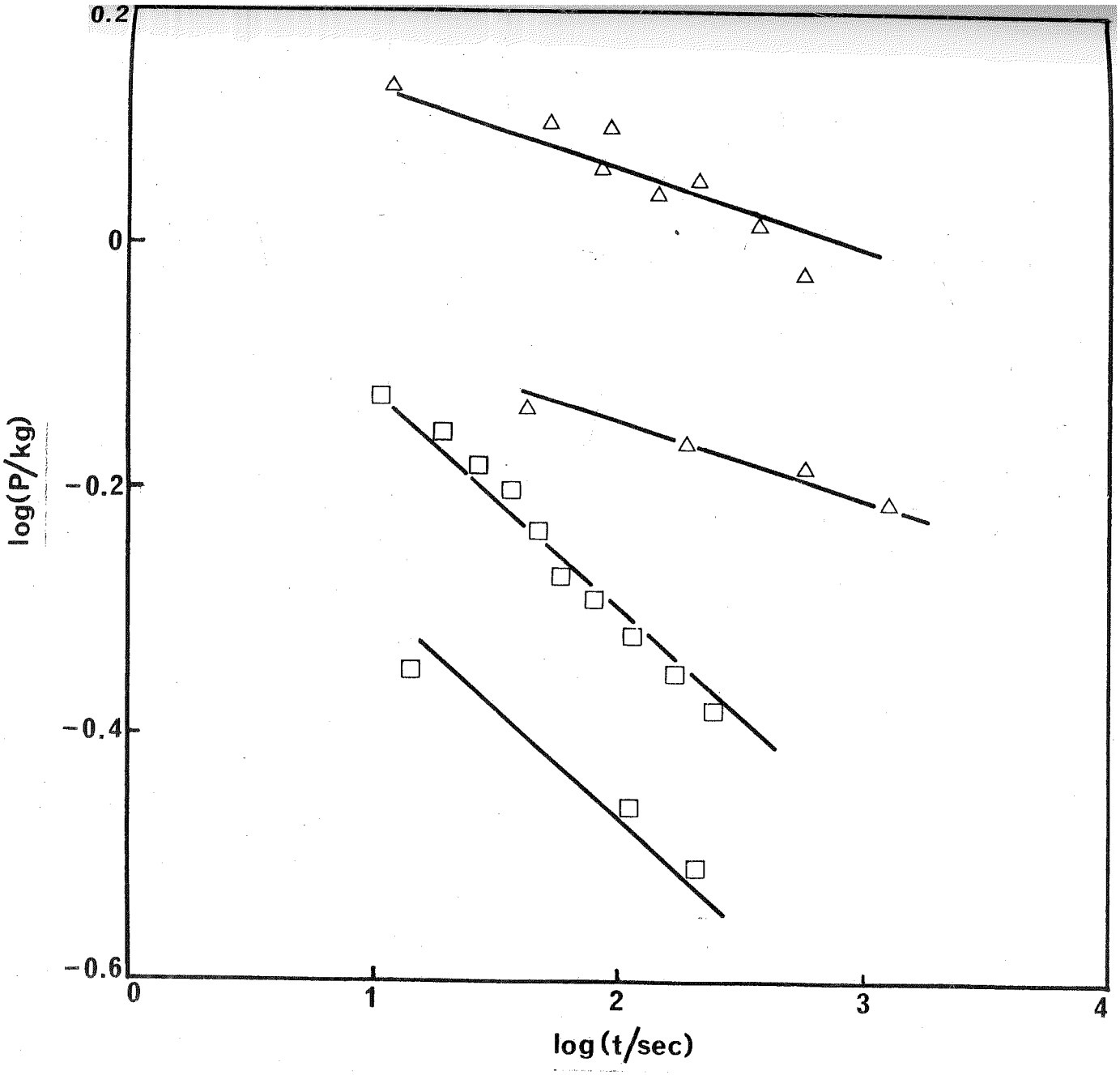
0.2
0
−0.2
−0.4
−0.6
log(P/kg)
0
1
2
3
4
log (t/sec)

(a) Theory

The total energy release rate G_T is the sum of two components (a) the energy absorbed by craze fibrils, G_A, and (b) the energy required to propagate the crack tip, G_P. That is

$$G_T = G_A + G_P \tag{5.98}$$

which can be represented by

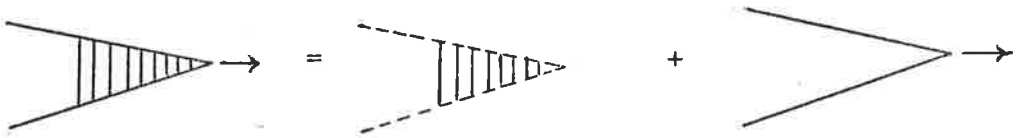

G_T = G_A + G_P

The SIF, K_c, calculated by the geometrical analysis $K_c = A_g P$ is related to G_T by

$$K_c^2 = G_T E \tag{5.99}$$

The derivation of K_c is based on the following assumptions:

(a) For convenience, craze matter is divided into bundles of unit area (Fig.5.47) where each bundle has experienced the same stress history during craze growth,

(b) Craze matter is in the rubbery state.

In assumption (a), strictly speaking, the same stress history of craze bundle requires the same strain rate. However, according to the results from tensile test of methanol-equilibrated HMW, as the strain rate increases from 10^{-3} sec^{-1} to 1 sec^{-1} (three decades), the yield stress only increases from 7 MN m^{-2} to 15 MN m^{-2}. Therefore, assumption (a) is plausible for a small range of crack (craze) velocities (strain rate of craze fibrils is proportional to crack or craze velocities, Eq.5.13) over two or three decades. The glass transition temperature of methanol-equilibrated PMMA, T_{sg},

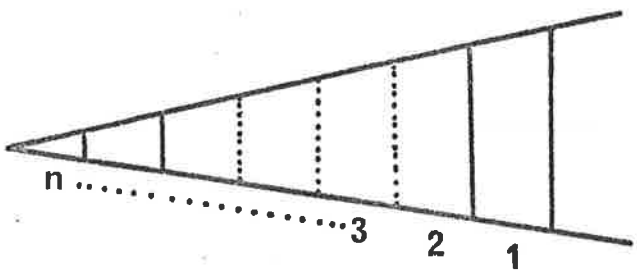

Fig.5.47 Craze matter is divided into bundles. Each bundle being of width corresponding to a unit along propagation direction.

is close to room temperature (Chapter 4) and it is reasonable to assume craze matter is in rubbery state [assumption (b)].

Now, the craze starts to develop by converting the bulk material into craze bundle 1 (1st step in Fig.5.48). As the tip propagates a unit length, the bulk material at the tip will convert into craze bundle 2 and craze bundle 1 moves to the second step (2nd step in Fig.5.48). Craze development then is a process of repeating the stress history of the preceding craze fibril until the front tip is arrested. Hence the energy absorbed per unit area by the craze matter as the tip propagates at nth step is the work expressed by the area under the stress vs. extension curve (nth step in Fig.5.48). This area also represents the work done by bundle 1 during the time of craze development from the 1st to the nth step.

In brief, the energy absorbed by craze fibrils per unit are, G_A, at time t is equal to the work done by the first craze bundle of one unit area from t=0 to t. This conclusion enables one to estimate G_A by examining the work done by the first unit of craze. The work done by a unit volume of material in rubbery state can be expressed by

$$W_A = \bar{N}_e \, RT \, f(\lambda_e) \tag{5.100}$$

and

$$\lambda_e = \frac{\ell}{\ell_o} \tag{5.101}$$

where $f(\lambda_e)$ is a function of extension ratio, λ_e, ℓ_o is the original length and ℓ is the length at time t (114).

The stress is defined by

$$\sigma = \frac{dW_A}{d\lambda_e} = \bar{N}_e \, RT \, \frac{df(\lambda_e)}{d\lambda_e} \tag{5.102}$$

The work done by bulk material at the front tip having the volume V and primordial thickness d_o* is W_A V. Therefore the energy

* Thickness of the original bulk material at the craze tip.

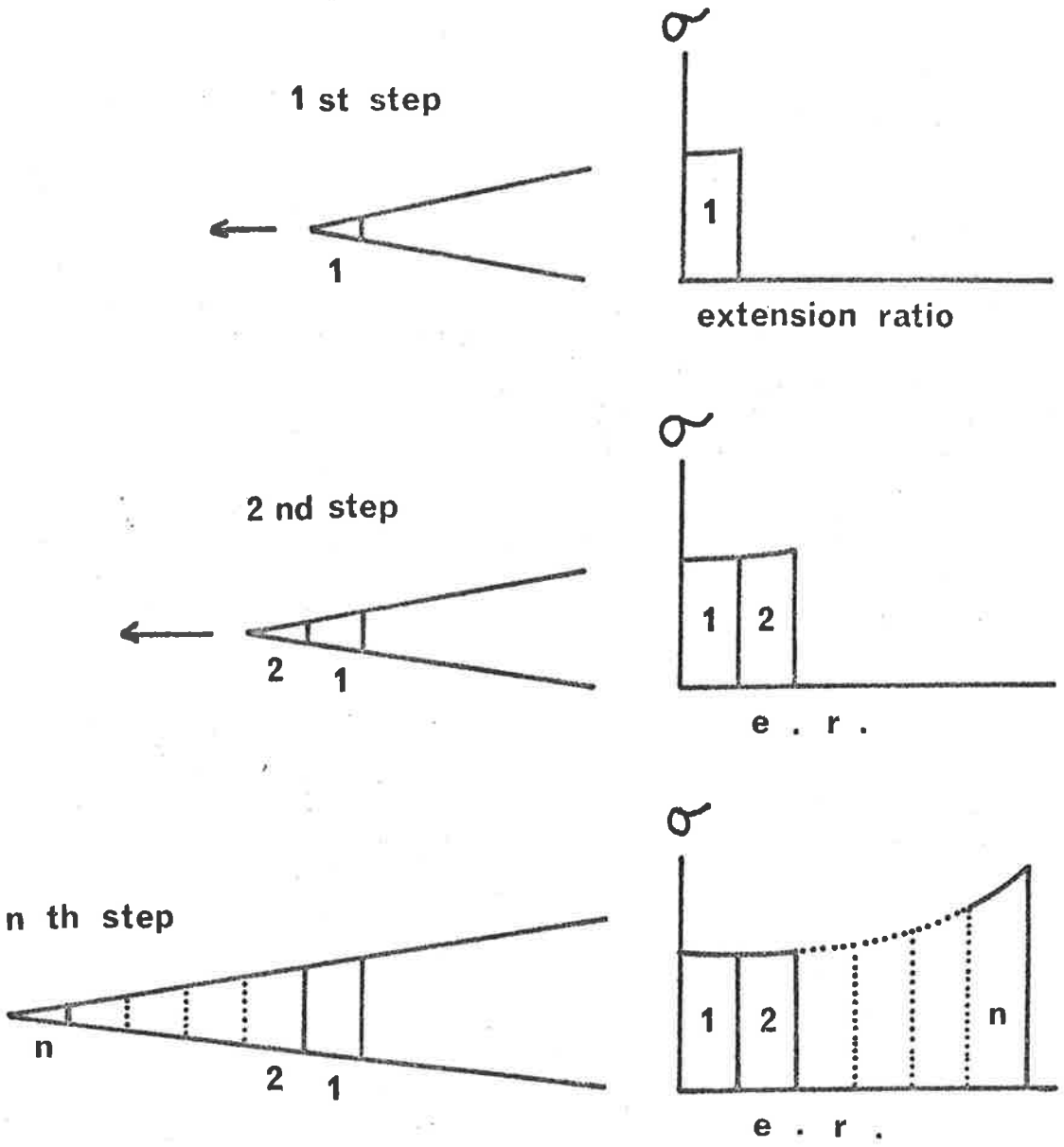

Fig.5.48 A model of craze development from lst step to nth step. Stress on craze fibrils, σ.

absorbed by the craze per unit area is expressed by

$$G_A = W_a d_o \tag{5.103}$$

If the stress distribution along the craze is assumed to obey Dugdale's model, the crazing stress can be described by

$$\sigma_c = \bar{N}_e RT a_\sigma \tag{5.104}$$

where a_σ is a stress constant depending on the inherent character of material. Eqs.5.100 and 5.103 become

$$W_A = \bar{N}_e RT a_\sigma \lambda_e \tag{5.105}$$

and

$$G_A = \bar{N}_e RT a_\sigma \lambda_e d_o \tag{5.106}$$

The extension ratio of the first bundle of craze fibrils is given by

$$\lambda_e = \frac{u_c}{d_o} \tag{5.107}$$

that is

$$G_A = \bar{N}_e RT a_\sigma u_c \tag{5.108}$$

Combining Eq.5.104 and Eq.5.106 gives

$$G_A = \sigma_c u_c \tag{5.109}$$

The release energy rate, G_P, of the crack propagation is given by

$$G_P = \sigma_{cP} u_{cP} \tag{5.110}$$

where σ_{cP} is the crazing stress at the front tip and u_{cP} is the COD of the crack propgation in Regime II.

By combination of Eqs.5.98, 5.99, 5.108 and 5.110, we obtain

$$K_c^2 = \bar{N}_e RT a_\sigma E u_c + E \sigma_{cP} u_{cP} \tag{5.111}$$

$$= E(\sigma_c u_c + \sigma_{cP} u_{cP})$$

If $\sigma_c u_c >> \sigma_{cP} u_{cP}$, then the SIF, K_c calculated by geometrical analysis $K_c = A_g P$ becomes

$$K_c^2 \simeq E \sigma_c u_c \tag{5.112}$$

$$\simeq G_A E$$

Consequently, the application of LEFM to long craze growth is justified when the range of propagating velocities is small (ranging from 2 to 3 decades). Williams and Marshall (17) have noted that for a long craze where the ratio of craze length and crack length is about ten; the use of $K_c = \sigma_c u_c E$ leads to only a factor of 2 in error.

As discussed in Section 5.4.3, the COD, u_c, is a function of MW expressed by

$$u_c = u_{c_1} + u_c(\infty) \frac{\bar{N}_e}{\bar{N}_e(\infty)} \tag{5.113a}$$

For $M_w \gtrsim 80{,}000$, u_c can be approximated as

$$u_c \simeq u_c(\infty) \frac{\bar{N}_e}{\bar{N}_e(\infty)} \tag{5.113b}$$

Hence, Eq.5.112 becomes

$$K_c \simeq \frac{\bar{N}_e}{\bar{N}_e(\infty)} E \sigma_c u_c(\infty)$$

$$= \frac{\bar{N}_e^2}{\bar{N}_e(\infty)} RT a_\sigma E u_c(\infty) \tag{5.114}$$

where R, T, a_σ, E and $u_c(\infty)$ are constants.

As mentioned in Section 5.4.2, the crazing stress, σ_c, in air is independent of MW down to values approaching the critical MW, M_c. However, Eq.5.104 has shown that the crazing stress σ_c in the presence of methanol depends on the entanglement density, $\bar{N}_e$, i.e. on the MW. Because the crazing stress corresponds to the yield stress in a tensile test for a good approximation, the MW dependence of σ_c can be understood by the yield stress of methanol equilibrated

PMMA samples. For example, at the same strain rate (~10^{-4} sec^{-1}), the tensile testing of methanol equilibrated HMW and LMW at 20°C gave the yield stress of 15 MNm^{-2} and 2 MNm^{-2} for HMW and LMW, respectively. Similar to the crazing stress, σ_c, Eq.5.114 showed that the SIF, K_c, is linearly proportional to the entanglement density, $\bar{N}_e$. Comparison of the calculated values and theoretical values of K_c (Eq.5.114) will be discussed in terms of the absorbed energy, G_A, in Part (b) of this Section.

The effect of temperature on the yield stress and on the SIF can be attributed to the same effect on the entanglement density, $\bar{N}_e$. At higher temperatures, more methanol is absorbed to plasticize the crack tip and this leads to a reduction in the entanglement density. Andrews et al. (60) reported a decrease in the yield stress with increasing temperature. Also, the transition of crazing behaviour at T = 0°C to cracking behaviour at T = 40°C in medium MW MMW (Fig.5.33) implies that at T = 40°C the entanglement density $\bar{N}_e$ reduces to zero due to heavy plasticization at the crack tip.

(b) Application:

The abosrbed energy, G_A, and the COD, u_c, of craze growth

To calculate the abosrbed energy, G_A, it is necessary to determine G_T and G_P (Eq.5.98), that is

$$G_A = G_T - G_P$$

The values of G_T can be estimated from log K_c vs. log v diagram because

$$G_T = \frac{K_c^2}{E}$$

The value of G_P can be estimated from Eq.5.110 where the crazing stress at the front tip, σ_{cP} ($\equiv \sigma_c$ by Dugdale's model), in methanol at 20°C was determined to be 7 MNm^{-2} by Graham et al. (102) for high MW PMMA and from tensile testing it was found that $\sigma_{cP} \equiv \sigma_c$ = 2 MNm^{-2} for medium MW (sample MMW). The COD of crack propagation,

u_{cP}, in Section 5.4.7 can be used to estimate G_P. According to previous results for the u_{cP} (Table 5.11) in the range of velocities 10^{-6} msec^{-1} < v < 10^{-5} msec^{-1}, the value of u_{cP} can be taken as 0.87 μm, that is

$$G_P = \sigma_{cP}\, u_{cP}$$
$$= (7 \times 10^6)(0.87 \times 10^{-6})$$
$$= 6.1 \text{ J m}^{-2}$$

for high MW sample (e.g. HMW) and

$$G_P = (2 \times 10^6)(0.87 \times 10^{-6})$$
$$= 1.7 \text{ J m}^{-2}$$

for medium MW sample (e.g. MMW).

The calculated values of G_A are listed in Table 5.15

TABLE 5.15: Calculated values of G_A at the initial SIF, K_i = 0.794 MNm^{-2} [E = 3500 MNm^{-2}].

Sample	M_w	v (msec^{-1})	G_P (Jm^{-2})	G_A (Jm^{-2})
A3	380,000	6.7x10^{-6}	6.1	180
		1.2x10^{-6}	6.1	126
		3.5x10^{-7}	6.1	98
A4	150,000	6.2x10^{-6}	6.1	178
		1.7x10^{-6}	6.1	113
		9.0x10^{-7}	6.1	86
A6	84,000	4.6x10^{-6}	6.1	107
		2.0x10^{-6}	6.1	72
		6.5x10^{-7}	6.1	56
A7	71,500	6.3x10^{-6}	1.7	12
HMW	787,000	6.4x10^{-6}	6.1	153
		1.1x10^{-6}	6.1	42
MMW	220,000	6.4x10^{-6}	1.7	88

The above calculation shows that most of the work done on the specimen by the applied load is absorbed by craze and only a few percent of the total energy is released to propagate the tip (G_p). Comparison of the G_A of different samples at the same propagating velocity has shown that high MW samples (e.g. A3 and HMW) have higher absorbed energy G_A than that of low MW samples (e.g. samples A7 and MMW). The decrease in G_A with velocity is attributed to the relaxation of σ_c and u_c with time. This problem will be discussed in Section 5.4.8.3.

A comparison of the theoretical values (Eq.5.114) and experimental values (Table 5.15) can be made by taking the ratio of $G_A(\alpha)/G_A(\beta)$ of sample α and sample β. Eq.5.114 gives

$$\frac{G_A(\alpha)}{G_A(\beta)} = \left(\frac{\bar{N}_e(\alpha)}{\bar{N}_e(\beta)} \right)^2 \qquad (5.115)$$

The entanglement density, $\bar{N}_e$, in methanol can be calculated by

$$\bar{N}_e = \bar{N}_e(\infty) \left(1 - \frac{M_{sc}}{M_n} \right) \qquad (5.53)$$

where M_{sc} = 38,000 for narrow MWD PMMA and M_{sc} = 178,000 for commercial PMMA (Chapter 4) in methanol at T = 20°C.

Table 5.16 shows the theoretical and experimental ratio of absorbed energy of samples α and β, $G_A(\alpha)/G_A(\beta)$.

TABLE 5.16: Theoretical and experimental values of ratio $G_A(\alpha)/G_A(\beta)$

Sample α/Sample β	Theoretical values (Eq.5.115)	Experimental values at $v = 6 \times 10^{-6}$ msec^{-1}
A4/A3	0.58	0.90
A6/A3	0.37	0.60
A7/A3	0.27	0.07
MMW/HMW	0.11	0.55

Except for the ratio of absorbed energy of A7/A3, the experimental values are generally higher than the theoretical. The difference between the two values shown in the above Table suggests that in contrast to cracking in air, the calculation of the entanglement density may not be based simply on

$$\bar{N}_e = \bar{N}_e(\infty) \left(1 - \frac{M_{sc}}{M_n}\right) \qquad (5.53)$$

Since this equation only includes the effect of the critical MW on the entanglement density in the equilibrium state. Rather, it is likely that in the presence of methanol, the craze fibrils have enhanced stretching ability (see calculation of u_c in next paragraph) and thus require longer time to reach their breaking point compared with the craze in air. In this case, the disentanglement process is a strongly time-dependent process in which the entanglement density is not only influenced by the amount of absorbed solvent but also by time-dependent disentanglement process under stress. Further study on the relation of the disentanglement kinetics under stress and the fracture toughness is necessary to provide a more comprehensive understanding of crazing behaviour.

The COD of craze growth can be estimated by $G_A = \sigma_c u_c$ (Eq.5.109), if the value of σ_c is known. Graham et al. (102) determined σ_c to be 7 MNm^{-2} at the arrest of the craze. Assuming that this value (σ_c = 7 MNm^{-2}) is still valid at low velocities ($v \simeq 10^{-7}$ $msec^{-1}$) then the COD, u_c, can be estimated (Table 5.17).

TABLE 5.17: The COD for craze growth in methanol at T = 20°C and σ_c = 7 MNm^{-2}

Sample	M_w	v ($msec^{-1}$)	$u_c = G_A/\sigma_c$ (μm)
A3	380,000	3.5×10^{-7}	14.8
A6	84,000	6.5×10^{-7}	8.8
HMW	787,000	1.1×10^{-6}	6.8

Compared to the COD for cracking in air (u_c = 2.56 μm) the calculated values of u_c for crazing in methanol illustrate the enhanced stretching ability of plasticized craze fibrils. It is noticed from the magnitude of the COD that the high MW and narrow MWD samples show higher stretching ability than the low MW and broad MWD samples. Another important point that must be remembered is that the above results can be considered as the "final" value of the COD because at $v \simeq 10^{-7}$ msec^{-1} the craze growth is practically arrested. Similar to the crazing stress, the COD, u_c, is a time dependent quantity. The COD increases with time to reach a final value when the craze is arrested. This problem will be discussed in the next Section.

5.4.8.3 Analysis based on Linear Elastic Fracture Mechanics (Williams-Marshall Theory)

Further examination and analysis of the initial SIF, K_i, dependence of the log K_c vs. log v relationship will be discussed within the framework of the LEFM concept (WM theory) in two parts. The first part is the analysis of the linear relationship between log K_i and v_i of the craze initiation step. The time-dependence of the crazing stress, the COD and the analysis of the craze propagation step (post-initial step) will be considered in the second part.

(a) Flow Controlled Craze Growth Mechanism

The linear relationship between log K_i and log v_i of the craze initiation step is shown by Figs.5.30, 5.31 and can be expressed in the form of

$$K_i \propto v_i^{0.5} \qquad (5.116)$$

Williams and Marshall (17) argued that in the early stages of craze growth (i.e. the initiation step), the craze mechanism will obey a flow controlled mechanism. Eq.2.44 expressing the theoretical relationship between v ($\equiv v_i$) and K_c ($\equiv K_i$) can be rewritten as

$$K_i = \sqrt{\frac{12\eta \Delta \sigma_o E_o}{P c}} \; v_i^{0.5} \qquad (5.117)$$

and the material constant, c, is defined as

$$c = \frac{\ell_v^2}{2d_o} \qquad (5.118)$$

where ℓ_v is the void spacing and d_o is the primordial craze thickness.

The agreement between the experimental and theoretical equations (Eqs.5.116 and 5.117) obviously suggests that the initiation step of craze growth obeys Williams and Marshall's flow controlled mechanism. Furthermore, plots of K_i^2 vs. v_i(Fig.5.49) yields straight lines with slope of 1.6×10^5 MN^2 s m^{-4} and 7.5×10^3 MN^2 s m^{-4} being the value of $(12 \Delta \eta \sigma_o E_o)/P c$[= $(24 \Delta \eta \sigma_o E_o d_o)/P \ell_v^2$] for HMW and MMW, respectively. The void spacing, ℓ_v, was calculated by Williams and Marshall (17) to be 25 nm, and this value was verified by Kambour and Holik's work (138). Other factors (Δ, η, σ_o, E_o and P) are constants, therefore the difference in the slope is attributed by the primordial craze thickness, d_o. Kramer et al. (139) have measured d_o to be 1 μm for high MW PMMA in methanol. From the values of the slope, assuming the d_o = 1 μm for HMW, d_o of MMW is determined to be 47 nm. The low magnitude of d_o for MMW is close to the primordial thickness of polystyrene in n-heptane (weak craze) and indicates that the craze fibril is more susceptible to breakdown than the craze fibrils of high primordial thickness (139).

It was also observed from the experimental data that a larger K_c is required in methanol than is required in air in the range of velocities $v > 10^{-5}$ m sec^{-1}. For example, at $v = 10^{-5}$m sec^{-1} for sample HMW, K_c = 1 MN m$^{-3/2}$ (log K_c = 0) (Fig.5.8) for cracking in air and K_i = 1.26 MN m$^{-3/2}$ (log K_c = 0.1) for crazing in methanol (Fig.5.30). It would have been desirable to have more data for the

Fig.5.49 A plot showing the relationship between the initial SIF, K_i, and the initial velocity, v_i. (a) HMW, (b) MMW.

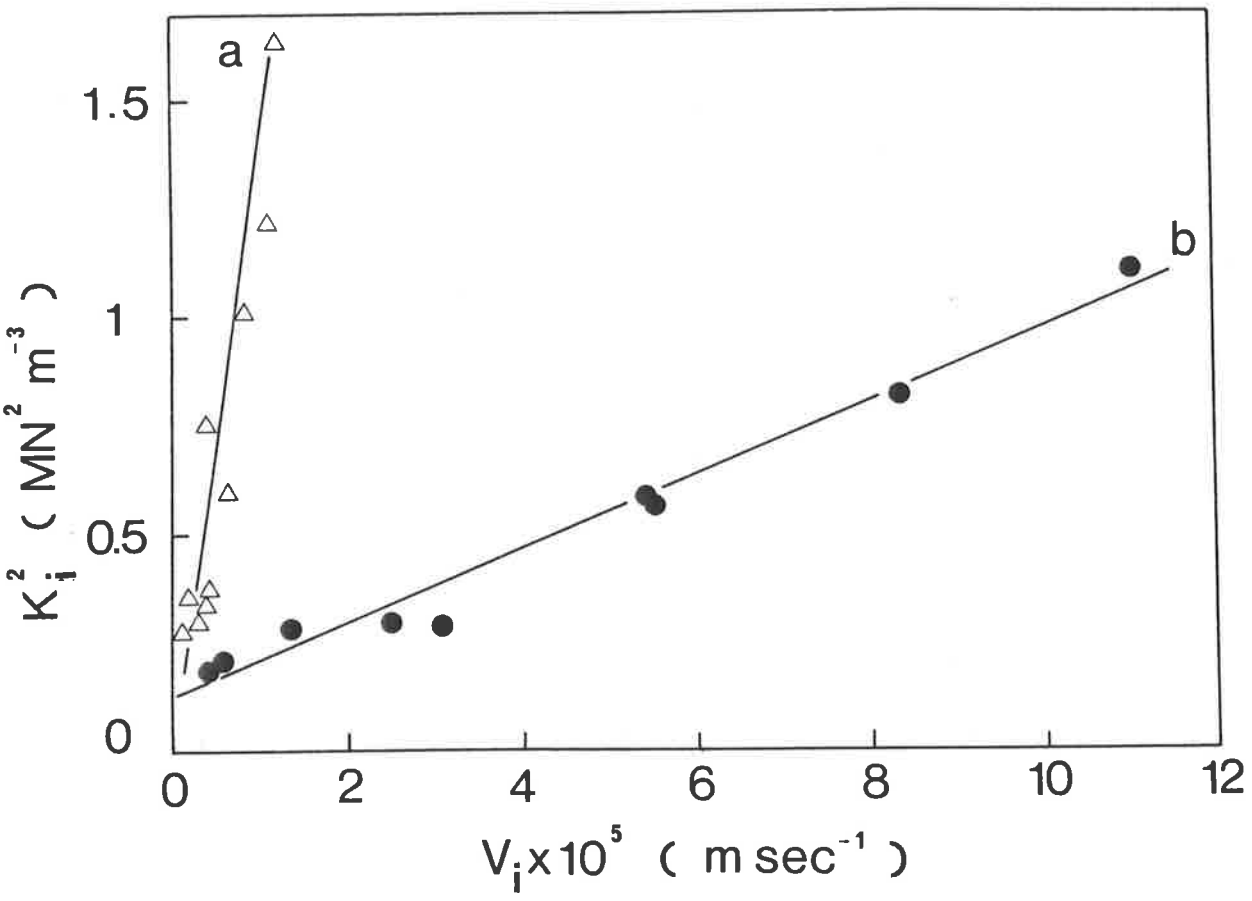
a
b
1.5
1
0.5
0
0
2
4
6
8
10
12
K_i^2 ($MN^2 m^{-3}$)
$V_i \times 10^5$ ($m\,sec^{-1}$)

crazing in methanol to confirm the trend at $v > 10^{-5}$ m sec^{-1}. Unfortunately, attempts to induce higher velocities in the DT geometry led to the development of multicracks. The same phenomena was observed in a wide range of velocities by Mai (99) for PMMA in ethanol and carbon tetrachloride. Re-examining Mai's data in log K_c vs. log v relationship, the graph divides into two parts of different slope. At $v < 10^{-5}$ m sec^{-1} the slope of log K_c vs. log v straight line is 0.5 and at $v > 10^{-5}$ m sec^{-1} the slope reduces to 0.07 (Fig. 5.50). A larger K_c for crazing in ethanol than for cracking in air is observed at $\log(v/m\ sec^{-1}) > -5.5$. Mai attempted to relate the larger K_c in ethanol crazing with void formation, but the explanation lacks support (99). Using $K_c^2 = \sigma_c\ u_c\ E$, however, the change in slope of Mai's data and the high SIF in ethanol can be clarified.

Mai's data of the log K_c vs. log v relationship (Fig.5.50), in fact, corresponds to the craze initiation step of this work. The slope of 0.5 at $\log(v/m\ sec^{-1}) < -5.5$ implies that the flow controlled mechanism is obeyed in this region. An increase in K_c leads to an increase in u_c until the magnitude of u_c reaches a limit where the slope of the log K_c vs. log v curve changes from 0.5 to 0.07. The second part of the curve having slope of 0.07 is parallel with the log K_c vs. log v curve in air. The relationship between K_c and v in this part of the curve which is analogous to that of cracking in air, depends only on the modulus E(v) because σ_c is a constant and u_c has reached a limiting value (105).

To fit Mai's data for craze growth of PMMA in ethanol, a limiting value of u_c of 90 μm at $K_i = 1.26$ MN $m^{-3/2}$ was selected. The theoretical log K_c vs. log v curve having the slope of 0.5 for $K_i < 1.26$ MN $m^{-3/2}$ and 0.07 for $K_i > 1.26$ MN $m^{-3/2}$ was drawn.

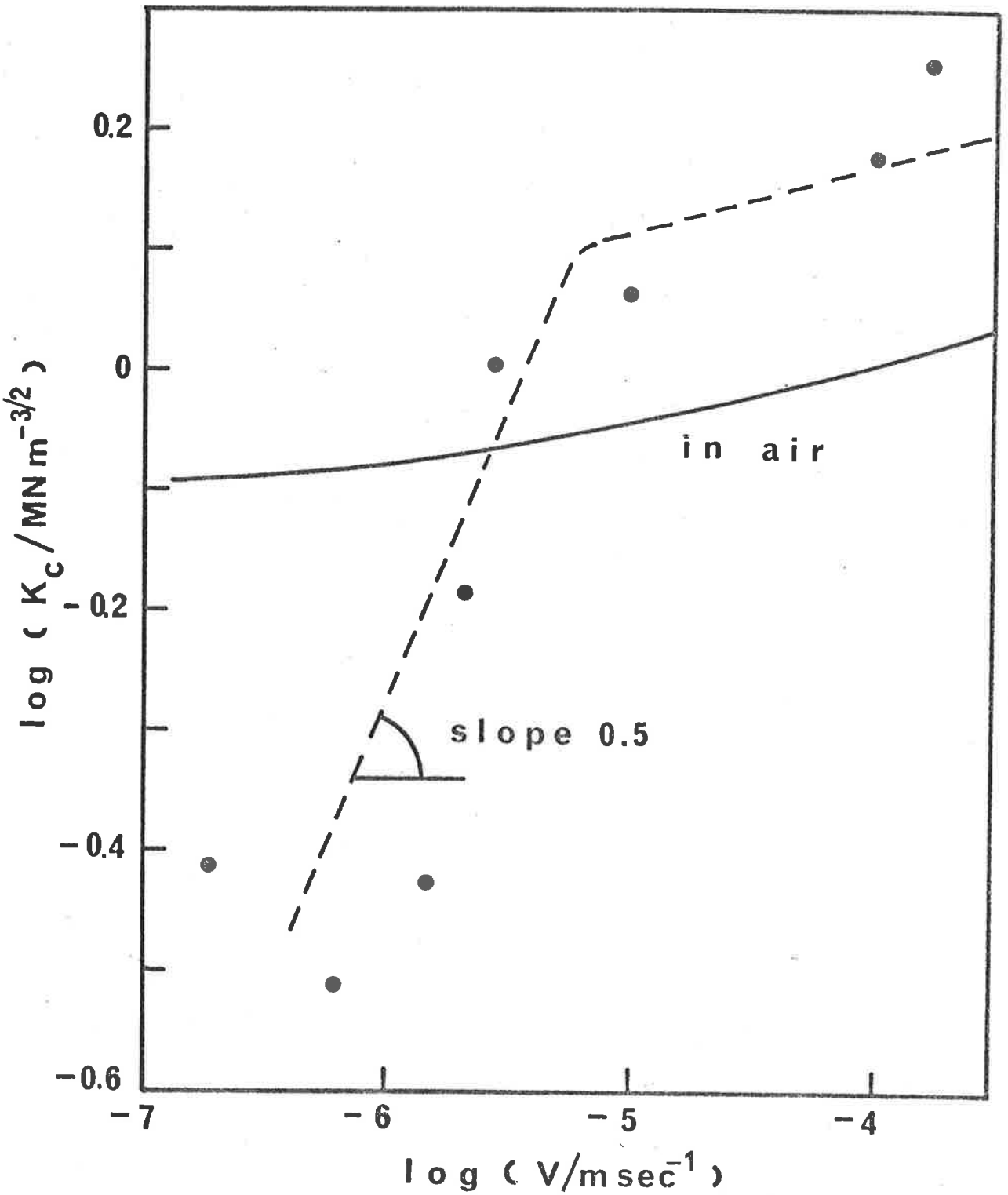

Fig.5.50 Environmental craze growth kinetics of PMMA in ethanol, Mai's data (99) (●) and the kinetic of crack growth in air (105) (solid line). The broken line is the theoretical curve, assuming that the limiting COD is 90 μm at $\log(K_c/MN\ m^{-3/2}) = 0.1$.

(b) Time Dependent Crazing Stress and COD.

Relaxation Controlled Craze Growth Mechanism.

In Section 5.4.8.2, it was shown that

$$K_c^2 \simeq \sigma_c u_c E$$

$$\simeq G_A E \qquad (5.112)$$

The applied load, P, decreases with time as craze developes (Fig.5.46) and so does the SIF, K_c ($K_c = A_g P$), that is,

$$K_c = K_o t^{-q} \qquad (5.119)$$

where K_o = constant. The COD, u_c, increases with time under the load due to the high ability of stretching of craze fibrils,

$$u_c = u_o t^{k} \qquad (5.120)$$

where time factors q and k are positive constants.

Hence, on combination of Eqs.2.32, 2.33, 5.112, 5.119, 5.120, we obtain

$$K_o^2 t^{-2q} = \sigma_o u_o E_o t^{k-m-n} \qquad (5.121)$$

that is

$$2q = -k + m + n \qquad (5.122)$$

the time factor n of modulus E is not influenced by the environment and has the value of 0.1 (17), whereas k, m and q are functions of the molecular properties of polymers and the nature of environment.

According to WM theory (17), at longer times, the kinetics of craze growth conforms to a relaxation controlled craze growth mechanism. Transition from a flow controlled mechanism at shorter times (craze initiation step) to relaxation controlled mechanism at longer time (propagation step) can be seen in the change of the slope of the log Δ vs. log t curves (Fig.5.51). Average crazing stress for the relaxation controlled mechanism was described as

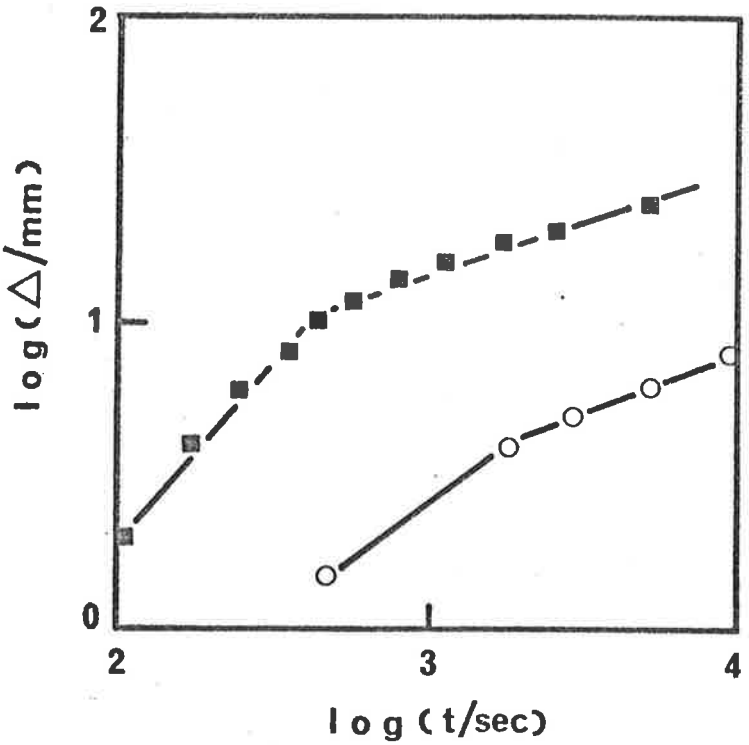

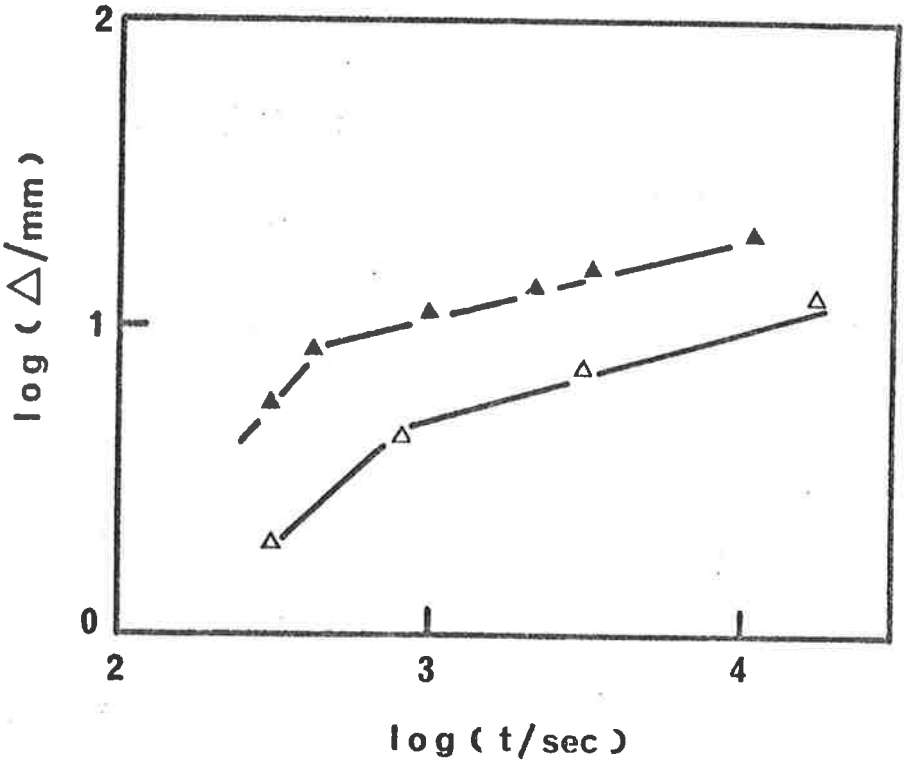

Fig.5.51 Growth of craze length, , with time. MMW (■), HMW (○), A7 (▲) and A2 (△).

$$\bar{\sigma}_c = \frac{\sigma_o t^{-m}}{1-m} \tag{2.38}$$

Assuming that no stress singularity exists at the tip, the craze length can be shown to be given by

$$\Delta = \frac{\pi}{8} \frac{K_c^2}{\sigma_c^2} \tag{2.25}$$

The expression for the SIF, $K_c^2 = \sigma_c u_c E$, as discussed in Section 5.4.8.2, proved to be a reasonable relationship for a long craze length, whereas Eq.2.25 is only true for a crack with small craze zone (Chapter 2). As a first approximation, by introducing a correction factor, ξ, the craze length can be assumed to be of the form

$$\Delta = \xi \frac{\pi}{8} \frac{K_c^2}{\sigma_c} \tag{5.123}$$

The introduction of the correction factor, ξ, will be justified later by experimental data.

Replacing σ_c by $\bar{\sigma}_c$ of Eq.2.38, Eq.5.123 becomes

$$\Delta = \xi \frac{\pi}{8} \frac{K_c^2}{\sigma_c^2} (1-m)^2 t^{2m} \tag{5.124}$$

and the craze velocity, v, is given by

$$v = \frac{d\Delta}{dt}$$

$$= 2m (1-m)^2 \xi \frac{\pi}{8} \frac{K_c^2}{\sigma_o^2} t^{2m-1} \tag{5.125}$$

Taking into account the relaxation of the SIF, K_c (Eq.5.119), Eq.5.125 becomes

$$v = 2m (1-m)^2 \xi \frac{\pi}{8} \frac{K_o^2}{\sigma_o^2} t^{2m-2q-1} \tag{5.126}$$

Plot of log v vs. log t gave a simular straight line independent of the initial SIF, K_i, for commercial HMW, MMW and narrow MWD PMMA as predicted by Eq.5.126 (Figs.5.52 a,b,c). The slope (= 2m-2q-1) varies from -0.75 to -0.80.

Fig.5.52 Plot of log v vs. log t for commercial PMMA and narrow MWD PMMA.

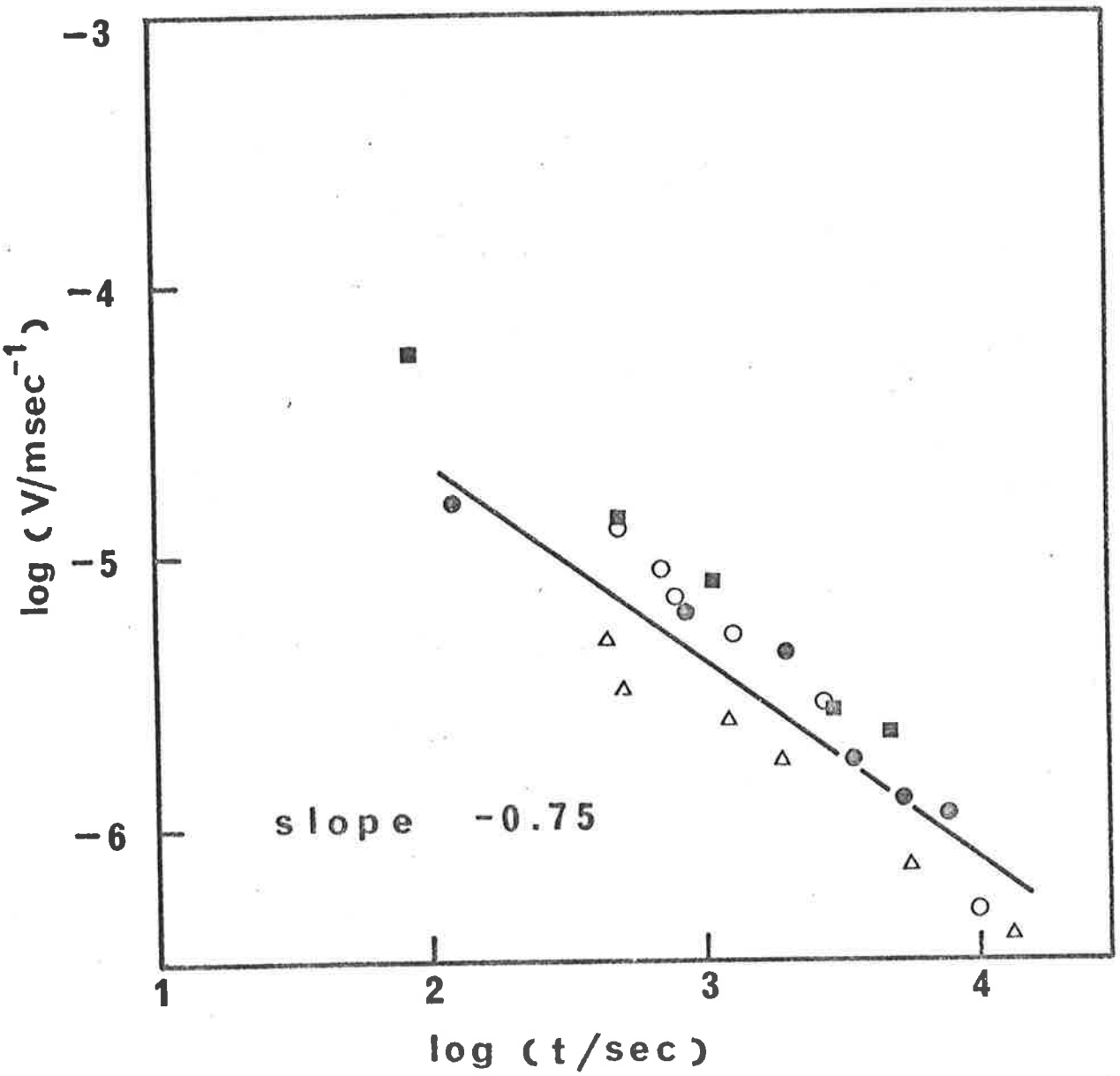

Fig.5.52a Sample HMW. Symbol represents data at various K_i.

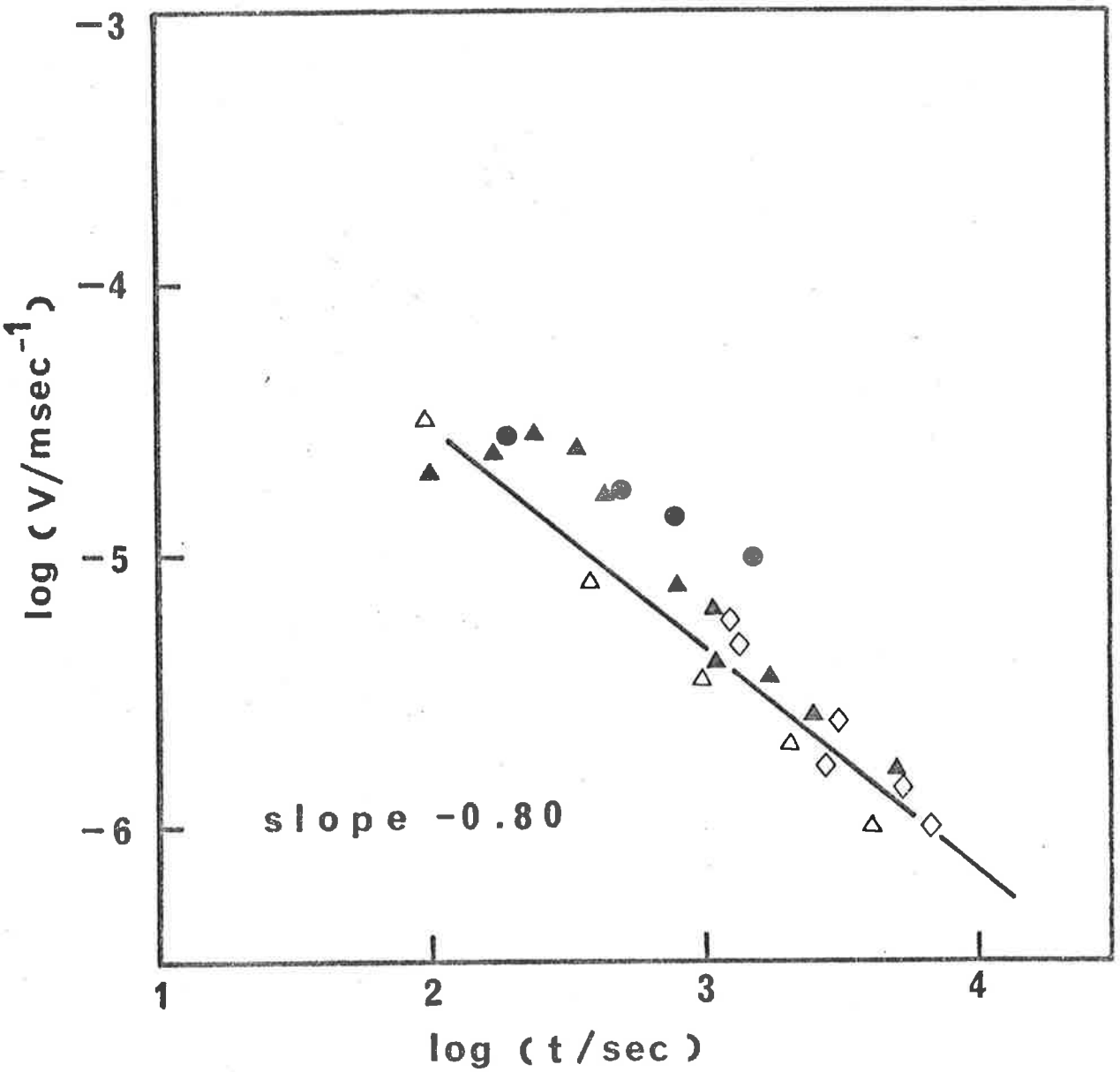

Fig.5.52b Sample MMW. Symbol represents data at various K_i.

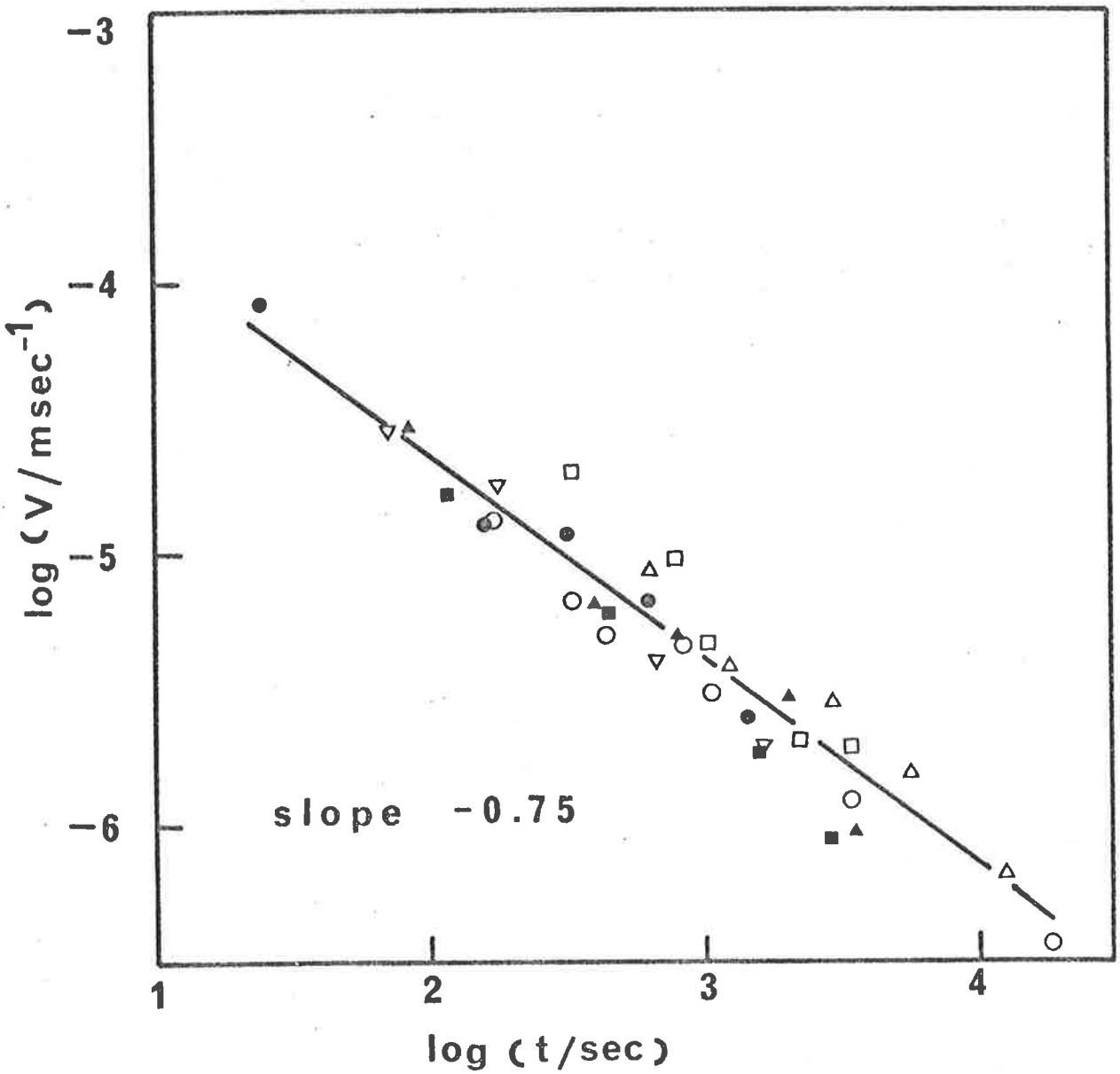

Fig.5.52c Narrow MWD PMMA. M_w = 71,000 (●), M_w = 84,000 (▽), M_w = 97,000 (▲), M_w = 120,000 (■), M_w = 380,000 (□), M_w = 450,000 (○) and M_w = 550,000 (△).

Taking the slope for log v vs. log t straight line as-0.8, the time factor (2m-2q-1) becomes

$$2m-2q-1 = -0.8 \qquad (5.127)$$

then the values of m and k can be estimated. For HMW, for example, q = 0.08 (Fig.5.46) and n = 0.1 (17), m and k can be estimated from Eqs.5.122 and 5.127 to be

$$m = 0.18$$

and

$$k = 0.12$$

Similarly, for MMW (Fig.5.46) q = 0.14, we obtain

$$m = 0.24$$

and

$$k = 0.06$$

These values are quite reasonable in terms of MW dependence. The larger m value and the smaller k value in lower MW PMMA (sample MMA) reveals a more rapid relaxation of the stress due to plasticization and a reduced stretching ability of craze fibrils under stress. It is also noted that the slope of log Δ vs. log t (Fig.5.51) under relaxation controlled mechanism (longer times region) is of the order of 0.25. From Eqs.5.119 and 5.124, the craze length, , and time are related by

$$\Delta \propto t^{2m-2q} \qquad (5.128)$$

Substituting the calculated values of m and q into (2m-2q), the calculated value of (2m-2q) are found to be 0.2 and this is in good agreement with the experimental value 0.25 (Fig.5.51).

Moreover, the slope of log K_c vs. log v straight line can be related to time-dependent factors by

$$\frac{d \log K_c}{d \log v} = \frac{d \log K_c}{d \log t} \Big/ \frac{d \log v}{d \log t} \qquad (5.129)$$

where d log K_c/d log t = -q (from Eq.5.119) and d log v/d log t = (2m -2q-1) (from Eq.5.126). Hence,

$$\frac{d \log K_c}{d \log v} = \frac{q}{2m-2q-1} \qquad (5.130)$$

Using values of q and m obtained previously, the value of d log K_c/d log v is estimated to be 0.10 for HMW (cf. experimental value of 0.12) and 0.17 for MMW (cf. experimental value of 0.16).

Rewriting Eq.5.125 in logarithmic form, we obtain

$$\log K_c = \tfrac{1}{2} \log(v\, t^{1-2m}) + \tfrac{1}{2} \log\left(\frac{8}{\pi} \frac{\sigma_o^2}{2m(1-m^2)\ \xi}\right) \qquad (5.131)$$

The introduction of the correction factor, ξ, in Eq.5.123 is justified only when the experimental data has a linear relationship in log K_c vs. log(v t^{1-2m}) plot. Taking m = 0.20 for high MW PMMA and m = 0.25 medium MW (calculated values of m were 0.18 and 0.24 for HMW and MMW, respectively), plots of log K_c vs. log(v t^{1-2m}) for samples HMW, MMW AND MH* show a linear relationship with a straight line of the slope of 0.5 although there is considerable scatter of data (Figs.5.53a,b,c).

The correction factor was found from the intersection to be $\xi \simeq 20$ using σ_o = 65 MN m^{-2}. Thus, the craze length derived from LEFM can be modified as a first approximation for the long craze growth as

$$\Delta = 20 \frac{\pi}{8} \frac{K_c^2}{\sigma_c} = \frac{5\pi}{2} \frac{K_c^2}{\sigma_c^2} \qquad (5.132)$$

Admittedly, the calculation of Δ for a long craze requires a rigorous theoretical treatment but the introduction of the correction factor, ξ, is a convenient way of showing the deviation from the craze length of a short craze.

* In methanol, fracture behaviour of MH is similar to MMW (Regime II)

Fig.5.53 Plot of fracture toughness vs. craze velocity in terms of log K_c vs. log (vt^{-2m}). Fig.5.53a: sample HMW (m = 0.2). Fig.5.53b: sample MMW (m = 0.25). Fig.5.53c: sample MH (m = 0.25).

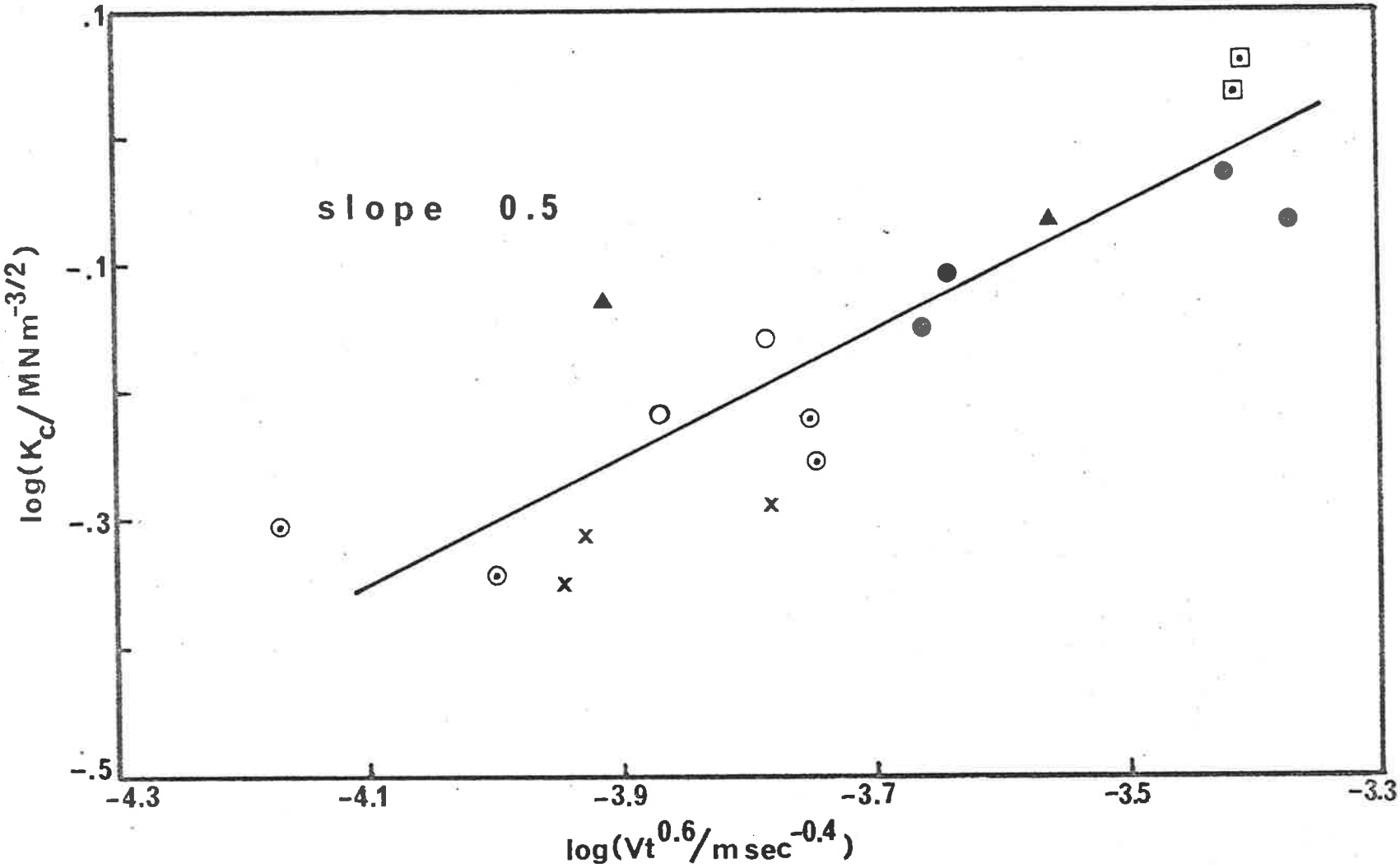

Fig.5.53a

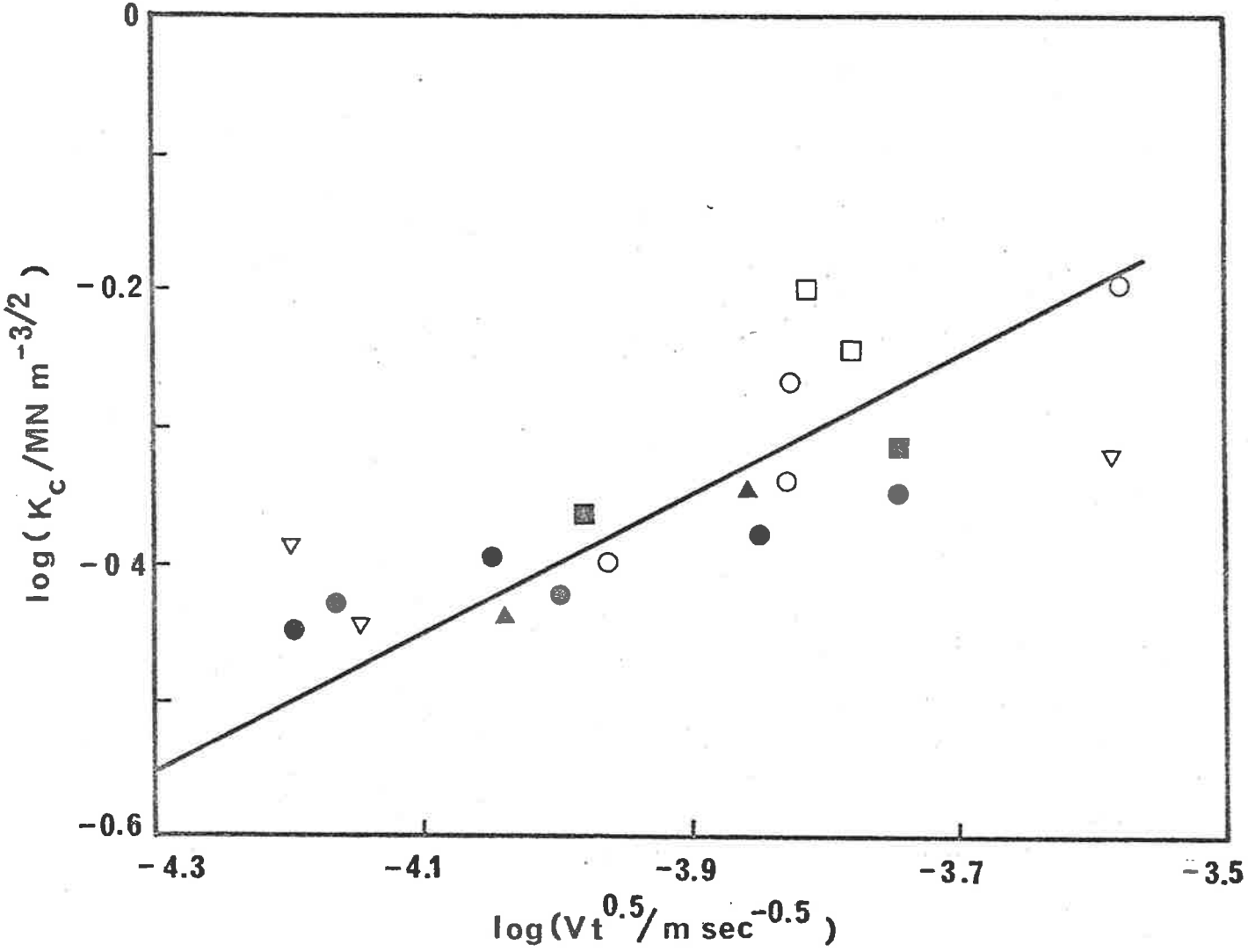

Fig.5.53b

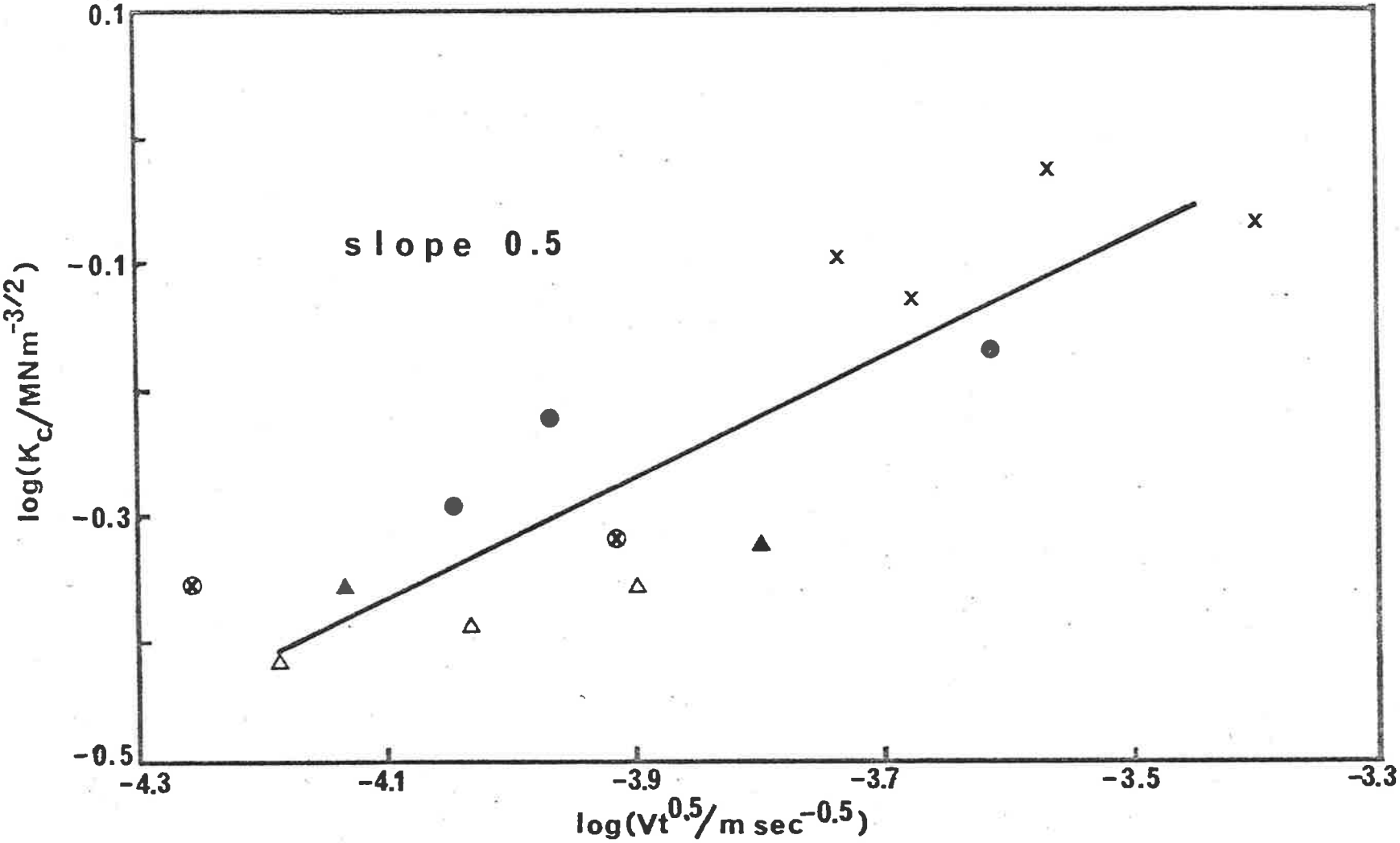
slope 0.5
0.1
-0.1
-0.3
-0.5
-4.3
-4.1
-3.9
-3.7
-3.5
-3.3
log(K_c/MNm^-3/2)
log(Vt^0.5/m sec^-0.5)

Fig.5.53c

5.4.9 Conclusions

The fracture mechanism of PMMA has been studied in relation to the MW, MWD and temperature in methanol and the following conclusions can be drawn.

(1) At room temperature (T=20°C), the log K_c vs. log v diagrams describing the fracture toughness of PMMA in a wide range of MW naturally divide into three distinct regimes: Regime I, Transition Regime and Regime II. Regime I is mature craze regime of PMMA having MW larger than the critical MW, M_c. Transition Regime is a weak craze regime of premature craze development. Regime II is a crack predominant regime of PMMA having MW smaller than M_c.

(2) A relationship was established between the stress relaxation curves of methanol equilibrated PMMA and the fracture behaviour in methanol expressed by the log K_c vs. log v diagram. This relationship suggests that entanglement density plays a crucial role in determining whether the breakdown mechanism occurs via rapid crack propagation or slow craze growth. Craze formation promoted by high entanglement density enhances the ability to absorb energy, i.e. high fracture toughness.

(3) The fracture behaviour of medium range MW is sensitive to temperature. At low temperature (T=0°C), the polymer shows a strong craze of slow craze development. At high temperature (T=40°C), the polymer shows rapid crack propagation. This fact can also be understood by the reduction of entanglement density as the temperature is increased and more solvent is absorbed.

(4) The crack predominant Regime II was satisfactorily treated by Zhurkov's and fracture mechanics (LEFM) approaches. The calculated results of the activation energy of the cracking process established that the crack mechanism is governed by a viscous flow process where the slippage of chain molecules over each other results in the secondary bond breakage.

(5) From the LEFM treatment, the COD, u_c and the craze length, Δ, of the cracking in methanol (Regime II) show a dependence on the SIF, K_c, and temperature. The craze length at the crack tip increases with K_c and temperature. The diffusion coefficient, D, also shows the same dependence on K_c and temperature, i.e. D increases with K_c and temperature. This coincidence suggests that the crack mechanism is controlled by diffusional behaviour of methanol at the crack tip and the enhancement of D by K_c and/or temperature gives rise to a larger plasticized craze zone.

(6) In contrast to crack predominant regime (Regime II), craze growth in Regime I shows a dependence on the initial SIF, K_i, in the log K_c vs. log vi diagrams. At the same K_i, the strong craze (Regime I) is characterized by a slower initial velocity and a smaller slope in log K_c vs. log v straight line than those of the weak craze (Transition Regime).

(7) The craze growth of Regime I and Transition Regime obeys Williams and Marshall's theory of flow controlled mechanism at shorter times (initiation step) and relaxation controlled mechanism at longer times (propagation step).

(8) A model for the craze growth was proposed and has proved that $K_c^2 \simeq \sigma_c u_c E$ for long craze growth, where K_c is calculated from geometrical analysis ($K_c = A_g P$). Equation of short craze length ($\Delta = \frac{\pi}{8} \frac{K_c^2}{\sigma_c}$) was modified for long craze length by introducing the correction factor ξ ($\Delta = \xi \frac{\pi}{8} \frac{K_c^2}{\sigma_c}$).

(9) A higher SIF, K_c, in methanol is required than in air at $v > 10^{-5}$ m sec^{-1}. This is due to the fact that in methanol craze fibrils produce a much larger COD, u_c, than the u_c in air ($K_c^2 \simeq \sigma_c u_c E$).

(10) Primordial craze thickness of a mature (strong) craze in Regime I (~1 μm) is larger than that of a premature (weak) craze of Transition Regime (~50 nm).

CHAPTER 6

EFFECT OF STEREOREGULARITY ON THE PHYSICAL PROPERTIES AND FRACTURE TOUGHNESS OF ISO- AND SYNDIO-TACTIC POLY(METHYLMETHACRYLATE) BLENDS

6.1 Introduction

Progress in organic synthesis and constant development of catalysts for polymerization has encouraged the synthesis of a considerable number of new polymers during the past two decades. Nevertheless, due to thermodynamic constraints very few polymers can form homogeneous mixtures. Miscibility rarely occurs in mixtures of polymers or even mixtures of polymers of the same chemical structure but different tacticity. Unlike metal alloys, the study of polymer "alloys" or polymer blends is still at an early stage of investigation. Although the numbers of blends are limited, from the technical point of view, new and useful polymer blends can provide novel properties to fulfill the demand of ever increasing technology. From the fundamental point of view, the relationship between molecular properties of the polymer blends and their bulk properties introduces a wide range of interesting and challenging research problems. Blends of iso- and syndio-tactic PMMA (i/s - PMMA) are not an exception.

Some of the earliest experiments dealing with the interaction between isotactic PMMA (i - PMMA) and syndiotactic PMMA (s - PMMA) were performed by Fox et al. (140). They reported that gelation occurred by mixing solutions of i-PMMA and s-PMMA; similar results were reported later by Fleischer and co-workers (141-142). This gelation process can be explained by the formation of stereocomplexes of i/s-PMMA. Liquori et al. (143) determined the structure of the gel by X-ray diffraction and concluded that the gel

consisted of stereocomplex crystallites formed in the ratio of one i-PMMA molecule to two s-PMMA molecules (i/s = 1/2 ratio). From the X-ray diffractogram, it was shown that the crystal structure of the stereocomplex was quite distinct from that of the individual constituents. The authors proposed a model in which extended s-PMMA chains fit cross-ways into the helical groove of the i-PMMA molecules. Although the occurrence of the gelation was discovered and the gel structure determined, the miscibility of i-PMMA and s-PMMA had not been investigated until Feitsma et al. (144) reported a broad single T_g implying the miscibility of the two polymers.

The miscibility of i-PMMA and s-PMMA and their ability to co-crystallize under suitable conditions suggests two interesting questions: (a) Does the addition of i-PMMA to s-PMMA affect the fracture toughness? (b) What are the physical properties of the i/s-PMMA blend such as the glass transition temperature, T_g, and the melting point, T_m, of the stereocomplexes? Investigation of the effect of stereoregularity on bulk properties of PMMA in the present work will be performed to answer these questions. The following paragraph will outline the development in the understanding of i/s-PMMA blends.

There have been a large number of reports since the pioneering study of the structure of i/s-PMMA blend of Liquori et al. (143). However, the studies were confined to the determination of the crystal structure of the stereocomplex and the effect of solvent on stereocomplex formation. In fact, a wide range of techniques such as viscometry, turbidimetry and high resolution NMR have been used to attempt to determine the controversial ratio of i-PMMA and s-PMMA in the stereocomplex structure. The ratio 1/2 (i/s) was observed by most workers (143,145-149), but other ratios of 1/1, 1/1.5 or even 2/1 have also been detected (150-153). Studies on the effect

of solvent on the stereocomplex co-crystallization were mostly contributed by Challa and co-workers (154-155). They classified three types of solvents: Type A, strongly complexing solvent; Type B, weakly complexing solvent and Type C, non-complexing solvent. Pyrlik et al. (156), on the other hand, have reported stereocomplex formation occurs even in very concentrated solutions of i-PMMA and s-PMMA in *o*-xylene. Feitsma et al. (144) have taken a further step and formed the stereocomplex in the solid state by annealing the blend at 140°C. Recently, Vorenkamp et al. (157) determined the ratio i/s to be 1/2 and suggested that this value is the predominant ratio regardless of the media (solid state or solution) and the history of crystallization process.

The crystallization processes described above, however, were confined to solution crystallization and thermal induced crystallization (TINC). Another method of achieving crystallinity is by solvent-induced crystallization (SINC). Generally, SINC is considered as a process in which solid amorphous polymer is crystallized by immersion in a liquid. The diffusion of liquid into the amorphous polymers enhances the movement of chain segments and allows a suitable juxtaposition of the segments for crystallization to occur. Although this method has been known for some time (158-159) and a number of studies have dealt with several aspects of SINC in poly(ethylene terephthalate) (160-162) and polycarbonate (163-164), little work has been done on solvent induced co-crystallization and especially the SINC of i/s-PMMA blend.

In Chapter 5, the study of the dependence of fracture toughness on MW of syndiotactic-like PMMA in air and in methanol has improved the basic understanding of the fracture mechanism. Now, the co-crystallization between i-PMMA and s-PMMA suggests a new approach to modify s-PMMA by blending with i-PMMA. The co-crystallization of i-PMMA and s-PMMA may give improved physical properties in

particular, an improvement in fracture toughness compared to that of the single components.

This Chapter is mainly intended to focus attention on the TINC, SINC and fracture toughness of i/s-PMMA blend of various i/s weight ratios of i-PMMA and s-PMMA in the presence of methanol. The melting point of crystallites, T_m, in the two crystallization processes (TINC and SINC) and the glass transition temperature, T_g, of the blends obtained from DSC and wide angle X-ray are discussed. It will be shown that the fracture toughness of i/s-PMMA blends in methanol can be understood on the basis of the co-crystallization of the blends. To distinguish the co-crystallization of i/s-PMMA from normal SINC (SINC of individual polymers), and to further understand the crystallization effect on the fracture toughness, the results of SINC and the fracture toughness of typical homogeneous blends of PMMA and poly(vinylidenefluoride) (PVF_2) are compared with those of i/s-PMMA blends.

6.2 Materials and Experiments

6.2.1 Materials

The component polymers used for the blends are syndiotactic-like narrow MWD PMMA synthesized by an anionic mechanism at low temperatures, isotactic or stereoblock PMMA synthesized by a pseudo-anionic mechanism using organo-magnesium initiators (Chapter 3) and commercial atactic PMMA prepared by a radical mechanism at high temperature. The stereoregularity of these components are listed in Table 3.5.

The blends of i-PMMA and s-PMMA were prepared by dissolving two samples at the required weight ratio in dichloromethane. The mixture was stirred at room temperature for at least 3 hours and subsequently precipitated in petroleum ether. The blend in powder form was dried overnight in a vacuum oven at 50°C. The specimen sheets for fracture toughness or dynamic mechanical

measurements were produced by pressing at 150°C in a hydraulic moulder using the procedure described previously. Compositions of the blends are listed in Table 6.1

TABLE 6.1: Compositions of i/s-PMMA blends*

s-PMMA	(syndiotactic triads)		i-PMMA	(isotactic triads)
MMW	(55%)	+	I.74	(74%)
LMW	(55%)	+	I.100	(100%)
A4a	(64%)	+	I.100	(100%)
S.73 h	(73%)	+	I.100	(100%)
S.73 h	(73%)	+	I.74	(74%)
S.73 ℓ	(73%)	+	I.74	(74%)

It was not appropriate to use every blend in each of the following investigations and therefore for the purposes of clarification the blends used in each section and their pertinent characteristics will be listed at the beginning of each discussion. The s-PMMA components in the above table are syndiotactic-like rather than highly syndiotactic. However, to distinguish from i-PMMA component, they are simply named s-PMMA.

6.2.2 Experimental

Crystallization was induced by two method thermal induced crystallization (TINC) and solvent induced crystallization (SINC).

Thermal induced crystallization involved heating sheet specimens of 0.1mm thickness at 140 ± 2°C in a hydraulic moulder press for 24 hours.

Solvent induced crystallization involved immersing sheet specimens in methanol at a crystallization temperature of T_{cr} = 20°C or 40°C until the sample reached a constant weight. The absorbed

* See Table 3.4 for details of MW and MWD and Table 3.6 for tacticity.

methanol was removed by pumping at 40°C in a vacuum oven for 7 days. However, infrared spectra of "dried" crystallized specimens indicated the presence of residual methanol. As was discovered later, the residual methanol produced endotherm peaks in DSC thermodiagrams. To avoid this problem, a precipitated powder form of the blend was used. The porous nature of the precipitated powder allowed absorbed methanol to be removed more easily by the above drying procedure. To allow the endotherm to be positively identified as the melting point of crystallites, the precipitated powder form of amorphous MMW (syndiotactic component in blends) was immersed in methanol in the same conditions as the blend samples. After immersion, MMW was dried and examined by DSC. This sample was amorphous and because the DSC thermodiagram did not reveal the presence of peaks, it could be concluded that the sample was free of methanol.

The glass transition temperature, T_g, and melting temperature, T_m, were measured by a Perkin-Elmer DSC II at a heating rate of 20°C per minute. The position of the maximum of the melting endotherm was taken as T_m. The presence of crystallites was also detected by wide angle X-ray scattering (WAXS) using Fe-filtered cobalt radiation.

Dynamic mechanical measurements were performed on 3.1 x 0.9 x 0.1 cm bars using a torsion pendulum at a frequency of ~1 Hz over a temperature range 20 to 140°C. The storage shear modulus G', the loss shear modulus, G", and loss tangent tan δ are calculated by the equations shown in Appendix 5.

6.3 Results and Discussion

6.3.1 Thermal Induced Crystallization (TINC)

The effect of MW and tacticity of s-PMMA on crystallinity of TINC in i/s-PMMA blend was investigated with the following blends

(1) MMW + I.74

(2) S.73 h + I.74

(3) S.73 ℓ + I.74

The molecular properties (MW, MWD and tacticity) were listed in detail in Chapter 3, but for clarity, these properties are briefly repeated in the following table.

Sample	MW	MWD or number of GPC peaks	Tacticity
MMW	220,000	2.1	55% syndio
S.73 h	2,700,000 200,000	bimodal	73% syndio
S.73 ℓ	30,000	approx. 2.5	73% syndio
I.74	2,000,000 110,000 35,000	trimodal	74% iso

The weight ratio of i-PMMA and s-PMMA was deliberately chosen to be 50/50 so that crystallization, if it did occur, could take place in a reasonable annealing time (144,157).

The effect of tacticity of s-PMMA components on crystallization is shown by X-ray diffractograms (Figs.6.1-6.3). In Figs. 6.1 and 6.2, the diffractograms show the development of crystallinity in blends (S.73 h + I.74) and (S.73 ℓ + I.74), whereas the diffractogram of blend (MMW + I.74) (Fig.6.3) remains a broad peak typical of an amorphous polymer after 24 hours annealing. The existence of a crystalline phase in the annealed blends (S.73 h + I.74) and (S.73 ℓ + I.74) is also supported by the presence of a melting endotherm in the DSC thermograms (Fig.6.4) at the same melting point T_m = 185°C as reported by Feistma et al. (144). It is of interest to note that while the melting temperature (T_m = 185°C) was not influenced by the MW of the s-PMMA component in blends (S.73 h + I.74) and (S.73 ℓ + I.74), the peak area of the melting

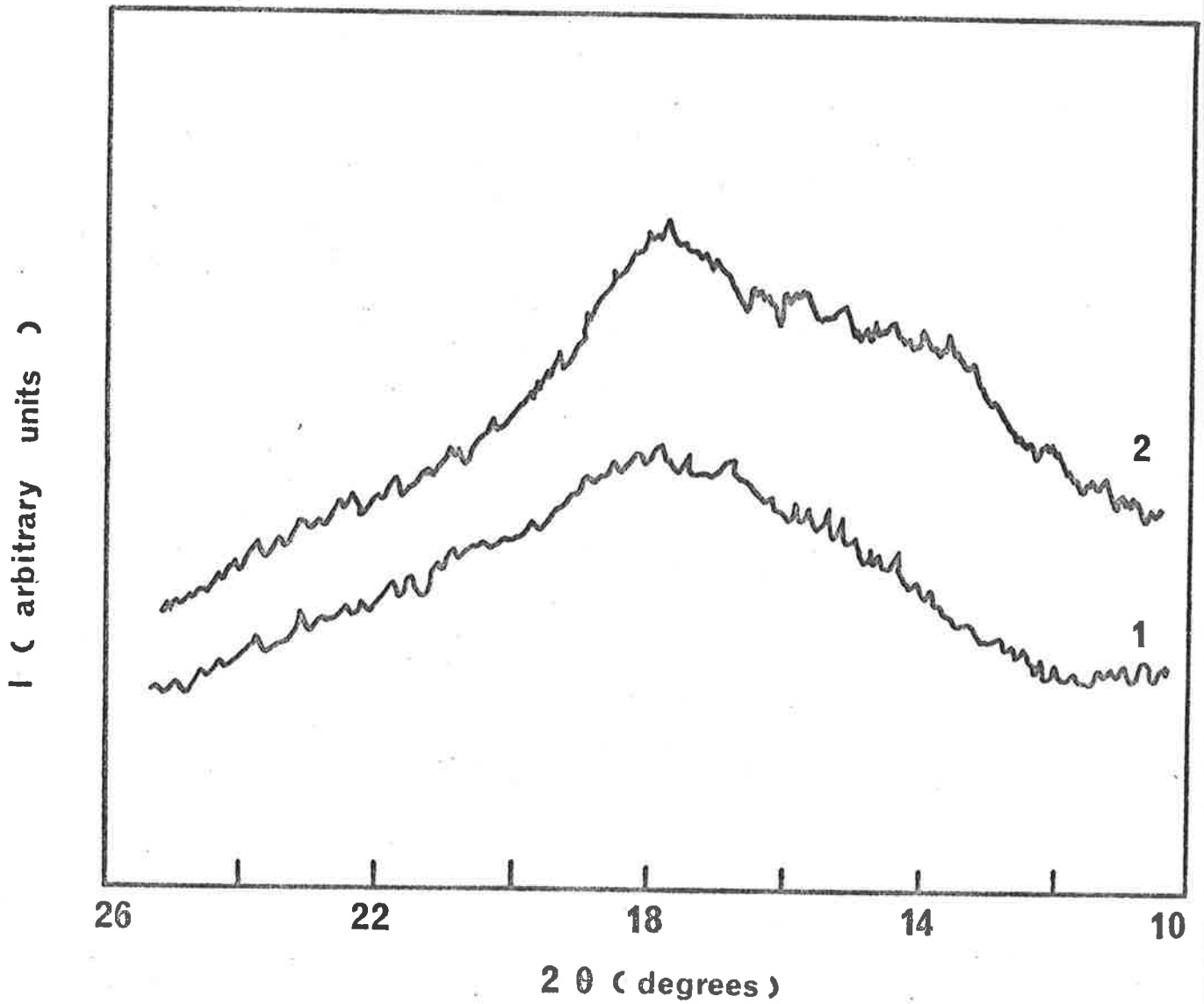

Fig.6.1 X-ray diffraction intensity, I, vs. diffraction angle 2θ. Development of crystallization by thermally induced crystallization at T_{cr} = 140°C in blend (S.73h + I.74) (i/s = 50/50), (1) zero hours, (2) 24 hours .

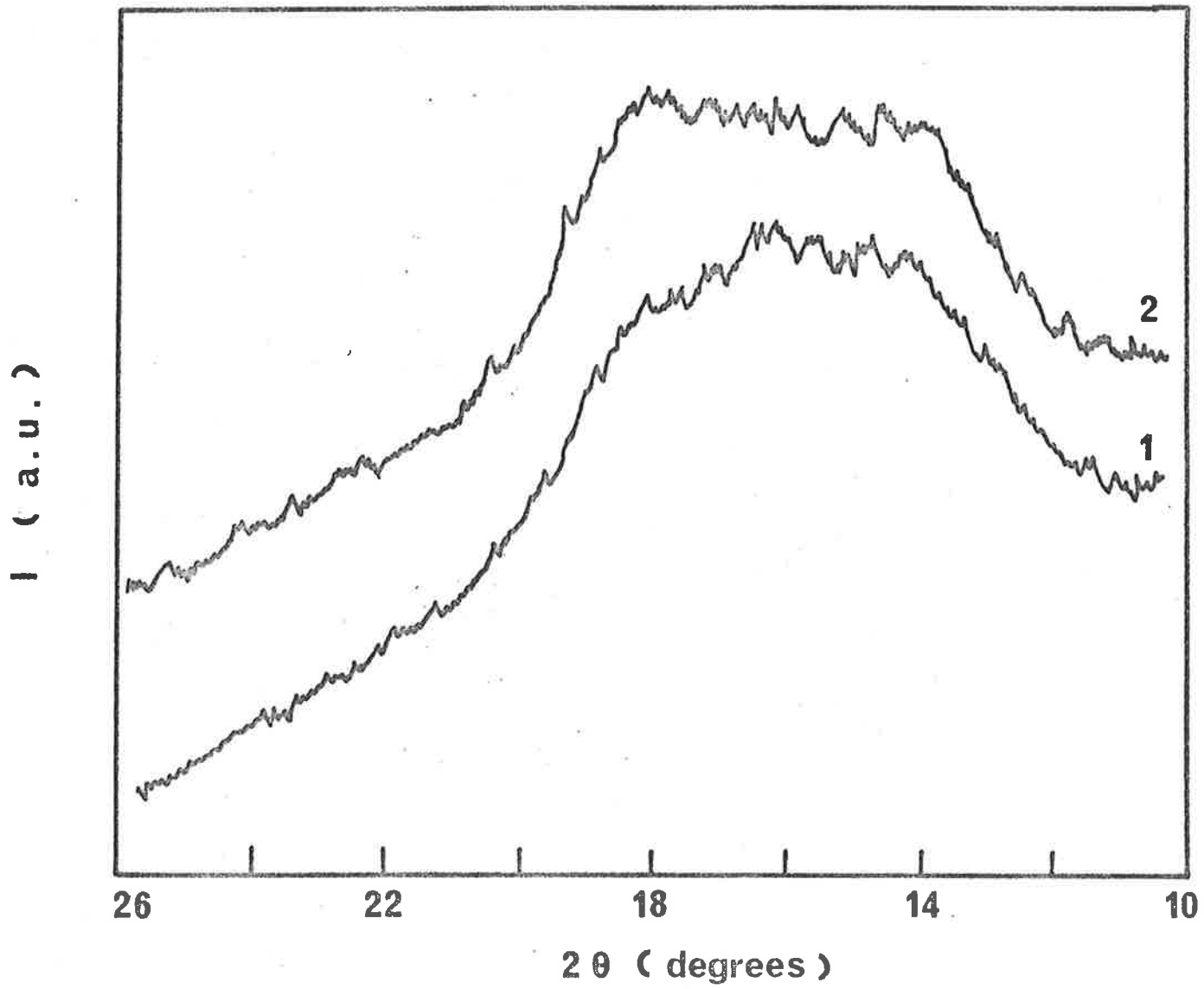

Fig.6.2 X-ray diffraction intensity, I, vs. diffraction angle 2θ. Development of crystallization by thermally induced crystallization at T_{cr}=140°C in blend (S.73ℓ + I.74)(i/s = 50/50), (1) 5 hours. (2) 24 hours.

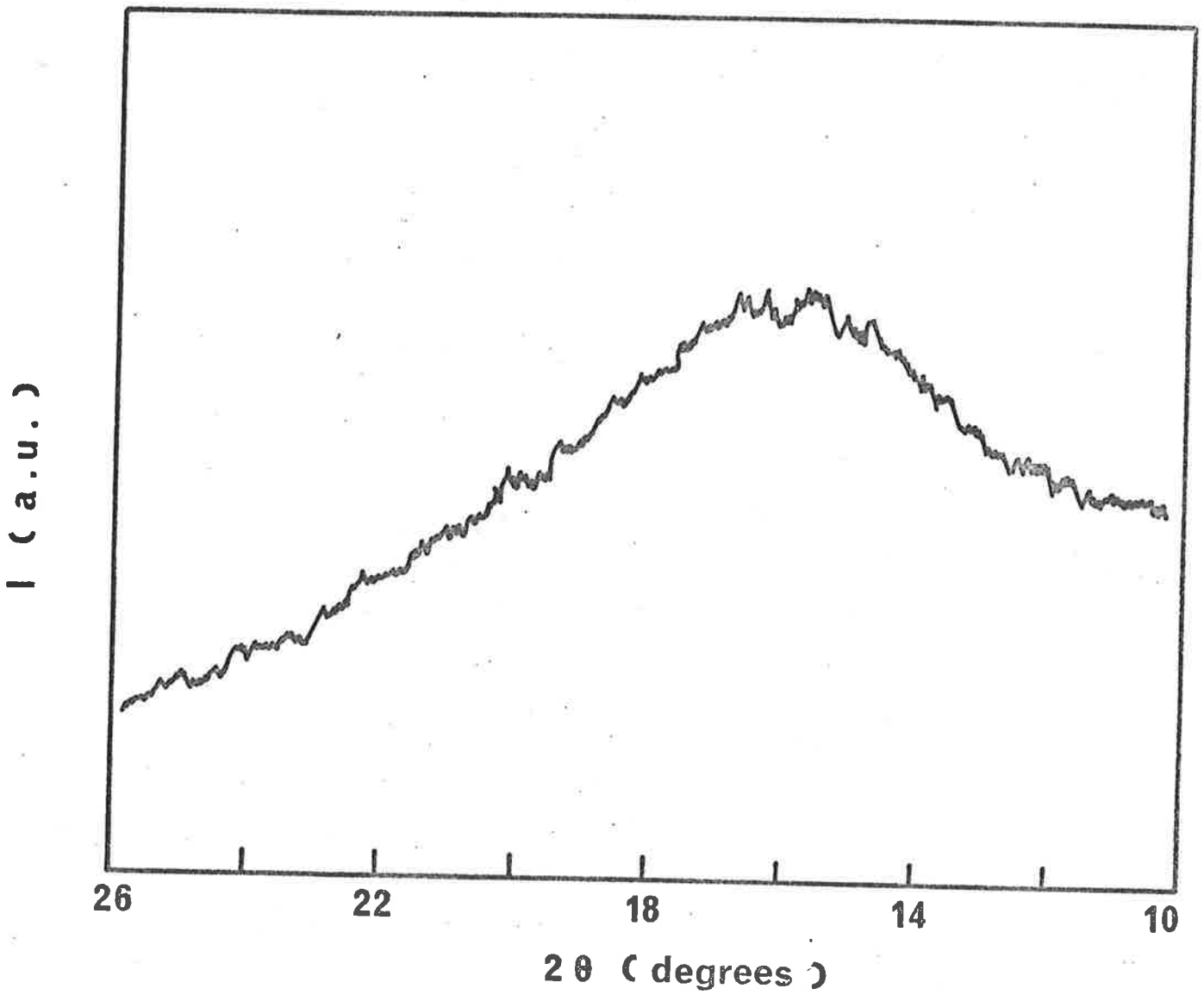

Fig.6.3 X-ray diffraction density, I, vs. diffraction angle 2θ. Blend (MMW + I.74) (i/s = 50/50) subjected to 24 hours annealing.

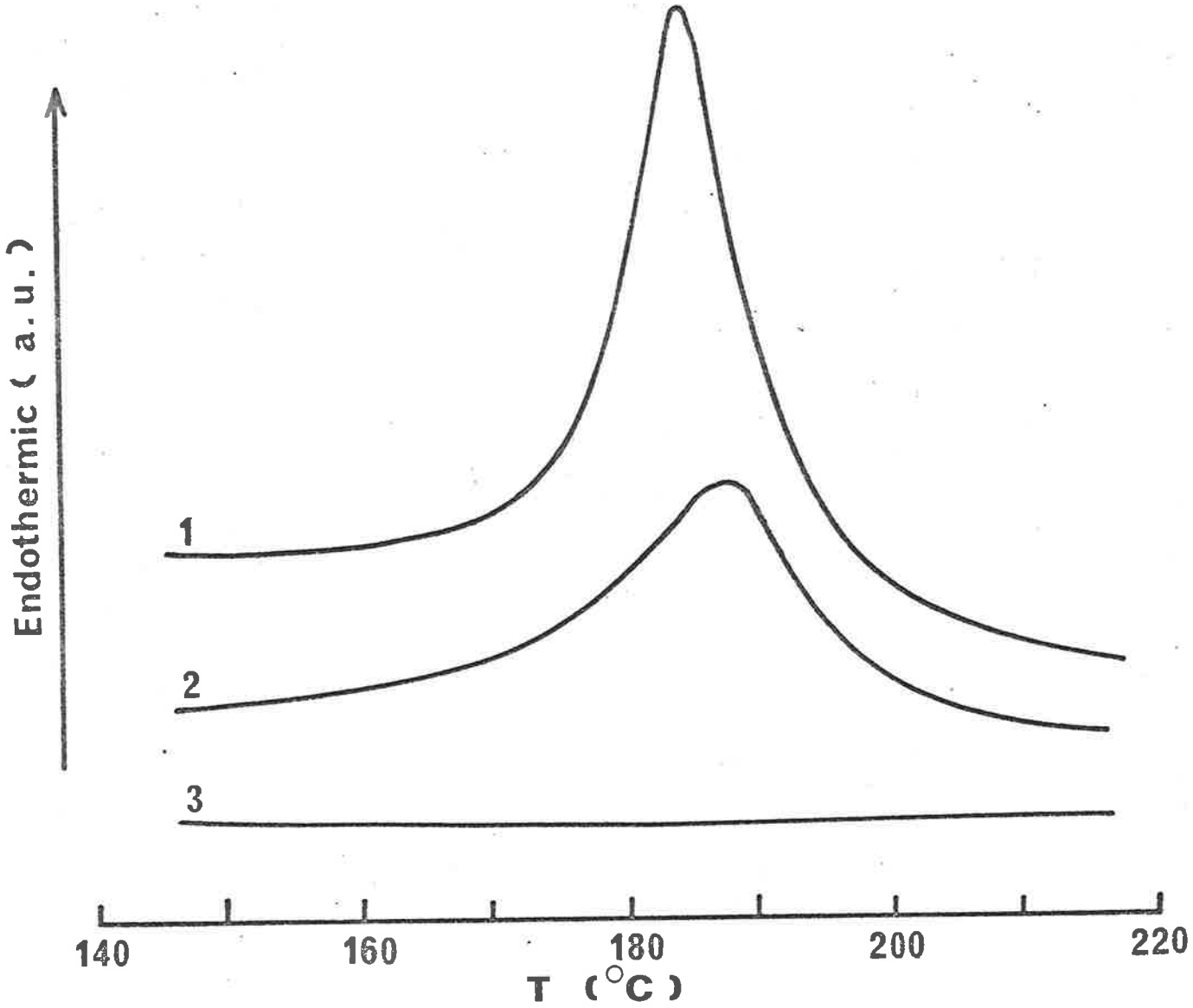

Fig.6.4 DSC thermodiagrams of i/s-PMMA blends (i/s = 50/50) subjected to 24 hours annealing at T_{cr} = 140°C. (1) Blend (S.73ℓ + I.74). (2) Blend (S.73h + I.74). (3) Blend (MMW + I.74).

endotherm of the latter is almost twice as large as that of the former.

The above observations clearly reveal the effect of tacticity and MW on the crystallization process. Firstly, the higher tacticity of the components resulted in less imperfection in the crystal structure of the stereocomplexes. Taking into account the work of Feistma et al. (144) on the TINC of the i/s-PMMA blends of high tacticity components (> 90% iso- and syndio-triads) where the crystallinity is indicated by peaks in the X-ray diffractograms, the imperfection, as shown by the breath of the crystalline peak, becomes higher for blends containing low tacticity components (Figs.6.1-6.2). Crystallization cannot be induced when the tacticity is less than a certain limit [e.g. blend (MMW + I.74)]. In this work, the limit was about 55% syndiotactic triads (MMW) and 74% isotactic triads. Secondly, the effect of MW on the percentage crystallinity, as shown by the area of the endotherm peaks of blends (S.73 h + I.74) and (S.73 ℓ + I.74) (Fig.6.4), suggests that the low MW component (S.73 ℓ) possesses a higher mobility so allowing a more rapid co-crystallization with i-PMMA. This suggestion, however, requires further investigation to ascertain the role of the MW in the kinetics of stereocomplex formation by TINC.

The mobility of molecular chains can also be enhanced by the diffusion of a liquid into the bulk material. The solvent effect on the stereocomplex formation of i/s-PMMA blends will be considered in the next Section.

6.3.2 Solvent Induced Crystallization (SINC)

The following blends were used for SINC

(1) MMW + I.74

(2) S.73 h + I.100*

(3) PMMA (sample MMW) + PVF_2**

* Sample I.100 (1) in Table 3.4 (Chapter 3).

** PVF_2 is a product of Kureha Chemical Ltd. and blend was produced by hot rolling at 200°C.

Sample	M_w	MWD or number of GPC peaks	Tacticity
MMW	220,000	2.1	55% syndio
S.73 h	2,700,000 200,000	bimodal	73% syndio
I.100*	3,500,000 400,000 100,000	trimodal	100% iso
I.74	2,000,000 110,000 35,000	trimodal	74% iso
PVF_2**	unknown	unknown	unknown

Methanol can induce crystallization in the amorphous blend (MMW + I.74) of low tacticity components. As noted in the previous Section, because of low syndiotacticity in the s-PMMA component (MMW), crystallization in this blend could not be induced thermally. This implies that the mobility of the chain segments is an important factor in the formation of crystallites by stereo-association. From Table 3.6 (Chapter 3), the ratio of the number-average length of syndiotactic block and that of isotactic block is $\bar{n}_r/\bar{n}_m$ = 7.08/1.25 = 5.66 for S.73 and 3.89/1.37 = 2.84 for MMW. Consequently, TINC requires a longer syndiotactic block than SINC for the association of i-PMMA and s-PMMA. The longer tactic block will compensate for the restriction caused by inter- and intra-molecular forces among polymer molecules during thermal crystallization.

Figs.6.5 and 6.6 show the X-ray diffractograms of a family of blends of various weight ratios of i-PMMA and s-PMMA of the blend (MMW + I.74) for T_{cr} = 20°C and 40°C. The diffractograms

* Sample I.100 (1) in Table 3.4 (Chapter 3).
** PVF_2 is a product of Kureha Chemical Ltd. and blend was produced by hot rolling at 200°C.

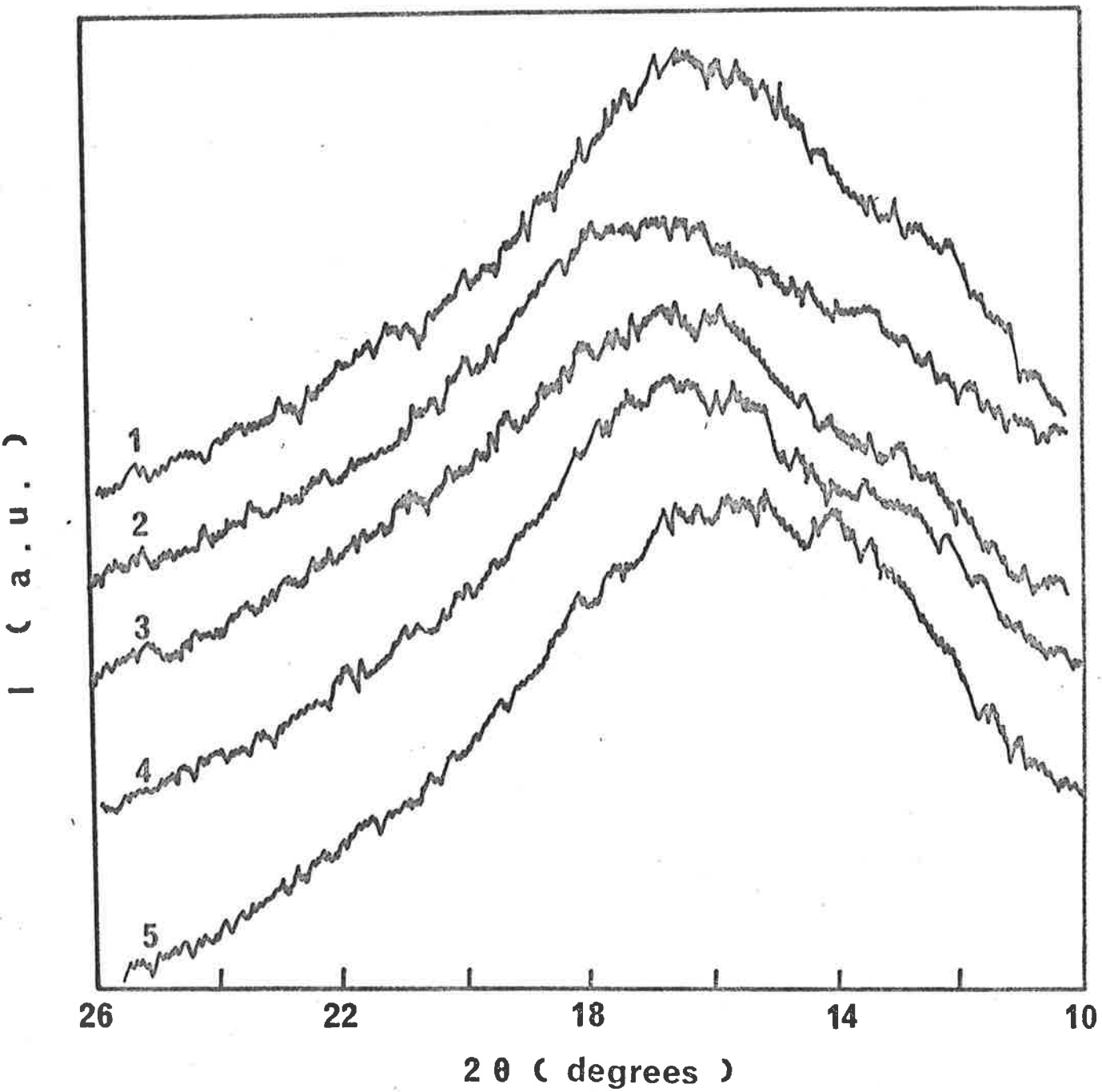

Fig.6.5 X-ray diffractodiagrams showing methanol induced crystallization for blend (MMW + I.74). (1) i/s = 50/50, (2) i/s = 40/60, (3) i/s = 30/70, (4) i/s = 20/80 and (5) i/s = 10/90.

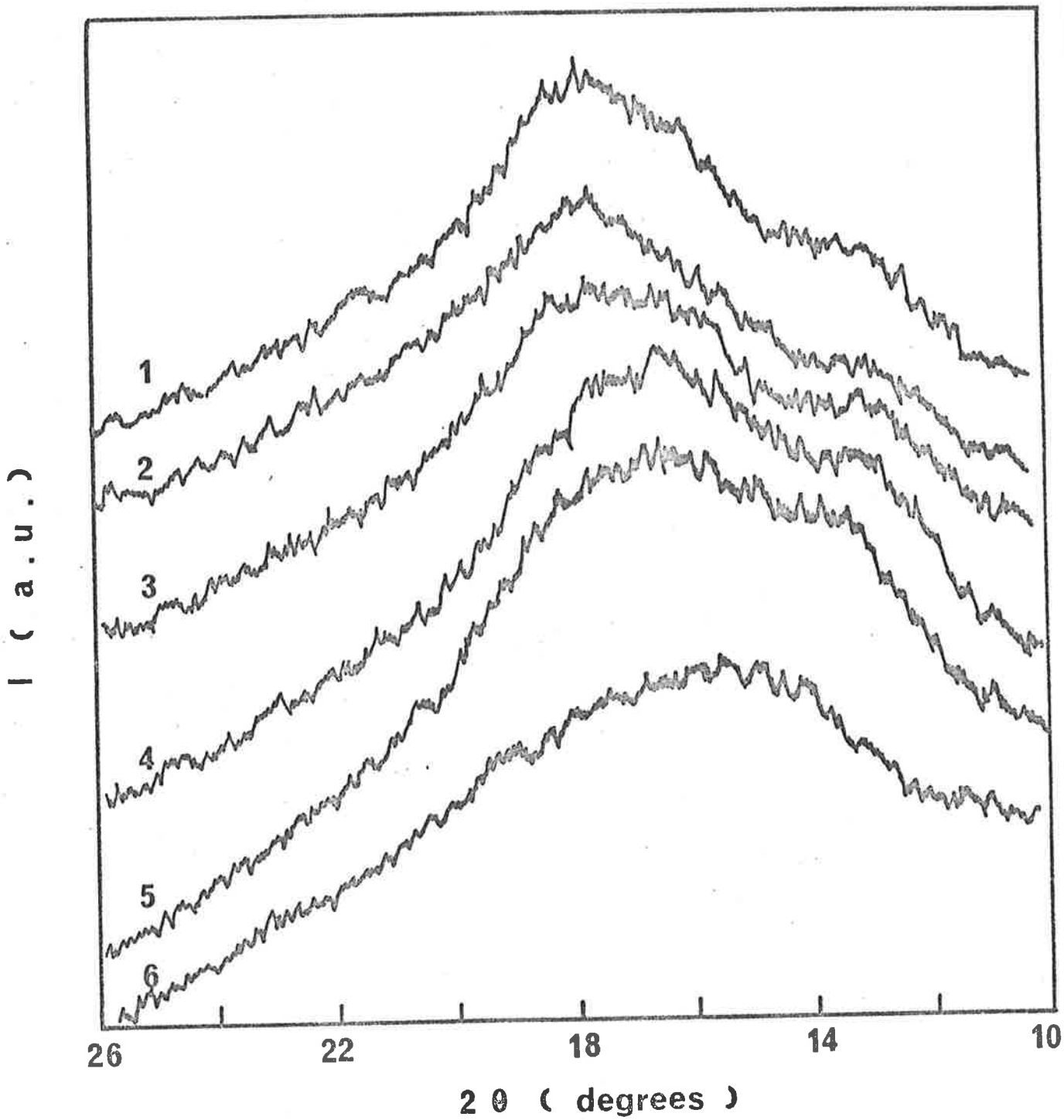

Fig.6.6 X-ray diffractograms showing methanol induced crystallization (T_{cr} = 40°C) for blend (MMW + I.74). (1) i/s = 50/50, (2) i/s = 40/60, (3) i/s = 30/70, (4) i/s = 20/80, (5) i/s = 10/90 and (6) i/s = 0/100 (MMW only) .

reveal the presence of two major crystalline peaks positioned at the same angle as those from TINC treatment (Fig.6.1). The crystallites induced by methanol were identified as crystalline stereocomplexes as the diffraction angles of the crystalline peaks (at 13° and 18°) are identical with that of crystallites induced by acetone (type A solvent)(Fig.6.7).

It is further noted that the location of the two major crystalline peaks are independent of the blend ratio and T_{cr}; also the crystalline peaks become more distinct at higher T_{cr} (T_{cr} = 40°C). A higher T_{cr} would mean a higher uptake of methanol thus giving a larger depression of T_g (Chapter 4). Therefore, the polymer molecules become more mobile encouraging the association of i-PMMA and s-PMMA.

For the blend of higher tacticity, e.g. blend (S.73 h + I.100), the diffractograms show sharper crystalline peaks at T_{cr} = 20°C and 40°C (Figs.6.8-6.9). The X-ray diffractogram for crystalline i-PMMA I.100 (induced by SINC in methanol at T_{cr} = 20°C) shows a different pattern from that of the i/s-PMMA crystalline stereocomplexes (Fig.6.10). Identical diffractograms for i/s-PMMA stereocomplexes and i-PMMA crystallites were obtained by Buter et al. (154) where i/s-PMMA stereocomplexes were crystallized from dimethylformamide (DMF) solution and i-PMMA was crystallized from heptanone solution.

The effect of solvent in SINC of stereocomplexes involves two factors; (a) the polarity of solvent and (b) the solvating power of the solvent where the solvent is known as a "good" or "poor" solvent for the polymer. Highly polar solvents classified by Challa's group (154-155) as Type A (i.e. strongly complexing solvents) promote the helical conformation of i-PMMA by the interaction between the polar ester group on the polymer chain and the polar solvent molecules. Such interaction encourages the forma-

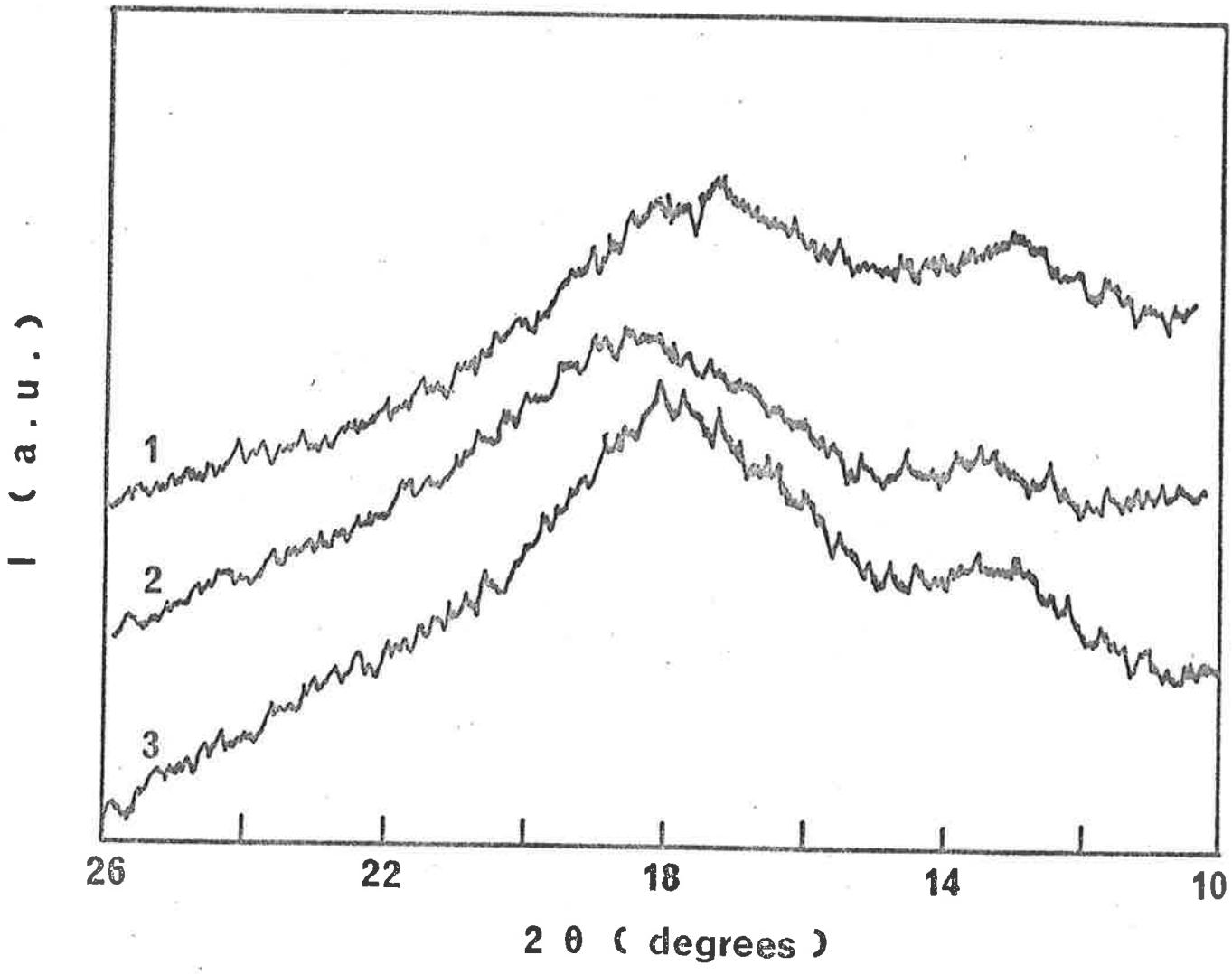

Fig.6.7 X-ray diffractograms showing acetone induced crystallization (T_{cr} = 20°C) for blend (MMW + I.74) (1) i/s = 50/50, (2) i/s = 40/60 and (3) i/s = 30/70.

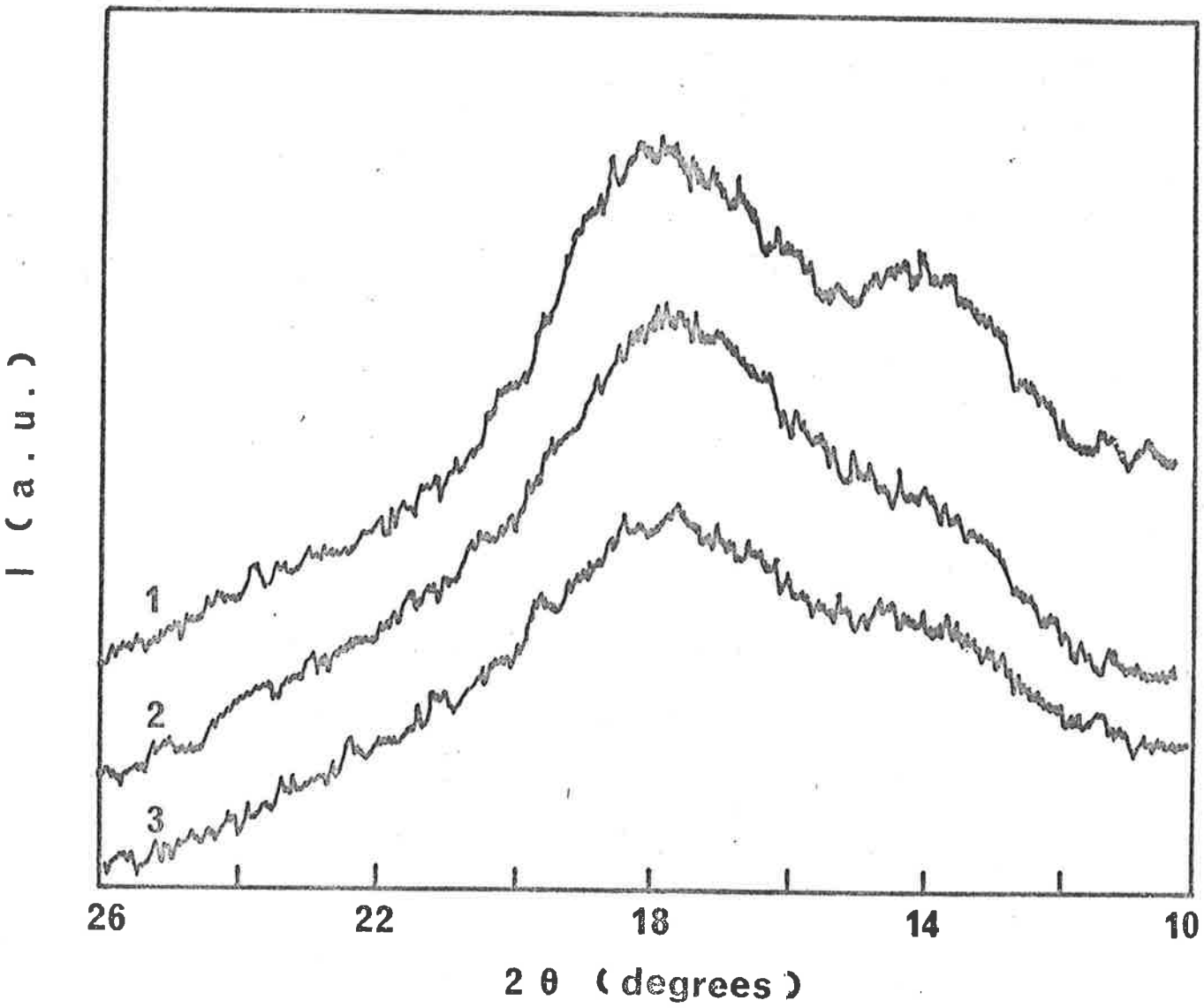

Fig.6.8 X-ray diffractograms showing methanol induced crystallization (T_{cr} = 20°C) for blend (S.74h + I.100). (1) i/s = 30/70, (2) i/s = 20/80 and (3) i/s = 10/90.

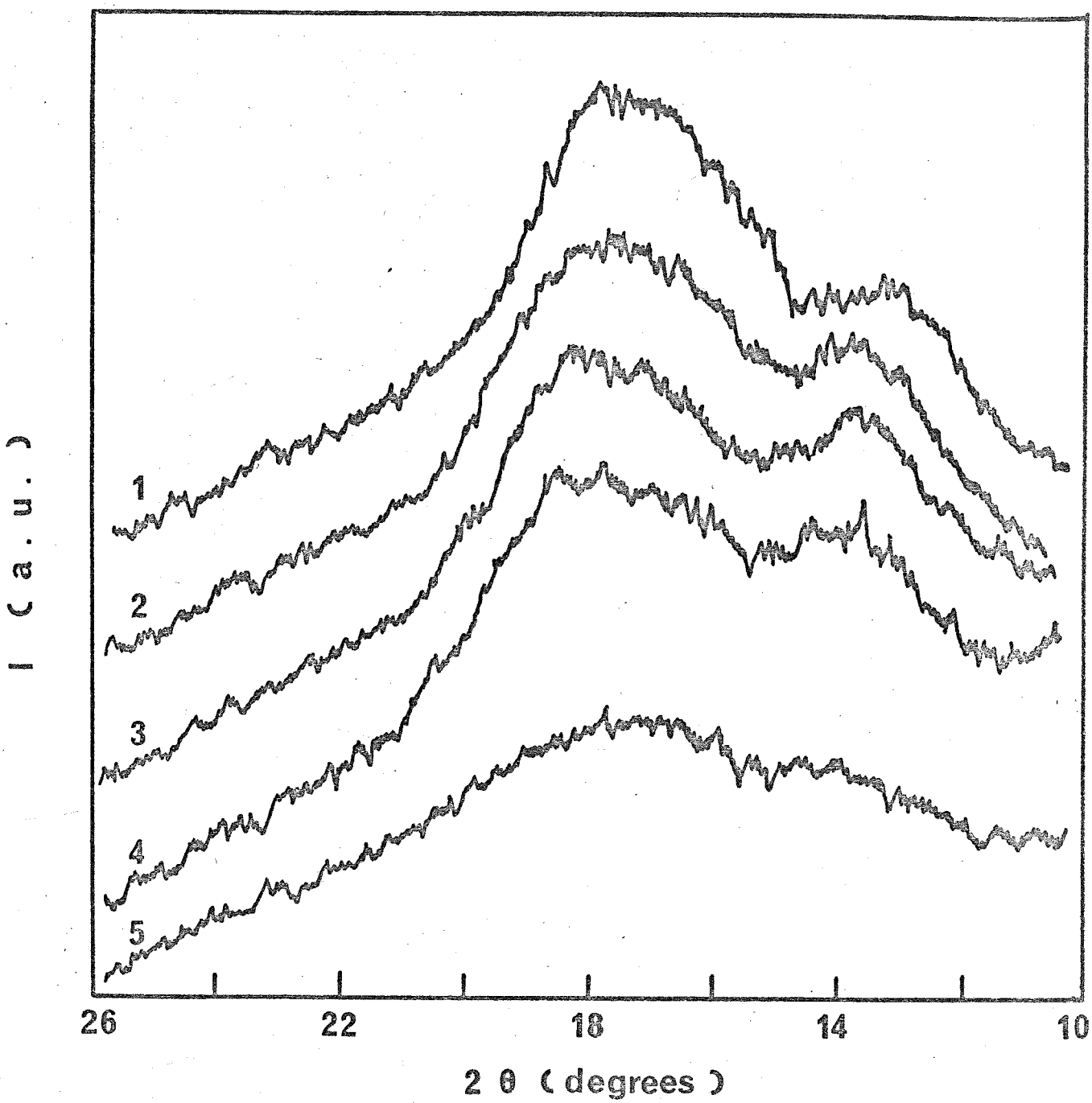

Fig.6.9 X-ray diffractograms showing methanol induced crystallization (T_{cr} = 40°C) for blend (S.74h + I.100). (1) i/s = 50/50, (2) i/s = 40/60, (3) i/s = 30/70 (4) i/s = 20/80 and (5) i/s = 10/90.

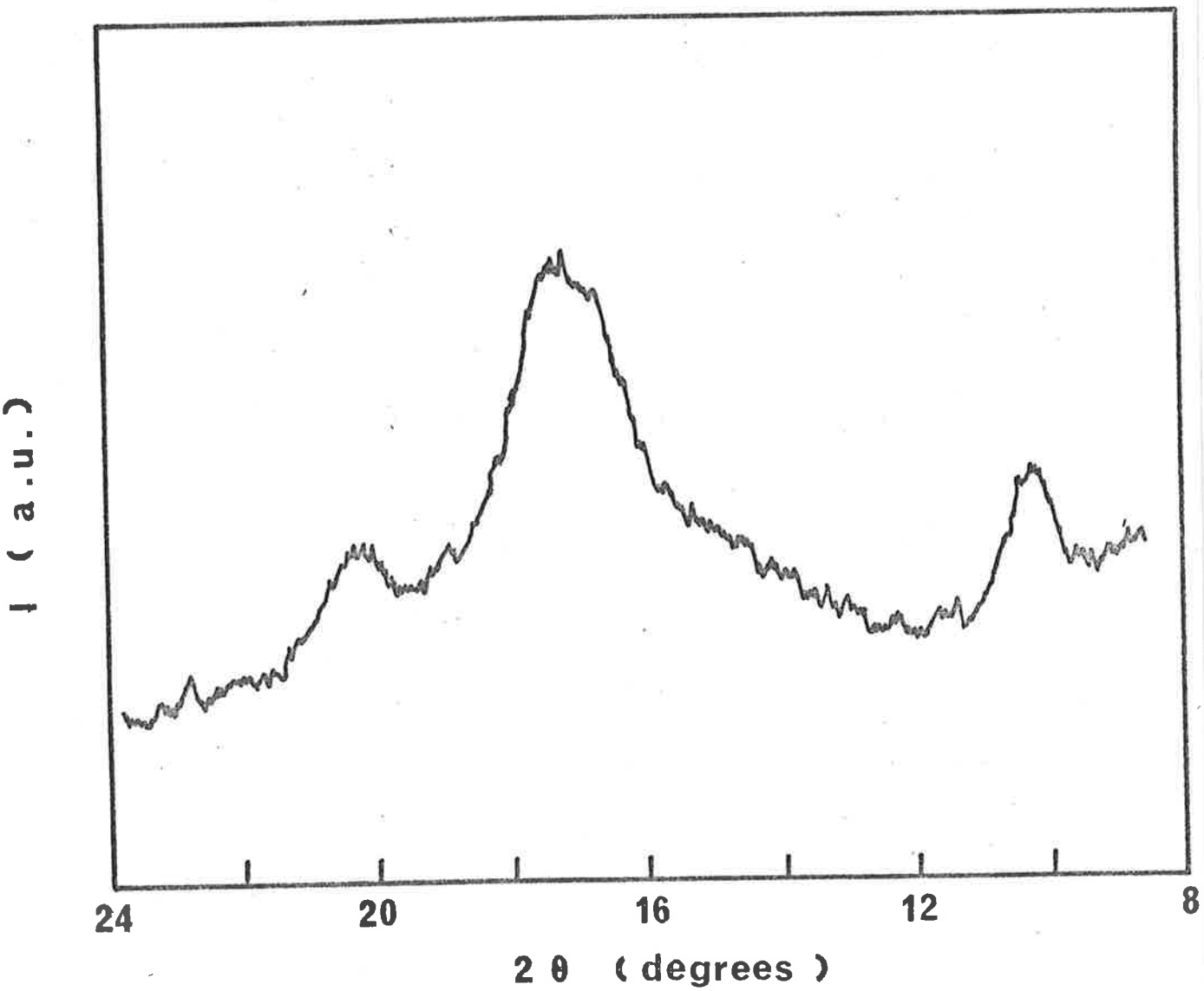

Fig.6.10 X-ray diffractogram showing methanol induced crystallization (T_{cr} = 20°C) for i-PMMA.

tion of i-PMMA helices in which the polar ester groups point outward from the helices and non-polar α-CH_3 groups are subjected to hydrophobic bonding in the centre of the helices (165). The chain segments of s-PMMA lie across the helices and the formation of stereocomplexes is facilitated. Acetone is a typical solvent of Type A. Type B are classified as non-polar solvents or weakly complexing solvents and examples are toluene and benzene. Type C are strongly solvating solvents, i.e. non-complexing solvents and dichloromethane is a typical example

Although Challa group's classification is well established at room temperature, some of Type A solvents such as acetone become a Type C solvent at elevated temperature. Acetone possesses two opposing actions: solvating power (good solvent) and the ability to encourage complexing between i- and s-PMMA. While acetone dissolves atactic PMMA and syndiotactic-like PMMA (e.g. s-PMMA used in this work), i/s-PMMA blends (i/s = 50/50 to 10/90 weight ratio) only swell in this solvent. The swelling reveals the nature of the two different actions of acetone on the blends. As a good solvent, acetone penetrates easily into the bulk but as a highly polar solvent, acetone at the same time facilitates the formation of stereocomplexes. Consequently, in a similar manner to the swelling of cross-linked rubber in a good solvent, the crystalline stereocomplexes behave like pseudo-crosslinks connecting the swollen amorphous phase. The solvating power is increased and become more predominant than complexing power at elevated temperatures and thus acetone behaves as a Type C solvent dissolving i/s-PMMA at T = 50°C.

By contrast, methanol, as a non-solvating solvent (poor solvent), slightly swells without dissolving the blend, but at the same time due to its high polarity, methanol promotes co-crystallization.

At high temperatures (T_{cr} = 40°C), the co-crystallization is enhanced by more absorbed methanol and this leads to a higher percentage crystallinity of stereocomplexes.

It is interesting to note that the sheet of i/s-PMMA blend did not become opaque after SINC or TINC. Obviously, the blends will not crystallize in the normal manner to give spherulites as in the SINC of poly(ethylene terephthalate) (162). Rather, the translucence of the specimen after crystallization suggests that the crystallites are smaller than the visible light wavelength (400 to 780 nm) and this could be referred as microcrystalline.

To understand the difference between the co-crystallization of i/s-PMMA stereocomplexes and the uni-crystallization of PVF_2 in (PMMA + PVF_2) blend, the SINC of the (PMMA + PVF_2) blend was carried out in both methanol and acetone. The blend (PMMA + PVF_2) and i/s-PMMA blend both show SINC but the main difference between the two blends, as shown by X-ray diffraction, is the co-crystallization of i/s-PMMA stereocomplexes and the uni-crystallization of PVF_2 in the (PMMA + PVF_2) blend. Comparing with i/s-PMMA blends, the X-ray diffractograms of the (PMMA + PVF_2) blend gave quite different results (Fig. 6.11). Curve (1) in Fig.6.11 shows a broad amorphous peak of the blend before SINC treatment (the blend was prepared at 200°C in a hot roller). In methanol, as shown in Curve (2), the original amorphous blend developed into two phases, a crystalline PVF_2 phase and an amorphous PMMA phase (shown by the broad peak on the right of the curve). In acetone, the crystalline peaks of PVF_2 become more distinct and the broad amorphous peak of PMMA disappears (Curve 3). The crystalline peaks in Curve 2 and Curve 3 have been identified as the crystalline peaks of PVF_2 by comparing with the diffractograms of the crystalline PVF_2 only.

The above observations suggests that, in contrast to i/s-PMMA blend where two components co-crystallize to form stereocomplexes.

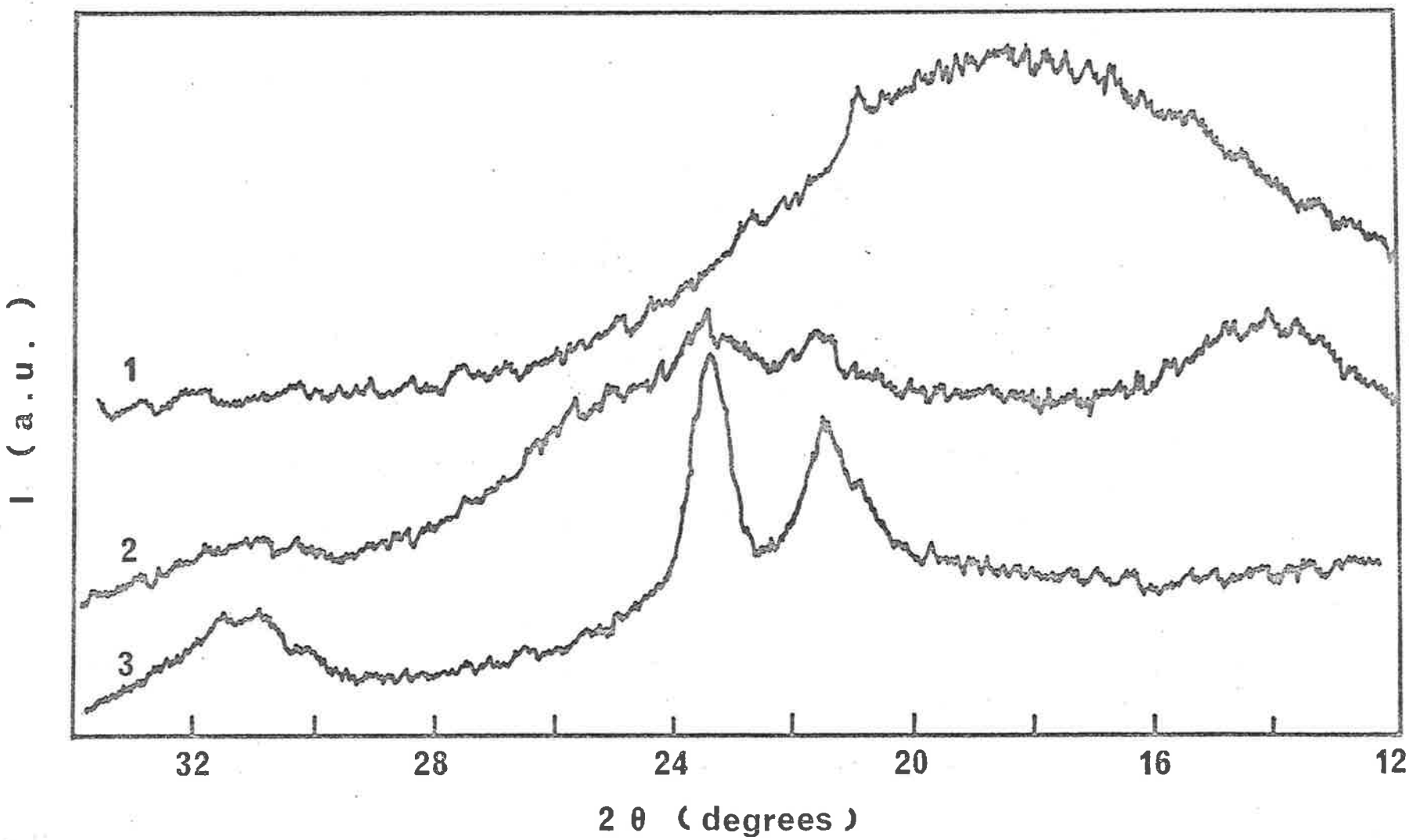

Fig.6.11 X-ray diffractograms of the (PMMA + PVF_2) blend (PMMA/PVF_2 = 70/30). (1) Amorphous (PMMA + PVF_2) blend, (2) methanol induced crystallization (T_{cr} = 40°C) and (3) acetone induced crystallization (T_{cr} = 40°C).

the PMMA component is not involved in the SINC in the (PMMA + PVF_2) blend. In methanol, the presence of amorphous PMMA phase suppresses the crystallization of PVF_2 as shown by a broad crystalline peak in Curve (2). However, in acetone, this solvent dissolved PMMA, facilitating the crystallization of PVF_2.

6.3.3 Glass Transition Temperature, T_g, Melting Temperature, T_m, and Dynamic Mechanical Properties

The following blends were used in this investigation

(1) MMW + I.74

(2) S.73 h + I.100*

(3) S.73 ℓ + I.74

(4) A4a + I.100**

Sample	M_w	MWD or number of GPC peaks	Tacticity
MMW	220,000	2.1	55% syndio
S.73 h	2,700,000 200,000	bimodal	73% syndio
S.73 ℓ	30,000	approx. 2.5	73% syndio
A4a	120,000	1.2	64% syndio
I.74	2,000,000 110,000 35,000	trimodal	74% iso
I.100*	3,500,000 400,000 100,000	trimodal	100% iso
I.100**	2,700,000 400,000	bimodal	100% iso

6.3.3.1 Glass Transition Temperature

While the X-ray diffractograms have convincingly proved the formation of crystalline stereocomplexes as a result of TINC or

* Sample I.100 (1) in Table 3.4.
** Sample I.100 (3) in Table 3.4.

SINC, it was considered necessary to provide supporting formation from T_g and T_m measurements.

Broadening of the glass transition temperature was observed for all blends (Figs.6.12a,b,c). The broadening was also observed by Feistma et al. (144) by DSC, and by Krause and Roman (166) by dilatometry of solution crystallized i/s-PMMA blend of high tacticity components. Feistma et al. stated that the broadening originated from the distribution of the non-complex polymer (i.e. amorphous phase), but did not suggest why the amorphous blends of i/s-PMMA possess a broad T_g in contrast with a sharp T_g exhibited by other polymer blends, for example (PMMA + PVF_2) (167-168) and poly(ethyl methacrylate) + PVF_2 (169). The existence of a single broad T_g or a single sharp T_g for blends poses the following question: Is the normal macroscopic techniques of observation of T_g adequate to determine polymer-polymer compatability? To answer this question, Kaplan (170) has proposed that there is a maximum domain size in which only one component can exist and yield a single distinct T_g. On the basis of examining a wide range of blends ranging from single phase to obvious two phase structures, Kaplan found a value of 15 nm is the domain size required to yield a sharp single T_g. At 15 nm to 100 nm domain size range, a broad T_g is observed and above 100 nm two distinct T_g's are formed (170). Consequently, the amorphous phase of i/s-PMMA blend is on the borderline of miscibility.

Blauer and Bletso (171) reported that i-PMMA is not miscible with so-called "heterotactic" PMMA* because they observed from dilatometry and storage shear modulus, G', measurements the presence of two distinct T_g's. Despite the fact that the tacticity of their

* It is presumed that the polymer described by Blauer and Bletso as "heterotactic" PMMA would almost certainly be atactic. A method of synthesis of highly heterotactic PMMA has not been reported.

Fig.6.12 Broadening of the glass transition temperature in i/s-PMMA blends.

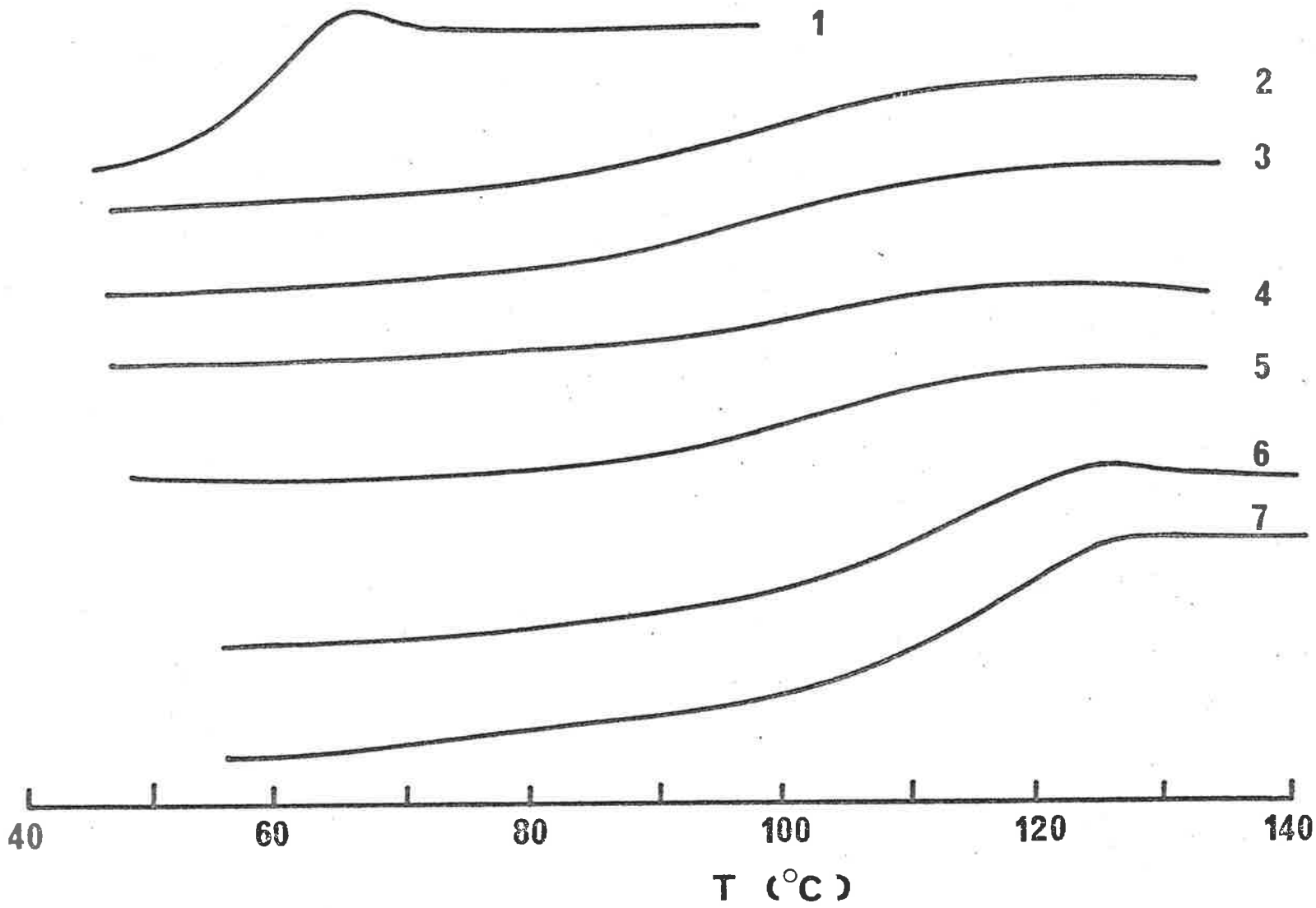

Fig.6.12a Blend (MMW + I.74). (1) i/s = 100/0 (I.74 only), (2) i/s = 50/50, (3) i/s = 40/60, (4) i/s = 30/70, (5) i/s = 20/80, (6) i/s = 10/90 and (7) i/s = 0/100 (MMW only).

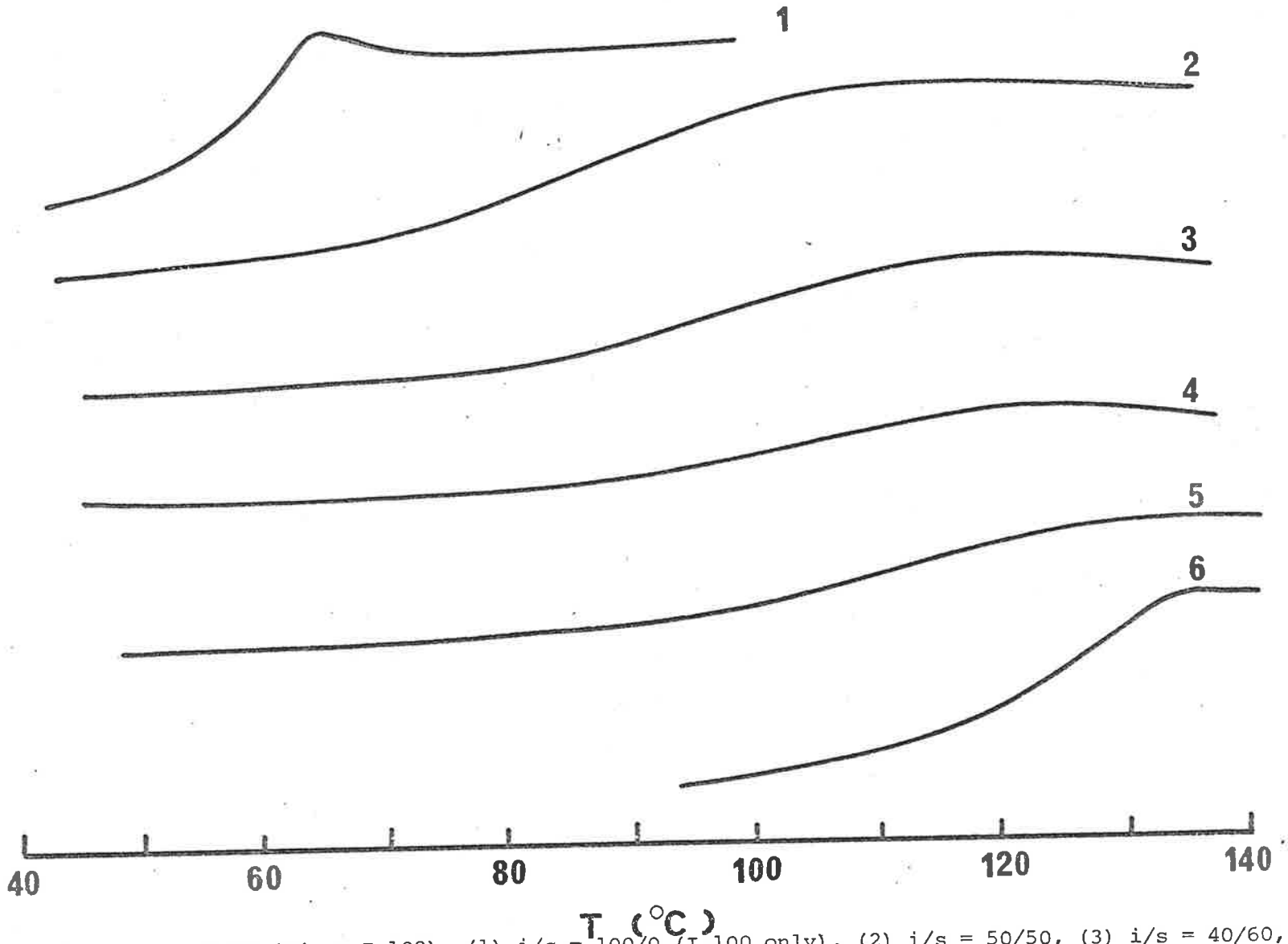

Fig.6.12b Blend (A4a + I.100). (1) i/s = 100/0 (I.100 only), (2) i/s = 50/50, (3) i/s = 40/60, (4) i/s = 30/70, (5) i/s = 20/80 and (6) i/s = 0/100 (A4a only).

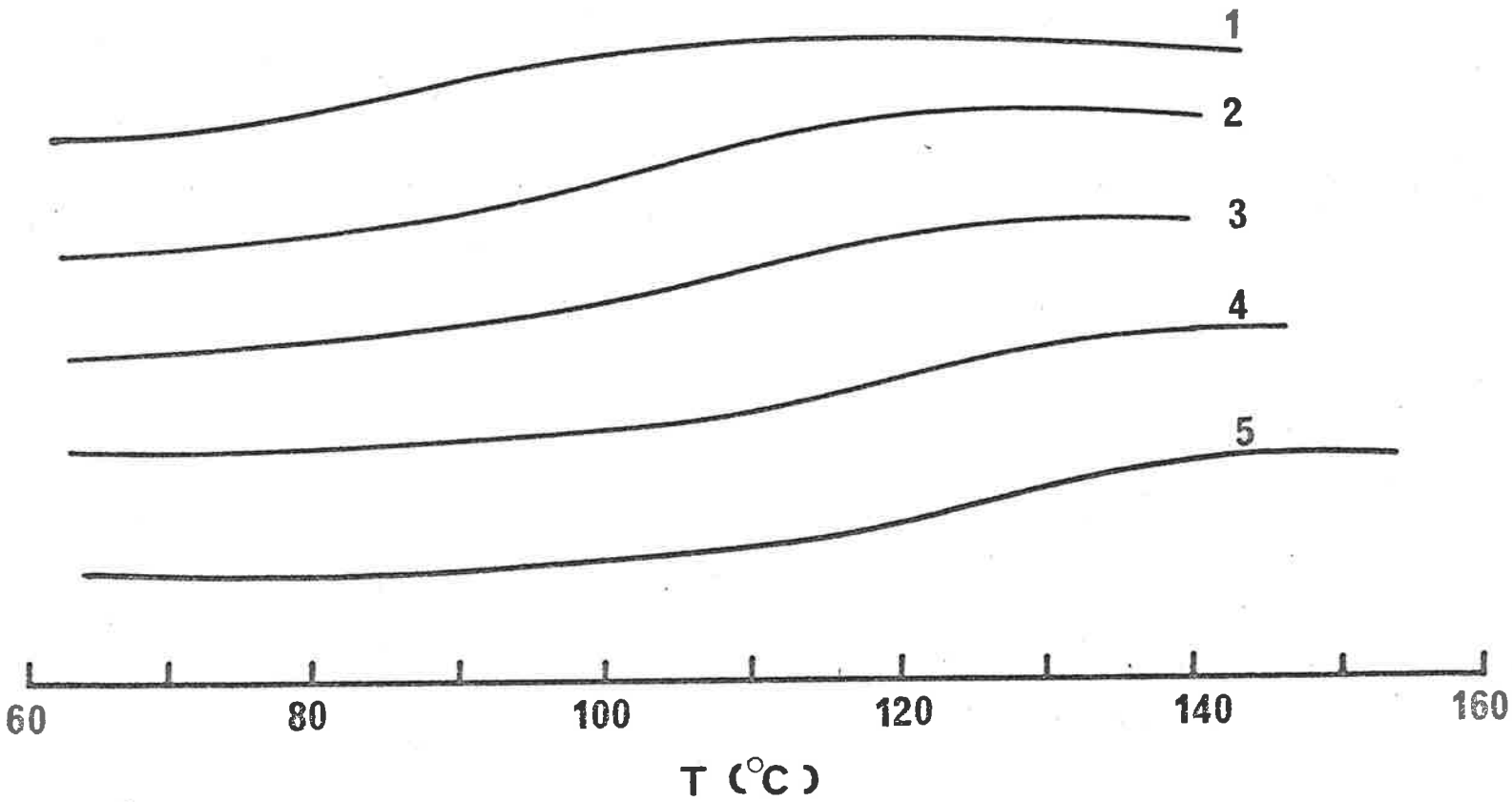

Fig.6.12c Blend (S.73h + I.100). (1) i/s = 50/50, (2) i/s = 40/60, (3) i/s = 30/70, (4) i/s = 20/80 and (5) i/s = 10/90.

polymers was not revealed, these authors' observation does suggest that there may exist PMMA polymer of sufficiently random tacticity that does not allow miscibility and this is an area that requires further investigation.

6.3.3.2 Melting Temperature, T_m, of Sterocomplex Crystallites.

The results of T_m measurements are summarized in Table 6.2.

TABLE 6.2: Melting Temperature of stereo complex crystallites induced at T_{cr} = 20°C and 40°C by methanol induced crystallization.

Blend	T_m(°C) (SINC/methanol T_{cr}=20°C)	T_m(°C) (SINC/methanol T_{cr}=40°C)
MMW + I.74	145 to 150	160 to 165
A4a + I.100	140 to 150	160 to 165
S.73 h + I.100	150 to 160*	160 to 165*

The melting points of the blends with exception for blend (S.73 h + I.100) of i/s = 10/90 have the following characteristics (Figs.6.13a,b-6.16).

(a) T_m and endotherm area of DSC thermodiagram increases with T_{cr} of the SINC process.

(b) T_m is almost independent of the weight ratios i/s and tacticity of components at a particular T_{cr}.

(c) T_m of stereocomplexes produced by SINC is lower than T_m of stereocomplexes produced by TINC (T_m = 185°C).

Increase in the T_m and endotherm area with the T_{cr} of SINC processes [Point (a)] implies that crystallites induced by SINC

* Blend (S.73 h + I.100) of i/s = 10/90 shows an exceptional T_m = 180°C for both T_{cr} = 20°C and 40°C.

Fig.6.13 The melting endotherm of methanol induced crystallization blend (MMW + I.74) at T_{cr} = 20°C (Fig.6.13a) and T_{cr} = 40°C (Fig.6.13b). (1) i/s = 50/50, (2) i/s = 40/60, (3) i/s = 30/70, (4) i/s = 20/80 and (5) i/s = 10/90.

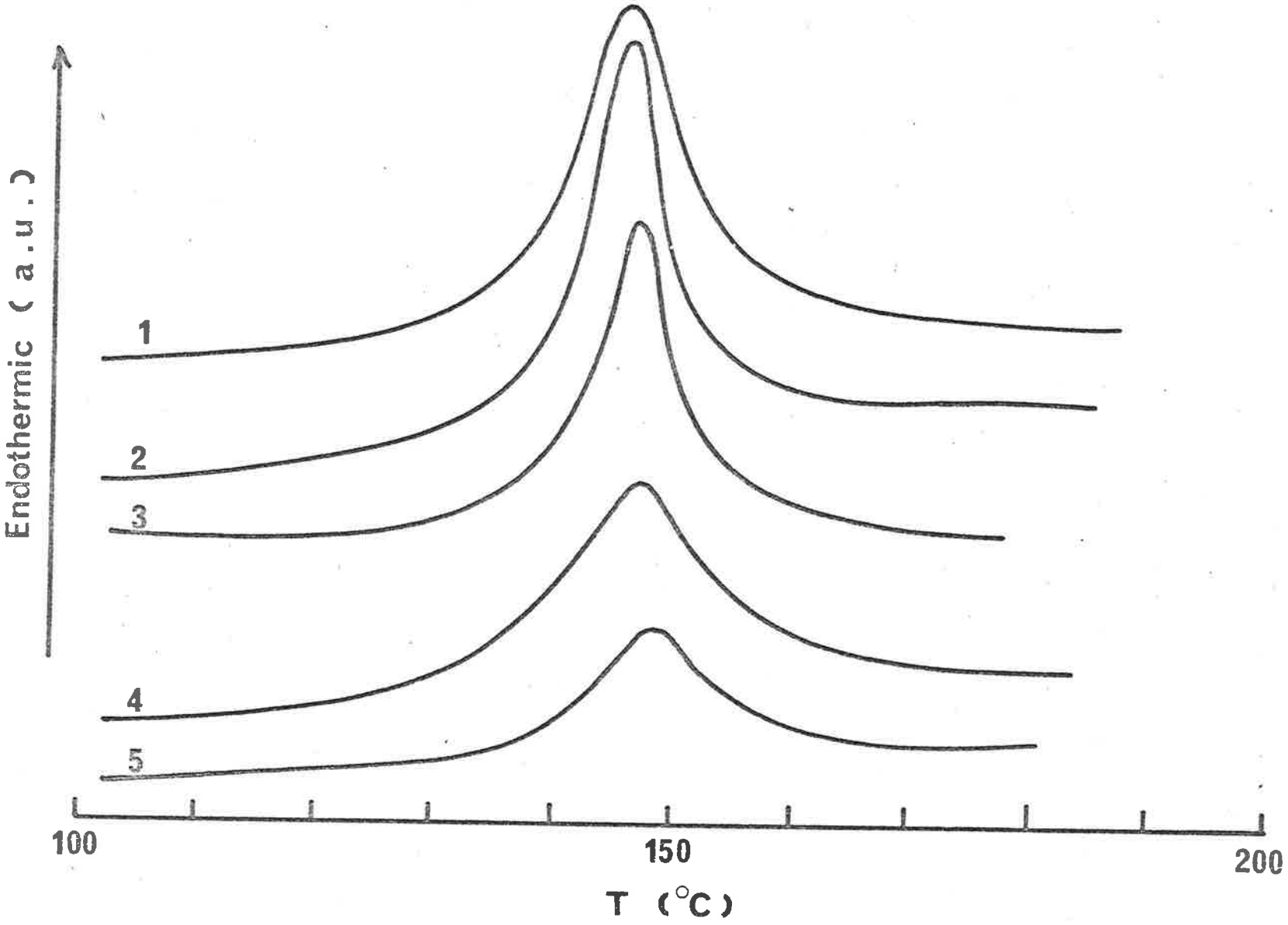

Fig.6.13a

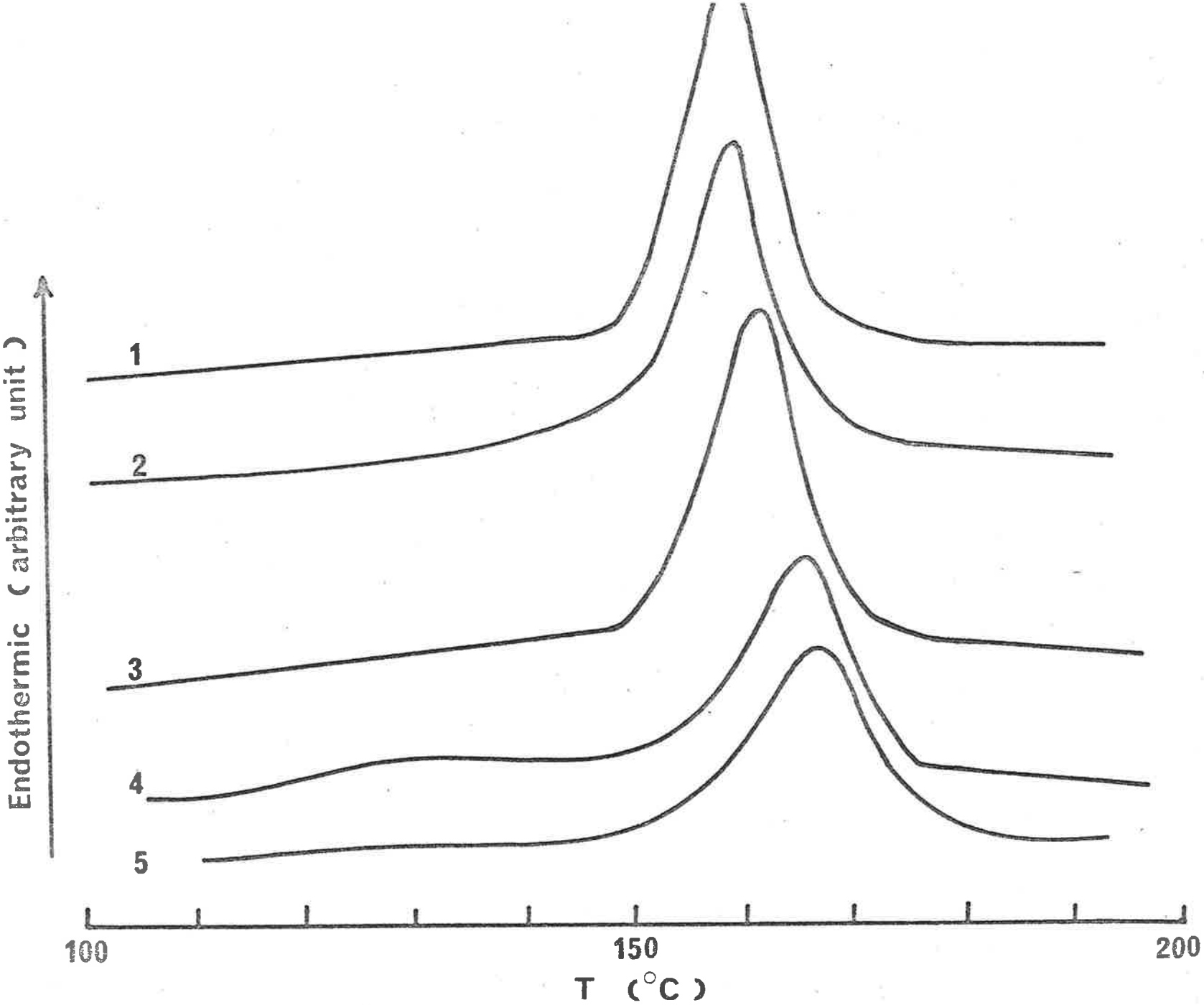

Fig.6.13b

Fig.6.14 The melting endotherm of methanol induced crystallization for blend (A4a + I.100) at T_{cr} = 20°C (Fig. 6.14a) and at T_{cr} = 40°C (Fig.6.14b). (1) i/s = 50/50, (2) i/s = 40/60, (3) i/2 = 30/70 and (4) i/s = 20/80.

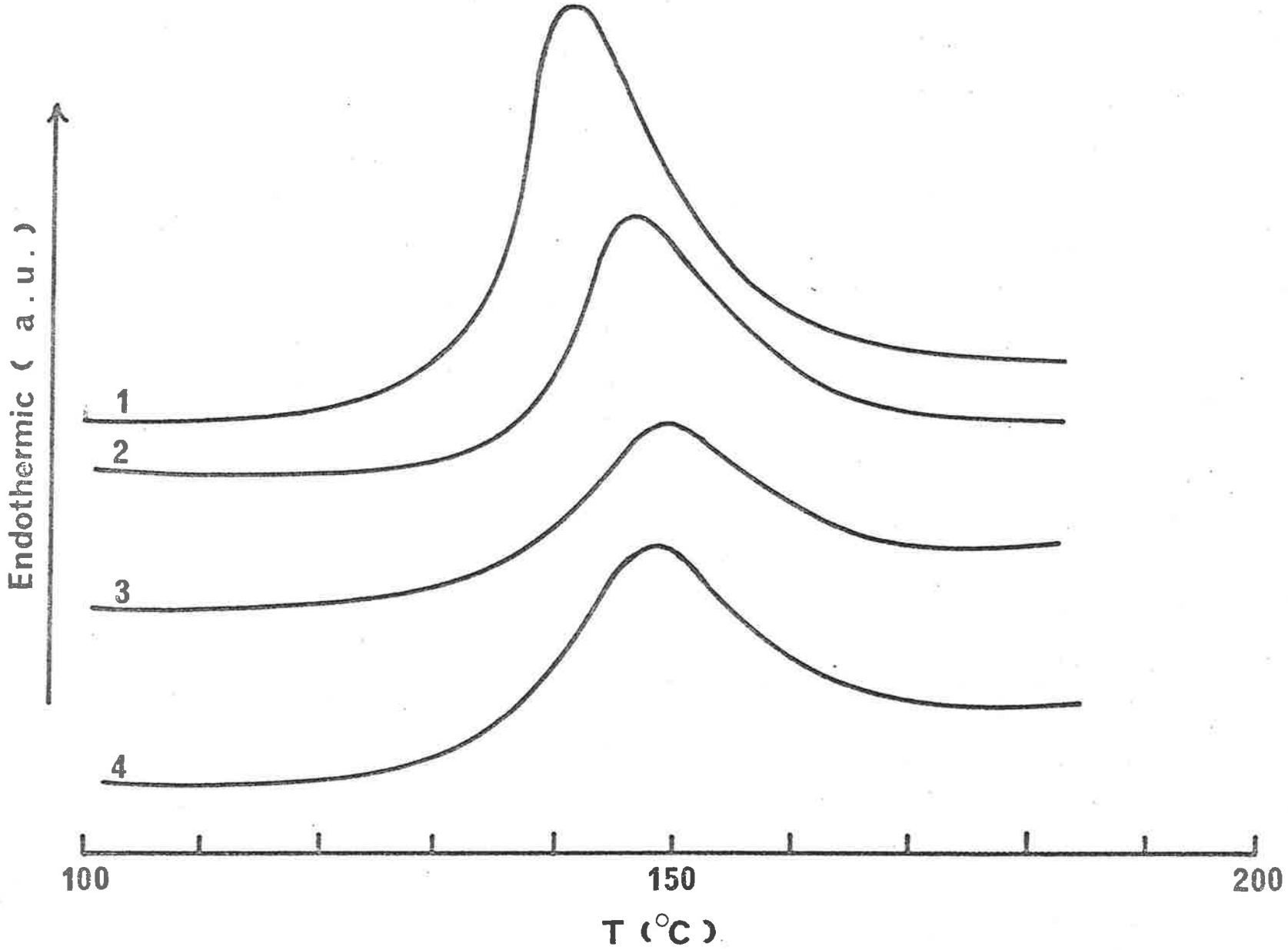

Fig.6.14a

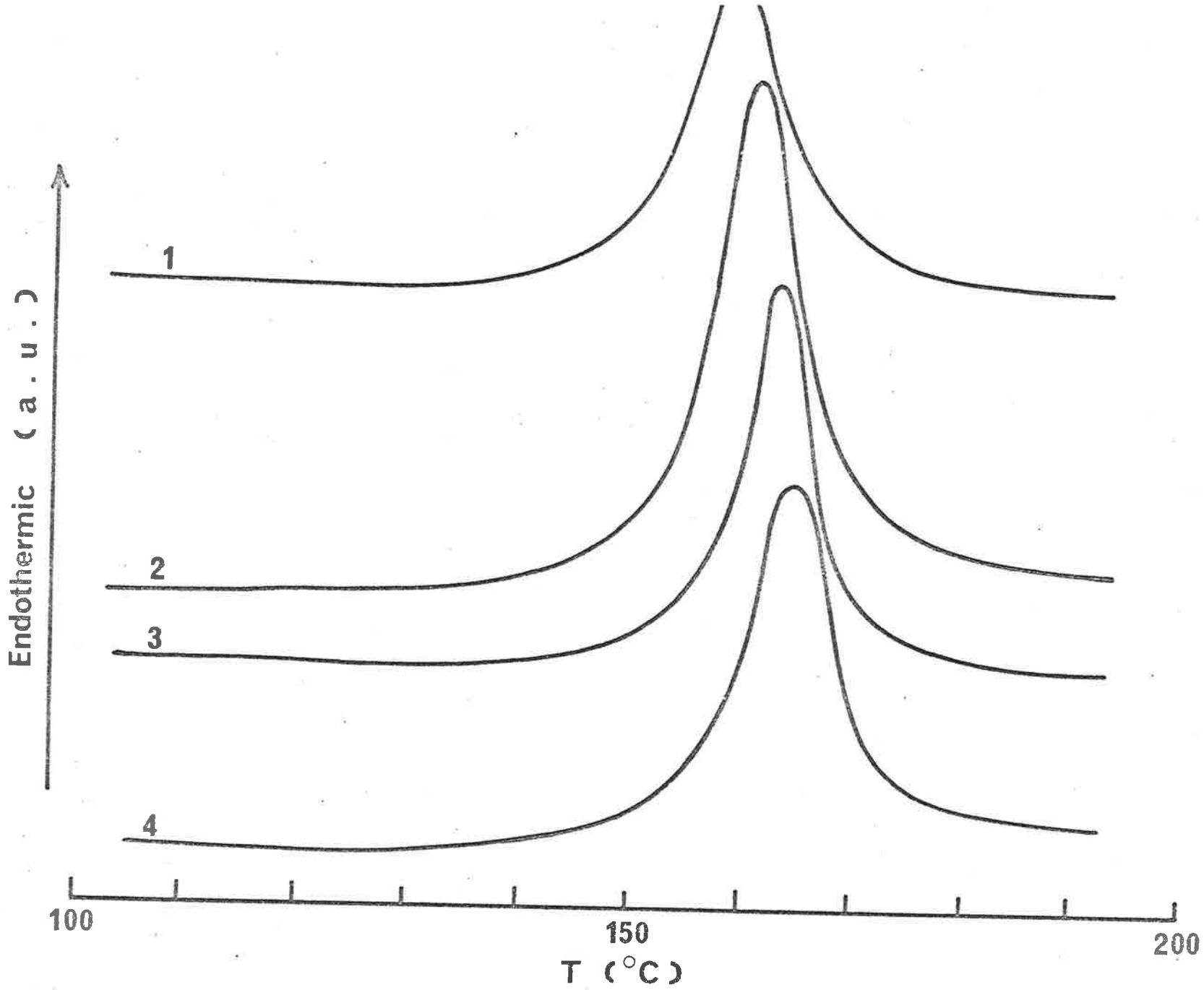

Fig.6.14b

Fig.6.15 The melting endotherm of methanol induced crystallization for blend (S.73h + I.100) at T_{cr} = 20°C (Fig. 6.15a) and at T_{cr} = 40°C (Fig.6.15b). (1) i/s = 50/50, (2) i/s = 40/60, (3) i/s = 30/70, (4) i/s = 20/80 and (5) i/s = 10/90.

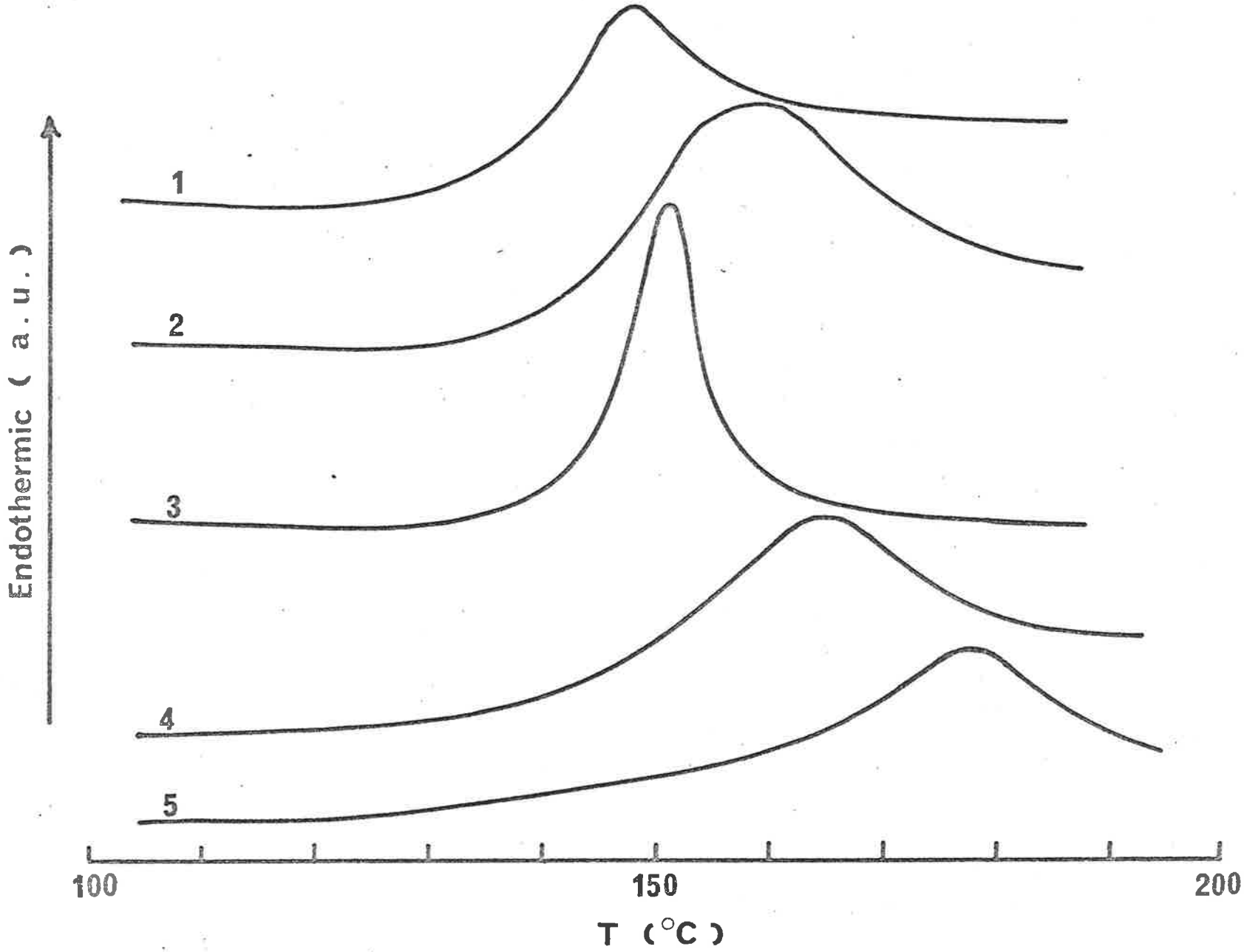

Fig.6.15a

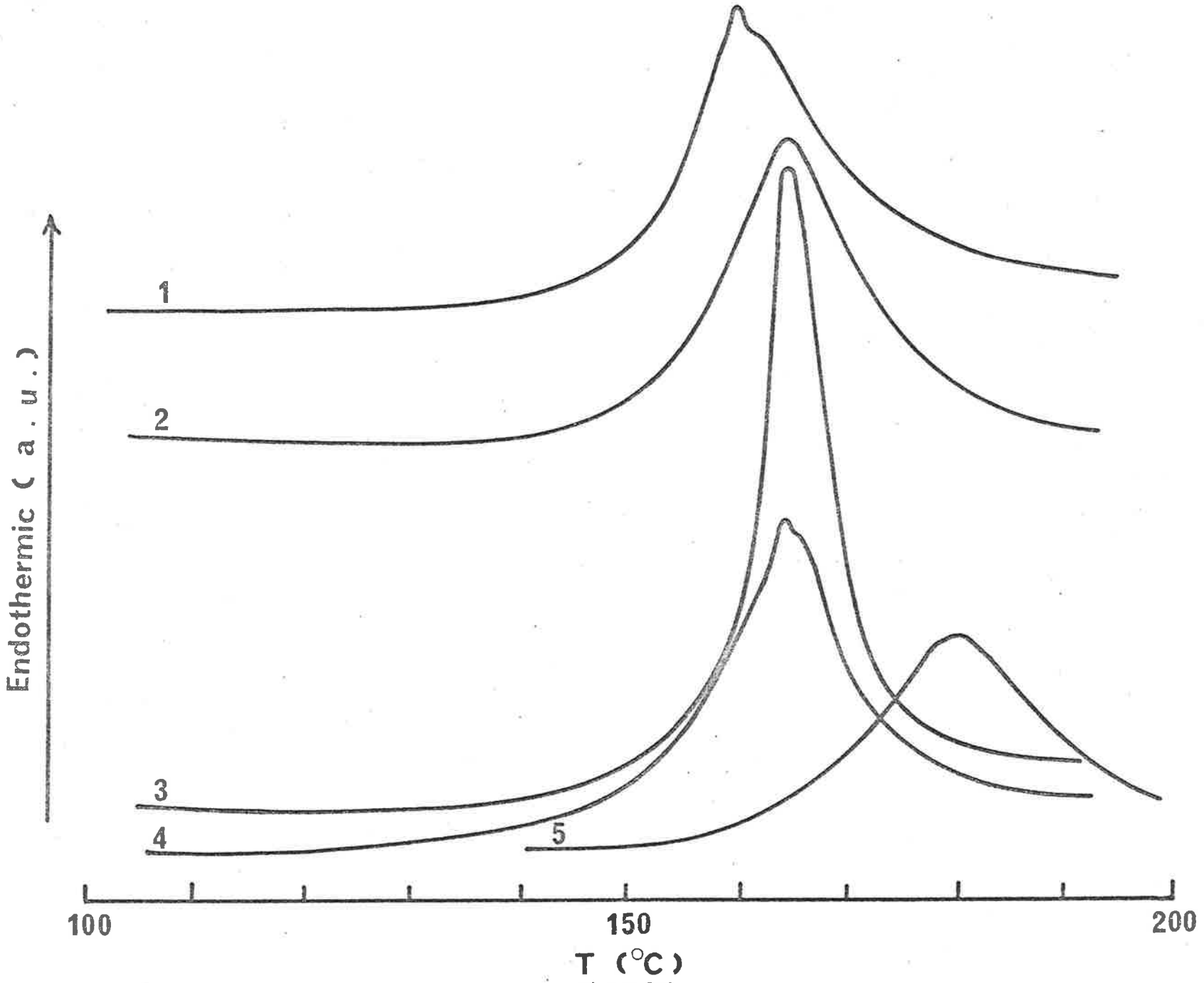

Fig.6.15b

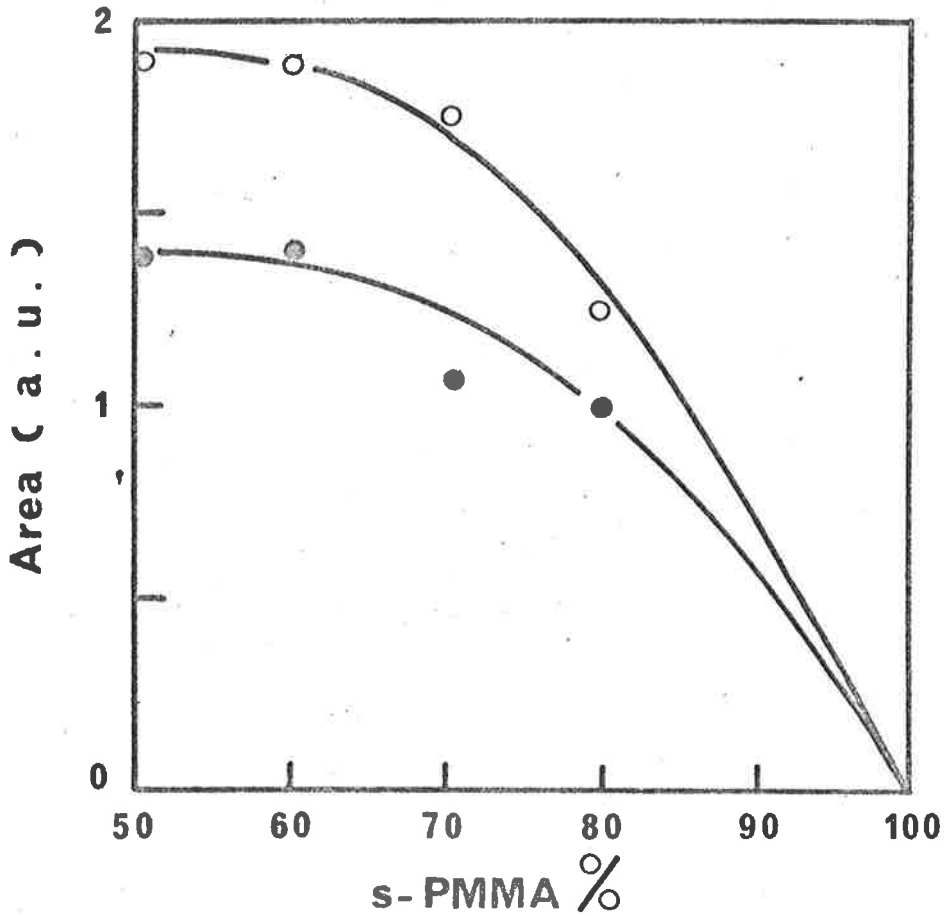

Fig.6.16 An example of increase in the endotherm area with crystallization temperature, T_{cr}, of methanol induced crystallization [blend (A4a + I.100)]. (●) T_{cr} = 20°C, (○) T_{cr} = 40°C.

have a larger size and/or a less imperfect crystal structure. This was confirmed by taking the pre-crystallized sample at T_{cr} = 20°C and re-immersing in methanol at T_{cr} = 40°C. The DSC thermodiagram of this sample shows a larger endotherm area and a single T_m = 165°C, that is, the endotherm has shifted from T_m = 150°C (for T_{cr} = 20°C) to T_m = 165°C (for T_{cr} = 40°C). Increasing T_{cr} from 20°C to 40°C has apparently enhanced chain mobility by lowering the T_g, thus encouraging the stereoassociation of longer tactic block and causing higher crystallinity.

In the NMR study of the formation and structure of the stereocomplex formed in solution, Spěváček and Schneider (150) have drawn the same conclusion that during heating the thermal stability of the associated segments (i.e. the melting point of stereocomplexes) increases with the length of associated sequences. Moreover, the observation in Point (b) suggests that the microcrystalline character of the stereocomplexes produced by SINC have a structure independent of the tacticity of the whole molecular chain, provided that tactic segments involving stereoassociation have an average length larger than a limiting value. This limiting value was not determined in this work because atactic PMMA of random tacticity was not available.

Although the T_m is not influenced by the tacticity of components of each blend, the tacticity does effect the percentage crystallinity of stereocomplexes. The higher tacticity components show a larger area of endotherm peak in the DSC thermodiagrams than that of stereocomplexes in i/s-PMMA composed of lower tacticity components. Figs.6.17a and 6.17b show the area of the endotherm peaks in the DSC thermodiagrams for the high tacticity blend (S.73 h + I.100) and low tacticity blend (MMW + I.74) at T_{cr} = 20°C and 40°C. These plots clearly reveal the higher crystallinity of (S.73 h + I.100)

for all i/s ratios. Moreover, the percentage crystallinity expressed by the magnitude of the endotherm area has a maximum at i/s ratios from 50/50 to 30/70 of low tacticity blends (MMA + I.74) and (A4a + I.100) (Figs.6.16-6.17a,b). This range covers all the controversial values of i/s (1/1, 1/1.5 and 1/2) reported by various workers (see Section 6.1). However, the maximum area of the endotherm for blend (S.73 h + I.100) composed of high tacticity components occurs at i/s = 30/70 ($\simeq$ 1/2) (Figs.6.17a,b). Re-examining the X-ray diffractograms reveals that blend (S.73 h + I.100) showed more distinct crystalline peaks than those for blend (MMW + I.74), implying that the lower tacticity blend yields a more imperfect crystal structure. Therefore, the i/s ratio of 1/2 for i/s-PMMA blends can be considered as a necessary ratio to yield the highest percentage crystallinity of a well-defined crystal structure. In other words, to achieve stereocomplexes of high degree of perfection it is necessary to use high tacticity components with the ratio i/s = 1/2.

In contrast to the difference in T_m of SINC at T_{cr} = 20°C and T_{cr} = 40°C where the T_m is mainly concerned with the geometrical factor, i.e. the size of stereocomplex, the difference between T_m of TINC and that of SINC [Point (c)] reflects different internal structure of the crystallites. This suggestion can be supported by the following experiment. Thermally-crystallized blend (S.73 ℓ + I.74) (See Section 6.3.1) was post-treated by immersing in methanol at T_{cr} = 40°C (SINC). The specimen was then dried in a vacuum oven for 7 days at T = 40°C. Fig.6.18 shows the DSC thermodiagrams of the blend before and after methanol treatment. The thermodiagram after treatment reveals the presence of two other peaks at T = 160°C and 140°C while the endotherm of crystallites of TINC remains at T_m = 185°C. The endotherm at T = 160°C is obviously the melting point of stereocomplexes by SINC and the peak at T = 140°C is pre-

Fig.6.17 Endotherm peak area vs. percentage of s-PMMA in blend methanol induced crystallization at T_{cr} = 20°C (Fig. 6.17a) and T_{cr} = 40°C (Fig.6.17b). (Curve 1) Blend (S.73h + I.100) and (Curve 2) blend (MMW + I.74).

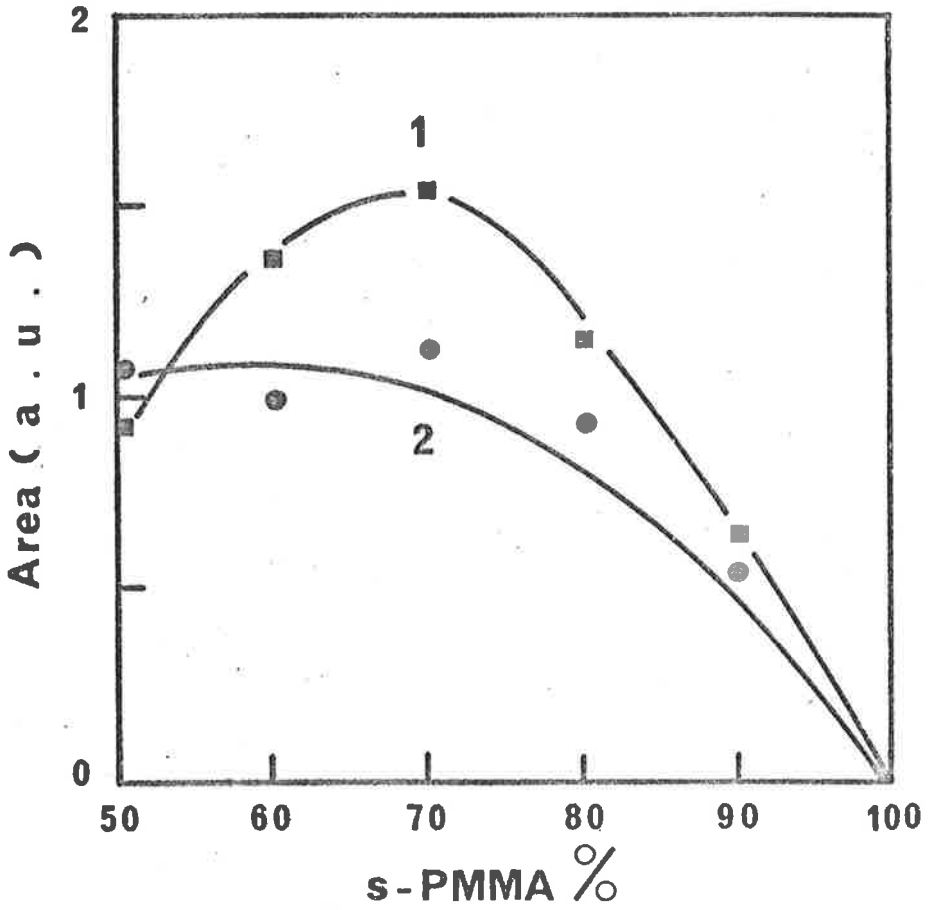

Fig.6.17a

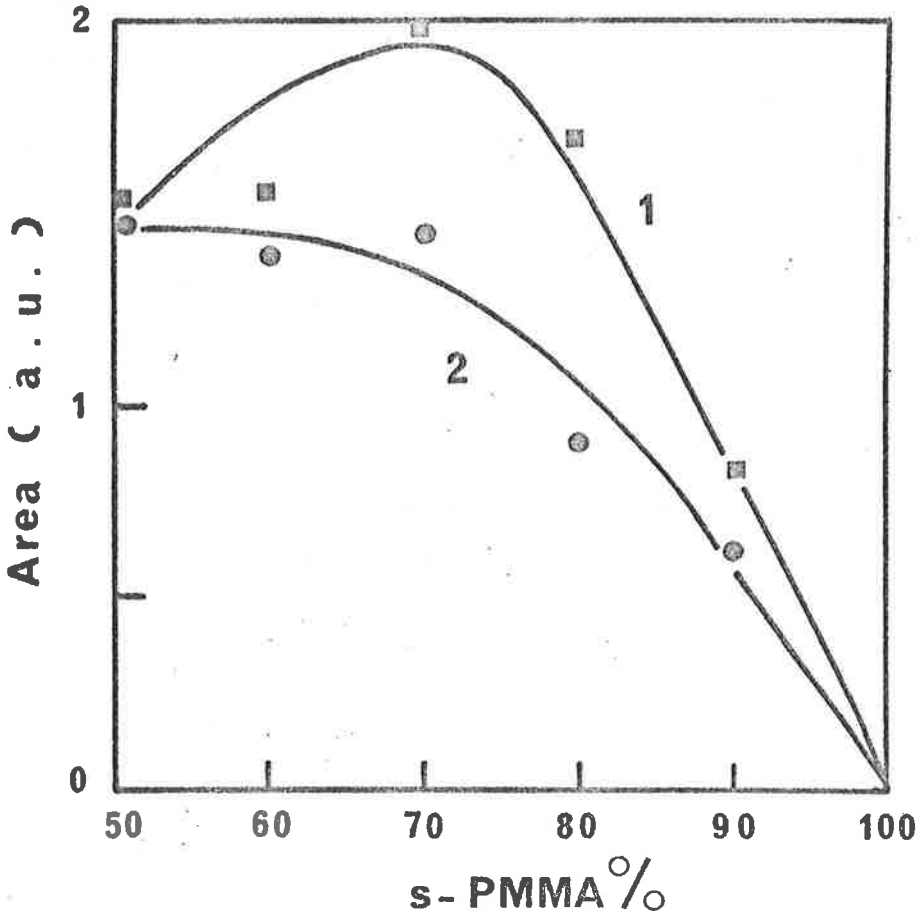

Fig.6.17b

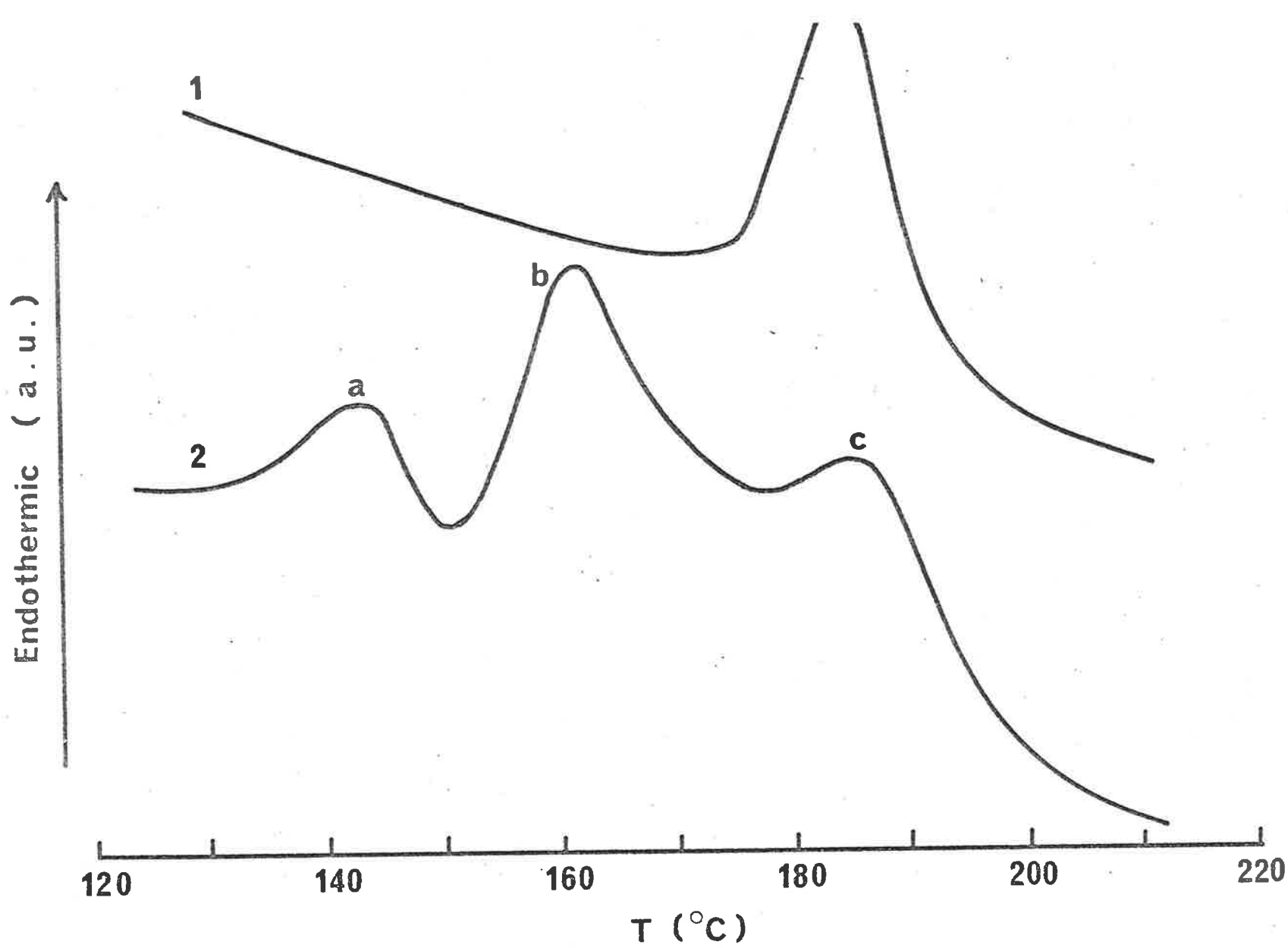

Fig.6.18 The melting endotherm of blend (S.73ℓ + I.74) (i/s = 50/50) initially subjected to thermally induced crystallization. (1) Before methanol induced crystallization and (2) after methanol induced crystallization (T_{cr} = 40°C).

sumed to be the endotherm of the residual methanol. The residual methanol could be eliminated by using a specimen in powder form, as previously mentioned (Sec.6.2.2), but when the powder form was initially treated by TINC at T = 140°C the powder partly melted into sheet form under heat. Methanol trapped in the sheet form can be difficult to completely remove by vacuum oven treatment.

The appearance of the SINC endotherm in addition to the existing TINC endotherm is evidence that the morphology of solvent-crystallized i/s-PMMA differs from that of thermally crystallized i/s-PMMA. In contrast to the increase of T_m by T_{cr} in SINC [Point (a)], the higher T_m of thermal-induced stereocomplexes as compared to that of solvent-induced stereocomplexes does not mean the stereo-association of a longer tactic block, because the chain segments are much more restricted in bulk than in the presence of solvent. The appearance of the SINC endotherm implies that solvent aids further association of the tactic chain segment which have been previously restricted by intra- and inter-molecular interactions during TINC. Vorenkamp et al. (157) reported an identical T_m for solution -crystallized (either from diluted or concentrated mixtures) and thermally-crystallized i/s-PMMA stereocomplexes. The above evidence of two distinct T_m of TINC and SINC, however, has confirmed that the crystallites produced by SINC do not belong to the same structural category as assigned by these authors.

6.3.3.3 Dynamic Mechanical Properties

To gain a further understanding of the crystalline stereocomplexes, dynamic mechanical measurements were performed on the moulded blend (S.73 h + I.100). After SINC in methanol at T_{cr} = 40°C, the specimen was dried in a vacuum oven at 40°C for several days prior to testing.

A general increase in modulus due to crystallization is shown in Fig.6.19. Although the difference between the amorphous

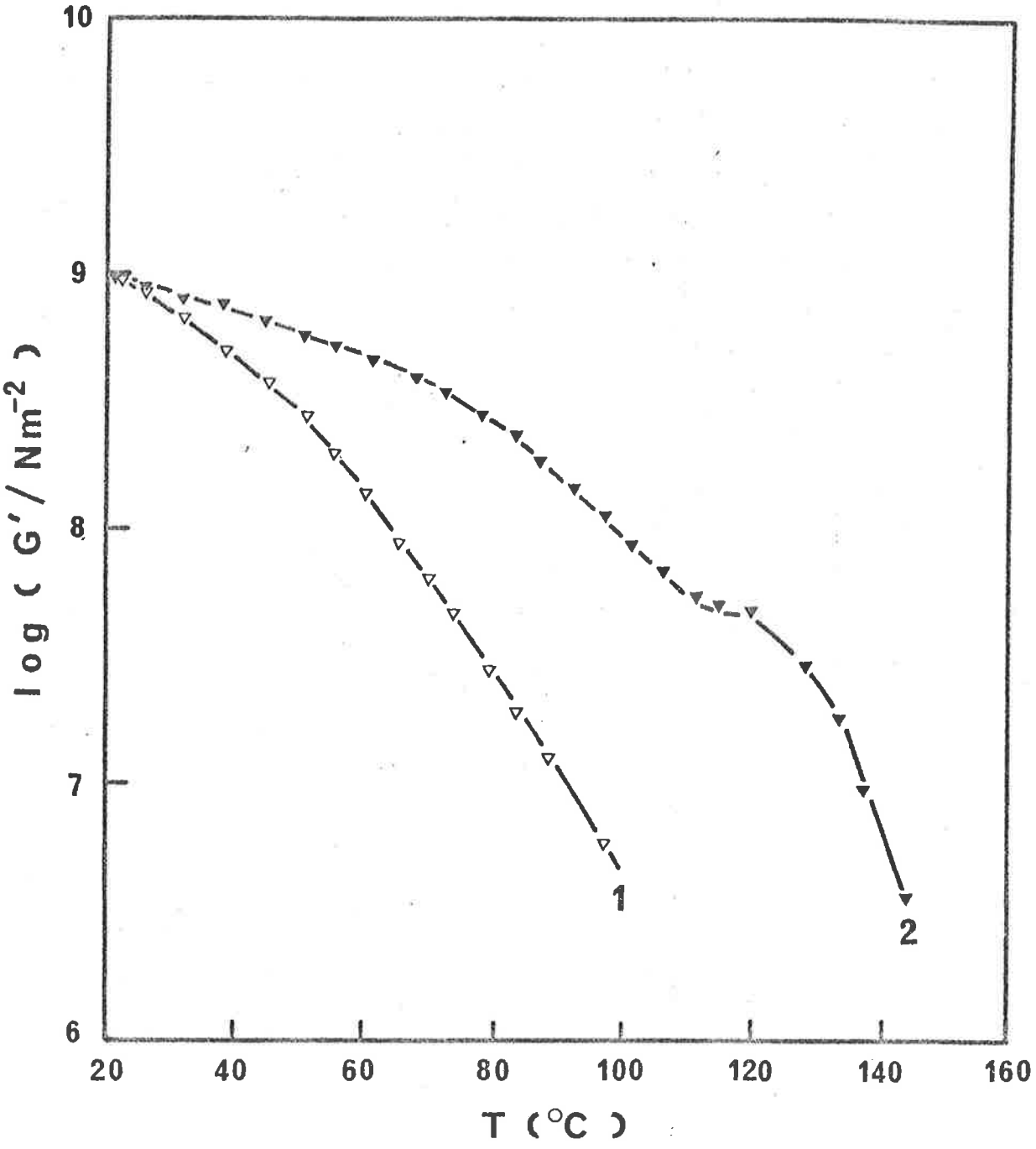

Fig.6.19 An example of the increase in modulus by crystallization, blend (S.73h + I.100) of i/s = 30/70. (1) Amorphous blend, (2) crystallized blend (methanol induced crystallization at T_{cr} = 40°C).

state and crystallized state is clearly revealed in plot of log G' vs. T (Fig.6.19), only a short rubbery zone is observed in the curve (Curve 2) for the crystallized state. The rubbery zone is confined between the glass transition zone and the melting zone of stereocomplexes ($T_m \simeq 150°C$) and mostly hidden by the broadening of the T_g of i/s-PMMA blend. The rubbery plateau is observed at $\log(G'/Nm^{-2}) = 7.5$ to 7.7 for blends of high crystallinity (i/s = 40/60 and 30/70) (Fig.6.20a) and almost disappears for blends of low crystallinity (i/s = 20/80 and 10/90) (Fig.6.20b).

An advantage of using dynamic mechanical measurments is that it provides a method of measuring the crystallinity of stereocomplexes. Other common methods such as density X-ray diffraction encounter some difficulties because firstly, the density of a 100% crystalline sample is required in the density method and this is unknown, and secondly, the broad crystalline peaks in X-ray diffractogram do not allow estimation of the percentage crystallinity with reasonable accuracy. However, from the study of polyethylene, Nielsen (172-173) was able to relate the value of the rubbery shear modulus, G, to the degree of crystallinity, w_c, and suggested that this emperical relationship could apply to other semi-crystalline polymers. The relationship is expressed by (173)

$$\log (G/Nm^{-2}) = 5.763 + 4.77\, w_c \qquad (6.1)$$

where the shear modulus, G, is defined as

$$G^2 = G'^2 + G''^2 \qquad (6.2)$$

In the rubbery region, we have

$$G'^2 \gg G''^2$$

and hence

$$G \simeq G' \qquad (6.3)$$

Fig.6.20 Storage shear modulus, G', and loss tangent, tan δ, vs. temperature for blend (S.73h + I.100) (methanol induced crystallization at T_{cr} = 40°C). Fig.6.20a: (1) i/s = 40/60 and (2) i/s = 30/70. Fig.6.20b: (3) i/s = 20/80 and (4) i/s = 10/90.

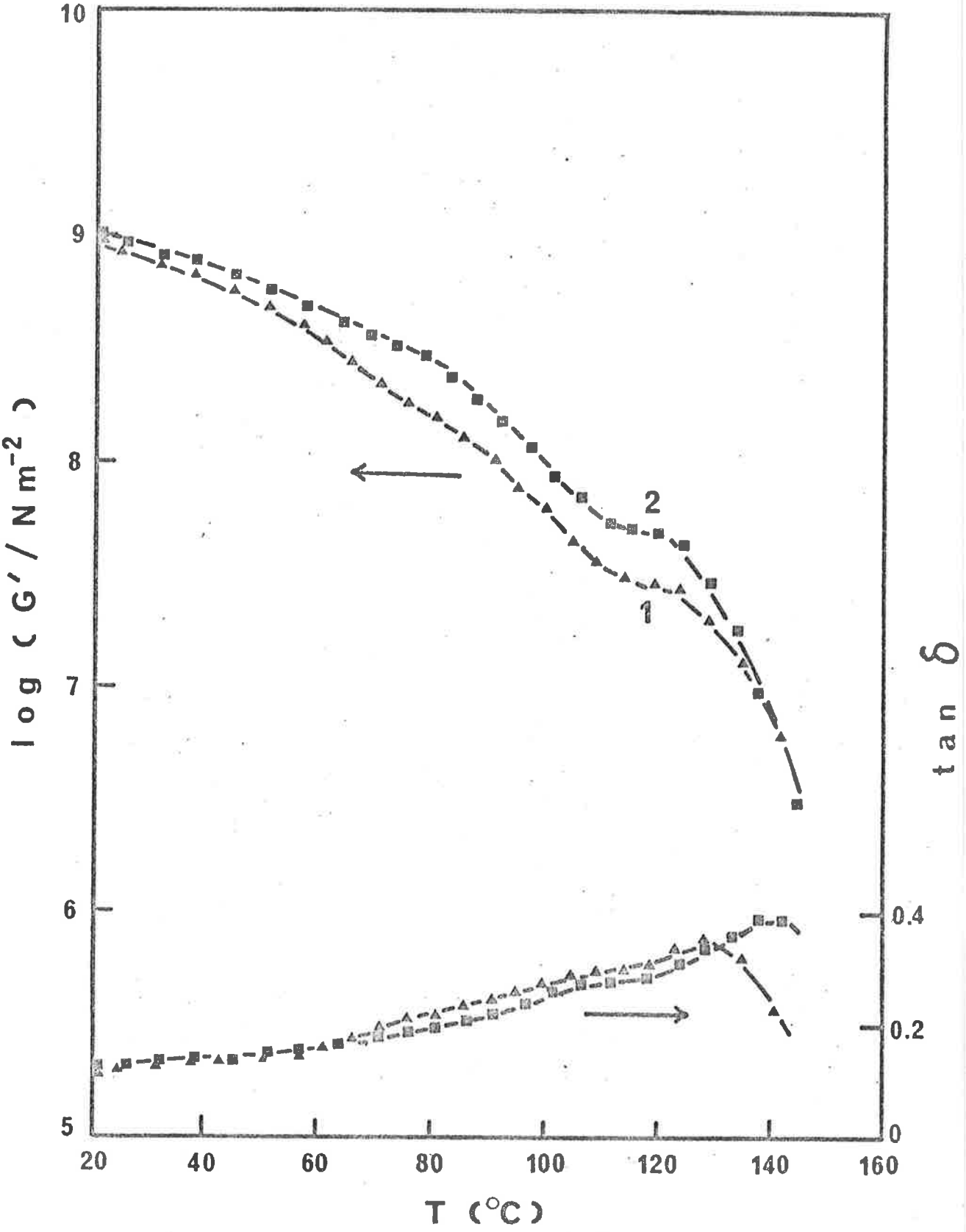

Fig.6.20a

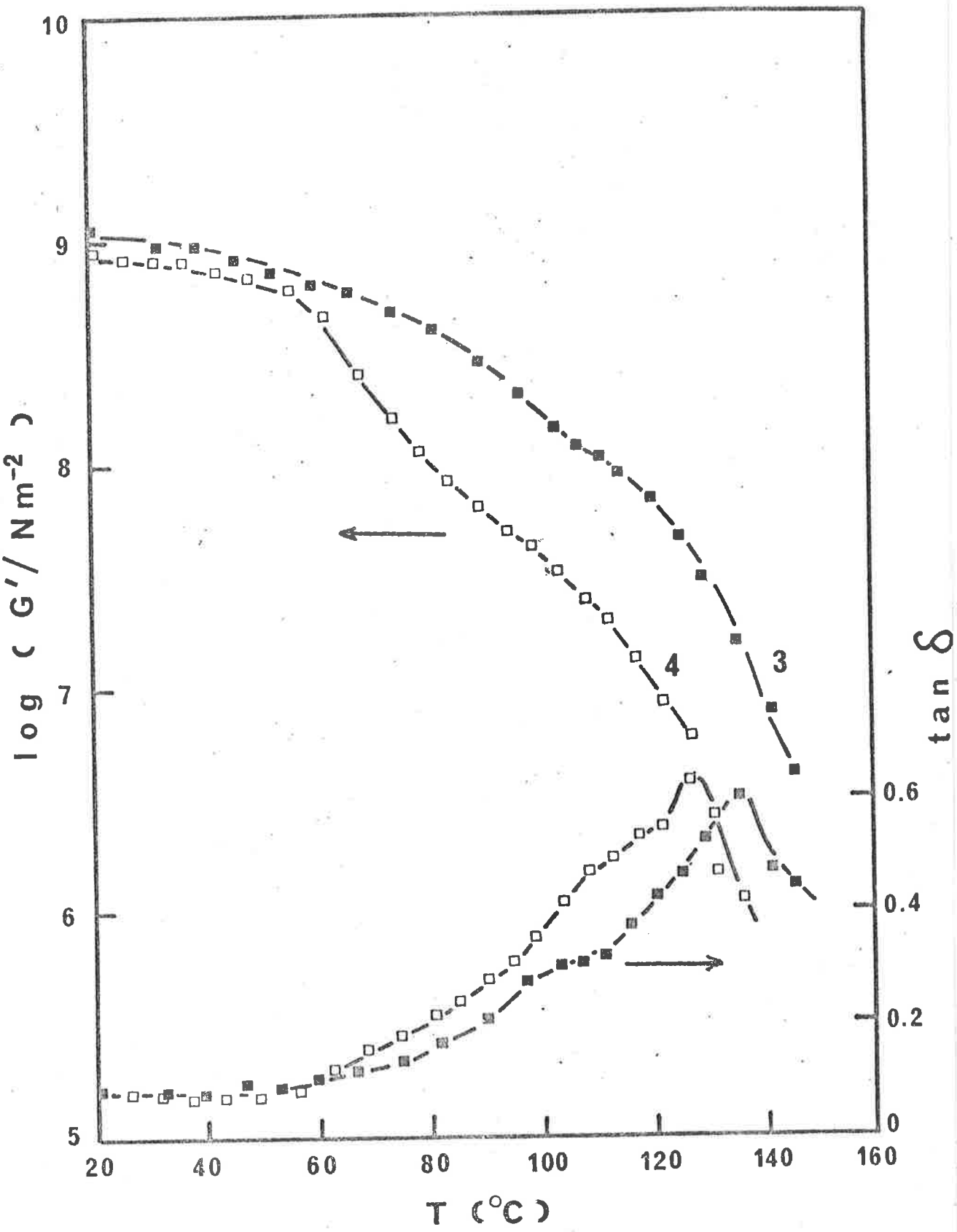

Fig.6.20b

For blend (S.73 h + I.100) of i/s = 30/70 at T_{cr} = 40°C, $\log(G'/Nm^{-2})$ = 7.6 (Fig.6.20a) and thus the crystallinity is calculated to be 35% (Eqs.6.1,6.3). Using this value a reference and comparing the area of the endotherm peaks obtained previously the percentage crystallinity of other i/s ratios and blends can be calculated (Tables 6.3a,b)

TABLE 6.3a: Percentage crystallinity of i/s-PMMA blends (methanol induced crystallization at T_{cr} = 40°C)

Blend \ i/s	50/50	40/60	30/70	20/80	10/90
(S.73 h + I.100)	27	27	35	30	14
(A.4a + I.100)	33	33	31	22	-
(MMW + I.74)	26	24	25	16	11

TABLE 6.3b: Percentage crystallinity of i/s-PMMA blends (methanol induced crystallinity at T_{cr} = 20°C).

Blend \ i/s	50/50	40/60	30/70	20/80	10/90
(S.73 h + I.100)	16	24	27	20	11
(A.4a + I.100)	24	24	18	17	-
(MMW + I.74)	19	17	20	17	10

The percentage of crystallinity by SINC in methanol for blend (S.73 h + I.100) at T_{cr} = 40°C is comparable to that obtained by solution crystallization in DMF (174).

6.3.4 Fracture Behaviour

The following blends were used in this investigation

(1) MMW + I.74

(2) A.4a + I.100*

(3) LMW + I.100**

Sample	M_w	MWD or number of GPC peaks	Tacticity	Fracture Behaviour at T=20°C	at T=40°C
MMW	220,000	2.1	55% syndio	Craze	Crack
A.4a	120,000	1.2	64% syndio	Craze	Crack
LMW	160,000	2.1	55% syndio	Crack	Crack
I.74	2,000,000 110,000 35,000	trimodal	74% iso	-	-
I.100*	2,700,000 400,000	bimodal	100% iso	-	-
I.100**	35,000	approx. 2.5	100% iso	-	-

The fracture tests were carried out in methanol at T = 20°C or 30°C with the sheet specimen. The sheets were prepared by the procedures previously described (Chapters 4 and 5). These blends were amorphous after moulding into sheets.

The s-PMMA components of the blends were deliberately chosen in the medium MW range and low MW range, because from the results of Chapter 5 these samples showed rapid crack propagation at T = 35°C or 40°C. The addition of i-PMMA to the s-PMMA presents the possibility of modifying the fracture toughness.

The fracture toughness of blends (MMW + I.74) and (A.4a + I.100) described by the log K_c vs. log v diagrams is shown in Figs.6.21-6.22. There is an obvious enhancement of the fracture

* Sample I.100 (3) (Table 3.4)

** Sample I.100 (2) (Table 3.4

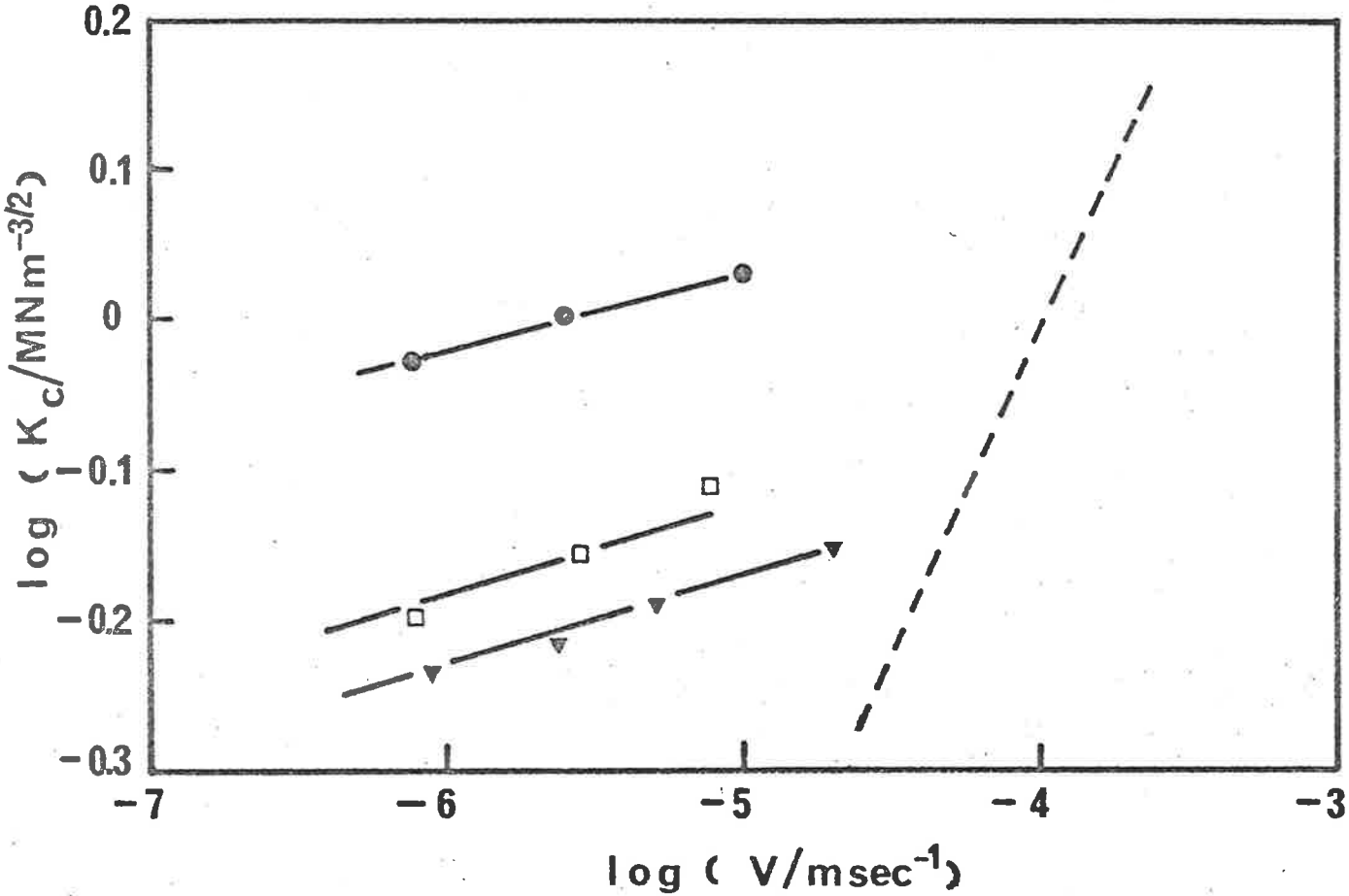

Fig.6.21 Plot of log K_c vs. log v for amorphous blend (MMW + I.74) fractured in methanol at T=20°C, i/s=30/70 (●), i/s = 20/80 (□) and i/s = 10/90 (▼). The broken line represents log K_i vs. log v_i linear relationship for MMW (see Fig.5.31) fractured at the same experimental conditions.

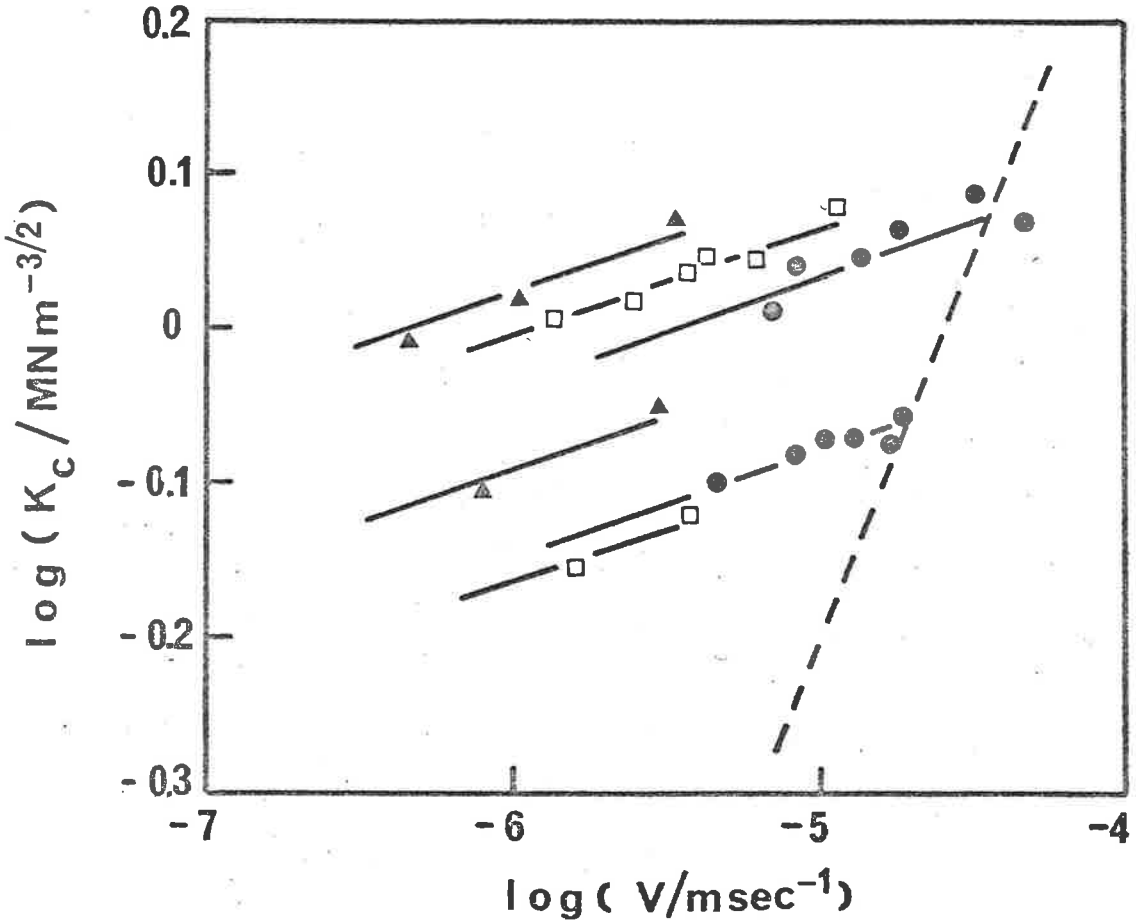

Fig.6.22 Plot of log K_c vs. log v for blend (A4a + I.100) fractured in methanol at T=20°C, i/s = 40/60 (▲), i/s = 30/70 (□) and i/s = 20/80 (●). The broken line represents log K_i vs. log v_i linear relationship for A4a fractured at the same experimental conditions.

toughness of the blend compared with the toughness of the s-PMMA component (MMW or A.4a). It can be seen from the log K_c vs. log v diagram of the corresponding s-PMMA component that the slope of the log K_c vs. log v straight line and the initial velocity, v_i, are larger than for the blend. For example, for the blend (MMW + I.74) the slope of log K_c vs. log v straight line have a value of 0.07 (cf. 0.16 for MMW) and blends of i/s = 30/70 or 20/80 has values of v_i about one decade smaller than that of MMW (Fig.6.21). The same phenomena can also be observed for blend (A.4a + I.100). Consequently, a smaller slope and a slower initial velocity implies that the blend has an increased toughness in the presence of methanol compared to the single s-PMMA component. Examination of the craze initiation step of the blends revealed a visible whitening at the crack tip —— a phenomena also observed in high MW syndiotactic-like PMMA (Chapter 5), whereas the single s-PMMA component was always started by a single crack. Under the optical microscope, this whitened area is revealed as a multicraze zone from which a single craze subsequently develops in the craze propagation step.

The enhancement of the toughness by adding i-PMMA becomes more pronounced at higher testing temperatures. The s-PMMA component (MMW or A.4a) shows a rapid crack propagation at T = 40°C, whereas the corresponding blends behave similarly to high MW syndiotactic-like PMMA (e.g. HMW) of high fracture toughness, i.e. a whitened zone appears and then is arrested after growing 2 mm. These observations were recorded from the i/s ratios from 50/50 to 20/80 for (MMW + I.74) and from 50/50 to 30/70 for (A.4a + I.100).

The experimental evidence suggests that by blending with i-PMMA the fracture toughness of MMW or A.4a is increased to the level of very high MW syndiotactic-like PMMA. There exist two possibilities for the enhancement of the toughness: (a) the effect of high MW i-PMMA, and (b) the SINC at the crack tip by methanol.

The high MW of the isotactic component is unlikely on its own to induce the increased toughness and the following experiment confirms this proposal. The fracture toughness results obtained from the blend (LMW + I.100)* (i/s = 40/60) composed of low MW components reveals a slow craze growth and similar log K_c vs. log v data at T = 20°C and 40°C to those of blends (MMW + I.74) and (A.4a + I.100) at the same i/s ratio. Thus, the SINC at the crack tip can be considered as a sole mechanism for the toughness enhancement. However, before discussing the details of the proposed mechanism it is necessary to consider the evidence for the existence of crystallites at the tip. Various direct methods were considered such as X-ray diffraction or electron diffraction. Not only is it difficult to examine the very small volume at the tip by these methods but SEM studies have already shown (Chapter 5) that rapid degradation of the polymer occurs under an electron beam.

The following alternative method was adopted. A sheet specimen for fracture test was subjected to SINC in methanol at T_{cr} = 40°C. The specimen was then dried in vacuum at 40 to 50°C for several days before testing. This pre-crystallized sheet of i/s-PMMA blend was tested in methanol at the same experimental conditions (i.e. at the same K_i, and temperature) with amorphous i/s-PMMA blend. As expected, the amorphous and pre-crystallized i/s-PMMA of the same i/s ratio gave identical log K_c vs. log v results.

Admittedly, one would like to have more positive evidence of the existence of crystallinity at the tip but without proof to the contrary, the mechanism involving SINC at the crack tip appears to be the most satisfactory. Any increase in solvent diffusivity near the tip caused by the high hydrostatic tension or increasing

* LMW shows rapid crack propagation from T = 0 to 40°C (Chapter 5) and I.100 has M_w = 35,000.

temperature would encourage the SINC at the tip. The crystalline stereocomplexes formed by SINC will act as pseudo-crosslinks by linking chain segments together reducing the slippage of molecule chains and thus stabilizing craze formation.

A similar phenomena can be observed in the log K_c vs. log v relationship of amorphous blend (PMMA + PVF_2) (Fig.6.23) in methanol. The ability of SINC by methanol of PVF_2 (Fig.6.11) suggests that the existence of crystalline PVF_2 phase at the tip will enhance the fracture toughness of the blend. As the amount of PVF_2 increases, a higher crystallinity will be achieved and this will result in a higher fracture toughness. The toughness enhancement can be observed in Fig.6.23 where higher amount PVF_2 in the blend shows a slower initial velocity, v_i, and smaller slope in the log K_c vs. log v straight line. It is interesting to obtain the data for the blend of PVF_2 rich blend. Unfortunately, the ratio of PVF /PMMA = 30/70 is the limiting ratio for the DT geometry, the ratio with higher PVF_2 content did not show fracture under this geometry due to softness. Moreover, the application of LEFM to the blend of higher PVF_2 content must be exercised with great care.

Further supporting evidence for the effect of crystallization on the enhancement of the fracture toughness can be observed in natural rubber (T_g = -80°C) (18). Strained-induced crystallization is a well-known phenomenon in natural rubber. The specimen was extended at a given strain to induce crystallites at -26°C and tested at temperature below the glass transition temperature (T_g = -80°C) to measure the fracture stress. By this method, Andrews (18) has found that specimens exhibit brittleness for zero pre-extension but yield and ductility above 200% pre-extension.

Finally, it is of interest to note that the toughness enhancement by crystallization contrasts with the ESC in nylons by zinc chloride and other inorganic salt solution (175). In this

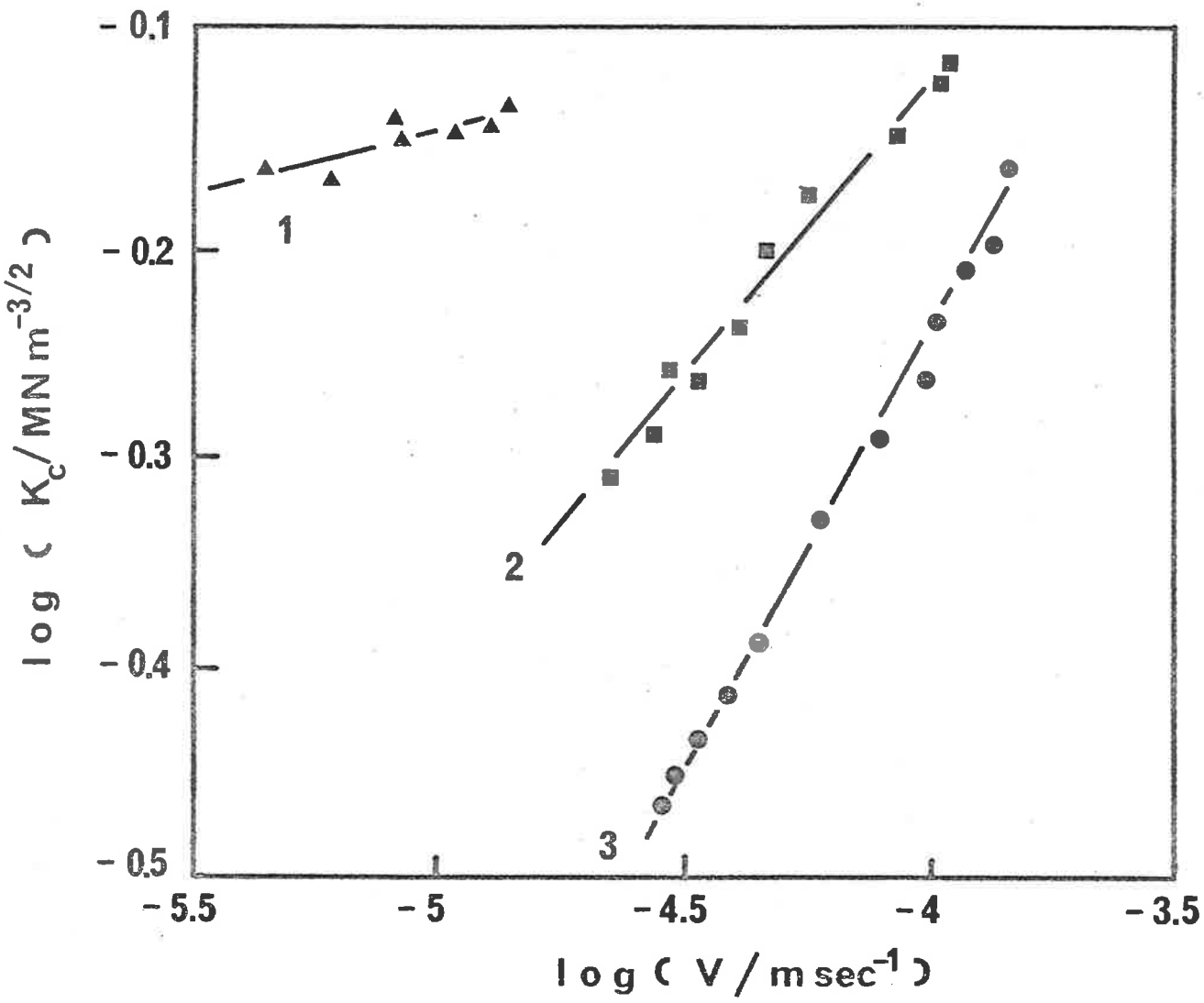

Fig.6.23 Plot of log K_c vs. log v for amorphous blend (PMMA + PVF_2) fractured in methanol at T=30°C. Ratios PVF_2/PMMA by weight are 30/70 (▲), 15/85 (■) and PMMA only (●).

system, the formation of a complex between the amide group of nylon and the solvated metal halide destroys the intermolecular hydrogen bonding network replacing it with intramolecular hydrogen bonding. The deficiency in intermolecular forces causes the complexed nylon to become more susceptible to ESC.

6.4 Conclusions

The following conclusions can be drawn.

(1) Higher tacticity components of i/s-PMMA blends are required to produce crystallinity by TINC than is required by SINC.

(2) The highest percentage crystallinity (35%) is produced by SINC from blends of high tacticity components with i/s ratio of 1/2.

(3) The different T_m of the crystallites from SINC at different crystallization temperature, T_{cr}, is attributed to the size of the stereocomplexes, whereas the higher T_m of crystallites from TINC as compared to T_m of crystallites from SINC indicates a difference in the internal crystal structure of the stereocomplexes induced by the two processes.

(4) Addition of i-PMMA to s-PMMA results in a new approach of modifying s-PMMA. The blend has a higher fracture toughness than the s-PMMA component in the presence of methanol. The enhancement of the fracture toughness is attributed to the SINC at the crack tip which produces crystallized stereocomplexes stabilizing craze formation.

CHAPTER 7

FURTHER COMMENTS ON THE EFFECT OF MOLECULAR WEIGHT, MOLECULAR WEIGHT DISTRIBUTION AND STEREOREGULARITY ON FRACTURE BEHAVIOUR

The prime aim of predicting the effect of polymer molecular properties on fracture behaviour and modifying the fracture toughness of PMMA has been satisfactorily achieved in this work. The fracture toughness vs. entanglements relationship is the key factor in understanding the mechanism of cracking and crazing in PMMA.

Current thinking is that the fracture toughness can be well correlated with the glass transition temperature of the plasticized crack tip, T_{sg}, or with the solvent solubility parameter, δ_s. The fracture toughness and T_{sg} (or δ_s) apparently shows a good relationship for most of amorphous polymer in various organic liquids, but it fails to interpret the MW, MWD and stereoregularity effects on the fracture toughness.

The intention is to clarify the deficiency of the fracture toughness vs. T_{sg} (or δ_s) correlation and to make further comments on the fracture toughness vs. entanglements correlation with supporting experimental evidence from a scanning electron microscopy (SEM) morphology study of the fracture of high MW PMMA in good solvents and i/s-PMMA blends.

The first well-documented study on the role of organic liquids in the crack/craze initiation of amorphous polymers can be attributed to Benier and Kambour (8). These authors investigated the effect of a wide range of organic liquids on stress-cracking or stress-crazing of poly(2,6-dimethyl-1,4-phenylene oxide) and

suggested two useful correlations exist between the critical strain*, ε_c vs. T_{sg} or ε_c vs. δ_s to predict the cracking or crazing behaviours. Benier and Kambour (8) found that the two correlations ε_c vs. T_{sg} and ε_c vs. δ_s are equivalent. The critical strain, ε_c, increases linearly with T_{sg} and shows a minimum at δ_s having a value close to δ_p, the polymer solubility parameter (i.e. at $|\delta_p - \delta_s| = 0$). Following Benier and Kambour, several other authors have related fracture mechanics parameter (e.g. K_c) with δ_c for PMMA (129), polystyrene and glass-filled polystyrene (128). Similarly to ε_c vs. δ_s correlation, the fracture toughness vs. δ_s correlation also shows a minimum of the fracture toughness at $|\delta_p - \delta_s| \simeq 0$.

The critical strain, ε_c, was a criterion for craze initiation which had been proposed for testing on unnotched specimens for some time before the LEFM concept was applied to polymers. However, because of variations in the inherent flaw sizes, there exists large scattering of the final craze length and the propagation velocities impeding accurate measurement of ε_c. Furthermore, in contrast to the SIF, K_c, the critical strain ε_c, does not represent the toughness of materials. Therefore, it is preferable to use K_c rather than ε_c to indicate the cracking or crazing behaviour in correlation with T_{sg} or δ_s.

It is tedious to measure the T_{sg} of a solvent equilibrated polymer film (see Chapter 4) and the fracture toughness vs. δ_s

* The critical strain, ε_c, is obtained by bending a rectangular sheet specimen on a three-point jig. The jig is then placed in a selected solvent and after a fixed time the separation of the craze boundaries is measured. The critical strain can be determined from the initial maximum strain and the length between two craze boundaries. Strictly speaking, ε_c is not a measure of fracture toughness but rather a quantity below which neither crack nor craze can be initiated. In this sense, although there is no direct theoretical relationship between fracture toughness and ε_c, the two quantities express the common characteristics —— the resistance of material to fracture.

correlation is a simple alternative expression of the fracture toughness vs. T_{sg} correlation. The equivalence of the two correlations relies on the fact that as the solvent solubility parameter, δ_s, approaches the polymer solubility parameter, δ_p, the more solvent will be absorbed and the larger the depression of the glass transition temperature. However, while the fracture toughness vs. T_{sg} correlation appears as a universal representation for both polar and non-polar liquids, the fracture toughness vs. δ_s correlation needs modification for the case of polar liquids. Vincent and Raha (9) suggested a more effective representation for stress-crazing and stress-cracking of the polymer by considering both the capacity of each liquid to hydrogen bond and the solubility parameter. These authors have applied the two-parameter representation (the hydrogen bonding parameter and the solubility parameter) to predict the cracking/crazing behaviours of PMMA, polyvinylchloride and polysulphones.

Although there have been many attempts at improving these physical parameter correlations, none of these approaches including the so-called "indisputable" T_{sg} correlation (a phrase used by Kramer (21)) can explain the effect of MW and temperature on the fracture toughness, and the enhancement of the toughness by blending i-PMMA with s-PMMA. Prior to pointing out the deficiency of these approaches, it is important to understand the physical significance of the solubility parameter.

Hildebrand (176) defined the solubility parameter of solvent, δ_s, as

$$\delta_s = \left(\frac{\Delta E_v}{V_s}\right)^{\frac{1}{2}} \qquad (7.1)$$

where ΔE_v = the energy of vaporization of solvent

V_s = the molar volume of solvent

$\frac{\Delta E_v}{V_s}$ = the energy of vaporization per unit volume or the cohesive energy density.

Hildebrand's equation can be applied to polymers where the solubility parameter, δ_p, is the solubility parameter of each segment of the polymer chain. The square of the difference $|\delta_s - \delta_p|$ is proportional to the enthalpy of interaction between one polymer segment and one solvent molecule (52). In the Flory-Huggins theory, the square of $|\delta_s - \delta_p|$ is related to χ_H by

$$\chi_H = \frac{V_s}{RT} (\delta_s - \delta_p)^2 \qquad (7.2)$$

where χ_H = the enthalpy term of Flory's polymer segment-solvent interaction parameter, χ (52).

The hydrogen bonding parameter as suggested by Vincent and Raha (9) in their two-parameter representation is independent of polymer chain length. Consequently, while the solubility parameter and the hydrogen bonding parameter are by definition independent of MW and stereoregularity, the crazing in high MW PMMA and the cracking in low MW PMMA occurring in the same experimental conditions, clearly indicates the failure of these approaches in predicting the fracture behaviour in organic liquids.

The "indisputable" T_g correlation also becomes uncertain in the light of this work. It was known from Chapter 4 that the T_{sg} of methanol equilibrated low MW PMMA is 5 to 10°C lower than that of methanol equilibrated high MW PMMA. However, according to Benier and Kambour's T_{sg} correlation, this small difference in T_{sg} is not expected to give a large drop in fracture toughness as observed from experiments (Chapter 5). The fracture toughness vs. T_g correlation also fails to account for the large decrease in the

fracture toughness of MMW in methanol when the testing temperature, T_{test}, increased from 30°C to 40°C (Fig.5.33). Increasing the T_{test} from 30°C to 40°C will result in an approximate ten degree decrease in T_{sg} (60), but this does not coincide with a large drop in the fracture toughness in the T_{sg} correlation. Furthermore, as known from the fracture data of the i/s-PMMA blends (Chapter 6, blend (MMW + I.74) for example) the fracture toughness in methanol (T_{test} = 20°C) is larger than that of the s-PMMA component (MMW) although the T_{sg} of blend and MMW are close to each other.

The conventional approaches face a dilemna in attempting to explain the effect of MW, MWD and stereoregularity on the fracture toughness because these approaches consider plasticization of polymers and subsequent depression of the glass transition temperature as the only phenomena occurring at the crack tip and failed to develop a satisfactory molecular mechanism involving the molecular properties of polymers.

As discussed in previous Chapters, fracture behaviour of PMMA can best be explained by the fracture toughness vs. entanglement correlation by taking into account (a) the entanglement density as a function of MW, (b) the disentanglement of polymer chains by solvent under high stress, and (c) the reinforcement of entanglement networks by crystallites. The reduction of entanglement density caused by absorbed solvent is attributed to an increase in the MW between entanglement loci, M_e. In a good solvent, in particular, the dissolution at the tip region results in an infinite M_e (zero entanglement density) and this will encourage a rapid disentanglement process at the crack tip leading to a rapid crack growth. This fracture behaviour can be understood by the following fracture test in good solvents of high MW PMMA (HMW) and by the study of fracture morphology.

In methanol, high MW PMMA such as HMW has a long craze growth and shown a honeycomb craze fracture surface (Fig.5.22). In a good solvent (e.g. butyl acetate or THF), on the other hand, HMW fractured with a rapid crack propagation in a manner analogous to the cracking of low MW PMMA in methanol and the fracture morphology of HMW in a good solvent has a mirror-like surface (similar to Fig.5.24 of LMW / methanol). The similarity between the fracture mechanism of HMW/THF and LMW/methanol suggests that there is no contribution from entanglement networks at the crack tip of HMW in good solvent during cracking. By dissolving the bulk material at the crack tip, the good solvent facilitates rapid disentanglement under stress leading to the de-stabilization of the craze.

The effects of the de-stabilization of the craze by solvent can be observed from another examination of the fracture surface of HMW cracked/crazed in a mixture of iso-propanol and methylethylketone (MEK) (1:1 by volume). PMMA and iso-propanol/MEK mixture (1:1) has a LCST at T = 25°C (53), so above this temperature, the polymer-solvent system is miscible in all proportions and below this temperature, phase separation will occur. By changing the temperature, the solvating power of the mixture can be varied to become a good solvent for the polymer at temperature above 25°C or a poor solvent at temperature much lower than 25°C. That is, if the temperature is far above 25°C the solvent mixture diffusing into bulk PMMA dissolves the tip zone. The dissolution of bulk material at the crack tip causes the collapse of the entanglement networks and thus allows rapid crack propagation. This cracking behaviour was observed at T = 40°C exactly in the same manner as in THF. The fracture surface is completely featureless surface under SEM. On the other hand, if the temperature is below 25°C, diffusion of the solvent mixture only partly disentangles the network and the

remaining entanglements enable the formation of stable craze. Figs. 7.1-7.2 show the fracture surface at T = 20°C and T = 5°C with the appearance of a "white" craze pattern that is reminiscent of the fracture surface from MMW/methanol at T = 20°C (Fig.5.25). It is further noted that at T = 5°C the decay of applied was much slower than with an initial velocity, $v_i \sim 10^{-2}$ msec^{-1} compared to $v_i \sim 10^{-4}$ msec^{-1} at T = 40°C.

In contrast, the stereocomplex formation in i/s-PMMA blend can be regarded as reinforcement of the entanglement network. As a good solvent, acetone is a cracking agent to PMMA and a featureless fracture surface of a LMW sample is shown in Fig.7.3 as evidence. However, as a strongly complexing solvent, acetone promotes the co-crystallization in i/s-PMMA. The crystallites act as pseudo-crosslinks preventing rapid disentanglement and thus promoting the craze formation (Fig.7.4). The amount of crystallinity induced in the same blend by toluene (a weakly complexing solvent) is not sufficient to support craze formation, therefore the fracture morphology in this solvent show typical smooth cracking surface (Fig.7.5).

Further to the experimental observations in Chapter 5, the above results concerned with the effect of organic liquids on the fracture mechanism in high MW PMMA and in i/s-PMMA blend again confirm that the fracture toughness of materials is direclty related to the craze formation which strongly depends on the number of entanglements existing in the bulk as well as in the craze fibrils. Therefore the fracture toughness or the critical strain is fundamentally correlated with the entanglements rather than with the glass transition temperature or the solubility parameter of the conventional concept. The following charts present a summary of Chapter 5, Chapter 6 and this Chapter.

Fig.7.1 "White" craze pattern appears on fracture surface of HMW in iso-propanol-MEK mixture at T=20°C. 500x.

Fig.7.2 More craze formation is observed on fracture surface of HMW in iso-propanol -MEK mixture at T=5°C, 500x.

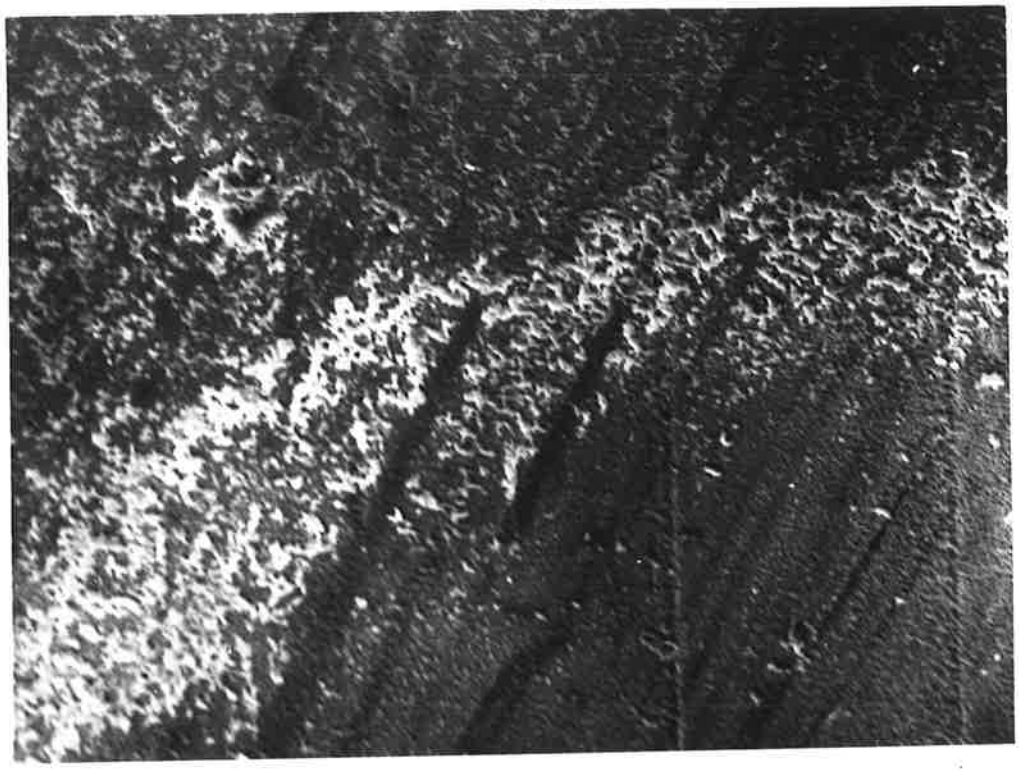

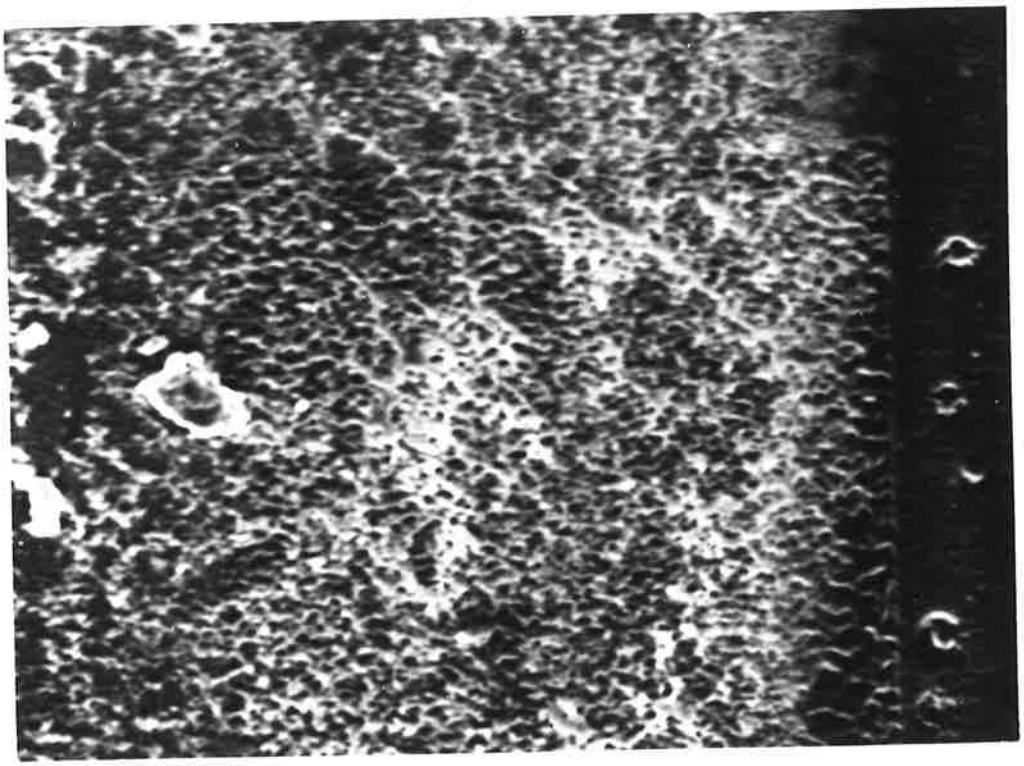

Fig.7.3 Mirror-like fracture surface of LMW in acetone at T=20°C, 100x.

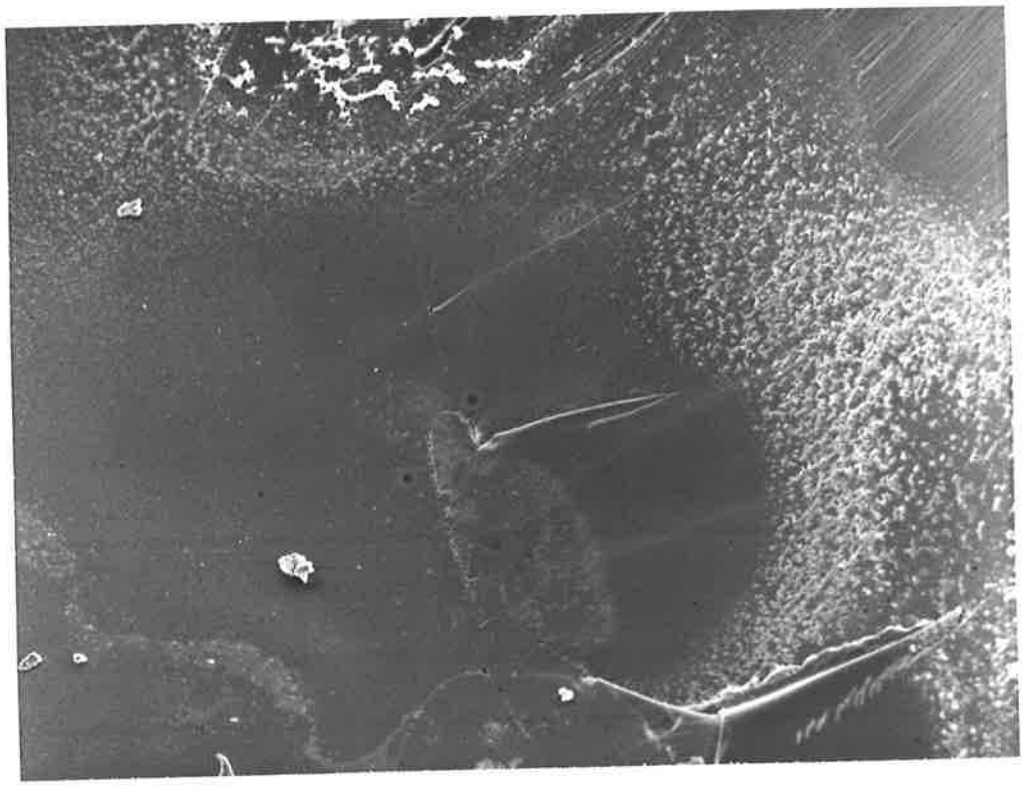

Fig.7.4 Fracture surface of (LMW + I.100) blend (i/s = 40/60) in acetone at T=20°C. (a) 100x (b) 500x.

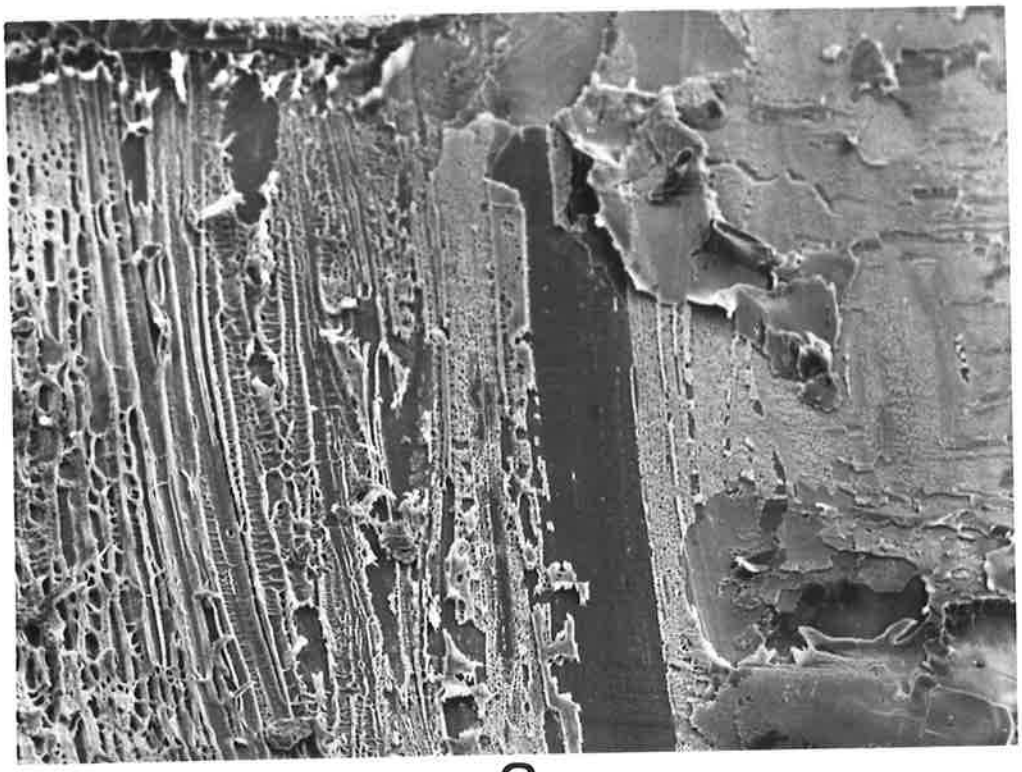

a

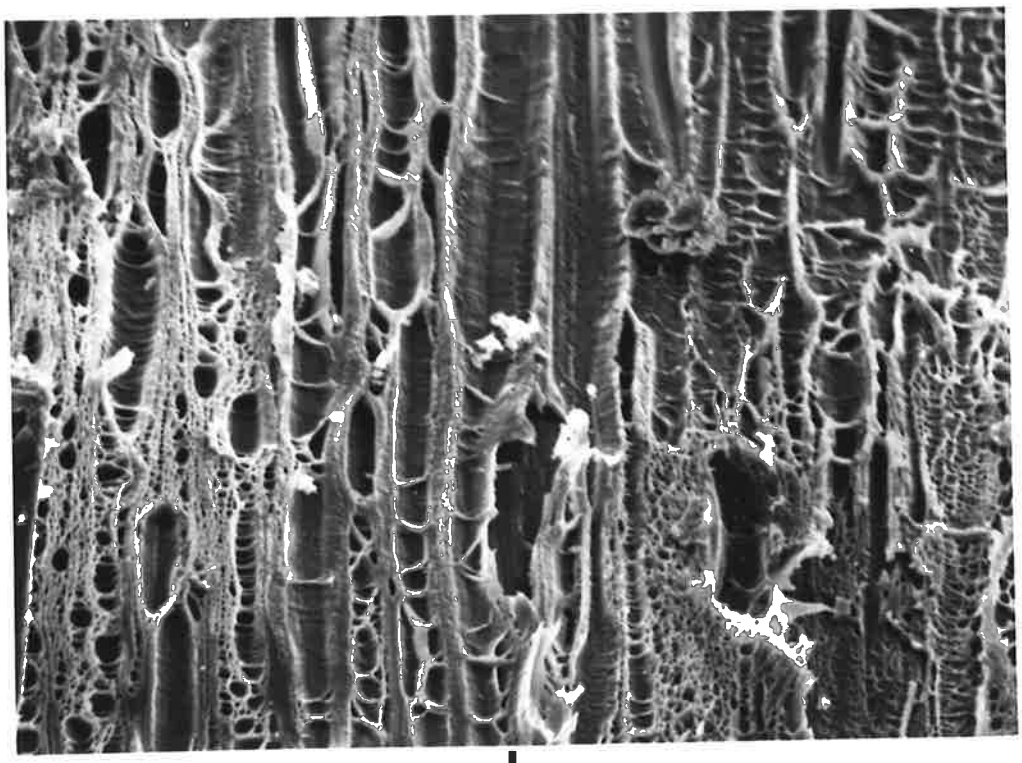

b

Fig.7.5 Fracture surface of (LMW + I.100) blend (i/s=40/60) in toluene at T=20°C, 100x.

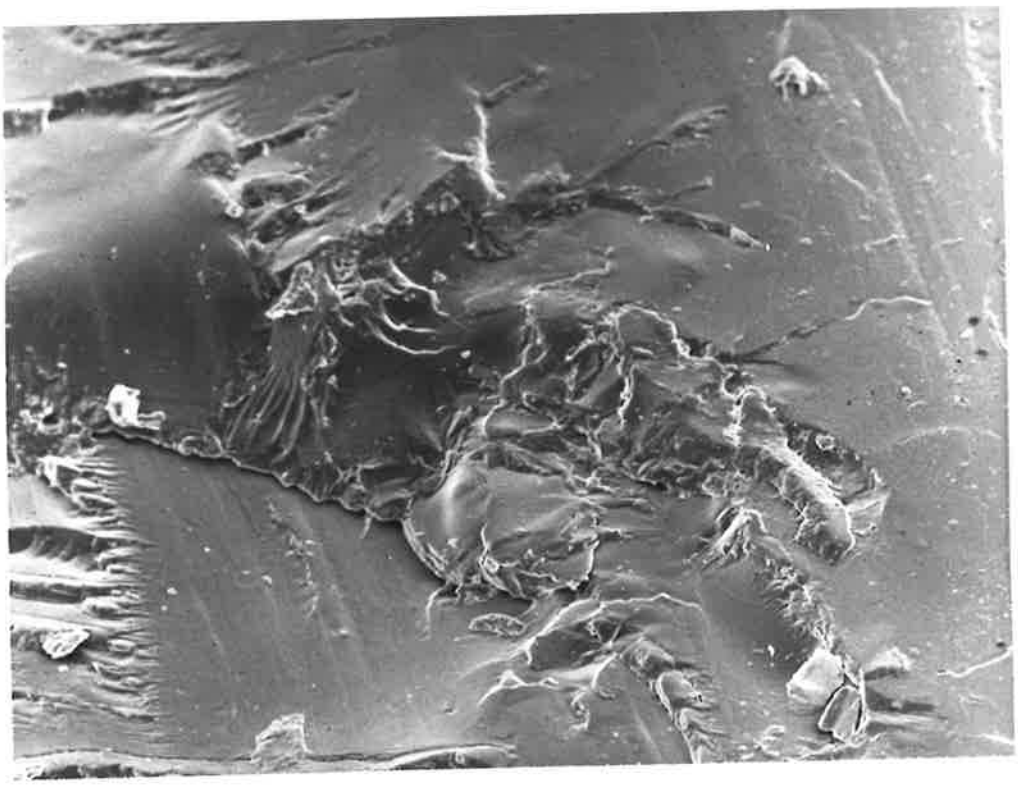

IN METHANOL

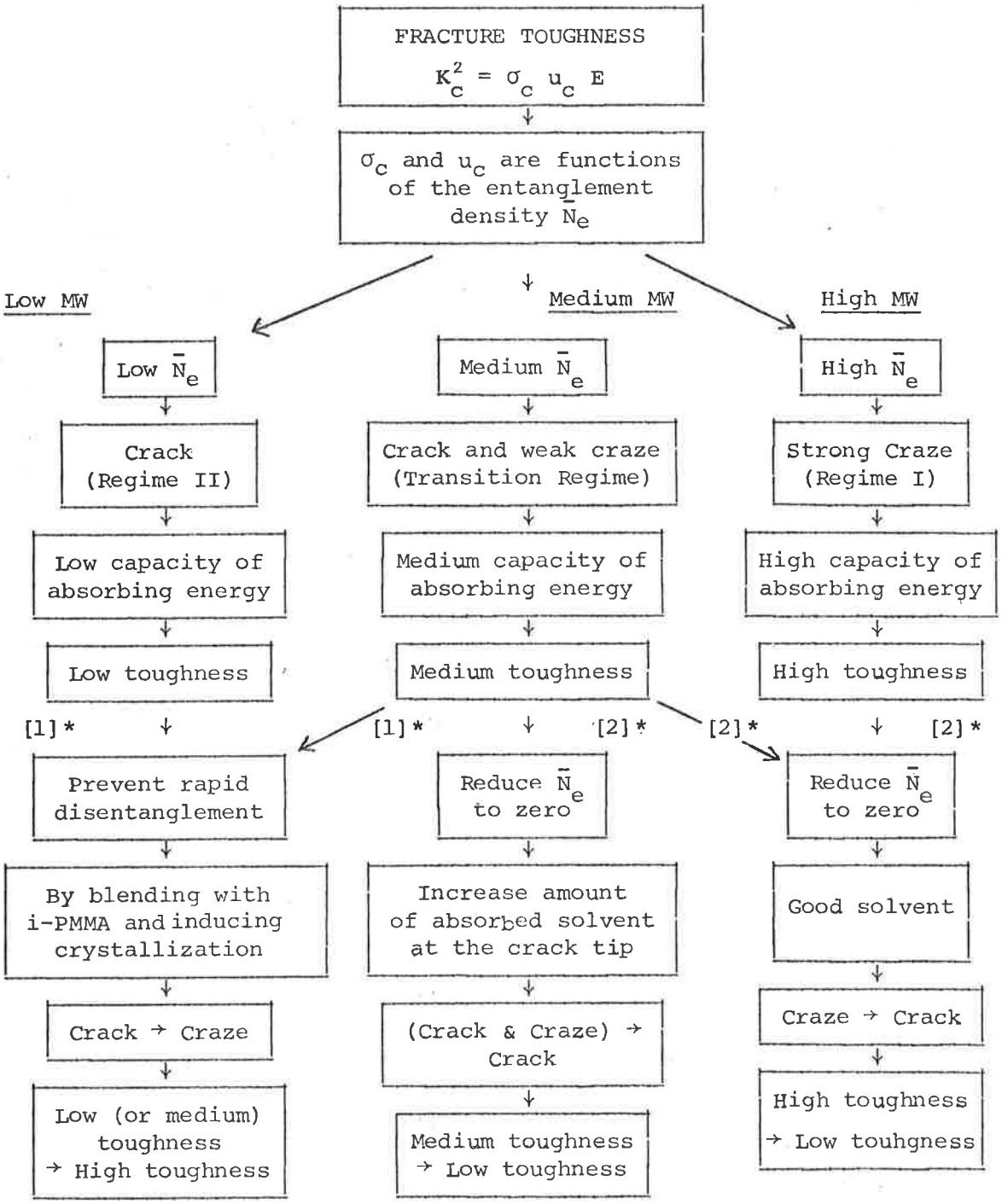

*[1] ≡ Reinforcement of entanglement networks,
[2] ≡ Acceleration of disentanglement process

IN AIR

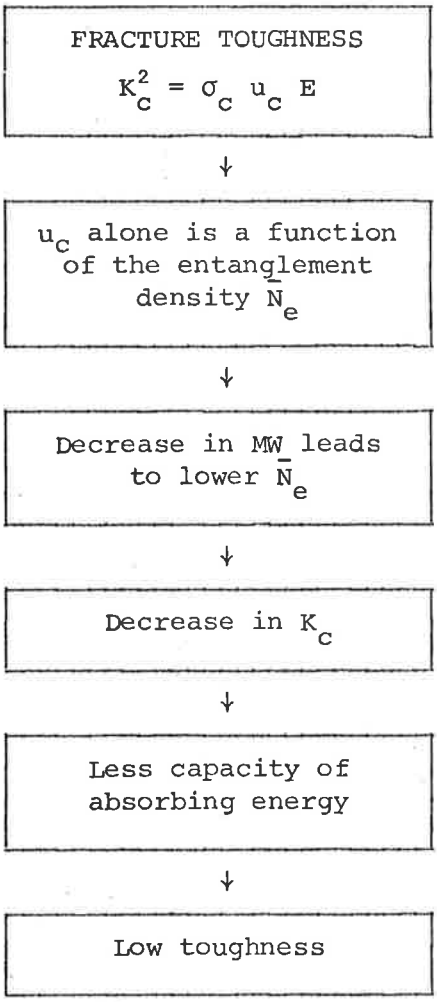

Over the last few decades there has been a constant endeavour to improve the understanding of the nature of entanglement coupling. The development of theories concerning this subject has been extensively reviewed by Ferry (67) and by Graessly (177). Because the main theme of this work has dealt with the entanglement concept, it is worthwhile to examine alternative descriptions of this concept before closing this Chapter. Hitherto, polymer entanglement networks have been customarily regarded as a system of rope-like entangled knots (loops, kinks etc.) at a number of points along the molecule chain. This model has been successfully used to explain the transition of the MW dependence of viscosity, η, in

polymer melts or solutions from $\eta \propto M$ (for $M < M_c$) to $\eta \propto M^{3.4}$ (for $M > M_c$), Bueche (71) has argued that the critical MW, M_c, characterizes the onset of entangled behaviour where the high MW dependence of viscosity in the range of $M > M_c$ is due to the dragging of one molecule by another leading to enhanced friction at the coupling points. While the rope-like entangling of chains has provided a satisfactory explanation for many polymer rheological properties, the nature of entanglement coupling is still open to speculation. The coupling has been arbitrarily regarded as a temporary coupling, a local kink or a long-range contour loop. This ill-defined nature of entanglement coupling leads to the more general concept for an "entangled" system in which movement of a given polymer is constrained by the topological effect at the points of entanglement or intersection of adjacent chains.

De Gennes (178) proposed that the motion of polymer molecules in a concentrated solution could be regarded as a snake-like (reptative) movement in a tube constraint. The tube is defined by the locus of the constraint imposed on motion of a given polymer chain by the other chains. Using this model, Klein (179) concluded that for semidilute and concentrated solutions the critical point at $M = M_c$ which represents the onset of entanglement in Bueche's description is the transition point from a free movement of polymer chains to constraint reptative movement of polymer chains. Bueche's classical picture of the transition from $\eta \propto M$ dependence to higher MW dependence, $\eta \propto M^{3.4}$ at the critical MW, M_c ($\simeq 2\ M_e$), can now be replaced by a more realistic view where the entanglement effect spreads along the length of the molecule, resulting in the reptative movement of the whole polymer chain. Although de Genne theoretically predicted $\eta \propto M^3$ (180) for the high MW range which is not in precise agreement with dependence of viscosity on MW, his

revolutionary model of the reptative movement of polymer chain, being probably the best model for describing the nature of entanglement "coupling", may foreshadow a leap forward in the development of the molecular theory of polymer rheology (181).

The treatment of the entanglement in this work is undoubtedly still in the framework of classical thinking. The central point of the treatment lies in the relationship between the fracture toughness and the entanglement density (the disentanglement process). However, in the light of de Genne's reptative model, the entanglement density $\tilde{N}_e$ and the characteristic MW, M_e or M_c, still play crucial roles in determining the dimension of the constraint tube for the reptative polymer chains. It is customary to consider craze fibrils as an extended entanglement network, stabilizing the craze by "hooking" together at entanglement loci. If de Genne's reptative model is fully verified by experiments, the new concept of entanglement may pose the question as to whether the restricted reptative movement is the main mechanism of the stabilization of the craze fibril. However, any attempt to answer this question awaits basic information on the existence of the reptative movement of chain molecules in polymer melts and solutions.

CHAPTER 8

RESEARCH TOPICS FOR FURTHER DEVELOPMENT

The mechanism of cracking and crazing in polymers requires an understanding of the stabilization and the failure processes of craze fibrils on the microscopic level. The study of the effect of molecular properties on the fracture toughness of PMMA in this work has clearly pointed out the important role of the entanglement concept on the molecular aspects of the fracture mechanism. However, there are some matters that arose during the investigation that would make fitting topics for further research.

(1) Application of particle scattering, X-ray diffraction or holographic interferometry to the observation of the front tip region to improve the understanding of the craze structure. For example, determination of the stress profile of crazing stress which could be done by holographic interferometry would aid the appreciation of the short craze growth behaviour in high MW PMMA and i/s-PMMA at high temperature in methanol.

(2) The rheological properties of polymer melts or solvent-equilibrated polymers under tensile stress is a key factor in understanding the mechanism of craze stabilization. A macroscopic test on the elongation of solvent-equilibrated polymer rod sample could provide basic information on the fracture process of the craze fibrils.

(3) The kinetics of disentanglement and the kinetics of crystallization under stress directly influence craze stabilization and therefore the fracture toughness of material. A kinetic study would increase our knowledge of the craze formation and the propagation velocity of the tip.

Some further problems that were noticed during the project but are of a more indirect nature are listed below:

(1) Study of the limit of the application of LEFM concept to the fracture process of polymers.

(2) Cavitation which occurs when PMMA is immersed in methanol. It has been suggested that phase inversion is a possible cause but this needs to be substantiated.

(3) The broad T_g of i/s-PMMA blends revealed the semicompatible nature of the blend. To what degree of tactic randomness in atactic PMMA will show an incompatible blend with i-PMMA and how the incompatibility will affect the fracture toughness.

(4) The study of the physical properties and the fracture toughness of i/s-PMMA blends has shown that the blend has distinct properties from its constituents. It would be interesting to extend this study to the case of stereoblock PMMA of iso- and syndio-tactic blocks where the competition between the crystallization of iso-iso, syndio-iso and syndio-syndio could be observed. This possibility, however, still requires a well-controlled method of sample preparation.

APPENDICES

APPENDIX 1

Viscometry Measurement

The Ubbelohde type viscometer has a distinct advantage over others in that measurement is independent of the amount of solution in the viscometer. The flow time is kept long (more than 100 sec) to minimize the error in timing the flow. The time counter is accurately controlled by two-light beam, set at an upper limit and at a lower limit. This viscometer allows the measurement at a series of concentrations to be easily made by successive dilution.

The measurements were made at a constant temperature of 24.94 ± 0.02°C. All solvents and solutions introduced into the viscometer were filtered through a sintered glass filter in order to avoid blockage of the viscometer capillary. After measurement of one solution was finished the viscometer was washed with solvent and then acetone before drying by a water pump.

At every concentration, at least three runs were made and the results shown are average values.

Viscometric runs of MG sample

t	c(g/100cc)	$\ln \eta_r/c$	η_{sp}/c
115.499	0		
121.234	0.218	0.2223	0.2277
120.280	0.182	0.2228	0.2274
119.595	0.156	0.2232	0.2272
119.066	0.136	0.2236	0.2270
118.670	0.121	0.2238	0.2268
118.353	0.109	0.2239	0.2266

Plot of $\ln \eta_r/c$ vs. c gives

Intercept = 0.2256

Slope = -0.01528

Plot of η_{sp}/c vs. c gives

Intercept = 0.2256

Slope = 0.009762

Hence, $(\eta) = 0.2256$ and $k' + k'' = 0.49$

APPENDIX 2

Methanol-Equilibrated PMMA Density and Molecular Weight between Entanglement Loci

The relationship between polymer density, ρ_p, and methanol equilibrated polymer density, ρ_s, are

$$\rho_s = \frac{m_p + m_d}{V_p + V_d} \qquad \text{(A2.1)}$$

where m is the mass at equilibrium absorption and V is the volume. The subscripts d and p identify the diluent and polymer, respectively. Rewriting Eq.A2.1 gives

$$\rho_s = \frac{m_p + m_d}{\frac{m_p}{\rho_p} + \frac{m_d}{\rho_d}} \qquad \text{(A2.2)}$$

where ρ is the density, $\rho_p = 1.18$ and $\rho_d = 0.80$ for methanol. At equilibrium uptake (T = 20°C), $W_1/W_2 = 0.22$, that is

$$W_p = \frac{m_p}{m_p + m_d} \qquad \text{(A2.3)}$$

$$= \frac{100}{100 + 22} = 0.82$$

Combining Eqs. A2.2 and A2.3 gives

$$W_p \rho_s = \left(\frac{m_p}{m_p + m_d}\right)\left(\frac{m_p + m_d}{\frac{m_p}{\rho_p} + \frac{m_d}{\rho_d}}\right) \qquad \text{(A2.4)}$$

$$= \frac{100}{\frac{100}{1.18} + \frac{22}{0.80}} = 0.89$$

The MW between entanglement loci, M_e, is expressed by

$$M_e = \frac{3 g_N (W_p \rho_s) RT}{E^\circ_{eN}}$$

$$= \frac{3 \times 1 \times 0.89 \times 8.314 \times 10^7 \times 316}{3.72 \times 10^6}$$

$$M_e \simeq 19{,}000$$

where $\rho_s = 1.09$ (at $W_1/W_2 = 0.22$)

APPENDIX 3

Calculation of the Depression in the Glass Transition Temperature

A3.1 T_{sg}/T_{og} from Chow's equation (Eq.4.30)

$$\gamma = \frac{V_u}{ZV_d}\,\frac{\phi_d}{1-\phi_d}$$

$$= \frac{106.51}{2\text{x}40.56} \text{ x } \frac{0.24}{(1-0.24)} = 0.415$$

$$\beta_c = \frac{ZR}{m_u\,\Delta C_{pp}}$$

$$= \frac{2\text{x}1.987}{100.12\text{x}0.07} = 0.567$$

Substituting γ and β_c values into Eq.4.30 gives

$$\frac{T_{sg}}{T_{og}} = 0.680$$

A3.2 T_{sg}/T_{og} from FH equation (Eq.4.34)

From the absorption data at T = 20°C the weight gain W_1 at equilibrium to the original weight of polymer W_2 is $W_1/W_2 = 0.22$ (i.e. $\phi_p = 0.76$ and $\phi_d = 0.24$). Let the original weight, W_1, be 1 g, then the weight of methanol will be 0.22g. Substituting into Eq.4.34 by using MW of methanol, $M_d = 32.04$ g mol^{-1}, $\Delta C_p = 1\text{x}\Delta C_{pp}$ = 0.07 cal deg^{-1}, we obtain

$$\ell n \left(\frac{T_{sg}}{T_{og}}\right) = \frac{1.987}{0.07}\left(\frac{0.22}{32.04}\,\ell n\ 0.24 + \frac{1}{M}\,\ell n\ 0.76\right)$$

where M = MW of PMMA. Hence,

$$\frac{T_{sg}}{T_{og}} = 0.757 \quad \text{for} \quad M = 500{,}000 \text{ and } 30{,}000$$

APPENDIX 4

Calculation of the Fracture Energy, γ_c, at various Molecular Weight Distributions

The energy γ_{c_2} is expressed by

$$\gamma_{c_2} = \gamma(\infty) \left(1 - \frac{M_c}{M_n}\right) S \qquad \text{(A4.1)}$$

where $\gamma(\infty) = 3 \times 10^2$ J m^{-2} and $M_c = 30{,}000$. The factor S is given by

$$S = \int_{\ln M_c}^{\infty} W(\ln M)\, d \ln M \qquad \text{(A4.2)}$$

where

$$W(\ln M) = \frac{\exp[-(\ln M - \ln M_p)^2]/2\sigma_D^2]}{2\sqrt{\pi}\,\sigma_D} \qquad \text{(A4.3)}$$

For PMMA, the energy γ_{c_1} is of the form

$$\gamma_{c_1} = 0.0068\, M_w^{\frac{1}{2}}$$

TABLE A4.1: $M_w/M_n = 2$, $\sigma_D = 0.832$

$M_n \times 10^3$	$M_w \times 10^3$	$M_m \times 10^3$	S	$(1-M_c/M_n)$	γ_{c1} (Jm^{-2})	γ_{c2} (Jm^{-2})	γ_c (Jm^{-2})	log γ_c
40	80	56.4	0.776	0.25	1.9	58.2	60.1	1.78
70	140	98.9	0.923	0.57	2.5	157.8	160.3	2.20
200	400	282.0	0.996	0.85	4.3	254.0	258.3	2.41
1000	2000	1411.0	1.0	0.97	9.6	300.0	309.6	2.49

TABLE A4.2: $M_w/M_n = 4$, $\sigma_D = 1.177$

$M_n \times 10^3$	$M_w \times 10^3$	$M_m \times 10^3$	S	$(1-M_c/M_n)$	γ_{c1} (Jm^{-2})	γ_{c2} (Jm^{-2})	γ_c (Jm^{-2})	log γ_c
40	160	80	0.797	0.25	2.7	59.8	62.5	1.78
70	280	140	0.905	0.57	3.6	154.7	158.3	2.20
200	800	400	0.986	0.85	6.1	251.4	257.5	2.41
1000	4000	2000	1.0	0.97	13.6	300.0	313.6	2.49

APPENDIX 5

Derivation of Storage Shear Modulus, Loss Shear Modulus and Loss Tangent

The equation of motion of free oscillation torsion pendulum is

$$I \frac{d^2y}{dt} + K (G' + iG'') y + R G_w y = 0 \qquad (A5.1)$$

where I = moment of inertia, y = angle of twist, G_w = shear modulus of the suspension wire, G' = storage shear modulus, G" = loss shear modulus.

The constant, K, involving geometric factors is expressed by

$$K = \frac{\mu b h^3}{16 \ell} \qquad (A5.2)$$

where b = width, h = thickness and ℓ = length of specimen, μ = shape factor.

The constant R, geometric factor of the suspension wire, is given by

$$R = \frac{\pi r^4}{2 \ell_w} \qquad (A5.3)$$

where r = radius of the wire and ℓ_w = length of the wire.

The solution of Eq. A5.1 is

$$y = y_o \exp (i\omega - \rho)t \qquad (A5.4)$$

where ω = angular frequency of oscillations and ρ = attenuation factor.

From Eqs.A5.1 and A5.4, we obtain

$$G' = I (\omega^2 - \rho^2)/K - R G_w/K \qquad (A5.5a)$$

$$G'' = 2 I \rho\omega/K \qquad (A5.5b)$$

and

$$\rho = \Delta\omega/2\pi \qquad (A5.5c)$$

where Δ = logarithmic decrement.

If the sample is removed from the pendulum it will oscillate at a frequency given by

$$\omega_o^2 = \frac{R\, G_w}{I} = \left(\frac{2\pi}{P_{or}}\right)^2 \qquad \text{(A5.6)}$$

where P_{or} = period of one oscillation when the sample is removed.

Eq.A5.6 gives

$$G_w = \frac{4\pi^2 I}{R P_{or}^2} \qquad \text{(A5.7)}$$

Combining Eqs. A5.5a,b,c and A5.7 we obtain

$$G' = \frac{4\pi^2 I}{P_r^2\, K}\left(1 - \left(\frac{\Delta}{2\pi}\right)^2 - \left(\frac{P_r}{P_{or}}\right)^2\right) \qquad \text{(A5.8a)}$$

$$G'' = \frac{4\pi I \Delta}{K\, P_r^2} \qquad \text{(A5.8b)}$$

and loss tangent, tan δ, is expressed as

$$\tan\delta = \frac{G''}{G'}$$

$$= \frac{\Delta}{\pi} \Big/ \left(1 - \left(\frac{\Delta}{2\pi}\right)^2 - \left(\frac{P_r}{P_{ro}}\right)^2\right) \qquad \text{(A5.8c)}$$

REFERENCES

(1) J.P. Berry, J. Polym. Sci., A2, 4069 (1964).

(2) R.P. Kusy and D.T. Turner, Polymer, 17, 161 (1976).

(3) R.E. Robertson, ACS Polym. Symp. (1975).

(4) G.L. Pitman and I.M. Ward, Polymer, 20, 895 (1979).

(5) P. Beahan, M. Bevis and D. Hull, J. Mat. Sci., 8, 162 (1974).

(6) ibid, Proc. Roy. Soc. Lond., A343, 523 (1975).

(7) S. Wellinghoff and E. Baer, J. Macromol. Sci., B11, 367 (1975).

(8) G.A. Benier and R.P. Kambour, Macromolecules, 1, 393 (1968).

(9) P.I. Vincent and S. Raha, Polymer, 13, 283 (1972).

(10) R.P. Kambour, C.L. Gruner and E.E. Romagosa, J. Polym. Sci., Polym. Phys. Ed., 11, 1879 (1973).

(11) A.N. Gent, J. Mat. Sci., 5, 925 (1970).

(12) A.C. Knight, J. Polym. Sci., A3, 1845 (1965).

(13) N. Vernuelpen-Heymans, J. Polym. Sci., Polym. Phys. Ed., 14, 93 (1976).

(14) N. Verhuelpen-Heymans, J. Mat.Sci., 11, 7 (1976).

(15) G.P. Marshall, L.E. Culver and J.G. Williams, Plastics and Polymers, Feb, 75 (1969) and April, 95 (1970).

(16) ibid, Proc. Roy. Soc. Lond., A319, 165 (1970).

(17) J.G. Williams and G.P. Marshall, idem, A342, 55 (1975).

(18) E.H. Andrews, "Fracture in Polymers", Oliver and Boyd, London (1968).

(19) S. Rabinowitz and P. Beardmore, "Craze Formation and Fracture in Glassy Polymers", in Critical Reviews in Macromolecules Science, Vol.I, E. Baer ed., CRC Press, Chemical Rubber Co., Cleveland, Ohio (1972).

(20) R.P. Kambour, Macromolecule Rev., 7, 1 (1973).

(21) E.J. Kramer, in "Developments in Polymer Fracture", Vol.1, E.H. Andrews ed., Applied Science Publisher, London (1979).

(22) R.P. Kusy and M.J. Katz, J. Mat. Sci., 11, 1475 (1976).

(23) J.P. Berry, J. Polym. Sci., A1, 993 (1963).

(24) L.J. Broutman and F.J. McGarry, J. Appl. Polym. Sci., 9, 609 (1965).

(25) K.P. Kambour and R.R. Russell, Polymer, 12, 237 (1971).

(26) S.N. Zhurkov, Int. J. Fract. Mech., 1, 311 (1965).

(27) G.P. Marshall, L.H. Coutts and J.G. Williams, J. Mat. Sci, 9, 1409 (1974).

(28) R.F. Boyer and H. Keskkula, "Encyclopedia of Polymer Science and Technology", Vol.13, John Wiley and Sons Inc., New York (1970).

(29) J.F. Rudd, J. Polym. Sci., B1, 1 (1963).

(30) A.A. Griffith, Phil. Trans. Soc. (Lond.), A221, 163 (1920).

(31) E. Orowan, in "Proc. Symp. on Fatigue and Fracture", p.139, J. Wiley, New York (1952).

(32) (a) G.R. Irwin, J. Basic Eng., 82, 417 (1960).
(b) G.R. Irwin and A.A. Wells, Mat. Rev., 10, 223 (1965).

(33) J.G. Williams, Adv. Polym. Sci., 27, 67 (1978).

(34) e.g. J.F. Knott, "Fundamentals of Fracture Mechanics", Butterworths, London (1973).

(35) D.S. Dugdale, J. Mech. Solids, 8, 100 (1960).

(36) P.J. Flory, "Principles of Polymer Chemistry", p.336, Cornell, New York (1953).

(37) M. Szwarc, Nature, 178, 1168 (1956).

(38) T.G. Fox, B.S. Garrett, W.E. Goode, S. Gratch, J.F. Kincaid, A. Spell and J.G. Stroupe, J. Am. Chem. Soc., 80, 1968 (1958).

(39) D.J. Worsfold and S. Bywater, J. Polym. Sci., 26, 299 (1957).

(40) F. Wenger, Makromol. Chem., 36, 200 (1960).

(41) M. Morton, R. Milkovich, D.B. McIntyre and L.J. Bradley, J. Polym. Sci., A1, 443 (1963).

(42) A. Roig, J.E. Figueruelo and E. Llano, J. Polym. Sci., C16, 4141, (1968).

(43) P.E.M. Allen and B.O. Bateup, European Polym. J., 14, 1001 (1978).

(44) P.E.M. Allen, M.C. Fisher, C. Mair and E.H. Williams, ACS, Polym. Preprint, Houston Meeting (1980).

(45) B.O. Bateup, Ph.D. Thesis, University of Adelaide (1974).

(46) M.C. Fisher and C. Mair, unpublished data.

(47) J.C. Moore, J. Polym. Sci., A2, 835 (1964).

(48) (a) L.H. Tung, J. Appl. Polym. Sci., 10, 375 (1966), (b) L.H. Tung, J.C. Moore and G.W. Knight, ibid, 10, 1261 (1966), (c) L.H. Tung, ibid, 10, 1271 (1966).

(49) Z. Grubisic, P. Rempp and H. Benoit, J. Polym. Sci., B5, 753 (1967).

(50) J.V. Dawkins, J. Macromol. Sci., B2, 623 (1968).

(51) D.N. Cramond, J.H. Hammond and J.R. Urwin, European Polym. J., 4, 451 (1968).

(52) C. Tanford, "Physical Chemistry of Macromolecules", John Wiley & Sons Inc. (1961).

(53) "Polymer Handbook", 2nd Ed., Interscience, New York (1975).

(54) D.D. Bly, J. Polym. Sci., C21, 13 (1968).

(55) (a) F.A. Bovey, "Polymer Conformation and Configuration", Academic Press, New York (1969).

(b) idem, "High Resolution NMR of Macromolecules", Academic Press, New York (1972).

(56) P.E.M. Allen and C.R. Patrick, "Kinetics and Mechanism of Polymerization Reactions", Chapter 7, Horwood, Chichester and Wiley, New York (1974).

(57) B.D. Coleman and T.G. Fox, J. Chem. Phys., 38, 1965 (1963).

(58) D.R.G. Williams, unpublished data.

(59) H.G. Krenz, E.J. Kramer and D.G. Ast, J. Mat. Sci., 11, 2211 (1976).

(60) E.H. Andrews, G.M. Levy and J. Willis, J. Mat. Sci., 8, 1000 (1973).

(61) A.V. Tobolsky and M. Takahashi, J. Appl. Polym. Sci., 7, 1341 (1963).

(62) G.S. Trick, ibid., 3, 253 (1960).

(63) D.R.G. Williams, unpublished data.

(64) T.K. Kwei, T.T. Wang and H.M. Zupko, Macromolecules, 5, 645 (1972).

(65) N. Thomas and A.H. Windle, Polymer, 19, 225 (1978).

(66) R.A. Ware and C. Cohen, J. Appl. Polym. Sci., 25, 717 (1980).

(67) J.D. Ferry, "Viscoelastic Properties of Polymers", 2nd ed., John Wiley and Sons Inc., New York (1970).

(68) S. Onogi, T. Masuda and K. Kitagawa, Macromolecules, 3, 109 (1970).

(69) T. Masuda, K. Kitagawa and S. Onogi, Polym. J., 1, 418 (1970).

(70) T.G. Fox and P.J. Flory, J. Appl. Phys., 21, 581 (1950).

(71) F. Bueche, "Physical Properties of Polymers", Interscience (1962).

(72) D.T. Turner, Polymer, 19, 789 (1978).

(73) R.F. Boyer, Macromolecules, 7, 147 (1974).

(74) R.B. Beevers and E.F.T. White, Trans. Faraday Soc., 56, 744 (1960).

(75) E.V. Thompson, J. Polym. Sci., A2, 199 (1966).

(76) J.M.G. Cowie, Eur. Polym. J., 11, 297 (1975).

(77) G.C. Berry and T.G. Fox, Adv. Polym. Sci., 5, 261 (1968).

(78) E. Kamei and S. Onogi, Polym. J., 8, 347 (1976).

(79) A.K. Doolittle, J. Appl. Phys., 22, 1471 (1951).

(80) R. Simha and R.F. Boyer, J. Chem. Phys., 37, 1003 (1962).

(81) S. Sharma, L. Mandelkern and F. Stehling, J. Polym. Sci, B10, 345 (1972).

(82) R. Simha and C. Weil, Macromol. Sci., Phys. Ed., B4, 215 (1970).

(83) R. Simha and R.F. Boyer, J. Polym. Sci., B11, 33 (1973).

(84) idem, ibid, B10, 345 (1972).

(85) J. Gibbs and E.A. DiMarzio, J. Chem. Phys., 28, 373 (1958) and 28, 807 (1958).

(86) I.S. Sanchez, J. Appl. Phys., 45, 4204 (1974).

(87) T. Nose, Kobunshi Bussei to Bunshi Kozo (Physical Properties of Polymers and Molecular Structures), p.57, Kagaku Zokan No.58, Kagaku Dozin (1973).

(88) F.N. Kelley and F. Bueche, J. Polym. Sci., 50, 549 (1961).

(89) C.A. Angell, J.M. Sare and E.J. Sare, J. Phys. Chem., 82, 2622 (1978).

(90) R.F. Fedors, J. Polym. Sci., Polym. Lett. Ed., 17, 719 (1979).

(91) E.A. DiMarzio and J. Gibbs, J. Polym. Sci., A1, 1417 (1963).

(92) T.S. Chow, Macromolecules, 13, 362 (1980).

(93) e.g. T.L. Hill, "An Introduction to Statistical Thermodynamics", Addison-Wesley, Mass. (1960).

(94) J.M. O'Reilly and F.E. Karasz, J. Polym. Sci., C14, 49 (1966).

(95) (a) A.J. Kovacs, Adv. Polym. Sci., 3, 394 (1963);
(b) G. Brown and A.J. Kovacs in "Physics of Noncrystalline Solids", North Holland, Amsterdam (1965).

(96) Y. Lipatov, Adv. Polym. Sci., 26, 63 (1978).

(97) J.G. Williams, Int. J. Frac. Mech., 8, 393 (1972).

(98) S.M. Wiederhorn, Proc. Int. Conf. Corrosion Fatigue, Connecticut, 731 (1971).

(99) Y.W. Mai, J. Mat. Sci., 10, 943 (1975).

(100) H.R. Brown and I.M. Ward, Polymer, 14, 469 (1973).

(101) G.P. Morgan and I.M. Ward, ibid, 18, 87 (1977).

(102) I.D. Graham, J.G. Williams and E.L. Zichy, ibid, 17, 439 (1976).

(103) J.R. Rice, "Fracture - An Advanced Treatise", H. Liebowitz ed., New York/London, Academic Press, Chapter 3, Vol.II (1963).

(104) H. Riedel, Mat. Sci. Eng., 30, 187 (1977).

(105) R.J. Young and P.W.R. Beautmont, Polymer, 17, 717 (1976).

(106) T. Saito, Polym. J., 11, 201 (1979).

(107) P.W.R. Beautmont and R.J. Young, J. Mat. Sci., 10, 1334 (1975).

(108) J.F. Fellers and B.F. Kee, J. Appl. Polym. Sci., 18, 2355 (1974).

(109) G.W. Weidmann and W. Döll, Colloid and Polym. Sci., 254, 205 (1976).

(110) S.J. Irael, E.L. Thomas and W.W. Gerberich, J. Mat. Sci., 14, 2128 (1979).

(111) R.N. Haward, H.E. Daniels and L.R.G. Treloar, J. Polym. Sci., Polym. Phys. Ed., 16, 1169 (1978).

(112) E.J. Kramer, J. Mat. Sci., 14, 1381 (1978).

(113) L.H. Peebles, "Molecular Weight Distribution in Polymers", Chapter 1, Interscience, New York (1971).

(114) L.R.G. Treloar, "The Physics of Rubber Elasticity", 2nd ed., Oxford University Press, Oxford (1958).

(115) J.F. Fellers and D.C. Huang, J. Appl. Polym. Sci., 23, 2315 (1979).

(116) J.P. Berry, J. Polym. Sci., 50, 107 (1961).

(117) J.J. Benbow and F.C. Roesler, Proc. Phys. Soc., 70B, 201 (1957).

(118) L.J. Broutman and F.J. McGarry, J. Appl. Polym. Sci., 9, 589 (1965).

(119) B.H. Bersted, J. Appl. Polym. Sci., 24, 37 (1979).

(120) M. Parvin and J.G. Williams, J. Mat. Sci., 10, 1883 (1975).

(121) H.H. Krausch, "Polymer Fracture", Springer-Verlag (1978).

(122) V.V. Matveyev, A. Ya. Gol'dman, V.P. Budtov, Ye. L. Ponomareva and A.M. Lobanov, Polym. Sci. USSR, 21, 413 (1979).

(123) R.P. Kusy and M.J. Katz, Polymer, 19, 1345 (1978).

(124) S.N. Zhurkov and V.E. Korsukov, J. Polym. Sci., Polym. Phys. Ed., 12, 385 (1974).

(125) K. Schönert, H. Umhauer adn W. Klemm, Proceedings of the Second International Conference on Fracture, p.474, Brighton, England (1969).

(126) J.A. Kies and A.B.J. Clark, ibid, p.483.

(127) A.G. Atkins, C.S. Lee and R.M. Caddell, J. Mat. Sci., 10, 1381 (1975).

(128) Y.M. Mai and A.G. Atkins, ibid, 11, 677 (1976).

(129) E.H. Andrews and L. Bevan, Polymer, 13, 337 (1972).

(130) N. Brown, J. Polym. Sci., Polym. Phys. Ed., 11, 2099 (1973).

(131) N. Brown and S. Fisher, ibid, 13, 1315 (1975).

(132) N. Brown, B.D. Metzger and Y. Imai, ibid, 16, 1085 (1978).

(133) K. Iisaka, Y. Nishimoto and K. Shibayama, ibid, 17, 791 (1979).

(134) N.G. McCrum, B.E. Read and G. Williams, "Anelastic and Dielectric Effects in Polymeric Solids", Wiley, New York (1967).

(135) W. Holzmüller, Adv. Polym. Sci., 26, 1 (1978).

(136) A.V. Tobolsky, J.J. Aklonis and G. Akovali, J. Chem. Phys., 42, 723 (1965).

(137) T. Fujimoto, N. Ozaki and M. Nagasawa, J. Polym. Sci. A2, 6, 129 (1968).

(138) R.P. Kambour and A.S. Holik, J. Polym. Sci., 10, 1334 (1975).

(139) E.J. Kramer, H.G. Krenz and D.G. Ast, J. Polym. Sci., Polym. Phys. Ed., 16, 349 (1978).

(140) T.G. Fox, B.S. Garret, W.E. Goode, S. Gratch, J.F. Kincaid, A. Spell and J.D. Stroupe, J. Am. Chem. Soc., 80, 1768 (1958).

(141) W.H. Watanabe, C.F. Ryan, P.C. Fleischer Jr. and B.S. Garrette, J. Phys. Chem., 65, 896 (1961).

(142) C.F. Ryan and P.C. Fleischer Jr., ibid, 69, 3384 (1965).

(143) A.M. Liquori, G. Anzuino, V.M. Coiro, M. d'Alagni, P. de Santis and M. Sarino, Nature, 206, 358 (1965).

(144) E.L. Feistma, A. de Boer and G. Challa, Polymer, 16, 515 (1975).

(145) H.Z. Liu and K.I. Kiu, Macromolecules, 1, 157 (1968).

(146) W.B. van den Berg, B. Hymans, P. Piet and D. Heikens, Nature, 217, 949 (1968).

(147) A.M. Liquori, P. de Santis, M. Savino and M. d'Alagni, J. Polym. Sci., Polym. Lett., 4, 943 (1960).

(148) J. Dayantis, C. Reiss and H. Benoit, Makromol. Chem., 120, 113 (1968).

(149) J. Biros, Z. Másа and J. Pouchlý, Eur. Polym. J., 10, 629 (1974).

(150) J. Spěváček and B. Schneider, Makromol. Chem., 175, 2939 (1975).

(151) idem, Polymer, 19, 63 (1978).

(152) idem, J. Polym. Sci., Polym. Lett., 12, 349 (1974).

(153) T. Miyamoto and H. Inagaki, Macromolecules, 2, 554 (1969).

(154) R. Buter, Y.Y. Tan and G. Challa, J. Polym. Sci., Polym. Chem. Ed., 11, 2975 (1973).

(155) G. Challa, A. de Boer and Y.Y. Tan, Int. J. Polym. Mat., 4, 239 (1976).

(156) M. Pyrlik, W. Borchard, G. Rehage and E.P. Uerpmann, Angnew Makromol. Chem., 36, 133 (1974).

(157) E.J. Vorenkamp, F. Bosscher and G. Challa, Polymer, 20, 59 (1979).

(158) J.J. Spence, J. Phys. Chem., 45, 401 (1941).

(159) W. Baker, C. Fuller and N. Pape , J. Am. Chem. Soc., 64, 766 (1942).

(160) H.G. Zachmann and W. Sherman, Kolloid Z.Z. Polym., 241, 916 (1970).

(161) E.L. Lawton and D.M. Cates, J. Appl. Polym. Sci., 13, 899 (1969).

(162) A.B. Desai and G.L. Wilkes, J. Polym. Sci., Symposium, 46, 291 (1974).

(163) P.R. Blakey and R.P. Sheldon, Nature, 195, 172 (1962).

(164) E. Turska and H. Janeczek, Polymer, 20, 855 (1979).

(165) H. Tadokoro, Y. Chatani, H. Kusanagi and M. Yokoyama, Macromolecules, 3, 441 (1970).

(166) S. Krause and H. Roman, J. Polym. Sci., A3, 1631 (1965).

(167) D.R. Paul and J.O. Altaminaro, ACS, Polym. Preprint, 10, 632 (1969).

(168) T. Nishi and T.T. Wang, Macromolecules, 8, 909 (1975).

(169) R.I. Imken, D.R. Paul and J.W. Barlow, Polym. Eng. Sci., 16, 593 (1976).

(170) D.S. Kaplan, J. Appl. Polym. Sci., 20, 2615 (1976).

(171) R.G. Bauer and N.C. Bletso, ACS, Polym. Preprint, 10, 632 (1969).

(172) L.E. Nielsen, J. Appl. Polym. Sci., 2, 351 (1959).

(173) idem, "Mechanical Properties of Polymers and Composites", Vol.1, Chapter 4, Marcel Dekker Inc., New York (1974).

(174) A. de Boer and G. Challa, Polymer, 17, 633 (1976).

(175) P. Dunn and G.P. Sansom, J. Appl. Polym. Sci., 13, 1641 (1969).

(176) J.H. Hildebrand and R.L. Scott, "Solubility of Nonelectrolytes", Reinhold, New York (1950).

(177) W.W. Graessly, Adv. Polym. Sci., 16, 1 (1974).

(178) P.G. de Gennes, J. Chem. Phys., 55, 572 (1971).

(179) J. Klein, Macromolecules, 11, 852 (1978).

(180) P.G. de Gennes, ibid, 9, 594 (1976).

(181) M. Doi and S.F. Edwards, J. Chem. Soc., Faraday Trans.2, 74, 1789 (1978); 74, 1802 (1978); 74, 1818 (1978) and 75, 38 (1979).